The vascularization of solid tumours: mathematical models of tumour angiogenesis and vascular tumour growth

Orme, Michelle Elaine

Award date:
1996

Awarding institution:
University of Bath

The Vascularization of Solid Tumours: Mathematical Models of Tumour Angiogenesis and Vascular Tumour Growth.

submitted by

Michelle Elaine Orme

for the degree of Ph.D.

of the

University of Bath

1996

ProQuest LLC
789 East Eisenhower Parkway
P.O. Box 1346
Ann Arbor, MI 48106-1346

Summary

In this thesis, we develop a number of mathematical models which describe the various stages of solid tumour growth prior to metastasis, from the initial appearance of the small avascular tumour nodule, to the vascularization of the tumour via angiogenesis, and the subsequent vascular tumour growth. From these continuum models, we wish to obtain an insight into the complex mechanisms behind tumour development. In the first chapter, we detail the biological background and highlight the link between tumour angiogenesis, tumour invasion and the dissemination of the disease. Our first model looks at how the growth of an avascular tumour can be modulated by the immune response of the host. In chapter (3), we look at the early stages of tumour angiogenesis, and we present two simple models for the formation of capillary buds and the formation of secondary branches. In the following chapter, we examine the growth of a vascularized tumour, and the interaction between the invasive tumour and the newly-formed capillary network. An alternative model is given in chapter (5), where a density-dependent diffusion equation is used as a qualitative description of solid tumour growth. We show the existence of travelling wave solutions with semi-infinite support for this equation. In chapter (6), we present a two-dimensional model of the growth of a tumour in heterogeneous host tissue and we analyse the numerical simulations from a surgical viewpoint. Finally, we present a two-dimensional model of tumour angiogenesis. By manipulating the model parameters, we simulate a variety of anti-angiogenesis strategies and analyse the effect on the pattern of capillary growth.

Acknowledgements

I would like to thank a number of people who have helped and supported me in various ways during my time at Bath University.

Firstly, I must thank my supervisor Dr. Mark Chaplain for all his help and enthusiasm. Thank you to the staff at the School of Mathematical Sciences, in particular Mark Willis for sorting out my computing problems. I would also like to acknowledge the financial support of the Engineering and Physical Sciences Research Council and The British Federation of Women Graduates.

A big thanks goes to all my friends, in particular my office mates at Bath, Chris Brooking for giving us all something to talk about, Emma Stott for tea and sympathy, Steve Benbow for organising various social events, Rob Laister for not organising various social events, Sandy Anderson, Luke Olsen, Chris Mills and anyone else who I've forgotten.

I would like to express my gratitude to my family, and especially to my Dad for his hand-drawn illustrations and all the time and effort that has gone into them. Finally, thanks to my husband, Mark, for keeping his sense of humour and for not looking too confused when I try to explain to him what I have been doing for the last three years.

> "My universe is within my fingers", he realized, "if I could just figure out how the damn thing works." *P. K. Dick, The Electric Ant.*

This thesis is dedicated to my grandad, Chill.

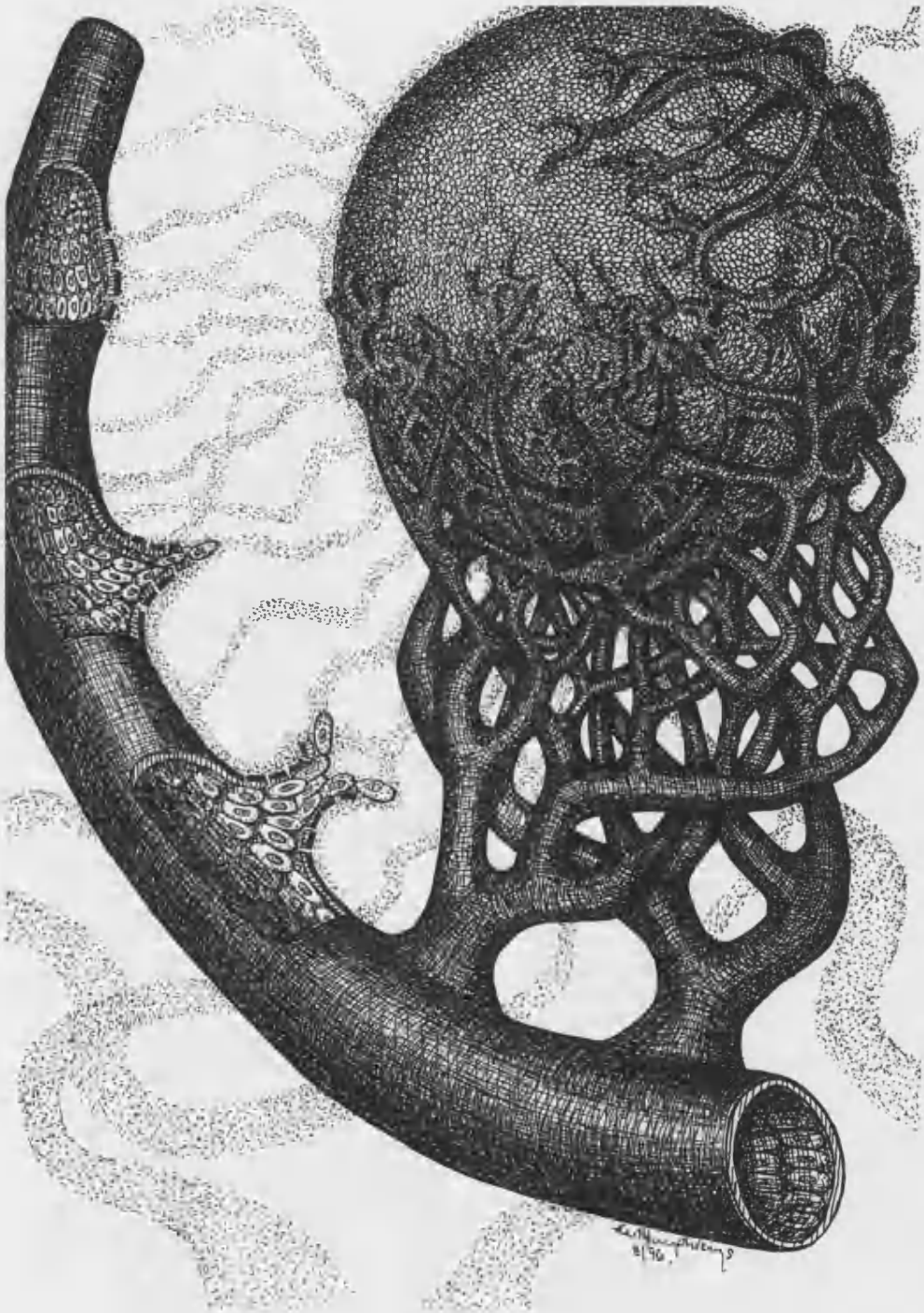

Contents

1 Introduction 1

1.1 The stages of solid tumour growth 2

1.1.1 Early tumour growth and the response of the immune system . . 2

1.1.2 The process of angiogenesis 6

1.1.3 The vascular phase of tumour growth: The consequences of tumour angiogenesis 9

1.2 Experimental models 10

1.3 Mathematical models 13

2 Early avascular tumour growth and cell-mediated immune response 15

2.1 The mathematical model 16

2.2 Numerical simulations 24

2.3 Discussion 30

3 Capillary sprout formation and secondary branching in tumour angiogenesis 33

3.1 A mathematical model of initial bud formation 34

3.1.1 Linear stability analysis 37

3.1.2 Estimation of parameters 41

3.1.3 Numerical simulations 43

3.2 The branching of capillary sprouts 45

3.2.1 Mathematical model of secondary branch formation 47

3.2.2 Linear stability analysis 49

3.2.3 Estimation of parameters 52

3.2.4 Numerical simulations 54

3.3 Discussion 62

4 Vascular tumour growth and invasion **63**

4.1 The mathematical model 64

4.1.1 Estimation of parameters 68

4.1.2 Numerical simulations 69

4.2 Travelling wave analysis 71

4.2.1 Case 1: $D = 0$. 75

4.2.2 Case 2: $D > 0$ 77

4.3 Discussion 80

5 Travelling waves for a density-dependent diffusion-reaction system modelling tumour growth and invasion **82**

5.1 The mathematical model 83

5.2 Travelling wave analysis of a density-dependent diffusion-reaction equation 86

5.2.1 First order approximation 88

5.2.2 Existence of a travelling wave solution for a density dependent diffusion equation 90

5.2.3 Existence of travelling wave solutions for $c^2 \geq M > 0$ 92

5.2.4 Existence of finite travelling waves 97

5.3 Numerical simulations 103

5.4 Discussion 114

6 Two-dimensional models of tumour invasion in heterogeneous host tissue **115**

6.1 A mathematical model of tumour invasion 116

6.2 Numerical simulations 118

6.3 Travelling wave analysis 124

6.4 Discussion 129

7 Two-dimensional models of tumour angiogenesis and anti-angiogenesis strategies **132**

7.1 The mathematical model 133

7.1.1 Estimation of parameter values 136
7.1.2 Model simplification which focuses upon the role of haptotaxis . 138
7.2 Numerical simulations 139
7.2.1 Anti-angiogenesis strategies 139
7.3 Alternative chemotaxis model 148
7.4 Discussion 150

8 Conclusions and future work **151**

Bibliography **154**

Appendices **163**

A Appendix to chapter 4 **163**
A.1 Analysis of the three-dimensional phase space 163
A.2 Analysis of the four-dimensional phase space 168

B Appendix to chapter 5 **171**
B.1 Local stability analysis of a density-dependent diffusion equation 171
B.1.1 At the critical point (0,0) 171
B.1.2 At the critical point P_1 176
B.1.3 At the critical point P_c 176

Chapter 1

Introduction

Any one cell in the body, which is capable of cell division, has the potential to become malignant [Ruddon, (1987)] and to proceed through various stages to eventually form a neoplasm or tumour. Neoplasia is the name used to describe a collection of diseases characterised by the uncontrolled, uncoordinated and excessive proliferation of cells.

Broadly speaking, tumours fall into two categories, benign or malignant. It is important to distinguish between these two types when deciding upon appropriate treatment. Table (1.1) summarises the basic differences between benign and malignant tumours [Ruddon, (1987)].

Benign Tumours	**Malignant Tumours**
Grow by expansion, do not invade.	Invade and destroy adjacent normal tissue.
Usually resemble normal tissue.	Anaplastic/Undifferentiated.
Grow slowly over several years.	Grow rapidly over weeks/months.
Remain localised.	Metastasise through blood/lymph system.

Table 1.1: *Differences between benign and malignant tumours.*

Whilst benign tumours can be life threatening if the growth is particularly large or near to essential organs, it is malignant tumours (or cancers) that pose the most serious threat to health. The most common type of malignant tumours are carcinomas (cancer of the epithelia), which are solid tumours of the internal and external surfaces of tissues and organs. Lung cancer, colorectal cancer, prostate cancer and breast cancer account for over 50% of all reported cancers in England and Wales [OPCS, (1989)].

In the majority of patients suffering from carcinomas, the disease has already spread (metastasised) before detection, resulting in multiple secondary tumours (metastases) which may occur in sites far removed from the primary cancer. Hence the disease cannot be cured by treating the primary tumour alone. Wide-spread metastases can be difficult to treat, can cause a number of unpleasant symptoms and often prove to be fatal. (The estimated annual death rate is 1 in 341 for men and 1 in 387 for women [OPCS, (1993)]). Thus, it is highly desirable to prevent metastasis from occurring and so it is important to investigate the mechanisms by which the cancer spreads *before* the secondary tumours have developed. In the first instance, this means understanding the different stages of solid tumour growth, from the initial appearance of the neoplasm, up to the point of metastases formation, and secondly, to identify the different ways by which the tumour growth can be, at the very least, contained, or ideally, removed altogether.

1.1 The stages of solid tumour growth

1.1.1 Early tumour growth and the response of the immune system

The growth of most solid tumours takes place in two stages [Folkman, (1985)]. In the first stage, the tumour is avascular, that is, it does not have a network of capillary blood vessels supplying it with nutrients. During this avascular stage, the tumour may be considered as being roughly spherical in shape and consists of a central necrotic core surrounded by a layer of quiescent cells which in turn is surrounded by a thin layer of proliferating cells [Sutherland, (1988)]. At this stage, the tumour is likely to be too small (1-3mm in diameter) to be detectable or may not produce any symptoms in the host. Thus, if left to grow unimpeded, the tumour may pass into the the next stage of growth (the vascular phase), and may subsequently metastasise. If, however, the immune system of the host recognises the abnormality in the nascent tumour, then the growth may be regulated by the immune response. This response may be sufficient to eradicate the tumour completely.

The immune cells, B-lymphocytes and T-lymphocytes (or B-cells and T-cells), are the key players in the immune response of invertebrate animals [Marrack & Kappler, (1986)]. Both B-cells and T-cells are derived from the bone marrow, but the T-cells undergo further development in the thymus gland. B-cells and T-cells circulate in the blood and lymph system but are usually concentrated in the lymph nodes (and also

the spleen in humans). These lymphocytes can recognise certain cell surface or free antigens, which are the molecules associated with foreign material (such as a virus or bacteria) or are produced by defective cells. Different viruses, for example, will produce different antigens and the ability of the host to defend against a virus depends upon the ability of the lymphocytes to recognise specific antigens. The lymphocytes also have the ability to distinguish between self and non-self, i.e. between cells evolving from the host or from an external source.

The response of the immune system to a virus or a malignant cell is initiated by the appearance of antigen in the host. The response of the B-cells is known as the Clonal Selection Theory. The antigen binds to a specific receptor on the B-cell membrane, which Marrack & Kappler, (1986) describe as analogous to a key fitting a lock. The B-cells start to produce clones which secrete *antibodies*, molecules similar in structure to the B-cell receptors to which the antigen was originally bound. This is known as a *humoral* immune response, and the B-cells and the antibodies are collectively known as immunoglobulins. The antibodies bind to the antigens and mark it for destruction by other immune cells such as macrophages or natural killer cells.

T-cells also respond to antigen by clonally dividing but will then differentiate into several kinds of T-cell.

- **Cytotoxic T-cells.** These cells bind to antigen on the surface of an infected cell or virus, and kill it by disrupting the cell membrane (lysis).
- **Suppressor T-cells.** These have the important role of regulating the immune response by inhibiting excessive immune reactions.
- **Helper T-cells.** These cells bind to antigen on the surface of the B-cells and release hormones which help the B-cells to proliferate.
- **Memory T-cells.** Cytotoxic T-cells can become memory cells, which continue to circulate in the blood and lymph system, long after the immune reaction has taken place. They can rapidly respond to any further appearance of antigen of the same kind. Therefore, after exposure to a small amount of antigen, the body can build up immunity to specific antigens, and hence, the use of vaccinations.

T-cells do not differentiate into cells that produce antibodies and so are only involved in the *cell-mediated* immune responses as described above.

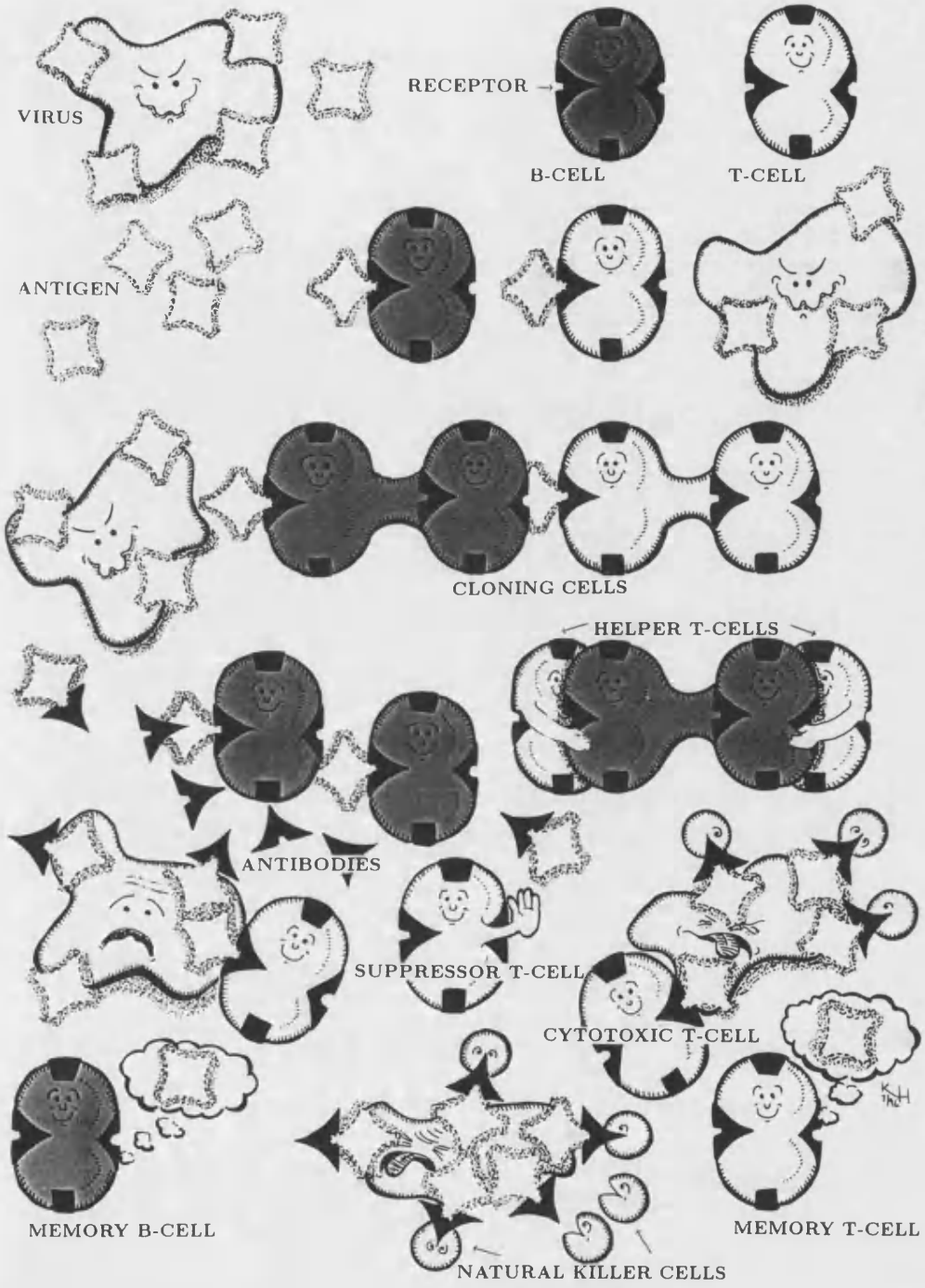

Figure 1-1: *Schematic diagram of the interactions of the T-lymphocytes and B-lymphocytes in response to an infection by a virus.*

The proteins that mark every cell as 'foreign' or 'self' are called MHC-encoded proteins (Major Histocompatibility Complex encoded proteins). These are encoded by genes in a specific region of the host DNA. There are millions of variants for the MHC encoding, such that two unrelated individuals are highly unlikely to have the same MHC-encoded proteins, (hence the occurrence of donor transplant rejections). Presumably, it is more difficult for the immune system to defend against neoplastic growth than external foreign invaders such as viruses or bacteria, since the tumour cells and the adjacent normal cells will have the same or similar proteins [Klein, (1980)]. Hence, the immune cells may not recognise the potential abnormality in the developing tumour and so the immune response may not be sufficient to produce an effect on the subsequent growth of the tumour. Tumours that induce a strong immune response are said to be immunogenic. Such tumours tend to be induced (by a carcinogenic virus, for example) rather than occur spontaneously [MacSween & Whaley, (1992)], [Prehn, (1994)].

During the avascular stage of growth, the tumour is small enough (1-3mm in diameter) to take in nutrients and expel waste products by diffusion alone. However diffusion is not sufficient to support any continued growth of the tumour. This is because the tumour consumes nutrients at a rate proportional to its volume whereas the supply of nutrients is delivered at a rate proportional to its surface area. The avascular tumour can sometimes become dormant and there is an indefinite period for which growth stops.

The inadequacy of diffusion as a means of transportation of vital nutrients has been demonstrated, for example, by LaBarbera & Vogel, (1982) and Edelstein-Keshet, (1988). By applying Fick's first law of diffusion across a wall (e.g of a cell) of thickness dx, the diffusive flux of nutrient across the surface is given by

$$J = DS\frac{dC}{dx},$$

where C is the concentration of nutrient, D is the diffusion coefficient and S is the surface area [Jones & Sleeman, (1983)], [LaBarbera & Vogel, (1982)]. Suppose then we have a spherical tumour, with radius r, volume $V = 4\pi r^3/3$ and surface area $S = 4\pi r^2$. Suppose further that the concentration of a given substance (e.g. oxygen) at the tumour surface is c_0 and that the tumour uses up the substance completely so that at $r = 0$, $c(0,t) = 0$ (cf. Greenspan, (1976)), where c is the concentration of the substance. The

total diffusive flux across the tumour surface will be approximately,

$$J = DS\frac{c_0}{r} = 4\pi D c_0 r,$$

where the gradient of the nutrient has been approximated by c_0/r, i.e. the concentration difference per unit distance [Edelstein-Keshet, (1988)]. The rate at which the substance is depleted will be proportional to the tumour's volume. If τ is a fixed constant representing the time it takes for the substance to be used up completely then

$$\text{rate at which substance used} = \frac{4\pi r^3}{3\tau}.$$

Hence,

$$\frac{\text{rate of supply}}{\text{rate used}} \simeq \frac{3Dc_0\tau}{r^2}.$$

In order to meet the demands of the tumour the rate of supply of the substance must be greater or equal to the rate at which the substance is used, i.e. the ratio must be greater than 1. Thus a minimum requirement is approximately

$$c_0 = \frac{r^2}{3D\tau}.$$

So the external substance concentration must be, at the very least, proportional to the radius of the tumour squared. This is unrealistic if the radius of the tumour is large. Hence, as the tumour grows, cells at the centre of the tumour become starved of nutrients and begin to die [Durand, (1990)], [Greenspan, (1976)]. Dormancy will occur when the necrosis at the centre of the tumour and the proliferation of the outer layer is in equilibrium, and the tumour may remain in this dormant state for months or even years [Paweletz & Knierim, (1989)]. The tumour can overcome this deficiency by acquiring a blood supply which can deliver nutrients directly into the tumour and can transport waste products away.

1.1.2 The process of angiogenesis

During the second stage of growth, the tumour becomes *vascular*, that is, it is penetrated by capillary blood vessels. A vascularized tumour can grow exponentially and there is the possibility of both invasion and metastasis [Folkman, (1985)], [Gimbrone *et al.*,

(1974)], [Muthukkaruppan *et al.*, (1982)]. Vascularization is realized by a process known as *angiogenesis*, that is, the formation of blood vessels. Angiogenesis occurs during physiological processes such as embryonic development, or during pathological processes such as wound healing, rheumatoid disease and of course tumour growth (see references in Paweletz & Knierim, (1989)).

The lining of many vessels such as veins and small lymphatic vessels is formed from a regular monolayer of endothelial cells (EC). The EC lie upon a continuous basement membrane (or basal lamina) and are in close contact with their neighbours. Studies have shown that EC play a crucial role in angiogenesis, and in fact it has been shown *in vitro*, that EC can construct capillary networks unaided by other cell types [Folkman & Haudenschild, (1980)].

Angiogenesis is initiated by the release of diffusible chemicals from the tumour, collectively known as tumour angiogenic factors (TAF), though it is not known what triggers this activity. There are two types of angiogenic factors, those that act directly on the EC and those that induce other cells into producing factors which act on the EC [Folkman & Haudenschild, (1980)] , [Folkman & Klagsbrun, (1987)]. Angiogenic factors induce one or more of the following activities in the EC:

1. the secretion of proteases and collagenases by the EC which degrade the basal lamina and the extracellular matrix.

2. the migration of EC towards the chemotactic stimulus.

3. the proliferation of EC.

For successful tumour vascularization, all three events must be carefully orchestrated. In recent years several angiogenic factors have been identified. A summary of these factors can be found in Folkman & Klagsbrun, (1987). The suggestion is that several angiogenic factors act together, either directly or indirectly, to promote angiogenesis. We now describe the above activities in more detail.

The tumour releases tumour angiogenic factors which diffuse into the surrounding tissue. The first reaction to this stimulus is that the EC in the neighbouring blood vessels and nearest to the chemical source start to alter their structure. The cells thicken and finger-like protrusions can be observed on the abluminal surface [Ausprunk & Folkman, (1977)] , [Paweletz & Knierim, (1989)]. Cell-associated proteases degrade the basement

membrane so that the EC loosen their contacts with their neighbours. Stimulated by the TAF the EC begin to migrate [Zetter, (1980)]. The EC accumulate in the region where the concentration of angiogenic factors has first reached a threshold level [Paweletz & Knierim, (1989)]. The vessel wall begins to bulge as EC pile up to form sprouts. The basement membrane does not contain gaps large enough to allow EC passage into the extracellular matrix beyond the vessel wall. Therefore the EC secrete proteases and collagenases which dissolve the basal lamina and the surrounding extracellular matrix enabling the capillary sprout to grow towards the tumour [Kalebic *et al.*, (1983)].

The capillary sprouts begin to grow in length by recruiting EC from the parent vessel. At some distance from the tip of the sprout EC begin to proliferate. There is evidence that migration and mitosis are independent events and that separate angiogenic factors are required to stimulate these activities of EC [Fenselau & Mello, (1976)], [Paweletz & Knierim, (1989)], [Zetter, (1980)]. The first stages of angiogenesis can be performed without cell proliferation [Sholley *et al.*, (1984)], with mitosis occurring after the capillary sprouts have started to grow. However, proliferation is essential for the completion of angiogenesis as gaps will develop in the parent vessel resulting in abnormal permeability [Ausprunk & Folkman, (1977)].

The EC in the outgrowing sprouts then start to reassociate with each other. The development of intracellular lumen, where vacuoles appear within the EC, and intercellular lumen, where vacuoles appear between the outgrowing sprouts, leads to the formation of tube-like structures [Konerding *et al.*, (1992)]. Branches form in a similar way whereby an intracellular vacuole becomes Y or T shaped before fusing with the primary lumen [Folkman & Haudenschild, (1980)]. Initially the sprouts are parallel with each other but tend towards each other as they elongate. Neighbouring sprouts will eventually fuse together at their tips to form loops (anastomoses). This signals the beginning of circulation of blood. It is essential that there is a flow of blood through the tumour since an effective system for transporting waste products away from the tumour is vital. As the vessels mature, the EC resynthesize a basal lamina in order to restore continuity. The looped vessels may bud or loops may fuse with other loops until a complex network of vessels develops. Finally, this network penetrates the tumour, providing it with the circulatory system and the supply of nutrients that it requires for growth. In order to support continued growth, the tumour's vascular system persistently remodels itself. Hence angiogenesis is an on-going process, continuing indefinitely until the tumour is

removed or killed, or until the host dies.

1.1.3 The vascular phase of tumour growth: The consequences of tumour angiogenesis

If the angiogenic process is successful, the tumour will then enter the vascular phase of growth. The neovasculature will penetrate the tumour and the necrotic core may temporarily disappear [Paweletz & Knierim, (1989)]. The sudden rise in metabolites throughout the tumour gives rise to an increase in tumour cell proliferation and a rapid increase in tumour volume [Muthukkaruppan *et al.*, (1982)], [Ruddon, (1987)]. This in itself could prove to be life threatening by compromising the function of adjacent organs. An avascular tumour can take months or years to grow a few millimetres in diameter, while a vascular tumour can achieve a diameter of a few centimetres in a matter of weeks.

The tumour vasculature is inferior to other capillary networks [Denekamp, (1984)], [Jain, (1994)], and that, coupled with the enormous build up of pressure caused by the unregulated tumour growth, leads to the collapse of the vasculature at the centre of the tumour. If oxygen levels fall, a tumour cell can become hypoxic, whereby the cell is no longer active [Denekamp, (1984)]. A hypoxic cell can be reactivated and function normally if the nutrient levels increase, but will eventually die if deprived of oxygen for long periods. Unfortunately, the internal architecture of the tumour and its inferior vasculature can lead to the failure of current forms of cancer therapy. After a dose of radiotherapy, only the outer proliferating layer of tumour cells is destroyed, and the inner layer of hypoxic cells (which is radioresistant), can become re-oxygenated, resulting in the regrowth of the tumour [Brown & Giaccia, (1994)], [Kennedy *et al.*, (1980)]. Furthermore, the poor circulation of blood through the tumour may lead to an inadequate distribution of chemotherapeutic drugs [Denekamp, (1984)], [Jain, (1994)]. In general, hypoxia has been regarded as a major problem in cancer therapy. However, recent research has suggested that the hypoxic portion of the tumour should be increased by attacking the highly vulnerable vasculature [Denekamp, (1984)], [Harris *et al.*, (1996)], and then preferentially killing the hypoxic cells by the use of bioreductive cytotoxic drugs [Brown & Giaccia, (1994)], [Harris *et al.*, (1996)], [Kennedy *et al.*, (1980)]. (These are drugs which are harmless in regions of high oxygen concentration,

but become activated in hypoxic areas). Such a strategy could be used in conjunction with conventional therapies, or on its own where destruction of normal healthy tissue must be kept at a minimum.

As well as the rapid increase in tumour growth and the appearance of hypoxic regions, the vascularization of a tumour can have other serious consequences. It has been suggested that angiogenesis is a precursor to a more malignant phase of the tumour growth [Blood & Zetter, (1990)], [Folkman, (1985)], [Gimbrone *et al.*, (1974)], [Paweletz & Knierim, (1989)] in that the vascularization of a tumour promotes the propagation of the more aggressively growing tumour cells [Ruddon, (1987)]. These malignant tumour cells actively invade and destroy the adjacent host tissue. At this stage, the malignant carcinoma loses its quasi-spherical shape and the outer edge of the tumour is covered with finger-like protrusions, resulting from the local invasion of the host tissue [Darling & Tarin, (1990)], [MacSween & Whaley, (1992)]. The irregular shape of such a tumour can cause complications during surgical excision of a cancer, since the tumour may only be partially visible and the surgeon is required to remove tissue beyond the observed tumour boundary in order to prevent regrowth.

Finally, the most important and somewhat devastating consequence of tumour vascularization is the increase in the risk of metastasis [Ellis & Fidler, (1995)], [McCulloch *et al.*, (1995)], [Norton, (1995)]. The immature tumour vasculature is easily invaded by the actively mobile tumour cells, and hence the disease can be spread around the body via the blood system. The outcome of the metastatic process varies extensively, since the formation of metastases is dependent upon a variety of different properties of the host and the tumour [Fidler, (1978)], [Nicolson, (1988)] as well as the potential of the tumour cells to survive in the circulation. However, there is a direct correlation between the intensity of the tumour vasculature and the metastatic potential of the tumour [Ellis & Fidler, (1995)], [McCulloch *et al.*, (1995)], [Norton, (1995)]. Indeed, the density of the tumour vasculature can now be used as a prognostic factor [Frank *et al.*, (1995)].

1.2 Experimental models of tumour growth and angiogenesis

Various techniques have been developed in order to examine the cascade of events that lead to neovascularization and the subsequent growth of the tumour. In this section,

we will briefly describe some of the main techniques.

Multicellular spheroids

The simplest experimental model of solid tumours are multicellular spheroids (MCS). These are three dimensional, multicellular aggregates, which are grown in tissue culture (for a review see Durand, (1990)). Multicellular spheroid models are used to study the growth kinetics of small populations of cells and the regrowth kinetics of the population in response to cytotoxic treatments. MCS models have similar growth kinetics to tumour nodules and they develop microregions of quiescent cells in much the same way as solid tumours do. Furthermore, they have simple geometry and are easy to manipulate. However, it is difficult to compare MCS models directly with *in vivo* tumours, since they do not incorporate the influence of the host on the tumour growth.

In vitro bioassays

It is known that angiogenesis is initiated by the release of tumour angiogenic factors by the tumour [Paweletz & Knierim, (1989)]. In order to identify these angiogenic factors, and to study their action, *in vitro* bioassays were developed which could examine EC migration [Zetter, (1980)], EC proliferation [Fenselau & Mello, (1976)] and degradation of the basement membrane by EC [Kalebic *et al.*, (1983)]. Typically, these assays involved cloning EC in a culture containing the test substance. To test for cell motility, the EC are put onto coverslips coated with gold, which is ingested as the EC migrate, leaving measurable tracks [Weiss, (1992)], [Zetter, (1980)]. Cell proliferation can be assessed by culturing the cells in the presence of test material and counting the cells at a fixed time [Fenselau & Mello, (1976)]. The Boyden chamber is a system which is widely used to examine chemotaxis, where two compartments, containing the culture medium, are separated by a filter with the test material added to the lower compartment [Weiss, (1992)]. The migration of the cells is assessed by counting the number of cells on the underside of the filter. Kalebic *et al.*, (1983) used a similar method, where collagen was placed in the top compartment with a chemotactic substance in the lower compartment, in order to examine the degradation of basement membrane collagen by migrating EC.

The use of these assays has led to several angiogenic factors being identified [Folkman & Klagsbrun, (1987)]. For example, EC react chemotactically to fibronectin [Bowersox

& Sorgente, (1982)], [Ungari *et al.*, (1985)] or heparin [Terranova *et al.*, (1985)], [Ungari *et al.*, (1985)], and display an increased growth rate in response to fibroblast growth factors (FGF) [Folkman & Klagsbrun, (1987)].

The cloning of EC in culture can additionally be used as a model for angiogenesis *in vitro*. Folkman & Haudenschild, (1980) reported that cloned capillary EC cultured in tumour-conditioned medium formed networks *in vitro*, which resembled capillaries observed *in vivo*. Such a method is useful for investigating the formation of capillary branches and anastomoses.

In vivo and animal models

Whilst *in vitro* experiments are relatively easy to deploy, they cannot simulate the situation within a whole organism. Studies on human tumours have previously been hampered by a lack of *in vivo* systems [Folkman, (1985)], [Schirrmacher, (1985)]. One of the earliest *in vivo* assays was the transparent chamber, developed by Sandison in 1928 (see references in Folkman, (1985)). This consisted of two metal plates fitted over each other to create a chamber, into which a tumour is implanted [Folkman, (1985)], [Weiss, (1992)]. Originally, the chamber was used in the ear of a rabbit, though later it was adapted for use in the hamster cheek pouch [Goodall *et al.*, (1965)].

Another useful method for the study of tumour angiogenesis is the corneal pocket test system [Gimbrone *et al.*, (1974)]. This method involves the implantation of a tumour fragment into the eye, (for example, a rabbit eye [Ausprunk & Folkman, (1977)], [Gimbrone *et al.*, (1974)], or a mouse eye [Muthukkaruppan *et al.*, (1982)]), a few millimetres from the edge of the cornea and the vascular bed. New capillaries grow towards the tumour implant and are examined with a slit lamp stereoscope.

One of the most simple and commonly used assay is the chick chorioallantoic membrane or CAM system [Folkman, (1985)], [Weiss, (1992)]. The CAM is separated from the egg shell membrane and exposed through a small window made in the shell. Test material is placed on the CAM, and examined a few days later for angiogenic activity. Using this system, a large number of samples can be tested relatively quickly.

Whilst the above test systems can be used to study tumour angiogenesis, cancer metastasis can be investigated using animal models such as the human tumour xenograph model (where human tumour cells are implanted into an immunosuppressed animal), or rodent tumours transplanted into a syngenic host [Schirrmacher, (1985)]. Both

models have the advantage of being more holistic methods to study tumour growth, but the disadvantage of not truly reflecting the growth of a spontaneous human tumour.

1.3 The use of mathematical models to study tumour growth

In this thesis, the mathematical models are derived with two key aims in mind. Firstly, we wish to obtain a better understanding into the complex mechanisms behind solid tumour development. Secondly, we wish to identify the potential mechanisms by which the tumour growth can be impeded with a view to preventing metastases.

In chapter (2), we develop a simple model of the early stages of solid tumour growth and how it is modulated by a cell-mediated immune response, and we determine several factors which influence the growth (or demise) of the tumour, such as the maximum avascular size and the immunogenicity of the tumour. In the subsequent chapters, we concentrate on what we consider to be the two key areas of tumour development;

1. The vascularization of the tumour via angiogenesis.

2. The invasion of the local tissue by the tumour.

A primary tumour is often vascularized, that is, it has its own blood supply and microcirculation. A vascularized tumour has two important advantages over an avascular tumour:

- The direct supply of nutrients into the tumour results in a rapid increase in growth, which compromises adjacent tissue.

- The tumour can shed cells into the blood stream which may consequently lead to metastases.

In chapter (3), we look at the very early stages of angiogenesis, and, in particular, the formation of capillary buds and secondary branches. Both of these processes are not widely understood and hence, this is an area worthy of further investigation. In chapter (7), we develop a two dimensional model of tumour angiogenesis, which captures the process of anastomosis (loop formation). Again, it is not known exactly how anastomosis occurs, but the formation of capillary loops is essential if blood is to circulate through the

tumour. Folkman, (1995) has proposed anti-angiogenesis as a potential strategy for the treatment of cancer. Mathematical models can help us to understand the mechanisms behind angiogenesis and to identify the different ways by which the angiogenic process can be interrupted. Hence, we use the model of chapter (7) to test a variety of anti-angiogenesis strategies by suitable manipulation of the model parameters and we analyse the effect on the resultant solution.

Tumour invasion is also a major problem in the treatment of cancer for several reasons.

- As the tumour cells invade they destroy normal tissue, which can cause complications for the patient, particularly if the tumour is adjacent to vital organs.
- A highly invasive tumour has no distinct edge which makes it difficult to remove surgically. Again, this is particularly serious if the tumour has infiltrated vital tissue, e.g. the brain.
- An invasive tumour can actively invade blood vessels and/or the lymph system and consequently metastasise.

Mathematical models can be used to explore the different ways in which the invasive properties of a tumour can be manipulated with a view to preventing metastasis.

In chapter (4), we develop a simple model for the growth of a vascularized tumour, with an emphasis on the interactions between the nascent invasive tumour and its vasculature. From this model, we estimate the speed at which the tumour invades the surrounding tissue. An alternative model of vascular tumour growth is given in chapter (5). In this chapter, we assume that tumour cell motility, tumour cell proliferation and tumour cell death are all events which are dependent upon the density of the tumour cell population, and changes in the model parameters related to these events correspond to changes in the behaviour of a tumour as it transforms from an *in situ* carcinoma to a more malignant invasive phenotype. In chapter (6), we present a two dimensional model of a solid tumour growing in heterogeneous host tissue and show how the structure of the host tissue affects the ability of the tumour to invade, and thus also affects the metastatic potential of the tumour. Finally, in chapter (8), we make various concluding remarks, suggest ways by which the models could be improved and highlight the key areas of solid tumour growth which have potential for future research for mathematicians and oncologists alike.

Chapter 2

Early avascular tumour growth and cell-mediated immune response

There are several mechanisms by which normal cell growth is regulated (e.g. apoptosis, contact inhibition, cell cycle control). Neoplastic tissue growth is, in general, described as uncontrolled and uncoordinated with adjacent normal tissue. A tumour can arise from a single cell which has escaped normal genetic control mechanisms after being exposed to some carcinogenic agent (e.g. a virus, radiation), and transformed into a malignant phenotype. After proliferation has occurred, the mutation will be reproduced in the daughter cells, resulting in the growth of a small cancerous nodule. If left to grow unimpeded, the tumour may eventually become vascularized and even metastasise. If, however, at an early stage, the host recognises the tumour cells as abnormal, the subsequent immune response can contain the growth or even eradicate the tumour altogether. A typical immune response is cell-mediated, whereby so-called effector cells (e.g. T-lymphocytes, natural killer cells, macrophages) bind with the tumour cells and subsequently kill them.

In this chapter, we develop a simple model of the early stage of solid avascular tumour growth and examine how it may be modulated by the reaction of the immune system. We identify several factors which determine whether the immune response is sufficient to produce a cancer free state, such as the maximum potential size of the avascular tumour, the extent to which the effector cells successfully induce lysis in the

tumour cells and the immunogenicity of the tumour. In the next section, we will derive the model equation and look at the stability of the cancer free steady state. In section (2.2), we briefly describe the numerical scheme used throughout this thesis, and present some numerical simulations for different values of the parameters relating to the immune response to the tumour.

2.1 The mathematical model

This model examines the development of a small avascular tumour and the simultaneous cell-mediated immune response. It is an extension of the model of growth mediated immune response in one space dimension by Adam, (1993). During the early stages of growth, the tumour may be considered roughly spherical in shape, so we take our model tumour to be radially symmetric. Let r be the distance from the centre of the tumour and $u(r,t)$ be the tumour cell density per unit volume. Conservation of mass gives us

$$\frac{\partial u}{\partial t} + \nabla.\mathbf{J} = f(u),$$

where $\mathbf{J}$ is the flux of tumour cells and $f(u)$ is the net production or loss term. At this early stage of growth, we assume the flux is simply given by

$$\mathbf{J} = -D\nabla u = -D\frac{\partial u}{\partial r}\mathbf{e}_r,$$

where $\mathbf{e}_r$ is the outward unit normal in the radial direction and D is the constant diffusion coefficient. $f(u)$ will contain terms describing the proliferation of the tumour cells and the reaction of the immune system to the tumour. We assume logistic type growth and hence our model equation, in spherical polar coordinates, is

$$\frac{\partial u}{\partial t} = \frac{D}{r^2}\frac{\partial}{\partial r}\left(r^2\frac{\partial u}{\partial r}\right) + su(1-\frac{u}{\kappa}) + S(u), \tag{2.1.1}$$

where $S(u)$ is a function describing the reaction of the immune system to the tumour (to be defined later), s is the mitotic growth rate and κ is the carrying capacity of the environment. To close the system, we impose the following boundary and initial conditions:

$$r \in [0,L], \quad \frac{\partial u}{\partial r}(0,t) = u(L,t) = 0, \quad u(r,0) = u_0(r), \tag{2.1.2}$$

where $u_0(r)$ is a sufficiently smooth monotonic decreasing function which models a tumour that has not developed a necrotic core at this stage. The boundary condition at $r = 0$ arises naturally from the geometry and symmetry assumption of the system. In Adam, (1993), the reference length L represented the typical organ size. The boundary condition, $u(L,t) = 0$, is biologically incorrect for this interpretation of L, as it implies that the *boundary of the organ* is hostile to the tumour such that no tumour cells can survive at the periphery. Tumours may sometimes be contained within an organ whenever adjacent anatomical structures are impermeable or resistant to compression (for example, cartilage), in which case a zero flux boundary condition is more appropriate. However, it is well known that, during the avascular stage, the growth of the tumour is self-limiting because the nutrient supply is not sufficient to support continued growth of the tumour [Paweletz & Knierim, (1989)]. Hence, we take L to be the maximum avascular tumour size where there is an equilibrium at the boundary between tumour proliferation and ischaemic death, i.e. $u(L,t) = 0$. An avascular tumour can become dormant when it is a few millimetres in diameter (L =O(mm)) though the critical size will depend upon the distance of the tumour from the nearest nutrient supply.

We will now derive the function $S(u)$ from first principles. Let E_0 denote free effector cells, U tumour cells, E effector cell-tumour cell complex and P dead tumour cells. The cell-mediated immune reaction is governed by two processes;

1. the binding of a tumour cell with an effector cell to form a complex, and

2. the cytotoxic action of the effector cell which induces lysis in the tumour cell.

Schematically, these processes can be represented as follows;

$$(1)\quad E_0 + U \underset{k_{-1}}{\overset{k_1}{\rightleftharpoons}} E, \qquad (2)\quad E \overset{k_2}{\rightharpoonup} E_0 + P. \tag{2.1.3}$$

Note that here, process (1) is reversible since the effector cells can sometimes release the tumour cells without killing them (cf. Adam, (1993) where it is assumed that the formation of a tumour cell-effector cell complex always results in a kill). Furthermore, the binding rate k_1 will depend upon the effector cells' ability to recognise the tumour cells as abnormal. Using the Law of Mass Action, which states that when two or more

reactants are involved in a reaction step, the rate of reaction is proportional to the product of their densities, we obtain the following system of ODEs:

$$\frac{d[U]}{dt} = -k_1[E_0][U] + k_{-1}[E], \tag{2.1.4}$$

$$\frac{d[E_0]}{dt} = -k_1[E_0][U] + k_{-1}[E] + k_2[E], \tag{2.1.5}$$

$$\frac{d[E]}{dt} = k_1[E_0][U] - k_{-1}[E] - k_2[E], \tag{2.1.6}$$

$$\frac{d[P]}{dt} = k_2[E], \tag{2.1.7}$$

where [ ] denotes the density per unit volume and k_{-1}, k_1, k_2 are proportionality constants. We can uncouple equation (2.1.7) from the rest of the system since P does not appear in the other equations. Note that

$$\frac{d[E_0]}{dt} + \frac{d[E]}{dt} = 0 \Rightarrow [E_0] + [E] = E_T, \ E_T \text{ a constant.}$$

This comes from the assumption that no effector cells are lost during this process. Hence, we have

$$\frac{d[U]}{dt} = -k_1 E_T[U] + (k_1[U] + k_{-1})[E]. \tag{2.1.8}$$

If we assume that lysis occurs much faster than the other processes [Adam, (1993)], [Lefever & Horsthemke, (1979)], [Prigogine & Lefever, (1980)], then the quasi-steady state assumption is $[\dot{E}] = 0$. Using this to eliminate E from equation (2.1.8), we obtain

$$\frac{d[U]}{dt} = \frac{-k_1 k_2 E_T[U]}{(k_{-1} + k_2 + k_1[U])}.$$

Let $A = k_2 E_T$, which is the maximum working rate, (i.e. all effector cells working at rate k_2) and $B = \dfrac{k_{-1} + k_2}{k_1}$, which is the ratio between the rate at which the effector cells become free and the rate of binding. Then

$$S(u) = -\frac{Au}{B + u}.$$

This term is qualitatively the same as in Adam, (1993) but is interpreted differently. Note that a large value of the parameter A indicates that the effector cells are more effective in killing the tumour cells and if B is small (k_1 large), then the effector cells are reacting quickly to the tumour cells (i.e. they are quick to recognise the abnormality

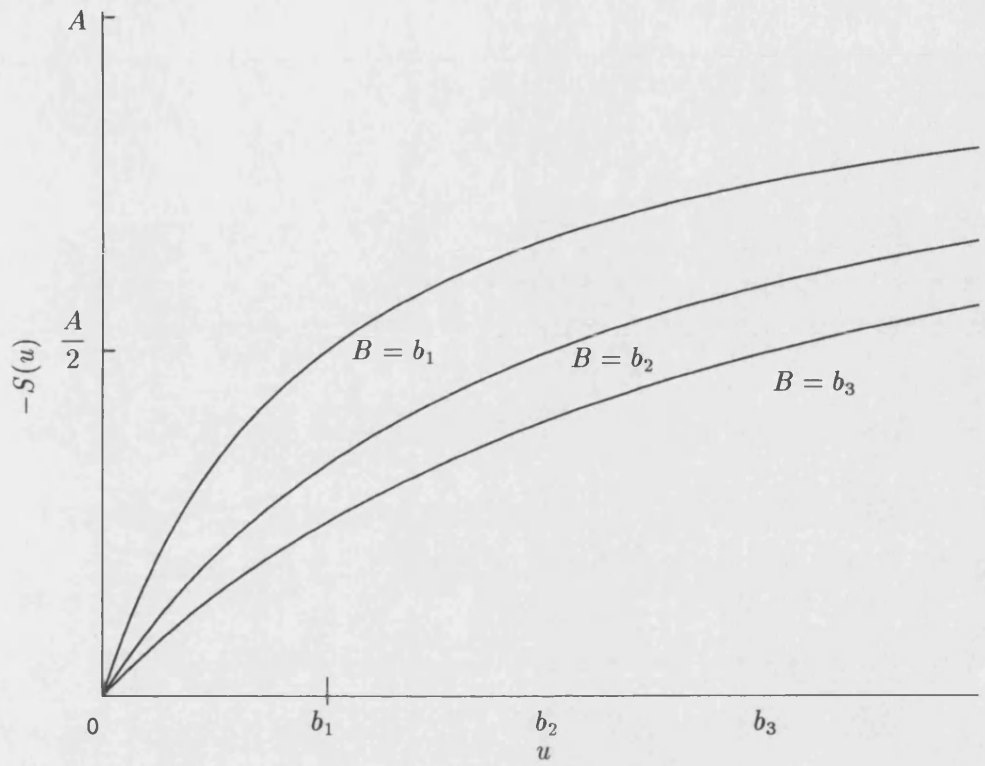

Figure 2-1: *Plot of the immune reaction term* $-S(u) = \dfrac{Au}{B+u}$ *for fixed* A *and different values of* B. *When* $u = B$, *the immune reaction is at half its maximum rate, so that the smaller the value of* B, *the quicker the effector cells are in recognising the tumour cells as abnormal. Hence* B *is a reciprocal measure of the immunogenicity of the tumour.*

and bind to the tumour cells). A tumour that produces a strong immune reaction is said to be immunogenic. Most immunogenic tumours are induced rather than spontaneous and are more common in animal models, but comparatively rare in human tumours [MacSween & Whaley, (1992)], [Prehn, (1994)]. We can interpret B as a reciprocal measure of the immunogenicity of the tumour, such that a small value of B indicates a highly immunogenic tumour. Figure (2-1) shows how the behaviour of $S(u)$ changes for different values of B.

We now introduce dimensionless parameters into the system by making the following substitutions;

$$u^* = \frac{u}{\kappa}, \quad r^* = \frac{r}{L}, \quad t^* = st, \quad d = \frac{D}{sL^2}, \quad a = \frac{A}{s\kappa}, \quad b = \frac{B}{\kappa}. \tag{2.1.9}$$

This change in parameters allows us to focus upon the model parameters relating to

the immune reaction (c.f. Adam, (1993)). Dropping the $*$'s for notational convenience, (2.1.1) and (2.1.2) become

$$\frac{\partial u}{\partial t} = \frac{d}{r^2}\frac{\partial}{\partial r}\left(r^2\frac{\partial u}{\partial r}\right) + u(1-u) - \frac{au}{b+u}, \tag{2.1.10}$$

$$r \in [0,1], \quad \frac{\partial u}{\partial r}(0,t) = u(1,t) = 0, \quad u(r,0) = u_0(r), \tag{2.1.11}$$

The spatially homogeneous steady state solutions are given by

$$f(u) = u(1-u) - \frac{au}{b+u} = 0.$$

We note that the trivial solution $u \equiv 0$ is a solution for all positive a, b. We will henceforth refer to this steady state as the cancer free state.

The non-trivial or cancerous steady state solution is given by

$$(1-u) = \frac{a}{b+u},$$

i.e. solutions of the quadratic equation

$$u^2 + (b-1)u + (a-b) = 0. \tag{2.1.12}$$

For $b > 1$, equation (2.1.12) has one positive real solution,

$$u_s = \frac{1-b}{2} + \frac{1}{2}\sqrt{(b-1)^2 - 4(a-b)}, \tag{2.1.13}$$

provided $a < b$, (see figure (2-2)). Given the non-dimensionalization (2.1.9), $b > 1$ implies that the effector cells are working at half their maximum rate when u is at the carrying capacity of the environment. Hence, the effector cells have difficultly in recognising the tumour cells as abnormal even if the population is large (a non-immunogenic tumour).

For $b < 1$, if $a \in (b, a_c)$ where $a_c = \dfrac{(1+b)^2}{4}$, there are two non-trivial real solutions of (2.1.12). For $a < b$, we have one solution of (2.1.12) and for $a > a_c$, there are no real solutions. Note that, the larger the value of a, the more efficient the effector cells are in inducing lysis in the tumour cells. A summary of the different solutions of (2.1.12)

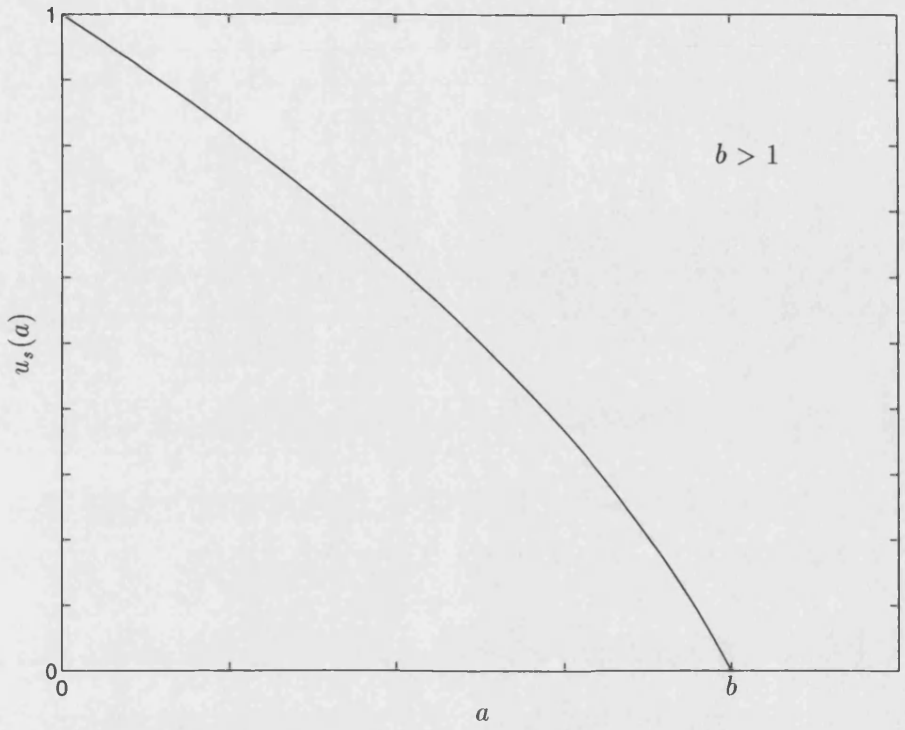

Figure 2-2: *When $b > 1$ (i.e. the tumour cell population needs to be large in order to provoke an effective response by the effector cells) and $a < b$, equation (2.1.12) has one positive real solution. These parameter values represent a weakly immunogenic tumour.*

for $b < 1$ is shown in figure (2-3).

Now consider the general problem,

$$\frac{\partial u}{\partial t} = \frac{d}{r^2}\frac{\partial}{\partial r}\left(r^2\frac{\partial u}{\partial r}\right) + f(u), \tag{2.1.14}$$

$$r \in [0,1], \quad \frac{\partial u}{\partial r}(0,t) = u(1,t) = 0, \quad u(r,0) = u_0(r), \tag{2.1.15}$$

possessing the trivial steady state solution $u^* = 0$. Linearising about this trivial steady state, we obtain the system

$$\frac{\partial u}{\partial t} = \frac{d}{r^2}\frac{\partial}{\partial r}\left(r^2\frac{\partial u}{\partial r}\right) + f'(0)u, \tag{2.1.16}$$

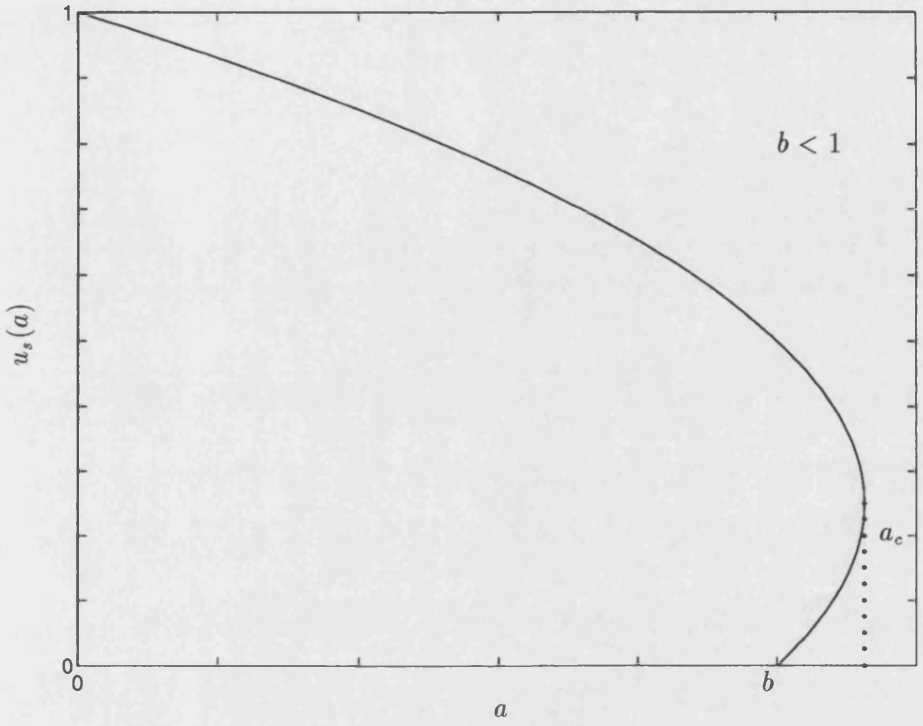

Figure 2-3: *When $b < 1$ (i.e. the effector cells respond at low tumour cell populations), equation (2.1.12) has one positive real solution when $a < b$ and two positive real solution for $a \in (b, a_c)$, where $a_c = \dfrac{(1+b)^2}{4}$.*

$$r \in [0,1], \quad \frac{\partial u}{\partial r}(0,t) = u(1,t) = 0, \quad u(r,0) = u_0(r). \tag{2.1.17}$$

The spatially-dependent steady states of the linear problem are given implicitly by setting $\dfrac{\partial u}{\partial t} = 0$ in (2.1.16) and the spatially-dependent steady state solutions are linear combinations of the eigenfunctions $\frac{1}{r}\sin(n\pi r), \quad n = 1, 2, 3, ...$ which also satisfy the boundary conditions. The general solution is of the form

$$u(r,t) = \sum_n a_n \exp(\lambda_n t) \frac{\sin(n\pi r)}{r}$$

where a_n can be determined by Fourier series expansion. Substituting this into equation

(2.1.16), we find that the λ_n are given by

$$\lambda_n = f'(u^*) - d(n\pi)^2.$$

The dominant mode and largest λ_n is given by $n = 1$. So $u^* = 0$ is stable provided $\lambda_1 < 0$, i.e.

$$d_c = \frac{f'(0)}{\pi^2} < d.$$

Now consider $f(u) = u(1-u) - \dfrac{au}{b+u}$ with a, b such that $f(u) = 0$ has one positive solution u_s, i.e. $b > a$. Then $f'(0) > 0$ and the cancer free state is unstable provided

$$d < d_c = \frac{b-a}{a\pi^2}.$$

Recall that, $d = \dfrac{D}{sL^2}$. Hence there is a critical domain size

$$L_c = \pi\sqrt{\frac{Da}{s(b-a)}},$$

such that when $L > L_c$ the cancer free state is unstable and hence the system evolves to a non homogeneous cancerous state. (Note that, if the domain size was fixed, then the cancer free state would be destabilised by a decrease in the diffusion coefficient below the critical level $D_c = sL^2 d_c$ or by a decrease in the tumour cell doubling time such that $s > s_c = D/d_c L^2$).

Now consider $f(u) = u(1-u) - \dfrac{au}{b+u}$ with a, b such that $f(u) = 0$ has two positive solutions,

$$u_{1,2} = \frac{1-b}{2} \mp \frac{1}{2}\sqrt{(1+b)^2 - 4a},$$

i.e. $b < 1$ and $a \in (b, a_c)$. Thus, $f'(0) < 0$, $f'(u_1) > 0$, $f'(u_2) < 0$. From the linear analysis, we see the spatially homogeneous steady states $u \equiv 0$ and u_2 are stable provided $b < 1$ and $a \in (b, a_c)$. Hence, we have bistability in the parameter region $a \in (b, a_c)$. Bistability has been observed in other models of tumour immunity [Adam, (1993)], [Lefever & Horsthemke, (1979)] and other ecological systems such as the spruce budworm models of [Ben-Yu *et al.*, (1986)], [Ben-Yu *et al.*, (1991)] and [Ludwig *et al.*, (1978)]. We can draw a further analogy between tumour cell-effector cell interaction models and predator prey models. In the spruce budworm models cited above, a critical

domain size L_c, could be obtained, such that a domain of size $L > L_c$ would support an outbreak of the insect population and for $L < L_c$ the budworm population was eradicated. Lefever & Horsthemke, (1979) highlighted the importance of fluctuating environmental factors in the growth or extinction of populations. In the next section, we will identify the factors important for a tumour 'outbreak'.

2.2 Numerical simulations

We solved equation (2.1.10) with boundary conditions (2.1.11) using a parabolic PDE solver available from the NAG library which integrates using the method of lines and Gear's method.

Note on numerical method

The method of lines approximates a system of partial differential equations with a system of time dependent ordinary differential equations by replacing the spatial derivatives with finite differences.

Suppose we have $NPDE$ PDE's. Discretise the space interval into $J+1$ mesh points, for example [0,1] can be discretised as follows;

$$\mathbf{x} = (x_0, x_1, ..., x_J), \quad x_j = j\Delta x, \quad j = 0, 1, .., J, \quad \Delta x = \frac{1}{J}.$$

Then replace the spatial derivatives with finite differences (e.g. three point differences) to obtain $(J+1) \times (NPDE)$ coupled ODEs.

Now consider the heat equation

$$\frac{\partial u}{\partial t} = \frac{\partial^2 u}{\partial x^2}.$$

Using the method of lines, we obtain the ODE system

$$\frac{\partial \mathbf{u}}{\partial t} = A\mathbf{u},$$

where

$$A = \frac{1}{(\Delta x)^2}\begin{bmatrix} -2 & 1 & 0 & 0 & .. & 0 \\ 1 & -2 & 1 & 0 & .. & 0 \\ 0 & 1 & -2 & 1 & .. & 0 \\ .. & .. & .. & .. & .. & .. \\ .. & .. & .. & .. & .. & .. \\ 0 & .. & 0 & 0 & 1 & -2 \end{bmatrix}, \qquad \mathbf{u} = (u_0, u_1, u_2, ..., u_J)^T,$$

It can be shown that A has eigenvalues between 0 and $\frac{-4}{(\Delta x)^2} \to -\infty$, as $\Delta x \to 0$ (stiffness). If the ODE system is solved using Euler's method (forward difference in time), we have

$$\frac{\mathbf{u}^{n+1} - \mathbf{u}^n}{\Delta t} = A\mathbf{u}^n, \qquad t = n\Delta t,$$

with the stability condition

$$\Delta t < \frac{(\Delta x)^2}{2},$$

where $\mathbf{u}^n$ is the vector $\mathbf{u}$ evaluated at the nth time step. Thus, by trying to increase the accuracy of the solution, i.e. by refining the mesh, we require a very small time step in order to maintain stability. If, however the ODE system is solved using backward Euler, for example, i.e.

$$\mathbf{u}^{n+1} - \Delta t A\mathbf{u}^{n+1} = \mathbf{u}^n,$$

then stability is unconditional. Hence, when using the method of lines to approximate a reaction-diffusion system, it is advisable to use an implicit method (e.g. Gear's method) to solve the ODE system, in order to avoid problems with stability.

In all simulations, we took the initial conditions to be

$$u_0(r) = \begin{cases} \dfrac{\exp(-r^2) - \exp(-0.01)}{1 - \exp(-0.01)}, & \text{for } 0 \le r < 0.1, \\ 0, & \text{otherwise,} \end{cases}$$

and fixed D and s such that the maximum avascular size, L, is determined by our choice of d. We estimated D to be in the range $10^{-9} - 10^{-10}\text{cm}^2\text{s}^{-1}$ [Chaplain & Stuart, (1993)], [Sherratt & Murray, (1990)], [Stokes *et al.*, (1991)] and s to be in the range $0.04 - 0.056\text{h}^{-1}$ [Sherratt & Murray, (1990)], [Stokes & Lauffenburger, (1991)], such that

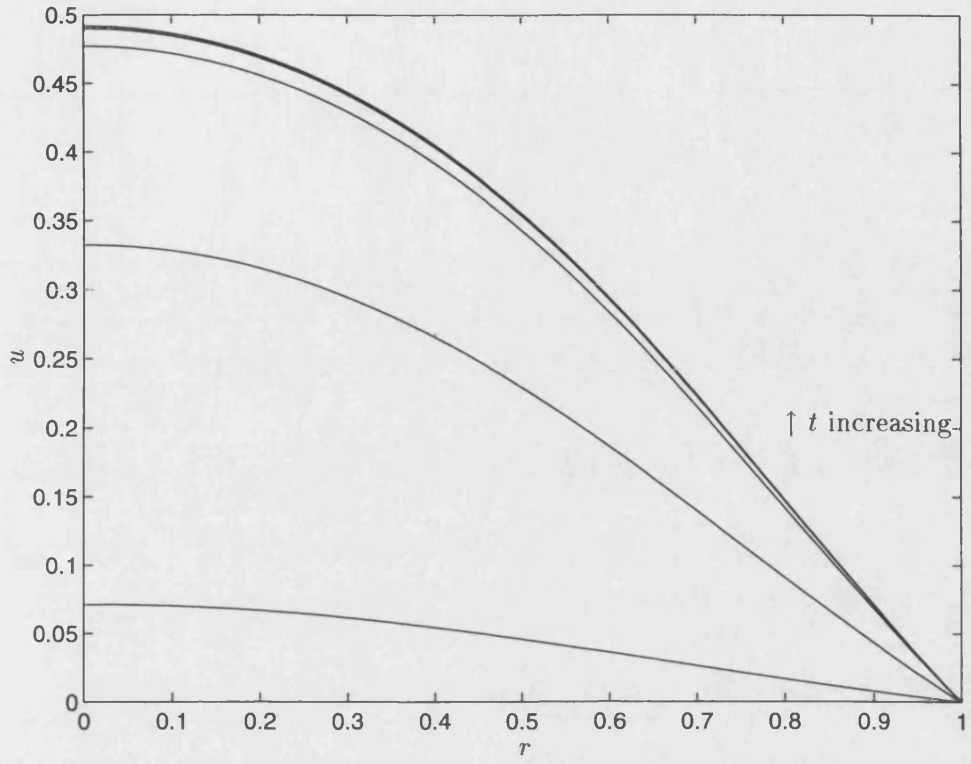

Figure 2-4: *Numerical solution of (2.1.10) with* $a = 0.5$, $b = 1.5$ *and* $d = 0.04$ *(with* $D/s = 10^{-4}cm^2$*) such that* $L > L_c$. *Linear analysis predicts that the cancer free state is unstable, so that the system evolves to an inhomogeneous (cancerous) steady state. Plots taken at time* $t = 10 - 50$. *The equilibrium state, which is 5mm in radius, is reached in about 52 days.*

in each simulation we took $\frac{D}{s} = 10^{-4}\text{cm}^2$.

We ran the simulations with different values of a and b to see whether the persistence or rejection of the tumour was dependent upon the immune reaction rates as well as the size of the domain. First, we considered values of a, b as in figure (2-2), i.e. $b > 1$ and $a < b$. The scenario here is that the effector cells are not very successful in identifying the tumour cells as abnormal, i.e. we have a tumour with a low immunogenicity. With $a = 0.5$ and $b = 1.5$, the critical domain size is $L_c = 0.0385$cm. Choosing $d = 0.04$, we have $L_c < L = 0.05$cm and hence the linear analysis predicts that the cancer free state is unstable. The numerical solution of the equation (2.1.10) for these parameters shows that the system evolves to a cancerous state (figure (2-4)). Hence, the immune response was insufficient to contain the tumour. Using the non-dimensionalization (2.1.9), the

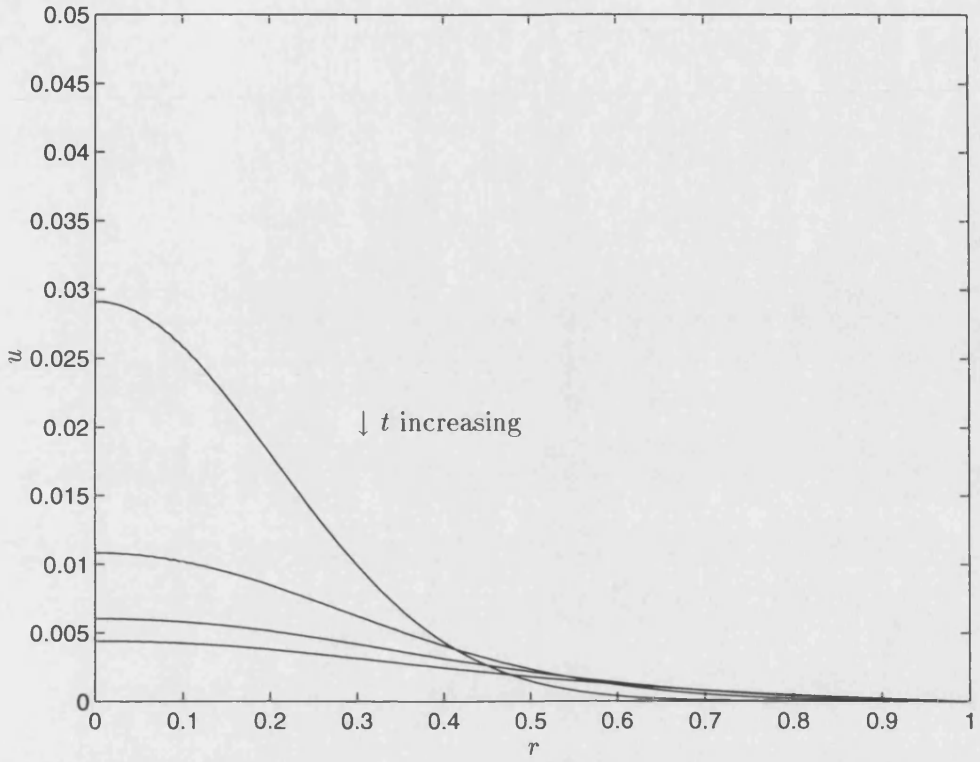

Figure 2-5: *Numerical solution of (2.1.10) with* $a = 0.5$, $b = 1.5$ *and* $d = 1$ *(with* $D/s = 10^{-4}cm^2$*) such that* $L < L_c$. *Linear analysis predicts that the cancer free state is stable and hence the tumour regresses within a couple of hours under the influence of the host defence system. Plots taken at time* $t = 0.02 - 0.08$.

tumour reaches an equilibrium state of 5mm in radius in about 52 days. However, if we choose $d = 1$, then we have $L_c > L = 0.01$cm. In this case, the linear analysis predicts the cancer free state to be stable. Figure (2-5) shows that, by reducing the size of the domain in this way, (i.e. by reducing the maximum potential tumour equilibrium size), the effector cells are able to eradicate the tumour. In dimensional terms, the immune reaction takes a few hours.

Next, we ran the simulations with parameters a and b as in figure (2-3) but with $a < b$, i.e. there is one positive solution to equation (2.1.12). In this case, the effector cells react and bind quickly to the tumour cells but the maximum working rate is quite low. With $a = 0.25$ and $b = 0.5$, the critical domain size is $L_c = 0.0444$cm. Choosing $d = 0.02$, we have $L_c < L = 0.07$cm. Again, the cancer free steady state is predicted to be unstable and figure (2-6) shows that the tumour evolves to a cancerous steady state despite the intervention of the effector cells. Using the non-dimensionalization (2.1.9),

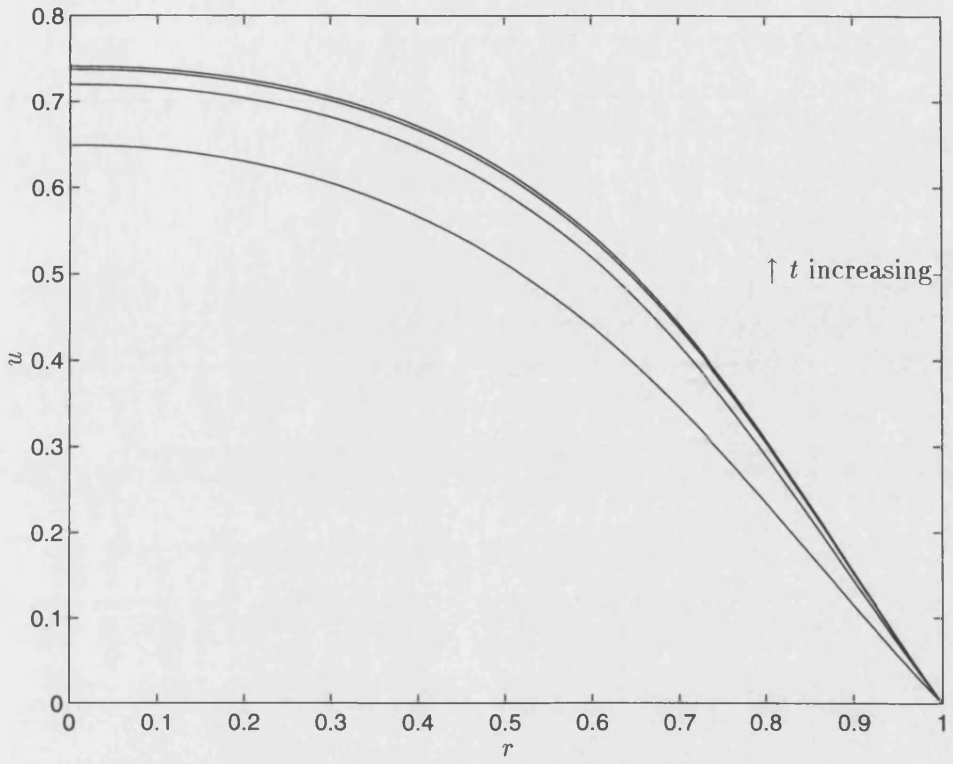

Figure 2-6: *Numerical solution of (2.1.10) with* $a = 0.25$, $b = 0.5$ *and* $d = 0.02$ *(with* $D/s = 10^{-4}cm^2$*) such that* $L > L_c$. *Linear analysis predicts that the cancer free state is unstable. The immune reaction is not sufficient to eradicate the tumour and so the growth persists. Plots taken at time* $t = 20 - 32$. *An equilibrium size of 7mm is reached within 33 days.*

the tumour reaches a size of 7mm in radius in about 33 days. Taking $d = 1$, we obtain $L_c > L = 0.01$cm so that the cancer free state is expected to be stable. The numerical solution of the system with these parameters shows that the tumour is eliminated within a few hours by the immune response (see figure (2-7)).

Finally, we choose parameters a and b to be as in figure (2-3), but with $a \in (b, a_c)$, $a_c = \dfrac{(1+b)^2}{4}$. In this case, the effector cells quickly interact with the tumour cells and induce lysis at an effective rate. This is the best case scenario. Linear analysis predicts that the system has multiple spatially homogeneous steady states such that the cancer free state and the cancerous state u_2 are both stable, with an intermediate unstable state u_1. Taking $a = 0.53$ and $b = 0.5$ and solving (2.1.10) with $d = 0.02$ such that $L = 0.07$cm, we obtain the solution as shown in figure (2-8). Here, the immune response is successful in removing the tumour. If however we increase L further, i.e. reduce d

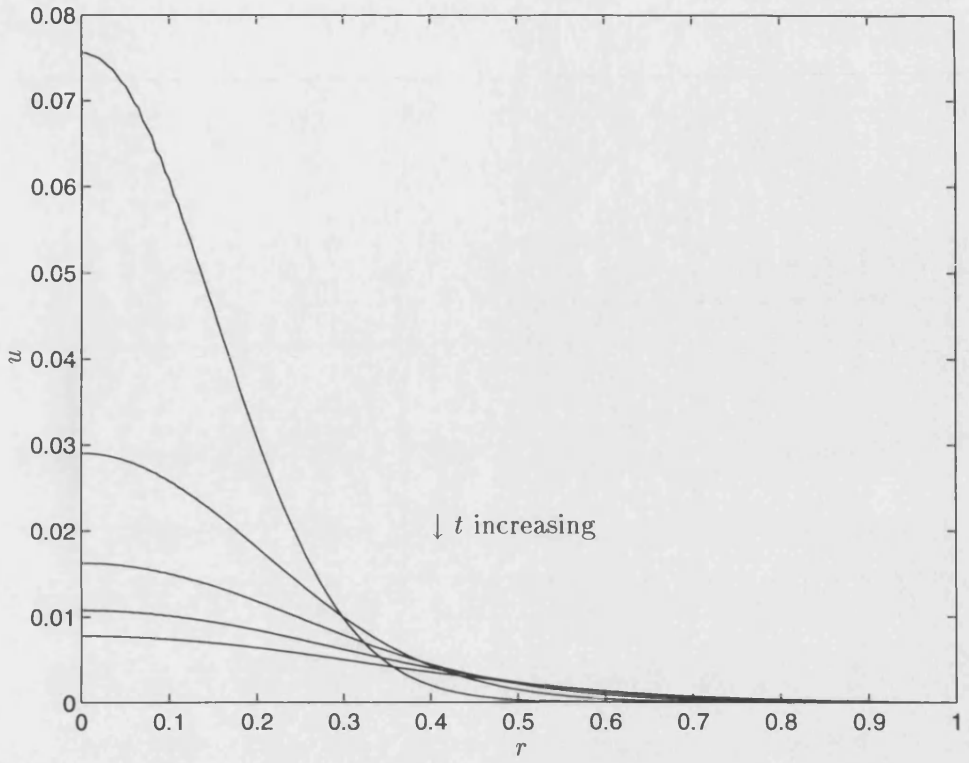

Figure 2-7: *Numerical solution of (2.1.10) with* $a = 0.25$, $b = 0.5$ *and* $d = 1$ *(with* $D/s = 10^{-4}cm^2$*) such that* $L < L_c$. *Linear analysis predicts that the cancer free state is stable and hence the tumour is removed by the immune system. Plots taken at time* $t = 0.01 - 0.05$. *The immune reaction takes just a few hours.*

such that $d = 10^{-4}$, $L = 1$, then the system evolves to a cancerous state as seen in figure (2-9). So despite the increased efficiency of the immune reaction, there is still the risk of a tumour outbreak if the size of the domain is sufficiently large to sustain the tumour outbreak.

Comparing the numerical simulations where there is bistability with the case where there is only one spatially homogeneous stable state, we notice several differences. The steady state solution obtained in figure (2-9), is more compact than the other cancerous states obtained in figures (2-4) and (2-6), and the nascent tumour has not reached its maximum avascular size (i.e. it has not reached the right-hand boundary). Furthermore, the time scales on which the tumour regresses (or grows to equilibrium) are different. In the bistability case, the tumour has reached an equilibrium of 1-2mm in radius in about 50 hours, whereas in the other cases where there is a tumour outbreak, the tumours take one or two months to reach 5-7mm in radius. Additionally, in the simulation shown

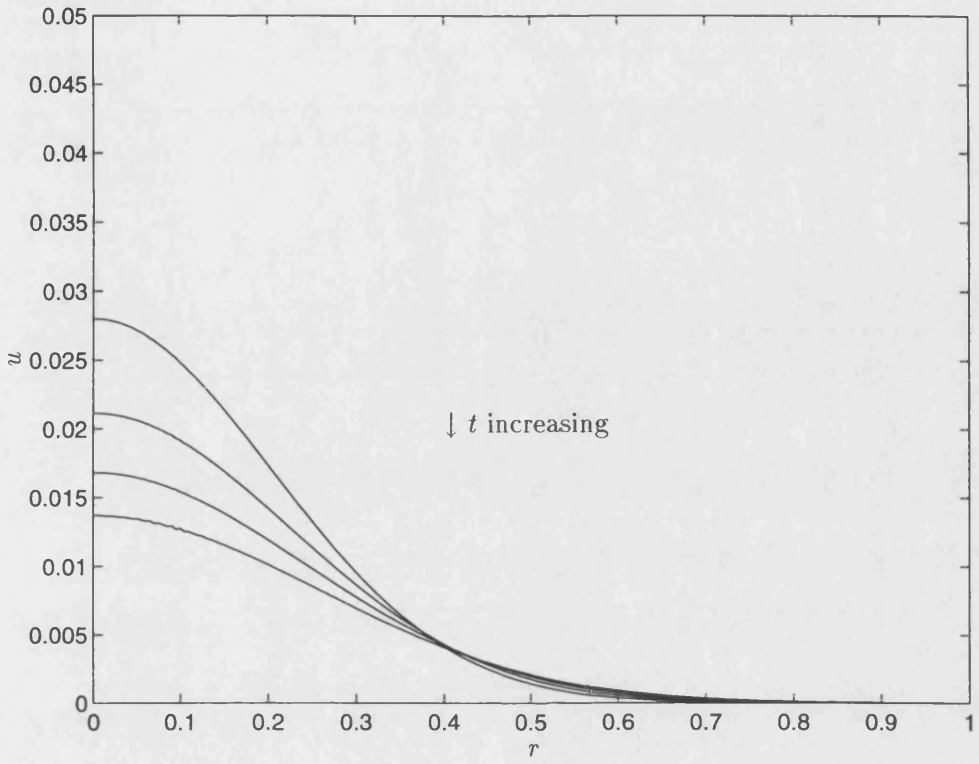

Figure 2-8: *Numerical solution of (2.1.10) with* $a = 0.53$, $b = 0.5$ *and* $d = 0.02$ *(with* $D/s = 10^{-4}\text{cm}^2$*). Linear analysis predicts that the (spatially homogeneous) cancer free state and the cancerous state* u_2 *are both stable. In this case, the system evolves to the cancer free state within 1 or 2 days. Plots taken at time* $t = 1.2 - 1.6$.

in figure (2-8), the immune reaction takes days to eliminate the tumour, compared to a few hours in the other simulations. This difference could be due to the two competing effects, i.e. the domain size is large enough to support a tumour outgrowth but the immune reaction is also sufficient to eradicate the tumour.

2.3 Discussion

The numerical simulations given here indicate that the growth of a tumour during the early stages of development is dependent upon a number of important factors. Of primary importance is the maximum avascular size of tumour (L) that can be supported by the environment. Any change in the supply of nutrients into the neighbourhood of the tumour can change this maximal size and can make the difference between whether the tumour grows to its avascular equilibrium or whether it is eradicated by the effector

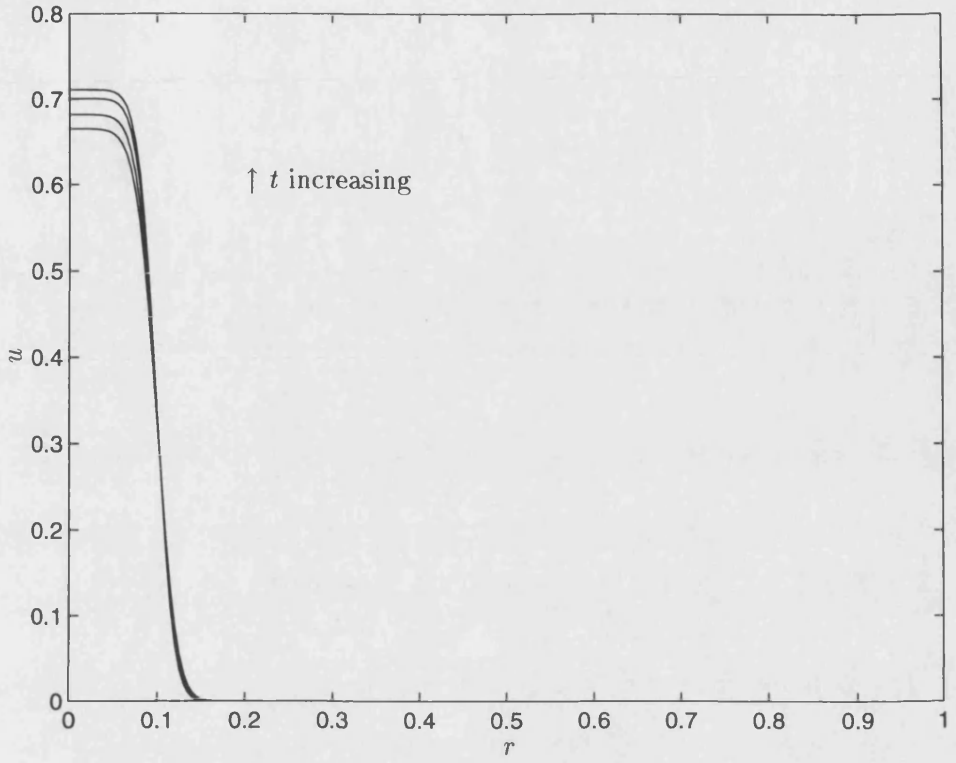

Figure 2-9: *Numerical solution of (2.1.10) with* $a = 0.53$, $b = 0.5$ *and* $d = 10^{-4}$ *(with* $D/s = 10^{-4}\text{cm}^2$*) such that* $L > L_C$. *Linear analysis predicts that the (spatially homogeneous) cancer free state and the cancerous state* u_2 *are both stable. In this case, the system evolves to a cancerous state. Note that the tumour is more compact which is indicative of a less malignant tumour or that the immune system has contained the tumour more efficiently. Plots taken at time* $t = 1.4 - 2$. *The tumour has taken 50 hours to establish an equilibrium size of about 1-2mm in radius.*

cells. Equivalently, a change in the motility or proliferation rate of the tumour can also affect whether or not a tumour persists or dies. These factors can change as the tumour grows and becomes increasingly malignant. Furthermore, the host's defence system must react quickly and effectively if the tumour is to be contained. This involves recognising the abnormality in the neoplastic tissue and successfully inducing lysis in the tumour cells. In experimental animal models, tumours induced by the use of carcinogenic agents are highly immunogenic and produce an immune response when transplanted into another host. Furthermore, the host will be protected from any subsequent challenge with the same tumour type [Prehn, (1994)], [Ruddon, (1987)]. On the other hand, tumours arising spontaneously in animals appear to be non-immunogenic

and do not immunise syngenic hosts. Whilst it is difficult to extrapolate the results obtained from transplanted tumours to spontaneous human cancers, there is some evidence that virally induced tumours can be used to vaccinate against some tumour growths (for example, individuals infected with Epstein-Barr virus do not get lymphoma [Ruddon, (1987)]). However, the immune system may fail to modulate the growth of many untransplanted tumours. This may be because spontaneously arising tumours are initially slow growing, so that only a very small quantity of antigen is produced [Prehn, (1994)] or evolve in such a way as to avoid the host's immune response [Ruddon, (1987)]. Nevertheless, advances are being made in the development of cancer 'vaccines' [Lineham *et al.*, (1996)].

We also note that, the maximum avascular size of the tumour in this model varies between 1-7mm, which is in good agreement with experimental observations [Gimbrone *et al.*, (1974)], [Paweletz & Knierim, (1989)]. Such a small tumour could persist undetected for many months or even years before passing on to the next stage of growth.

Chapter 3

Capillary sprout formation and secondary branching in tumour angiogenesis

Angiogenesis is a precursor to a more malignant phase of tumour growth, wherein the tumour cells are aggressively invading the surrounding tissue. The result of angiogenesis is the rapid, uncontrolled growth of the tumour and an increased risk of the disease spreading via the blood system. In this chapter, we look at the early stages of the angiogenic process, namely, the formation of capillary buds and secondary branches. In particular, we focus upon the potential role that haptotaxis, i.e motion directed by gradients of adhesion, may play in the early stages of angiogenesis.

Initially the EC are uniformly distributed along the walls of the parent vessel (e.g limbus). The release of diffusible substances from the tumour triggers an angiogenic response in the EC. The EC become mobile and form clusters of cells which are the beginning of the capillary buds. These buds will eventually sprout and will form the primary capillary vessels in the tumour's vascular system. There is clear experimental evidence that the mechanism by which the cells move involves haptotaxis, i.e. the cells move up an adhesive gradient, especially in the early stages. Studies have shown that compounds such as fibronectin are secreted by the EC during the angiogenic process [Clark *et al.*, (1982)a], [Paweletz & Knierim, (1989)] and it is known that fibronectin increases cell to cell and cell to matrix adhesiveness [Clark *et al.*, (1982)b] , [Yamada & Olden, (1978)] . It can be reasonably supposed therefore, that fibronectin aids angio-

genesis by directing migration [Clark *et al.*, (1982)a], [Clark *et al.*, (1982)b], [Paweletz & Knierim, (1989)], [Ungari *et al.*, (1985)] . Chemotaxis is also certainly involved in angiogenesis [Chaplain & Stuart, (1993)], but in this chapter, we will focus our attention on the potential role of haptotaxis.

The TAF which diffuse from the tumour create a chemical gradient. In this model, we assume that initially the EC secrete fibronectin in response to the TAF and hence move up an adhesive gradient of their own creation. Carter, (1965) suggested that a chemotactic substance may act indirectly by altering the surface of a cell and so increasing its adhesiveness. Fibronectin can bind to cell membranes by means of a specific fibronectin receptor thereby anchoring the cell to the ECM [Ruddon, (1987)]. An adhesive gradient will be created since the surface nearest the chemical stimulus will be altered.

In the following section we develop a mathematical model for the initial formation of capillary sprouts, i.e. the budding process mentioned previously, and present the results of numerical simulations. In the second half of this chapter, the modelling of the branching process is considered and numerical simulations are presented.

3.1 A mathematical model of initial bud formation

We initially focus on the early stages of angiogenesis and consider the EC within the parent vessel, e.g. the limbus. Let $n(\mathbf{x},t)$ be the endothelial cell density per unit area and $c(\mathbf{x},t)$ the concentration of fibronectin. We assume that there are only two contributions to cell flux at this early stage of the angiogenic process—random motion and haptotaxis. Thus the total cell flux $\mathbf{J}_n$ is given by

$$\mathbf{J}_n = \mathbf{J}_{\text{diffusion}} + \mathbf{J}_{\text{haptotaxis}},$$

where $\mathbf{J}_{\text{diffusion}} = -d_n(n)\nabla n$ and $\mathbf{J}_{\text{haptotaxis}} = a(c)n\nabla c$, and where d_n, a are the diffusion and haptotaxis coefficients respectively. For simplicity we will assume that these are both constant. If N is the measure of the total number of cells per unit area and rN is the linear mitotic growth rate, then the net cell production can be modelled using a logistic-type growth rate and is given by $rn(N-n)$.

We assume that the fibronectin is simply secreted by the EC and diffuses locally

into the surrounding area. The flux of the chemical fibronectin is given by $\mathbf{J}_c = -d_c \nabla c$, where d_c is the diffusion coefficient of the chemical, again assumed to be constant. It is assumed that the production of fibronectin by the cells is given by the Michaelis-Menten production term $\frac{Sn}{(\beta + n)}$ and that the decay term is $-\gamma c$, where S, β, γ are positive constants.

Angiogenic activity is confined to a small localised region of the parent vessel wall nearest the tumour [Paweletz & Knierim, (1989)] . Initially, the vessel wall simply consists of a monolayer of EC. After the release of the TAF, some of the EC loosen their contacts with their neighbours and try to penetrate the basement membrane. Subsequently several EC follow the primary EC and pile up behind each other, creating a bulge in the wall of the capillary. Hence we need only consider the model in one spatial dimension in order to focus attention on clusters of cells rather than the overall shape of the buds. We assume that a region of increased cell density indicates the initiation of a cell cluster leading to a capillary bud. Figure (3-1) is a schematic representation of the capillary budding and branching processes.

Conservation of mass gives us

$$n_t + \nabla . \mathbf{J}_n = f(n, c),$$

$$c_t + \nabla . \mathbf{J}_c = g(n, c),$$

where f, g contain the appropriate source and sink terms as detailed in the previous paragraphs. Hence the system of equations in one spatial dimension is

$$n_t = \underbrace{d_n n_{xx}}_{diffusion} - \underbrace{a(nc_x)_x}_{haptotaxis} + \underbrace{rn(N-n)}_{mitosis}, \tag{3.1.1}$$

$$c_t = \underbrace{d_c c_{xx}}_{diffusion} + \underbrace{\frac{Sn}{(\beta + n)}}_{production} - \underbrace{\gamma c}_{decay} . \tag{3.1.2}$$

During angiogenesis, EC in the parent vessel actively move towards the tumour [Ausprunk & Folkman, (1977)]. Experimental evidence [Muthukkaruppan *et al.*, (1982)] clearly shows that only a finite region of the parent vessel is involved in producing buds and hence we will take our spatial domain D to be finite. Given this geometry it is not unreasonable to treat the system as closed and impose zero flux boundary conditions

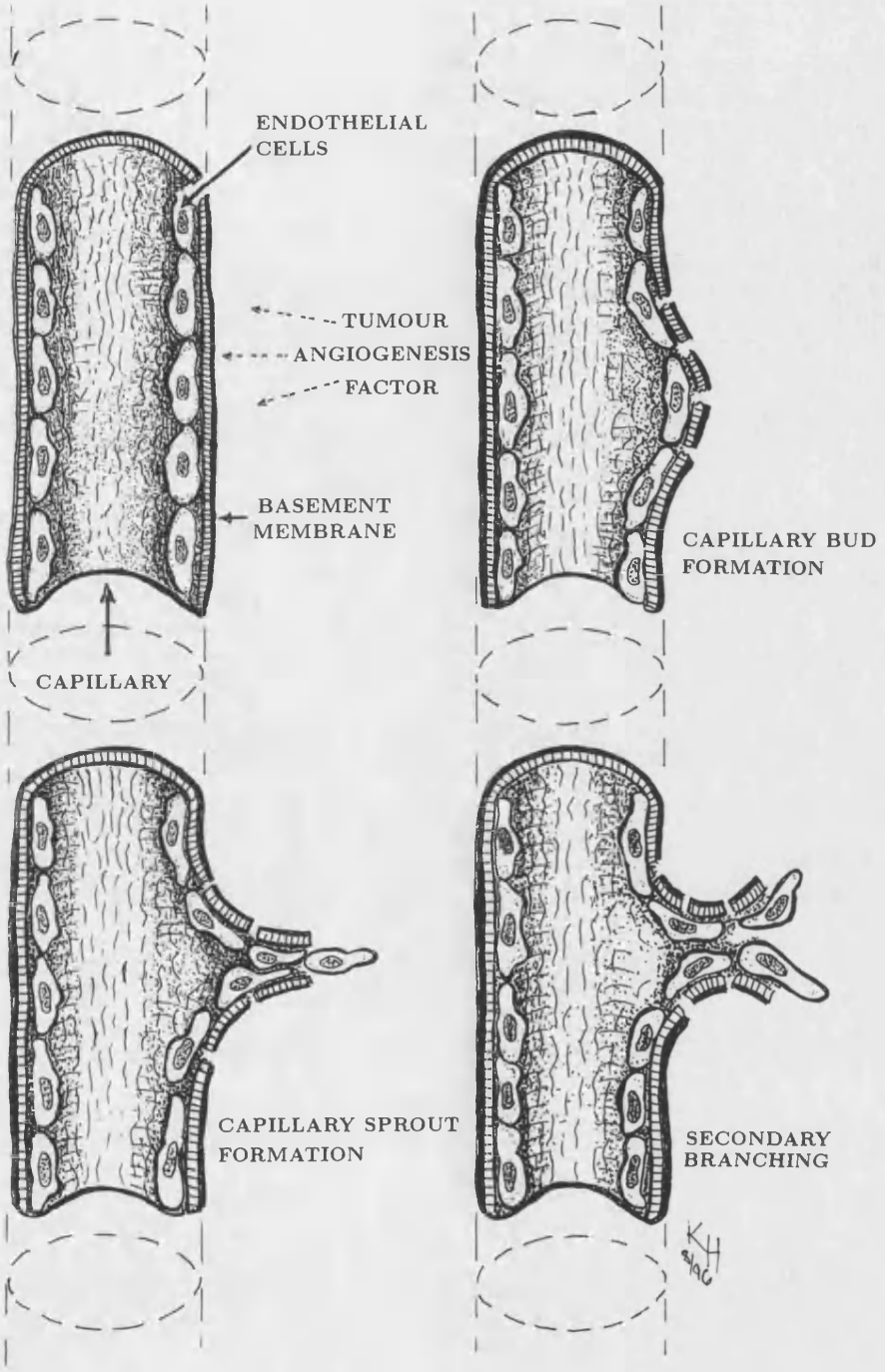

Figure 3-1: *A schematic diagram showing the initiation of a capillary bud, the formation of a capillary sprout and the growth of a secondary branch.*

as follows:

$$d_n n_x - anc_x = 0\ ,\ c_x = 0 \ \text{ on } x \in \partial D,$$

$$\text{i.e. } n_x = c_x = 0 \text{ on } x \in \partial D.$$

We introduce dimensionless variables into the model in the following manner:

$$x^* = \left[\frac{\gamma}{d_c s}\right]^{\frac{1}{2}} x,\ t^* = \frac{\gamma t}{s},\ n^* = \frac{n}{\beta},\ c^* = \frac{\gamma c}{S},$$

$$N^* = \frac{N}{\beta},\ d^* = \frac{d_n}{d_c},\ a^* = \frac{aS}{\gamma d_c},\ r^* = \frac{r\beta}{\gamma},$$

where s is a scale factor with reference to the size of the domain [Myerscough & Murray, (1992)]. After non-dimensionalizing and dropping the asterisks for notational convenience, the equations become

$$n_t = dn_{xx} - a(nc_x)_x + srn(N-n), \tag{3.1.3}$$

$$c_t = c_{xx} + s\left[\frac{n}{n+1} - c\right], \tag{3.1.4}$$

$$n_x = c_x = 0,\ x = 0,\ 1. \tag{3.1.5}$$

These equations model the initial response of EC to the angiogenic stimulus, i.e. the secretion of fibronectin, proliferation and clustering.

3.1.1 Linear stability analysis

The following analysis is standard, but we include it here for completeness. We now look for spatially homogeneous steady states of the above system which are easily seen to be

$$(n,c) = (0,0) \text{ and } (n,c) = (N, \frac{N}{N+1}).$$

The trivial state is not biologically relevant. We thus linearize about the non-trivial steady state in the usual manner by substituting

$$n = N + u \text{ and } c = \frac{N}{N+1} + v,$$

where $| u |, | v |$ are small, into the above equations to obtain the linearized system:

$$u_t = du_{xx} - aNv_{xx} - srNu, \tag{3.1.6}$$

$$v_t = v_{xx} + s\left[\frac{u}{(N+1)^2} - v\right]. \tag{3.1.7}$$

We look for solutions of the form $(u, v) \propto \exp(\sigma t + ikx)$, and hence we obtain the quadratic dispersion relation

$$\sigma^2 + \sigma[k^2(1+d) + s + srN] + k^2\left[d(k^2+s) + srN - \frac{saN}{(N+1)^2}\right] + s^2rN = 0. \tag{3.1.8}$$

The dispersion relation will have two roots and these will either be real or complex conjugates.

In the absence of any spatial variation, we insist that the homogeneous steady state be linearly stable, so that any instability will be diffusion driven. So by putting $k^2 = 0$ in the dispersion relation and solving for σ, we obtain

$$\sigma_1 = -rNs, \ \sigma_2 = -s.$$

Since all parameters are positive, σ_1 and $\sigma_2 \leq 0$ and so the spatially homogeneous steady state is linearly stable. We require $Re(\sigma(k^2)) > 0$, for some k, for instability and spatial heterogeneity. When $\sigma = 0$, we have

$$dk^4 + k^2\left[ds + rNs - \frac{aNs}{(N+1)^2}\right] + rns^2 = 0,$$

giving

$$k^2 = \frac{aNs - (ds + rNs)(N+1)^2}{2d(N+1)^2} \pm \frac{1}{2d}\left[\left(ds + rNs - \frac{aNs}{(N+1)^2}\right)^2 - 4drNs^2\right]^{\frac{1}{2}}. \tag{3.1.9}$$

Experimental studies have shown that there is no significant increase in the rat

of EC mitosis during the first stages of angiogenesis [Ausprunk & Folkman, (1977)]. Mitosis occurs only after the first sprouts have formed. It has been postulated that mitosis is a secondary reaction to angiogenesis resulting from abnormal permeability of the host vessels. Normal EC have a long half life and cell division is rare, occurring only when repair and remodelling of large wounds is essential [Paweletz & Knierim, (1989)]. It has also been shown that fibronectin even inhibits cell proliferation to some extent [Bowersox & Sorgente, (1982)]. We will therefore consider the case where there is no mitosis and where there is mitosis (at some low background level) separately.

No mitosis (r=0)

Consider the case where there is no mitosis i.e. $r = 0$, then the system is similar to the model as examined in Myerscough & Murray, (1992). Then from equation (3.1.9) we have the two roots

$$k^2 = \begin{cases} 0 \\ \dfrac{aNs}{d(N+1)^2} - s = k_2^2. \end{cases}$$

Hence the dispersion relation passes through the origin, which is to be expected when there is no proliferation of cells. By differentiating the dispersion relation with respect to k^2 and with $r = 0$ we obtain

$$\frac{d\sigma}{dk^2}(k^2(1+d) + s + 2\sigma) + \sigma(1+d) + 2dk^2 + ds - \frac{saN}{(N+1)^2} = 0.$$

Setting $\sigma = 0$,

$$\frac{d\sigma}{dk^2} = \frac{aNs}{(s + k^2(d+1))(N+1)^2} - \frac{ds + 2dk^2}{s + k^2(d+1)}.$$

So, $\dfrac{d\sigma}{dk^2} > 0$ at the origin provided $\dfrac{aNs}{d(N+1)^2} - s > 0$, i.e. $k_2^2 > 0$. The maximum occurs at $\dfrac{d\sigma}{dk^2} = 0$, i.e. at k_M^2 where

$$\sigma_M(1+d) + 2dk_M^2 + ds - \frac{saN}{(N+1)^2} = 0.$$

But if the maximum value is $\sigma = 0$ then $k_M^2 = 0$ as the dispersion relation passes through the origin as shown in figure (3-2). Hence $a_c = \dfrac{d(N+1)^2}{N}$ is the critical value of a. So provided $a > a_c$ we will have instability.

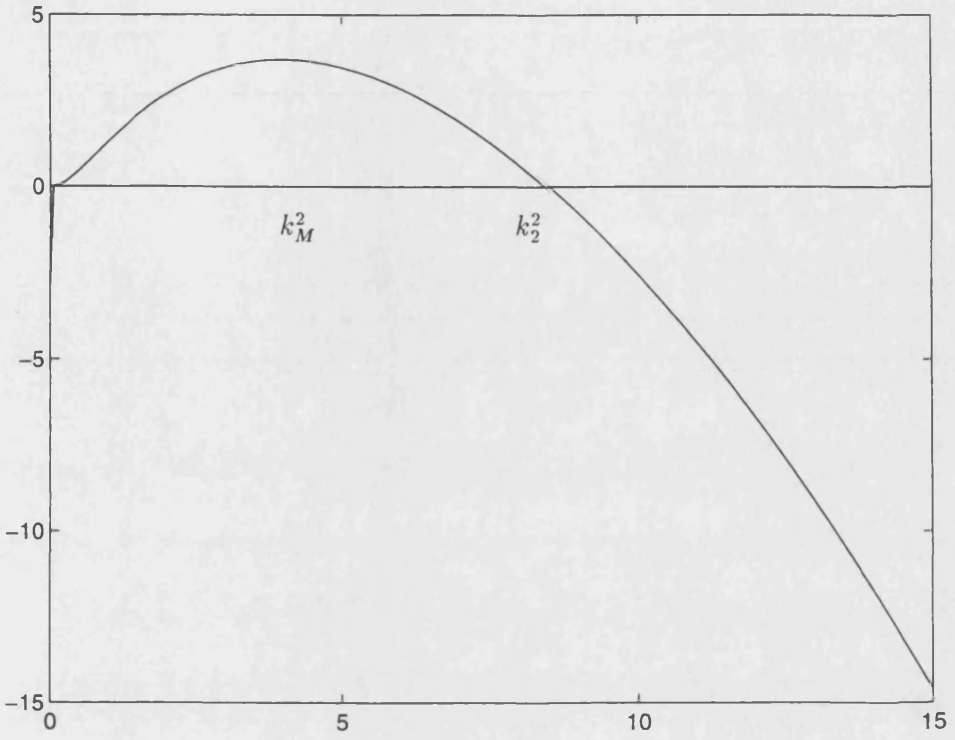

Figure 3-2: *A typical dispersion relation where* $r = 0$ *and* $a > a_c$ *so that there is instability for* $0 < k^2 < k_2^2$.

Mitosis included $(r > 0)$

In this model we will include some mitosis, but at a reduced rate in order to account for the effect of fibronectin on the proliferation of EC [Bowersox & Sorgente, (1982)]. With $r > 0$, the critical value of k^2, k_c^2, occurs when equation (3.1.9) has only one root. i.e.

$$\left(ds + rNs - \frac{aNs}{(N+1)^2}\right)^2 - 4drNs^2 = 0, \tag{3.1.10}$$

$$k_c^2 = \frac{1}{2d}\left(\frac{aNs}{(N+1)^2} - ds - rNs\right) = s\left(\frac{rN}{d}\right)^{\frac{1}{2}}. \tag{3.1.11}$$

So the critical value of a, a_c, is given by equation (3.1.10). A typical dispersion is shown in figure (3-3). Again when $a > a_c$ the system will be unstable for sufficiently small r. Also as $r \to 0$, $k_c^2 \to 0$ and $a_c \to \dfrac{d(N+1)^2}{N}$ which agrees with our earlier observations.

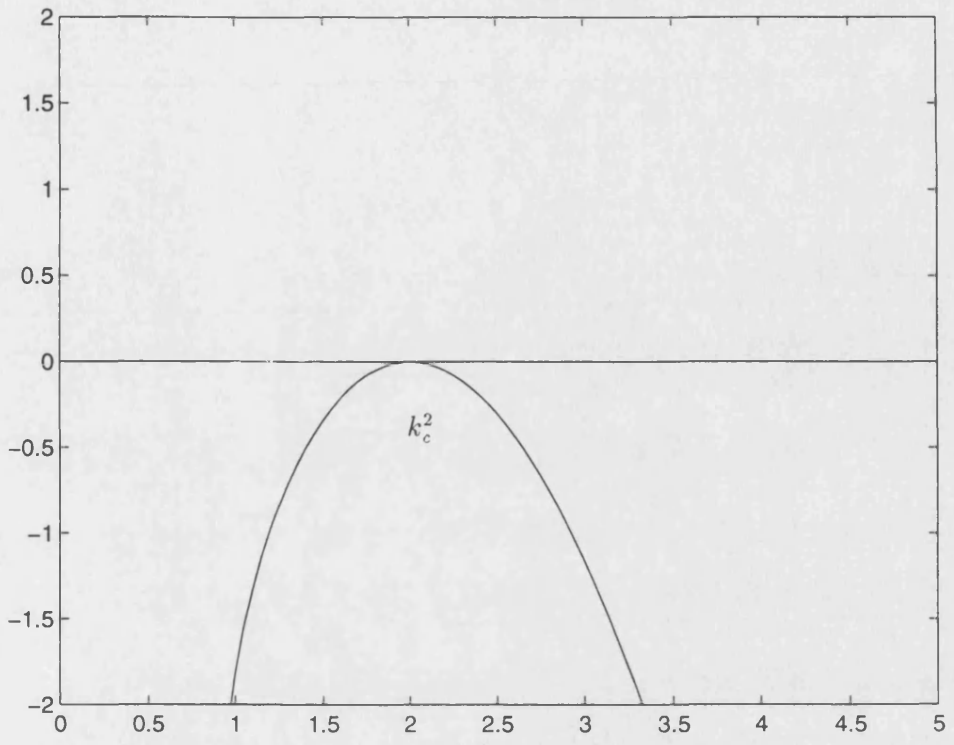

Figure 3-3: *A typical dispersion relation with $r > 0$ and $a = a_c$ so that σ has only one root k_c^2. In this case we are on the border of stability/instability.*

3.1.2 Estimation of parameters

Wherever possible experimental data was used to estimate the parameter values d, a, s, r and N. For simplicity we took S, $N = 1$.

Michaelis-Menten parameter β

We assume that the secretion of fibronectin by the EC is governed by Michaelis-Menten kinetics. Fibronectin molecules inside the EC form a complex by combining with receptors on the cell membrane. They are then carried across the membrane and deposited outside the cell. Upon derivation of the Michaelis-Menten term $\frac{Sn}{\beta + n}$, we observe that β represents the ratio between the rate at which the receptors become empty and the rate at which the receptors become occupied (see chapter 2 section (2.1)). Hence a reasonable estimate is $\beta = 1$.

Diffusion coefficient d

Sherratt & Murray, (1990) used estimated diffusion coefficients in their model of epidermal wound healing. For the diffusion of the cells they gave values of $3 \times 10^{-9}\text{cm}^2\text{s}^{-1}$, $3.5 \times 10^{-10}\text{cm}^2\text{s}^{-1}$ and $6.9 \times 10^{-11}\text{cm}^2\text{s}^{-1}$, and for the diffusion of the chemical in question they had $3.1 \times 10^{-7}\text{cm}^2\text{s}^{-1}$ and $5.9 \times 10^{-6}\text{cm}^2\text{s}^{-1}$. This gives a range for d of 9.6×10^{-1} to 1.2×10^{-5}. In their study of individual endothelial cells, Stokes *et al.*, (1991) calculated a random motility coefficient of $(7.1 \pm 2.7) \times 10^{-9}\text{cm}^2\text{s}^{-1}$ for endothelial cells migrating in a culture containing an angiogenic factor αFGF [Folkman & Klagsbrun, (1987)], heparin and fetal calf serum. Taking the diffusion of the chemical as above, we obtain the range 1.4×10^{-2} to 7.5×10^{-4} for d. In the numerical simulations which follow, we chose a value for d of 10^{-3}, which lies in the middle of the range.

Rate of Mitosis r

For the rate of mitosis we took the range 0.04h^{-1} (estimated in Sherratt & Murray, (1990)) to 0.056h^{-1} (estimated in Stokes & Lauffenburger, (1991)). However according to Bowersox & Sorgente, (1982) fibronectin inhibits cell proliferation by 23%. Hence we have a range of 0.0308h^{-1} to 0.043h^{-1} for cell mitosis. We chose a value of 0.034, again in the middle of the range. Yamada & Olden, (1978) reported on the turnover rate of cell surface fibronectin. Fibronectin has a generation time of 18 hours with half remaining after 36 hours. This gives a half life of 18 hours and so the rate of decay is given by $\gamma = \frac{1}{18} ln2 \simeq 0.0385 h^{-1}$. Hence we took the mitotic parameter $r = \frac{0.034}{0.0385} \simeq 0.88$.

Haptotaxis coefficient a

The Boyden chamber can be used to analyse cell migration. Using this method, Ungari *et al.*, (1985) found that fibronectin mobilized EC at a dose between $5\mu g/\text{ml}$ to $20\mu g/\text{ml}$. Bowersox & Sorgente, (1982) found that the maximum response by EC was at $100\mu\text{g/ml}$ and Terranova *et al.*, (1985) found that doses of fibronectin between 10^{-8}M and 10^{-10}M stimulated cell migration. However, the data from this method fails to give complete information about the haptotaxis coefficient. Therefore we ran several numerical simulations and found that the best results were obtained with a value of $a = 3.8$. Hence, using the values of γ and d_c which we found previously, this leads to a dimensional value of $1.46 \times 10^{-7}\text{cm}^2\text{s}^{-1}\text{M}^{-1}$ for the haptotactic coefficient.

Size of domain s

The parameter value s represents the finite region of the capillary vessel that is affected by the TAF. s will depend on the distance between the tumour and the capillary. As a scale reference, we will take $s = 1$ when the tumour is at a maximum distance from the capillary but still close enough for angiogenesis to take place [Gimbrone *et al.*, (1974)]. From the summary of corneal implants as reported in Balding & McElwain, (1985), the distance between the tumour and the host vessel should be in the range 0.8mm to 2.5mm in order to achieve an angiogenic response. Gimbrone *et al.*, (1974) observed that capillary sprouts did not grow until the tumour implant was placed within 2.5±0.5mm from the limbal vessels. Therefore we estimate our domain size parameter s to be in the range 1 to 3. By increasing the size of the domain we can obtain a larger variety of pattern.

3.1.3 Numerical simulations

The non-dimensionalized system of equations was solved using a routine available from the NAG library which integrates parabolic partial differential equations via the method of lines and Gear's method. The parameter values used were as specified in the previous section and we imposed zero flux boundary conditions. Initial conditions were taken to be small random perturbations about the steady state $(1, 0.5)$. As predicted by the linear stability analysis the system evolved into a spatially inhomogeneous solution (see figures (3-4) and (3-5)). The peaks in the cell density show that the cells have moved from their evenly distributed positions and have clustered together to form buds. These buds are assumed to sprout towards the tumour and become the primary capillary vessels in the vasculature of the tumour. Our simulation shows that two clusters form initially, which is consistent with observations made by Muthukkaruppan *et al.*, (1982) in their experiments with mouse cornea. The distribution of the chemical fibronectin and the distribution of the cells are similar. Thus the cells have moved towards areas of high chemical concentration. As fibronectin is closely associated with cell adhesion, we assume that the main mechanism by which the cells move is via haptotaxis. The maxima in the chemical concentration coincide with the intensity of the TAF diffusing from the tumour i.e. the point of initial contact between the parent vessel and the TAF is the area where the first sprouts will be observed.

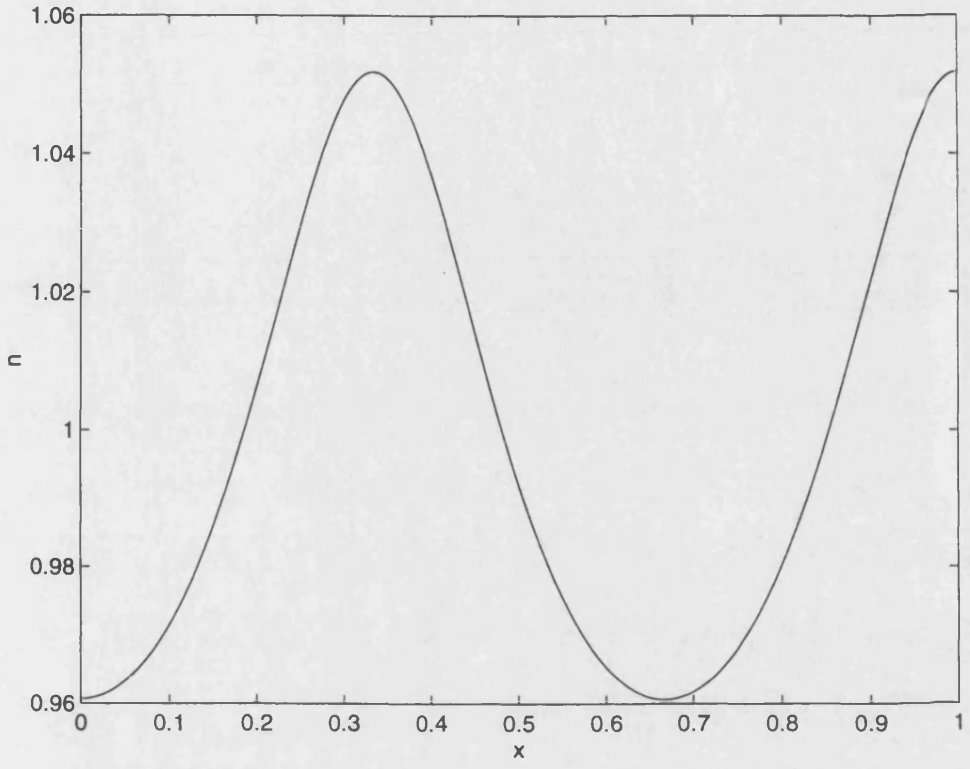

Figure 3-4: *The density pattern of the endothelial cells after being perturbed from an initially homogeneous steady state. Two peaks appear indicating that two buds have formed. Parameter values are* $d = 10^{-3}$, $a = 3.8$, $s = 3$, $r = 0.88$ *and* $N = 1$.

This model illustrates the principle of local activation and lateral inhibition [Oster & Murray, (1989)] . Once a peak in fibronectin concentration has been established, EC will actively move up the adhesive gradient and hence the concentration of chemical in that area will increase. Even more cells will move into that particular area and so on. Zones of inhibition will be created as cells move away from areas of low chemical concentration. These are indicated by the minima in figures (3-4) and (3-5). This highlights the importance of domain size in producing a pattern. If the domain were too small, the cells would become saturated with fibronectin and would not be able to detect gradients in the chemical/adhesive sites. Hence the zones of inhibition would disappear and so would the pattern.

In the next section we focus upon EC within the capillary sprout in order to investigate the secondary branching process. Once again the role of haptotaxis in this process is focussed upon.

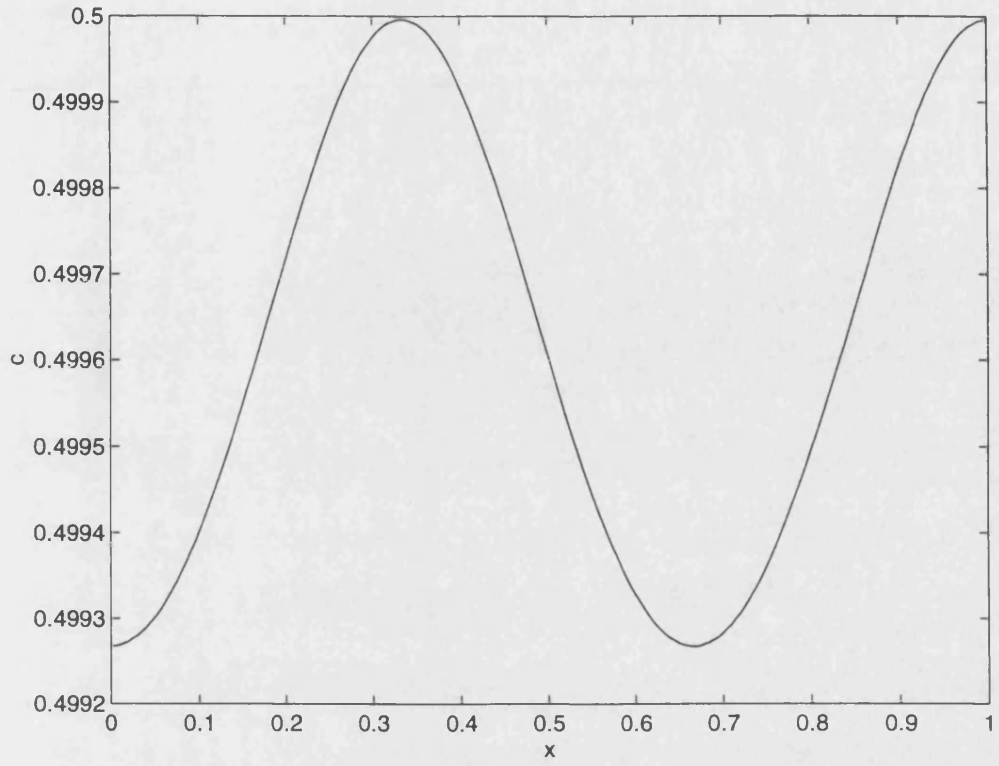

Figure 3-5: *The distribution of fibronectin after being perturbed about an initially homogeneous steady state. The pattern matches that of the endothelial cells, indicating that the cells have moved towards the areas of high fibronectin concentration. Parameter values are* $d = 10^{-3}$, $a = 3.8$, $s = 3$, $r = 0.88$ *and* $N = 1$.

3.2 The branching of capillary sprouts

We now consider events concerned with the EC after the formation of capillary buds. Having broken through the basement membrane, the buds elongate and form sprouts by recruiting EC from the parent vessel. As the sprouts grow towards the tumour, secondary side branching occurs, whereby the sprouts themselves bud in a similar manner to those which developed from the parent vessel (see figure (3-1)).

There are two separate processes involved in the creation of branching structures such as capillary networks, namely

1. the growth of branches,

2. the splitting of one branch into two.

As the resultant patterns depend upon the timing and the location of a splitting branch,

there are often significant differences between branching structures so that each one is distinct. Balding & McElwain, (1985) observed several similarities between fungal growth and neovascularization and subsequently based their model for capillary growth on the model of fungal colonies by Edelstein, (1982).

Similar structures to those observed in angiogenesis are known to arise during the growth and development of bryozoans and fungi. Growth in bryozoans occurs at the tips of the branches and the cells lying inside a growing tip secrete cuticle as the branch grows. The new cuticle is inserted directly into the existing cuticle, which spreads out carrying cells and adhesive sites with it. The older cuticle is pushed outwards and calcifies forming the outer layer of the branch. The direction of branch growth depends upon the location of the cells within the tip and the splitting of a cell cluster into two coincides with the splitting of one branch into two. Hence the splitting of a cell cluster is the initial event which determines branching.

The model of bryozoan growth proposed by Goldwasser *et al.*, (1989) may be adapted to describe other branching structures, in particular as the basis for a model mechanism describing the branching of capillary sprouts during angiogenesis. The growing capillary sprout tip is analogous to the growing tip of a bryozoan in that branching occurs when a cell cluster splits into two [Konerding *et al.*, (1992)]. From experimental observations it is known that during angiogenesis the EC secrete a matrix consisting of fibronectin, laminin and collagen IV [Paweletz & Knierim, (1989)] and the movement of the EC is determined, at least in part, by the distribution of adhesive sites on this matrix. We can attribute the loss of matrix to the reformation of a basement membrane during the maturation of the newly formed capillary sprouts. It is known that EC move up and down the new capillary sprout [Paweletz & Knierim, (1989)] and this motion cannot be explained either by directed cell motion alone, such as chemotaxis, or by random motility. However, it is known that convection plays a major role in the transport of tissue [Murray, (1989)] and we assume that as the matrix spreads out the EC are to some extent passively carried with it. As proliferation occurs near the tip of the capillary sprout [Ausprunk & Folkman, (1977)], [Paweletz & Knierim, (1989)], we do not need to include mitosis in the model, since we focus attention on the latter part of the sprout.

3.2.1 Mathematical model of secondary branch formation

Once again the model is constructed in a one-dimensional domain in order to focus attention on the endothelial cell clusters, rather than the emerging shape of the capillary sprout tip. Let $\rho(x,t)$ be the density per unit length of the matrix, $a(x,t)$ the density per unit length of the adhesive sites and $n(x,t)$ the density per unit length of the EC.

Mathematical models of tumour angiogenesis certainly rely on chemotaxis as the principal mechanism governing the motion of the capillary network [Chaplain & Stuart, (1993)], [Stokes & Lauffenburger, (1991)]. However chemotaxis alone is insufficient to account for all the events associated with angiogenesis especially those such as secondary side branching and anastomosis. Chemotaxis is implicit in this model in that all the events of angiogenesis occur after the release of TAF by the tumour, and the cells at the tips of the sprouts are assumed to react to the chemotactic stimulus through migration and proliferation. It is these cells at the tips which primarily orientate the direction of the sprouts. In this section we focus attention on EC behind the proliferating cells which are located near the sprout tip and as far back as the parent vessel (e.g. limbus) and hence it can be assumed, based on experimental evidence cited previously, that the movement of the EC (within the region of the sprout under consideration) in this case is governed by a combination of diffusion, haptotaxis and convection.

The model is based on two processes [Paweletz & Knierim, (1989)]:

1. The spreading of the matrix with the convection of EC and adhesive sites with it.

2. The secretion of matrix and adhesive sites by the EC.

The convection of cells and adhesive sites will be at the same rate at which the matrix spreads out. Assuming that the matrix spreads out at a constant rate, c say, and that the velocity is $-\rho_x$, then the convective flux is proportional to $-c\rho_x$, i.e. flux of the adhesive sites is $\mathbf{J}_a = -ca\rho_x\mathbf{n}$, where $\mathbf{n}$ is a unit vector. For the source and sink terms, we assume a linear production by the EC and linear decay of the matrix and adhesive sites, but as proliferation of EC occurs near the tip, we omit a cell production term for the reasons cited above. Hence the model equations are

$$\rho_t = \underbrace{d_1\rho_{xx}}_{diffusion} + \underbrace{\zeta n}_{production} - \underbrace{\lambda\rho}_{decay}, \tag{3.2.12}$$

$$a_t = \underbrace{d_2 a_{xx}}_{\text{diffusion}} + \underbrace{c(a\rho_x)_x}_{\text{convection}} + \underbrace{bn}_{\text{production}} - \underbrace{\mu a}_{\text{decay}}, \tag{3.2.13}$$

$$n_t = \underbrace{d_3 n_{xx}}_{\text{diffusion}} - \underbrace{h(na_x)_x}_{\text{haptotaxis}} + \underbrace{c(n\rho_x)_x}_{\text{convection}}, \tag{3.2.14}$$

where c is the rate at which the matrix spreads, ζ is the rate of secretion of matrix per cell, λ is the loss of matrix per unit matrix, b is the rate of secretion of adhesive sites per cell, μ is the decay of adhesive sites, d_1, d_2, d_3 are the diffusion constants, and h is the rate at which cells move up an adhesive gradient.

Let N be the mean endothelial cell density throughout the capillary sprout, L_0 the original length of the domain, i.e. the length of the initial sprout bud, and L the current sprout length. The above system of equations can be non-dimensionalized by making the following substitutions:

$$n^\star = \frac{n}{N},\ x^\star = \frac{x}{L},\ t^\star = \frac{\mu L_0^2 t}{L^2},\ a^\star = \frac{ah}{\mu L_0^2},\ \rho^\star = \frac{\rho c}{\mu L_0^2},$$

$$\lambda^\star = \frac{\lambda}{\mu},\ \gamma^\star = \frac{L^2}{L_0^2},\ \zeta^\star = \frac{cN\zeta}{\mu^2 L_0^2},\ b^\star = \frac{bhN}{\mu^2 L_0^2},\ d_i^\star = \frac{d_i}{\mu L_0^2},\ i = 1,2,3.$$

Dropping the asterisks for notational convenience, the system of equations becomes,

$$r_t = d_1\rho_{xx} + \gamma(\zeta n - \lambda\rho), \tag{3.2.15}$$

$$a_t = d_2 a_{xx} + (a\rho_x)_x + \gamma(bn - a), \tag{3.2.16}$$

$$n_t = d_3 n_{xx} - (na_x)_x + (n\rho_x)_x. \tag{3.2.17}$$

To close the system we impose non-zero flux boundary conditions for the matrix and the adhesive sites, but zero flux boundary conditions for the cells. The reasoning behind these conditions is that the endothelial cells stay entirely within the domain of the capillary sprout [Paweletz & Knierim, (1989)] whereas the matrix and the adhesive sites spread out beyond the domain, (i.e. sprout), so there is a certain amount of leakage at the boundaries. We therefore take boundary conditions as follows:

$$\begin{aligned} d_1\rho_x &= \mp k \quad \text{at } x = 0 \text{ and } x = 1 \text{ respectively,} \\ d_2 a_x + a\rho_x &= \mp l \quad \text{at } x = 0 \text{ and } x = 1 \text{ respectively,} \\ dn_x - na_x + n\rho_x &= 0 \quad \text{at } x = 0 \text{ and } x = 1 \text{ respectively,} \end{aligned} \tag{3.2.18}$$

where k and l are positive constants representing the rate of loss of matrix and adhesive sites respectively. In section (3.2.4), we will discuss the significance of the parameters k and l

3.2.2 Linear stability analysis

Assuming that the number of cells in the domain remains constant, i.e. there is no proliferation in the region that we are considering, then we choose $n = 1$ as an appropriate scaled steady state. The non-trivial spatially homogeneous steady state is therefore $(\frac{\zeta}{\lambda}, b, 1)$. After linearizing about this steady state , we look for solutions of the form

$$\mathbf{r} = \begin{bmatrix} \rho - \frac{\zeta}{\lambda} \\ a - b \\ n - 1 \end{bmatrix} \propto \exp(\sigma t + ikx),$$

where k is the wave number of the perturbation and σ is the rate of growth of the perturbation with wave number k, as per previous section.

The linearized system of equations takes the form $\sigma\mathbf{r} = A\mathbf{r}$ where A is a 3×3 matrix. The dispersion relation between σ and k is given by $\det[\sigma I - A] = 0$ which is:

$$\begin{aligned} \sigma^3 &+ \sigma^2[k^2(d_1 + d_2 + d_3) + \gamma(\lambda + 1)] \\ &+ \sigma[k^4(d_1(d_2 + d_3) + d_2 d_3) + \gamma k^2(d_1 + \lambda d_2 + (1 + \lambda)d_3 - b + \zeta) + \gamma^2\lambda] \\ &+ k^2[k^4 d_1 d_2 d_3 + \gamma k^2(\zeta(b + d_2) + \lambda d_2 d_3 + (d_3 - b)d_1) \\ &+ \gamma^2(\zeta + \lambda(d_3 - b))] = 0. \end{aligned} \tag{3.2.19}$$

If $\mathrm{Re}(\sigma) < 0$ then $\exp(\sigma t + ikx) \to 0$ as $t \to \infty$, so the system will be stable to small perturbations. If $\mathrm{Re}(\sigma) > 0$ the perturbations will grow. The imaginary part of σ gives rise to periodic solutions. When $k = 0$, the system is spatially homogeneous, and the dispersion relation becomes

$$\sigma^3 + \gamma(\lambda + 1)\sigma^2 + \gamma^2\lambda\sigma = 0, \tag{3.2.20}$$

which has the solution $\sigma = 0$ and two negative roots. Hence the system is stable to spatially homogeneous solutions. When $k \neq 0$ the dispersion relation will either have

three real roots or one real root and two complex conjugate roots. The root whose real part is the greatest in magnitude will determine the pattern which is formed. If this root is real and positive for a range of k, the initially uniform cell distribution will evolve into a spatially heterogeneous one. If this root is complex and its real part is positive then the perturbation will be oscillatory in nature.

In the following analysis, the theory used is standard for coefficients of polynomials, such as Descartes rule of signs (see Murray (1989)). We will have a change in stability when $\sigma = 0$, i.e. $p(k^2) = 0$ where $p(k^2) = a_1k^4 + a_2k^2 + a_3$, and

$$a_1 = d_1d_2d_3,$$

$$a_2 = \gamma\left((d_3 - b)d_1 + \zeta(b + d_2) + d_2d_3\lambda\right),$$

$$a_3 = \gamma^2(\zeta + \lambda(d_3 - b)).$$

If $a_2 > 0$ and $a_3 > 0$, then $p(k^2)$ has no positive solutions for k^2. Consider $a_3 < 0$, i.e. $b > d_3 + \frac{\zeta}{\lambda}$, then $p(k^2)$ has one positive root. If $a_3 > 0$ but $a_2 < 0$, then $p(k^2)$ has two positive roots, i.e. if $b < d_3 + \frac{\zeta}{\lambda}$ and

$$b(\frac{\zeta}{\lambda} + d_1 - \zeta) > d_3(\frac{\zeta}{\lambda} + d_1) + d_2\zeta + d_2d_3\lambda.$$

We will have exponential growth provided $p(k^2) < 0$. So if $b > d_3 + \frac{\zeta}{\lambda}$, we will have instability for k^2 in the range $0 < k^2 < k_B^2$ and if

$$0 < b < d_3 + \frac{\zeta}{\lambda}, \quad d_1 < \zeta,$$

or if

$$\frac{d_1d_3 + d_2\zeta + d_2d_3\lambda}{d_1 - \zeta} < b < d_3 + \frac{\zeta}{\lambda}, \quad d_1 > \zeta,$$

then we have instability for $k_A^2 < k^2 < k_B^2$ where $k_{A,B}^2$ are the roots of $p(k^2)$.

Returning to the dispersion relation, we now consider the signs of the coefficients of the cubic equation (3.2.19), i.e. the signs of

$$A_1 = k^2(d_1 + d_2 + d_3) + \gamma(\lambda + 1),$$

$$A_2 = k^4(d_1(d_2+d_3)+d_2d_3)+\gamma k^2(d_1+\lambda d_2+(1+\lambda)d_3-b+\zeta)+\gamma^2\lambda,$$

$$A_3 = k^2 p(k^2).$$

If $A_3 < 0$ then (3.2.19) has only one positive root which will be real. If $A_3 > 0$ and $A_2 > 0$, the dispersion relation will have no positive roots. However if $A_3 > 0$ and $A_2 < 0$ then the dispersion relation has two positive roots. So consider $q(k^2) = 0$ where $q(k^2) = b_1k^4 + b_2k^2 + b_3$ and

$$b_1 = d_1(d_2+d_3)+d_2d_3,$$

$$b_2 = \gamma(d_1+\lambda d_2+(1+\lambda)d_3-b+\zeta),$$

$$b_3 = \gamma^2\lambda.$$

If $b_2 > 0$ then $q(k^2)$ has no positive roots. If $b_2 < 0$ then $q(k^2)$ has two positive roots. So when

$$b > d_1+\lambda d_2+(1+\lambda)d_3+\frac{\zeta}{\lambda}+\zeta,$$

$q(k^2) < 0$ for $k_1^2 < k^2 < k_2^2$, where $k_{1,2}^2$ are the roots of $q(k^2)$.

There exists another bifurcation point at which two of the real roots become complex. This point k_C^2 say, is given by solving

$$|\beta| = 2\alpha^{3/2},$$

for k^2 where

$$\alpha = \left(\frac{A_1}{3}\right)^2 - \left(\frac{A_2}{3}\right), \quad \beta = 2\left(\frac{A_1}{3}\right)^2 - \left(\frac{A_1A_2}{3}\right) + A_3.$$

A summary of the changes in the roots of the dispersion relation as b increases are as follows.

- For $0 < b < d_3+\frac{\zeta}{\lambda}$ (provided $d_1 < \zeta$), the dispersion relation has only one positive root and hence we have instability for $k_A^2 < k^2 < k_B^2$.
- For $d_3+\frac{\zeta}{\lambda} < b < d_1+\lambda d_2+(1+\lambda)d_3+\frac{\zeta}{\lambda}+\zeta$ the dispersion relation has only one positive root and hence instability for $0 < k^2 < k_B^2$.

For $b > d_1+\lambda d_2+(1+\lambda)d_3+\frac{\zeta}{\lambda}+\zeta$ the changes in the dispersion relation as k^2 increases are as follows:

- For $0 < k^2 < k_B^2$ the dispersion relation has one positive and two negative real roots.
- For $k_B^2 < k^2 < k_C^2$ all the roots are real and negative.
- For $k_C^2 < k^2 < k_1^2$ two roots are complex with negative real parts and one root is real and negative .
- For $k_1^2 < k^2 < k_2^2$ the dispersion relation has one negative real root and two complex roots with positive real parts.
- For $k_2^2 < k^2$ the two complex roots have negative real parts.

For example, if we choose parameters $d_1 = 1$, $d_2 = 1$, $d_3 = 10$, $\lambda = 20$, $\gamma = 15$, $\zeta = 10$ and let $10.5 < b < 241.5$, we would expect the system to evolve into a spatially heterogeneous state. We obtain the dispersion relation as shown in figure (3-6) with $b = 155$. So for $0 < k < 5.15$, we will have exponential growth of perturbations (according to linear stability analysis).

Another example is if we take $b = 300$. For this parameter set we obtain the dispersion relation as shown in figure (3-7) where two of the roots of the dispersion relation have become complex with positive real part. In this case we would expect oscillating solutions, which correspond to EC migrating up and down the sprout [Paweletz & Knierim, (1989)].

3.2.3 Estimation of parameters

Wherever possible parameters were estimated from experimental papers. When this proved difficult, the parameters which yielded the best numerical results, were chosen.

From Balding and McElwain (1985) and Gimbrone *et al.* (1974), the tumour must be placed at a distance of 0.08–0.3cm from the limbal vessel. Hence, we will take the initial length $L_0 = 0.001$cm and let L vary between 0.003–0.015cm so that $9 < \gamma < 225$.

Using the results from Yamada and Olden (1978), we estimate the decay of the matrix to be 0.0385h^{-1}. If we take $\lambda = 20$ then the decay of the adhesive sites μ is $1.925 \times 10^{-3}\text{h}^{-1}$. The choice of λ was arbitrary due to the lack of empirical data.

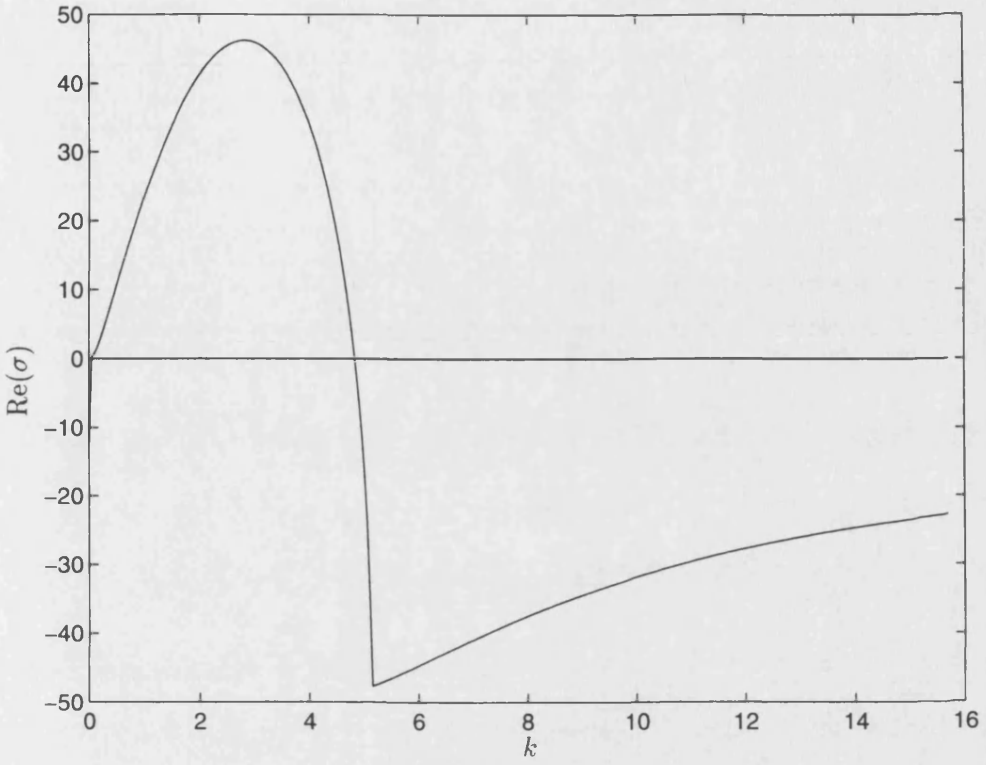

Figure 3-6: *A dispersion relation where σ is real and positive for $0 < k^2 < 5.15$ and hence we have instability for this range. Parameter values are $d_1 = 1$, $d_2 = 1$, $d_3 = 10$, $b = 155$, $\lambda = 20$, $\zeta = 10$, $\gamma = 15$.*

Yamada and Olden (1978) also reported that fibronectin is relatively immobile, with a diffusion coefficient $< 5 \times 10^{-12}\text{cm}^2\text{s}^{-1}$. So taking the diffusion coefficient of the matrix and the diffusion coefficient of the adhesive sites to be $5.35 \times 10^{-13}\text{cm}^2\text{s}^{-1}$ and the diffusion coefficient of the cells to be ten times higher, we have $d_1 = d_2 = 1$ and $d_3 = 10$. By making the diffusion of the cells lower than in the previous section, we are able to emphasise and focus upon the other transport mechanisms which we believe to be more important.

Terranova *et al.* (1985) found that doses of fibronectin between $10^{-8} - -10^{-10}\text{M}$ stimulated cell migration and Yamada and Olden (1978) gave the generation time of fibronectin to be 18 hours. Assuming that 10^{-8}M of fibronectin is produced by N cells in 18 hours, where N is the mean cell density, we estimate the rate of the secretion of the matrix as $\frac{10^{-8}}{18} N^{-1}\text{h}^{-1}\text{M}$. Again choosing ζ arbitrarily to be 10, we find that $c = 1.854738 \times 10^{-5}\text{cm}^2\text{s}^{-1}\text{M}^{-1}$, which seems a reasonable estimate for the convection rate. Assuming that the secretion of the adhesive sites is ten times higher than that

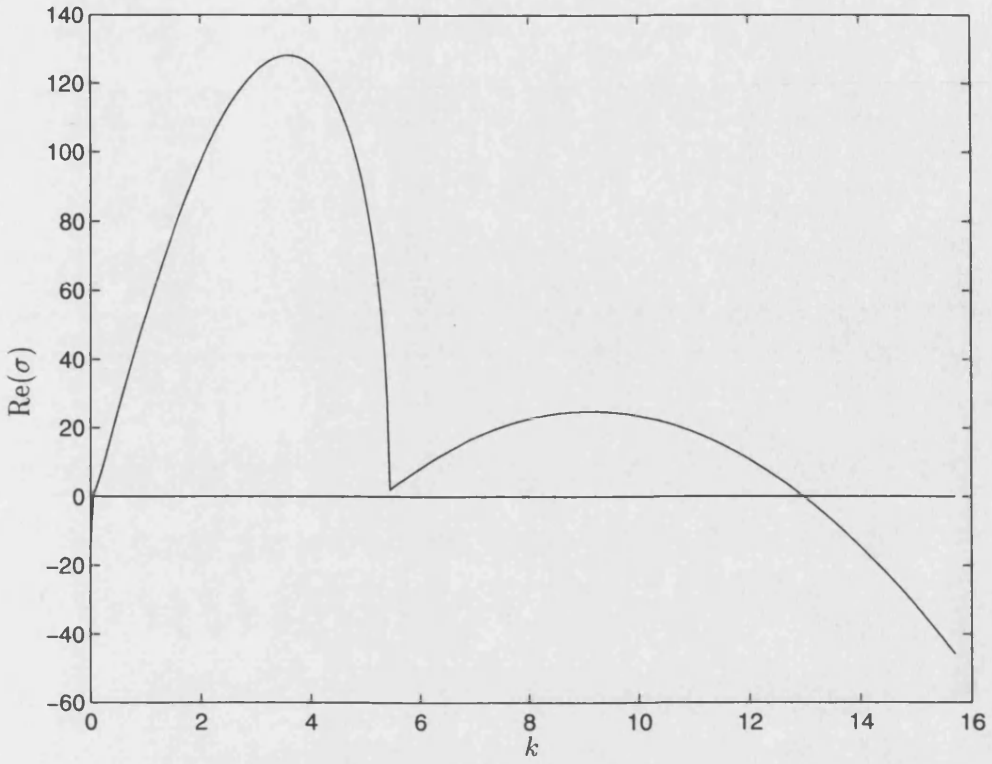

Figure 3-7: *A dispersion relation where σ is complex with positive real part. Parameter values are* $d_1 = 1$, $d_2 = 1$, $d_3 = 10$, $b = 300$, $\lambda = 20$, $\gamma = 15$, $\zeta = 10$.

of the matrix and choosing $b = 155$ (example 1) and $b = 300$ (example 2), we obtain $h \simeq 2.87 \times 10^{-5}\text{cm}^2\text{s}^{-1}\text{M}^{-1}$ and $h \simeq 5.56 \times 10^{-5}\text{cm}^2\text{s}^{-1}\text{M}^{-1}$, respectively.

In theory the values for k and l could be determined experimentally. However, in the absence of reliable empirical data, we will discuss the significance of these parameters in the next section.

3.2.4 Numerical simulations

We used the numerical scheme available from the NAG library (as described in chapter(2), section (2.2)), to solve the non-dimensionalized system of equations (3.2.15)-(3.2.17). In principle, the model should display a variety of solutions, as predicted by the linear analysis. In practice, some of the solutions predicted by the linear stability analysis proved difficult to obtain.

The initial conditions we used were perturbations about the steady state

$$\rho = \frac{\zeta}{\lambda}, \quad a = b \text{ and } n = 1. \tag{3.2.21}$$

We experimented with small random perturbations of $O(0.01)$ as well as a sine wave with small amplitude. This did not affect the resulting solution but the numerical scheme ran best with random initial conditions. However, some of the solutions could only be obtained using initial conditions which were far away from the steady state. As stated earlier, we impose non–zero flux boundary conditions for the matrix and the adhesive sites, but zero flux boundary conditions for the cells. This seems reasonable as we are only considering the splitting of an EC cluster rather than the actual formation and elongation of the branches. To model the formation of the branches themselves we would need to consider a moving domain.

The boundary conditions (3.2.18) can be written as follows,

$$\begin{aligned} d_1\rho_x &= \mp k, \\ d_1 d_2 a_x &= \mp(d_1 l - ak), \\ d_1 d_2 d_3 n_x &= \mp(d_1 l - (d_2 + a)k). \end{aligned} \tag{3.2.22}$$

When written in this form, it is clear that our choice of k and l can affect the value of the solution for n at each boundary. We assume that we must choose k and l such that

$$d_1 l - (d_2 + a)k > 0, \tag{3.2.23}$$

so that the sign of n_x is consistent with the signs of ρ_x and a_x at each boundary. Furthermore, the initial choice of a, i.e. our choice of the parameter b, can also affect the value of n_x. In the examples that follow, we took $d_1 = d_2 = 1$. Hence our assumption is $l > ak$ at $x = 0, 1$. In each of the numerical simulations that follow, we took $k = 0.0001$ and $l = 1$, since initially $a = b$, where $155 \leq b \leq 300$. We found that if we fixed $l = 1$ and varied k such that $k < 0.001$, i.e. (3.2.23) is satisfied, then the numerical solution for n did not change significantly. However if we let k vary so that $k > 0.001$, then the numerical simulations broke down. Therefore, the solutions were sensitive to changes in the flux parameters. We conclude from this that the boundary conditions are important

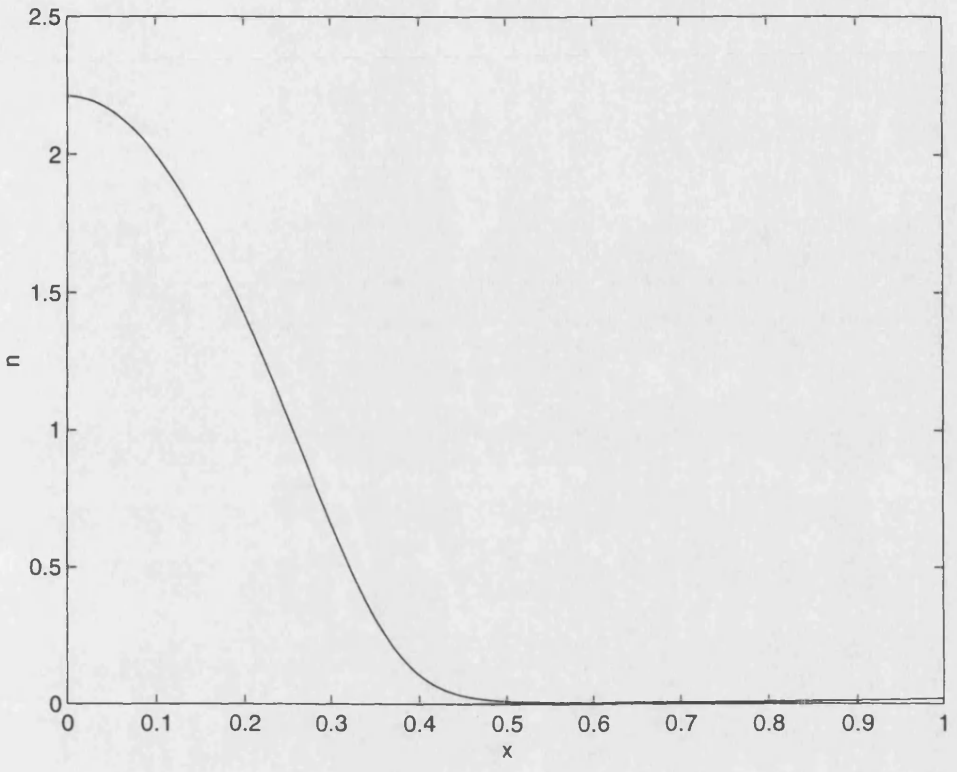

Figure 3-8: *Endothelial cell density profile obtained using parameter values* $d_1 = 0$, $d_2 = 0$, $d_3 = 10$, $b = 169$, $\lambda = 20$, $\zeta = 10$, $\gamma = 13$. *Figure illustrates formation of one EC cluster towards* $x = 0$. $x = 0$ *corresponds to a location close to sprout tip, but behind proliferation compartment,* $x = 1$ *corresponds to location of parent vessel, e.g. limbus.*

in the formation of the patterns obtained here.

By using the parameter values $d_1 = 1$, $d_2 = 1$, $d_3 = 10$, $b = 155$, $\lambda = 20$, $\gamma = 15$, $\zeta = 10$ in the numerical scheme, we obtain figure (3-8) where the density of the cells is greater at one end of the domain indicating the formation of one EC cluster. We can increase the number of EC clusters formed by increasing our value of γ, which is representative of the size of the domain. If we take $\gamma = 60$ we obtain two cell clusters (figure (3-9)). Throughout our numerical investigation, solutions of this type were typical. It has been observed experimentally [Folkman & Haudenschild, (1980)], [Paweletz & Knierim, (1989)] that the most common form of branching in capillaries is Y or T shaped. According to the linear analysis, if we choose $\gamma = 200$, we should obtain three cell clusters. However this solution was hard to capture and appeared transient. We obtained the solution in figure (3-10) using initial conditions for a away from the steady state $a = b$, i.e. initially we took $a = 200$. Hence as the domain increases,

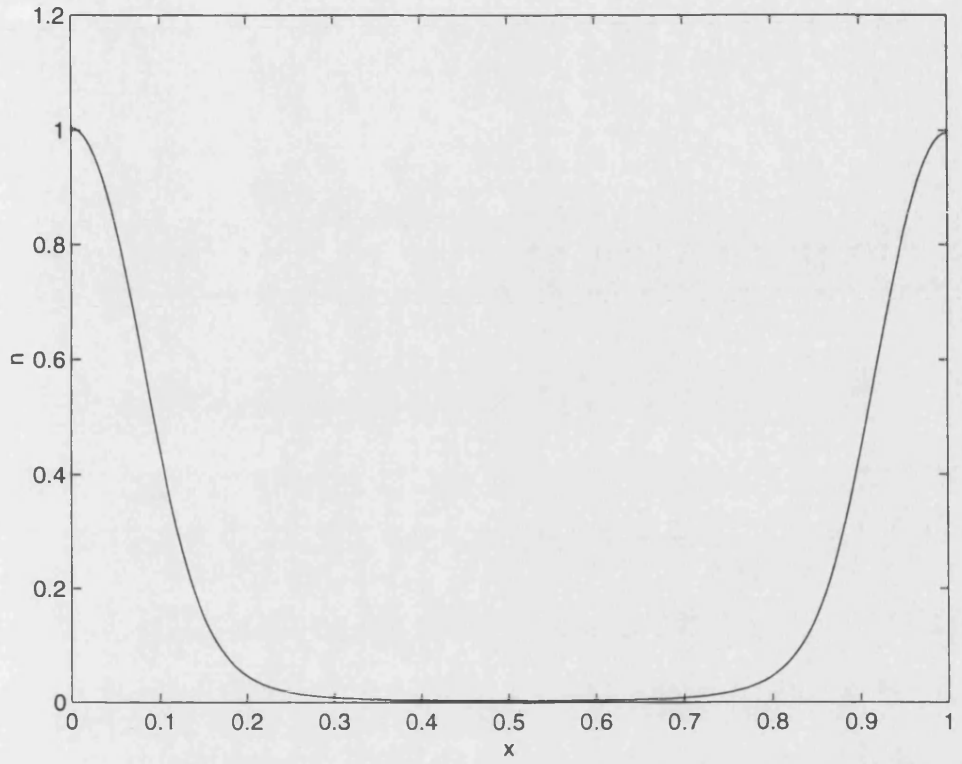

Figure 3-9: *Endothelial cell density profile obtained using parameter values* $d_1 = 0$, $d_2 = 0$, $d_3 = 10$, $b = 169$, $\lambda = 20$, $\zeta = 10$, $\gamma = 52$. *Figure illustrates formation of two EC clusters corresponding to side branches. By increasing* γ, *we model an increase in domain size, i.e. an increase in capillary sprout length.* $x = 0$ *corresponds to a location close to sprout tip, but behind proliferation compartment,* $x = 1$ *corresponds to location of parent vessel, e.g. limbus.*

i.e. the capillary sprout grows, the more side branches there are. Thus the number of side branches appearing depends on the size of the sprout, which is consistent with experimental observations.

By using the parameter values $d_1 = 1$, $d_2 = 1$, $d_3 = 10$, $b = 300$, $\lambda = 20$, $\gamma = 15$, $\zeta = 10$ we would expect oscillatory solutions from the linear stability analysis. However by using the initial conditions (3.2.21), we obtained a solution similar to that shown in figure (3-9). Oscillating solutions could be obtained by using initial conditions far away from the steady state, i.e. large perturbations. In the examples that follow we took initial conditions for a and ρ to be $a = 200$ and $\rho = 0.5$. One oscillating solution, whereby peaks of cells form from the initial conditions and momentarily merge before

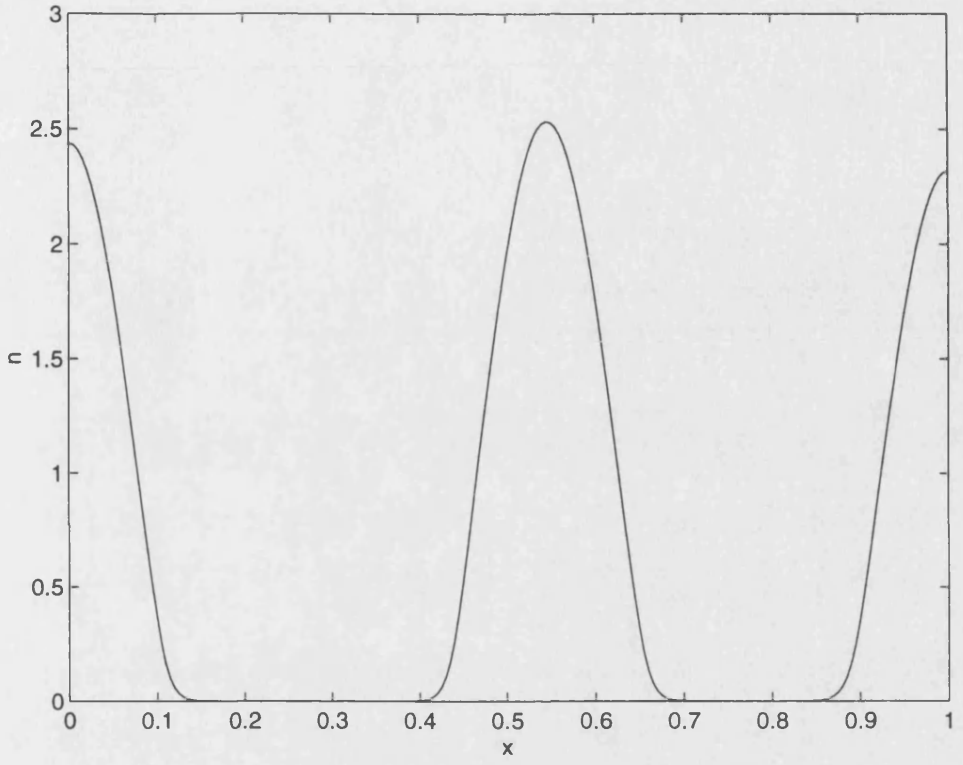

Figure 3-10: *Endothelial cell density profile obtained using parameter values* $d_1 = 0$, $d_2 = 0$, $d_3 = 10$, $b = 169$, $\lambda = 20$, $\zeta = 10$, $\gamma = 108$. *Figure illustrates formation of three EC clusters corresponding to three side branches. By increasing* γ *further, we model an increase in domain size, i.e. an increase in capillary sprout length.* $x = 0$ *corresponds to a location close to sprout tip, but behind proliferation compartment,* $x = 1$ *corresponds to location of parent vessel, e.g. limbus.*

splitting again, is illustrated in figure (3-11). This models the observation that the EC are continually rearranging themselves, moving up and down the capillary sprout [Paweletz & Knierim, (1989)]. This also reflects the transient behaviour of branching structures. Each time a cell cluster is produced there is the possibility of a daughter branch forming and hence no two branching structures are exactly alike.

The linear stability analysis has shown that there is a critical value of the parameter b above which the solutions oscillate. Furthermore, by increasing the value of γ, we increase the number of cell clusters formed. It is interesting to note that similar effects can be obtained by varying parameters ζ and λ. For example, an increase in ζ has the same effect on the dispersion relation as an increase in b and a decrease in γ simultaneously. An increase in λ has the exact opposite effect on the dispersion rela-

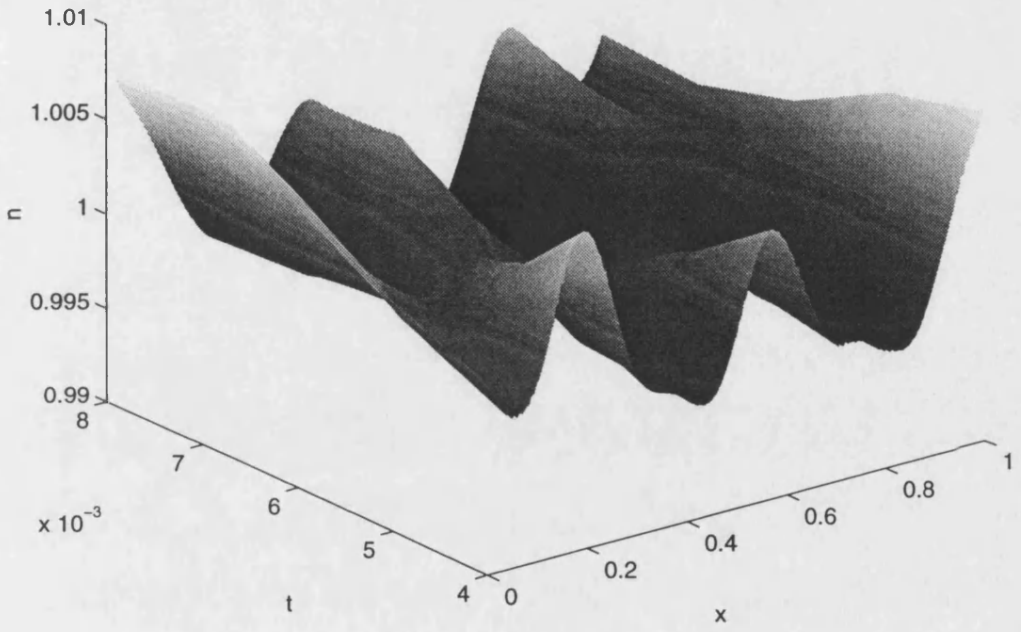

Figure 3-11: *A simulation showing cell clusters merging and then splitting again. Parameter values are* $d_1 = 1$, $d_2 = 1$, $d_3 = 10$, $b = 300$, $\lambda = 20$, $\gamma = 15$, $\zeta = 10$. *This models the observation of EC migration within the capillary sprout.* $x = 0$ *corresponds to a location behind proliferating cells (near tip),* $x = 1$ *corresponds to parent vessel e.g. limbus.*

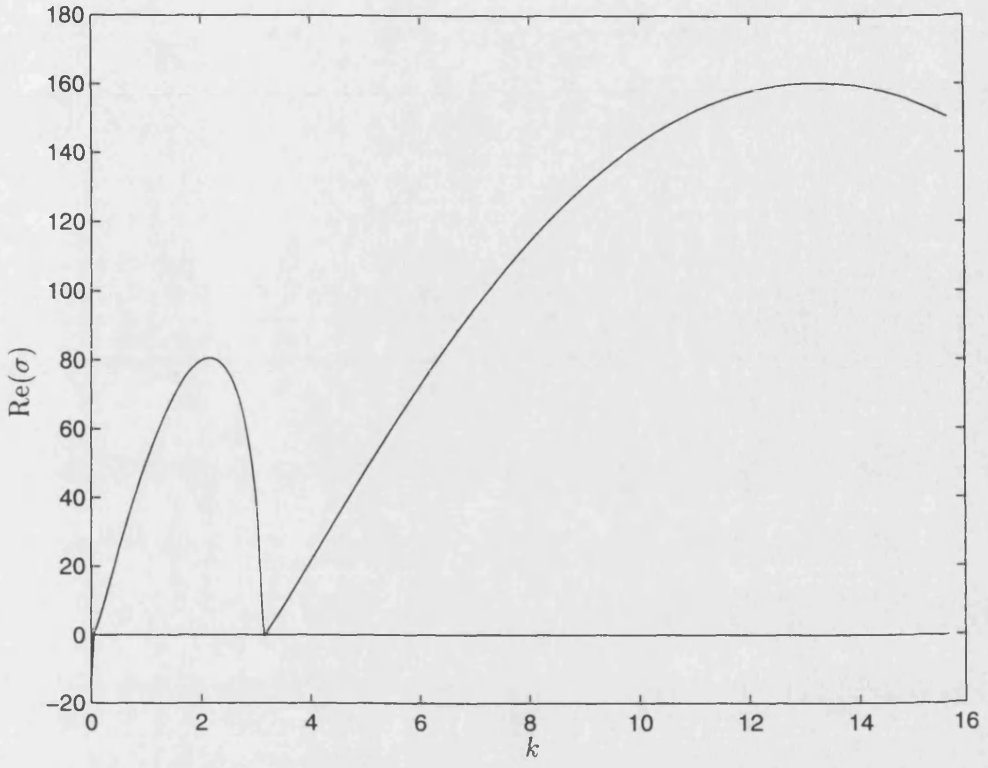

Figure 3-12: *A dispersion relation where the complex mode dominates. Parameter values are* $d_1 = 1$, $d_2 = 1$, $d_3 = 10$, $b = 300$, $\lambda = 20$, $\gamma = 15$, $\zeta = 30$.

tion as an increase in ζ. If we use the same parameters as in the last example but set $\zeta = 30$, then the dispersion relation is as in figure (3-12). From this we infer an increase in oscillatory behaviour. The numerical solution using these parameter values (figure (3-13)) has clusters of cells travelling to the right in a wave–like manner. Again, this demonstrates the persistent remodelling of the capillary network.

The difficulty in obtaining some of the predicted solutions in the numerical simulations indicates that the boundary conditions and initial conditions are very important in this model. Furthermore, the parameter values must be chosen very carefully. [Saunders & Ho, (1995)] also found this to be true of a simple reaction–diffusion system modelling segmentation and they concluded that this is a disadvantage of prepattern models in general, which do not have a mechanism for self–correction. A more robust model, such as a mechanochemical model where pattern formation occurs sequentially, would allow more freedom in the choice of parameters and would be less sensitive to the boundary and initial conditions. However, we would expect any model of branching to display transient behaviour in order to capture the uniqueness of each branching structure.

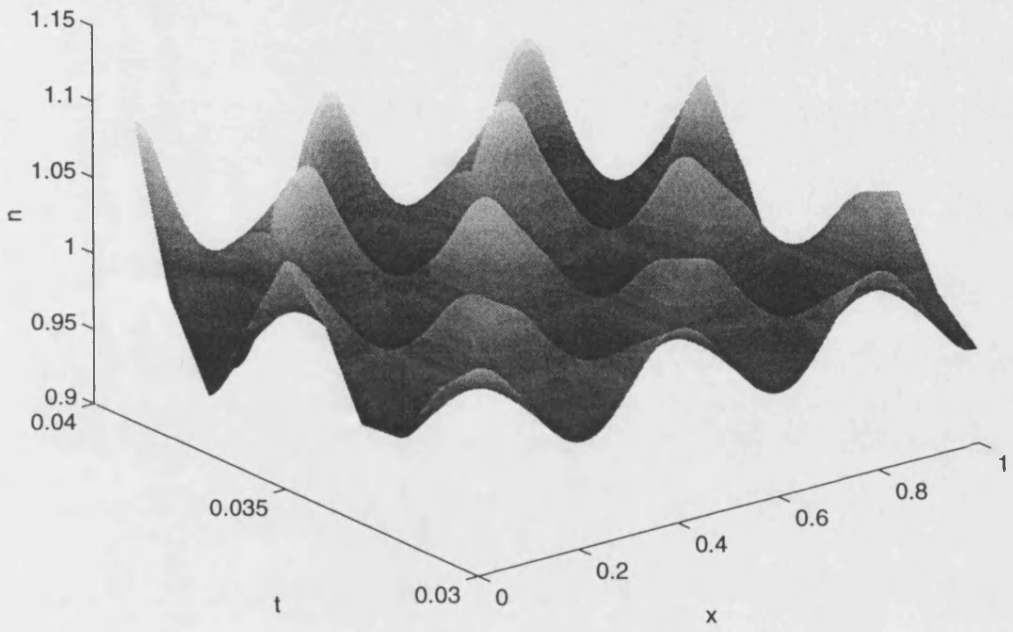

Figure 3-13: *A simulation showing increased oscillatory EC behaviour when the complex eigenvalue has a positive real part. Parameter values are* $d_1 = 1$, $d_2 = 1$, $d_3 = 10$, $b = 300$, $\lambda = 20$, $\gamma = 15$, $\zeta = 30$. *Here we have three clusters of cells moving to the right in waves.*

3.3 Discussion

The mathematical models for capillary bud and capillary side-branch formation in this have been developed using empirical data wherever possible and the numerical solutions of the models are in good agreement with experimental observations of tumour angiogenesis.

It is our belief that all of the events associated with angiogenesis cannot be fully explained by chemotaxis alone. We have shown that haptotaxis is a potentially important mechanism in at least two of the stages of angiogenesis and is worthy of further study. Schor & Schor, (1983) found that components of the ECM, such as fibronectin, increased the ability of EC to react to angiogenic factors positively. Furthermore, they discovered that EC did not react to an angiogenic stimulus when grown on denatured collagen or plastic material. Haptotaxis has also been implicated in the formation of anastomoses [Paweletz & Knierim, (1989)]. Though this important event in angiogenesis is well documented and it is known that capillary sprouts fuse together at their tips, the precise reason for this remains unexplained. Perhaps some mechanism which induces cell-cell adhesion may be involved. The role that haptotaxis may play may also suggest a potential anti-angiogenesis strategy by developing drugs which reduce the adhesive properties of EC to the matrix. We will explore this possibility in chapter (7).

We note that a one dimensional model of the early stages of angiogenesis is not particularly descriptive of the overall form of the capillary network. We only look at the formation and splitting of cell clusters and not the overall shape of the developing sprout and side branches. Finally we note that the mathematical models that we have considered are minimal in that they include the most basic of equations concerning the chemical and cell distribution. We could elaborate the models further to include other factors such as the effect of traction forces on the matrix (see for example Maini, (1989)). It may be possible to gain some useful information on lumen formation and anastomosis by producing two dimensional simulations of these models. We could also consider non-constant diffusion/haptotactic coefficients. Nevertheless, these simple models have produced the desired results by encapsulating the formation of capillary buds and the side branching of capillary sprouts, and have demonstrated the important potential role haptotaxis may play in the angiogenic process.

Chapter 4

Vascular tumour growth and invasion

In this chapter, we develop a simple mathematical model of the vascularization and subsequent invasive growth of a solid spherical tumour.

A vascularized tumour rapidly increases in mass [Paweletz & Knierim, (1989)]. This enormous growth in tumour volume results in the collapse of the vasculature at the centre of the tumour and a necrotic core will develop surrounded by a peripheral zone of live cells or 'tumour vascular envelope' [Paweletz & Knierim, (1989)]. Furthermore, the growth of the tumour during this stage is accompanied by the invasion of the surrounding tissue. Invasion is closely linked to metastasis, whereby tumour cells enter the blood or lymph system and hence secondary tumours or metastases may arise at distant sites in the body. Hence it is desirable to prevent a tumour from reaching the vascular phase of growth [Blood & Zetter, (1990)], [Folkman, (1985)], [Folkman & Haudenschild, (1980)], [Langer *et al.*, (1976)].

The key elements that are encapsulated in this model are the development of a central necrotic core due to the collapse of blood vessels at the centre of the tumour and a peak of proliferating tumour cells advancing towards the main blood vessels together with the regression of newly–formed capillaries. In the second part of the chapter, we conduct a travelling wave analysis on a simplified version of the model and obtain bounds on the parameters such that the solutions are non-negative and hence biologically relevant. Furthermore, we obtain an estimate for the speed of invasion of the host tissue by the tumour cells.

4.1 The mathematical model

This model examines the development of the tumour vascular envelope from the onset of vascularization to the eventual invasion of the (parent) blood vessel which may consequently lead to metastasis. We assume that the tumour has successfully induced angiogenesis, that is, a network of capillary vessels has just reached the tumour boundary. We do not explicitly model the concentration of TAF, though this is implicitly incorporated into the model by presuming that the TAF indirectly influences vessel proliferation.

Following Liotta *et al.*, (1977), let $n_1(\mathbf{x},t)$ be the tumour cell density per unit volume and $n_2(\mathbf{x},t)$ be the density or surface area of capillary vessels per unit volume. Conservation of mass gives us

$$\frac{\partial n_1}{\partial t} + \nabla.\mathbf{J_1} = f(n_1,n_2), \tag{4.1.1}$$

$$\frac{\partial n_2}{\partial t} + \nabla.\mathbf{J_2} = g(n_1,n_2), \tag{4.1.2}$$

where $\mathbf{J}_i$, $i = 1,2$, is the cell flux and $f(n_1,n_2)$ and $g(n_1,n_2)$ are functions describing interactions between tumour cells and capillary vessels. These also contain source and sink terms which will be made explicit below. We assume that there is a small amount of random motion of both tumour cells and capillary vessels which can be modelled by a diffusion term with constant diffusion coefficient, i.e. $\mathbf{J}_i = -D_i\nabla n_i$, $i = 1,2$. Many mathematical models of prevascular tumours rely solely on diffusion as a mechanism for tumour growth [Adam & Maggelakis, (1990)], [Greenspan, (1972)]. In a malignant invasive tumour, there is clearly a movement of tumour cells into the capillary mass. Indeed, the appearance of metastases is a clear indication that tumour cells have invaded the blood system [Darling & Tarin, (1990)]. We assume that tumour cells react to blood vessels in a similar manner to that of 'taxis', that is, the tumour cells move up a gradient of capillary vessels. Hence the flux of tumour cells is given by

$$\mathbf{J_1} = \mathbf{J}_{\text{diffusion}} + \mathbf{J}_{\text{taxis}} = -D_1\nabla n_1 + \chi n_1 \nabla n_2, \tag{4.1.3}$$

where, for simplicity, we assume χ is a constant.

The functions f and g are carefully chosen to describe the particular behaviour and interaction of the tumour cells and blood vessels.

For the tumour proliferation rate, we assume that during its avascular stage the tumour has reached its maximum size and has become dormant. Folkman (1985) reports that tumour cells lying nearest to a capillary have the highest [^{3}H]thymidine labelling index and that the index decreases as the distance from the capillary increases. Hence we assume that the proliferation rate is dependent on the surface area of capillary vessels n_2. We also assume that, given an adequate supply of nutrients, the proliferation of tumour cells is very rapid since tumour-induced angiogenesis can continue indefinitely until the tumour is eradicated or the host dies [Folkman, (1985)]. Hence we model the tumour cell proliferation rate by rn_1n_2.

The vascular proliferation rate is assumed to be of a Michaelis-Menten form which saturates as n_2 increases, so that there is a finite limit to the proliferation rate. The normal turnover rate of endothelial cells is quite low on the time-scale that we are considering [Paweletz & Knierim, (1989)]. In normal endothelium, the labelling index was found to be as low as 0.01% per hour in some cases [Denekamp, (1984)]. The proliferation of capillary vessels is initiated by the release of TAF and so is dependent on the density of tumour cells n_1. We therefore take the vessel proliferation term to be $\frac{Sn_1n_2}{\beta + n_2}$.

In this model we assume that the main cause of tumour cell death is nutrient deficiency [Denekamp, (1984)]. Capillary vessels may fail to reach some parts of the tumour or tumour cell overcrowding and high internal pressure may cause the vessels to collapse [Denekamp, (1984)], [Jain, (1994)]. If the oxygen concentration in a tumour cell is inadequate for normal cell functions, the cell becomes hypoxic which leads to a reduction in cell activity. A hypoxic cell can return to normal if nutrient levels increase but will eventually die if deprived of oxygen for too long. In this model we assume that once a cell has become hypoxic it will subsequently die. In the discussion section we will suggest a way of incorporating temporarily hypoxic tumour cells into a model. Let N_2 be some reference vessel surface area such as the surface area per unit volume at the point of vascularization. We choose $\alpha n_1(1 - \tanh((n_2 - N_2)/N_2))$ as our tumour cell death term as this gives us a smooth switch from high to low death as n_2 increases, which is qualitatively what is desired. Furthermore, there is a finite limit to tumour cell death as $n_2 \to 0$, which suggests that the tumour becomes increasingly necrotic as the nutrients in its environment decrease (figure(4-1a)).

The death of vasculature is mainly due to the overcrowding of vessels and tumour

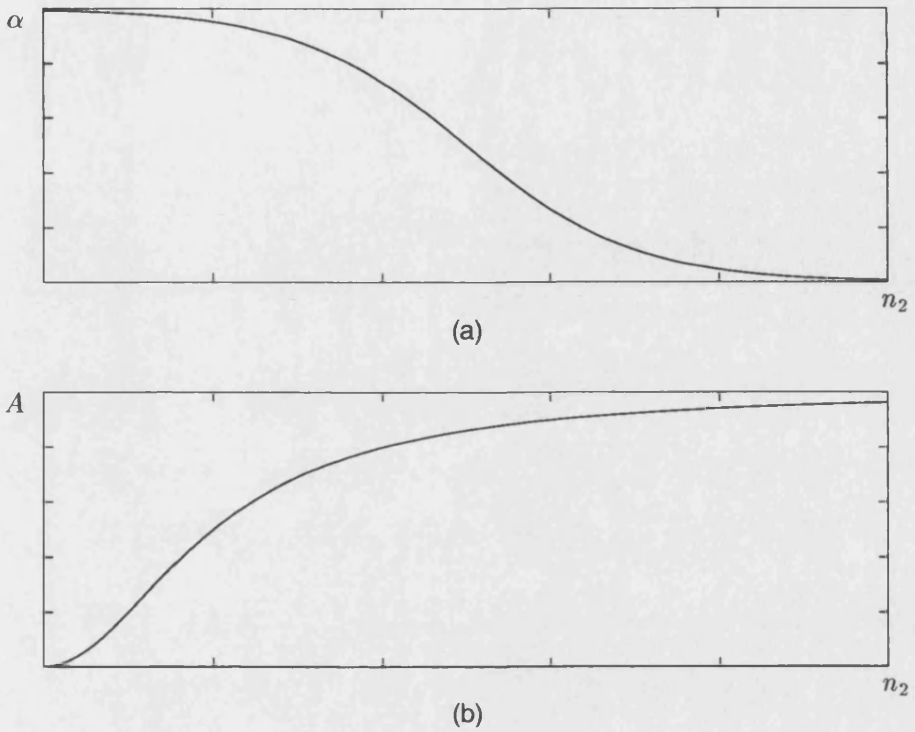

Figure 4-1: *The qualitative forms of the two cell death terms. Figure (a) is a typical tumour cell death term* $\alpha(1 - \tanh((n_2 - N_2)/N_2))$ *while figure (b) shows the vessel death term* $An_2^2/B + n_2^2$.

cells, and hence we would expect a sharp increase in vessel death as n_2 increases and also a term which depends on n_1. We therefore chose $\dfrac{An_1n_2^2}{B+n_2^2}$ as our vessel death term. This term has previously been used to describe spruce budworm death due to overcrowding and predation [Ludwig *et al.*, (1978)]. In a similar manner, tumour cells invade the blood vessels which collapse due to the massive increase in tumour volume (figure(4-1b)).

Hence, the reaction terms f and g are

$$f(n_1, n_2) = rn_1n_2 - \alpha n_1\left(1 - \tanh\frac{(n_2 - N_2)}{N_2}\right), \tag{4.1.4}$$

$$g(n_1, n_2) = \frac{Sn_1n_2}{\beta + n_2} - \frac{An_1n_2^2}{B + n_2^2}. \tag{4.1.5}$$

As stated in the introduction, we assume that the tumour is a solid spherical mass and that all growth is in the radial direction only, i.e. we have radial symmetry. If

R is the distance from the centre of the tumour, under the assumptions made on f and g, and from equations (4.1.1) and (4.1.2), we therefore have the following partial differential equation model for vascular tumour growth and invasion:

$$\frac{\partial n_1}{\partial t} = \frac{D_1}{R^2}\frac{\partial}{\partial R}\left(R^2\frac{\partial n_1}{\partial R}\right) - \frac{1}{R^2}\frac{\partial}{\partial R}\left(R^2\chi n_1\frac{\partial n_2}{\partial R}\right) + rn_1n_2 - \alpha n_1\left(1-\tanh\frac{(n_2-N_2)}{N_2}\right), \quad (4.1.6)$$

$$\frac{\partial n_2}{\partial t} = \frac{D_2}{R^2}\frac{\partial}{\partial R}\left(R^2\frac{\partial n_2}{\partial R}\right) + \frac{Sn_1n_2}{\beta+n_2} - \frac{An_1n_2^2}{B+n_2^2}. \quad (4.1.7)$$

We now non-dimensionalize the above system in the usual way. Let L be some reference length such as the distance from the tumour boundary to the parent vessel, let $\tau = L^2/D_2$ be our reference time and N_1 a reference tumour cell density. By making the following substitutions;

$$n_1^* = \frac{n_1}{N_1},\ n_2^* = \frac{n_2}{N_2},\ R^* = \frac{R}{L},\ t^* = \frac{t}{\tau},$$

$$D = \frac{D_1}{D_2},\ \chi^* = \frac{\chi N_2}{D_2},\ r^* = rN_2\tau,\ \alpha^* = \alpha\tau,$$

$$\beta^* = \frac{\beta}{N_2},\ B^* = \frac{B}{N_2^2},\ A^* = \frac{AN_1\tau}{N_2},\ S^* = \frac{SN_1\tau}{N_2},$$

and dropping the asterisks for notational convenience, we obtain the dimensionless system

$$\frac{\partial n_1}{\partial t} = \frac{D}{R^2}\frac{\partial}{\partial R}\left(R^2\frac{\partial n_1}{\partial R}\right) - \frac{1}{R^2}\frac{\partial}{\partial R}\left(R^2\chi n_1\frac{\partial n_2}{\partial R}\right) + rn_1n_2 - \alpha n_1\left(1-\tanh(n_2-1)\right), \quad (4.1.8)$$

$$\frac{\partial n_2}{\partial t} = \frac{1}{R^2}\frac{\partial}{\partial R}\left(R^2\frac{\partial n_2}{\partial R}\right) + \frac{Sn_1n_2}{\beta+n_2} - \frac{An_1n_2^2}{B+n_2^2}. \quad (4.1.9)$$

To close the system we impose the following boundary conditions;

$$\frac{\partial n_1}{\partial R} = 0,\ \frac{\partial n_2}{\partial R} = 0,\ \text{at } R = 0, \qquad \frac{\partial n_1}{\partial R} = 0,\ n_2 = 1,\ \text{at } R = 0.$$

The first set of boundary conditions arises naturally from the symmetry of the system. The position $R = 1$ corresponds to the location of the parent vessels (e.g. limbus). Once the tumour cells reach the right-hand boundary the assumptions of the model will no longer hold, since other interactions become important (e.g. the active invasion of the limbus by the tumour cells). Various initial conditions will be considered in section 4.1.2.

4.1.1 Estimation of parameters

Whenever possible experimental data was used to estimate our parameter values. Where this was difficult, we chose parameters that gave the correct qualitative behaviour of the tumour cells and the blood vessels.

A summary of data on corneal implants was given by Balding & McElwain, (1985). A tumour will successfully induce angiogenesis if placed at a distance between 0.8mm [Muthukkaruppan *et al.*, (1982)] and 3mm [Gimbrone *et al.*, (1974)] from the limbal vessels. The time for vascularization is approximately 8 to 12 days [Ausprunk & Folkman, (1977)], [Gimbrone *et al.*, (1974)], [Muthukkaruppan *et al.*, (1982)]. This gives a value for $D_2 \simeq 10^{-7}\text{cm}^2\text{s}^{-1}$, for $\tau \simeq 10$ days and $L \simeq 0.3$cm. Sherratt & Murray, (1990) estimated the diffusion coefficient of cells in their model of epidermal wound healing and used diffusion coefficients ranging from $3\times10^{-9}\text{cm}^2\text{s}^{-1}$–$6.9\times10^{-11}\text{cm}^2\text{s}^{-1}$. In their study of individual endothelial cells, Stokes *et al.*, (1991) measured the motility parameters for endothelial cells. The mean random motility coefficient for endothelial cells, migrating in a medium containing the angiogenic factor αFGF, was $7.1 \pm 2.7 \times 10^{-9}\text{cm}^2\text{s}^{-1}$. A reasonable estimate of the diffusion coefficient of tumour cells would be in the range 10^{-9} to $10^{-11}\text{cm}^2\text{s}^{-1}$. This would give a range for D of 10^{-4} to 10^{-2}. We would expect the diffusion of tumour cells to be small in comparison with the directed movement of the tumour cells in response to a gradient of blood vessels, which is clear from experimental studies. We therefore chose the taxis coefficient to be ten times that of the tumour cell diffusion, so that, with $N_2 = 10^3$, an approximate range for χ is 1 to 100. The parameter r corresponds to the tumour proliferation rate which we would expect to be fairly high since we are modelling aggressive invasion. If tumour cell proliferation was about 0.1% per hour then $r \sim O(10^2)$. α represents the maximum death rate in the absence of capillary vessels. Denekamp, (1984) stated that the lifespan of a nutrient-deprived hypoxic cell is 5 to 10 hours. The proportion of hypoxic cells in a tumour can

be up to 80% . Hence a reasonable range for α is 1–20. For the capillary vessels, the parameters S and A represent the maximum proliferation and death rates respectively, whereas β and B are measures of the critical value at which proliferation or death is switched on. A low value of β or B means a low threshold. The tumour's vasculature is highly vulnerable [Paweletz & Knierim, (1989)], [Denekamp, (1984)] and hence we chose a low death threshold value, $B = 0.01$, and a high maximum death rate, $A = 100$, in comparison to the proliferation threshold, $\beta = 1$, and the maximum proliferation rate $S = 10$.

4.1.2 Numerical simulations

The system of equations was solved using a routine available from the NAG library which integrates the system using the method of lines and Gear's method. Three different sets of initial conditions were used and these are shown in figure (4-2).

In the first case, we tried similar initial conditions to those used by Liotta *et al.*, (1977) in their model of tumour vascular growth, i.e. unit step functions (figure (4-2a)). Assuming that the tumour is placed at a distance of 3mm from the parent vessel and that its radius is about 1mm, we take the tumour boundary to be situated at $R = 0.25$. The results are given in figure (4-3). Figure (4-3a) shows a peak of tumour cells moving across the domain towards the parent vessel and there is a decline in tumour cell density at the centre, indicating that a necrotic core is beginning to develop. Figure (4-3b) shows that the capillary vessels have infiltrated the tumour mass and they have slightly regressed from the advancing front of tumour cells. However, the vessels have not, as would be expected, degenerated at the centre of the tumour.

In the second case, a more realistic initial profile for the tumour cells was chosen with a Gaussian distribution of cells centred at $R = 0.2$ (figure (4-2b)). This corresponds to a newly vascularized tumour nodule with central necrosis surrounded by a layer of live proliferating and highly mobile tumour cells. Again, the results show (figure (4-4a)) a peak of advancing tumour cells penetrated by capillaries. Figure (4-4b) shows that the regression of vessels is slightly more pronounced and after time $t = 0.03$ the density of vessels at the centre of the tumour begins to decrease, which is an improvement on the simulations shown in figure (4-3b).

Finally, we took an initial profile of capillary vessels from a model of angiogenesis by Chaplain & Stuart, (1993) (figure (4-2c)). The taxis coefficient χ is reduced in

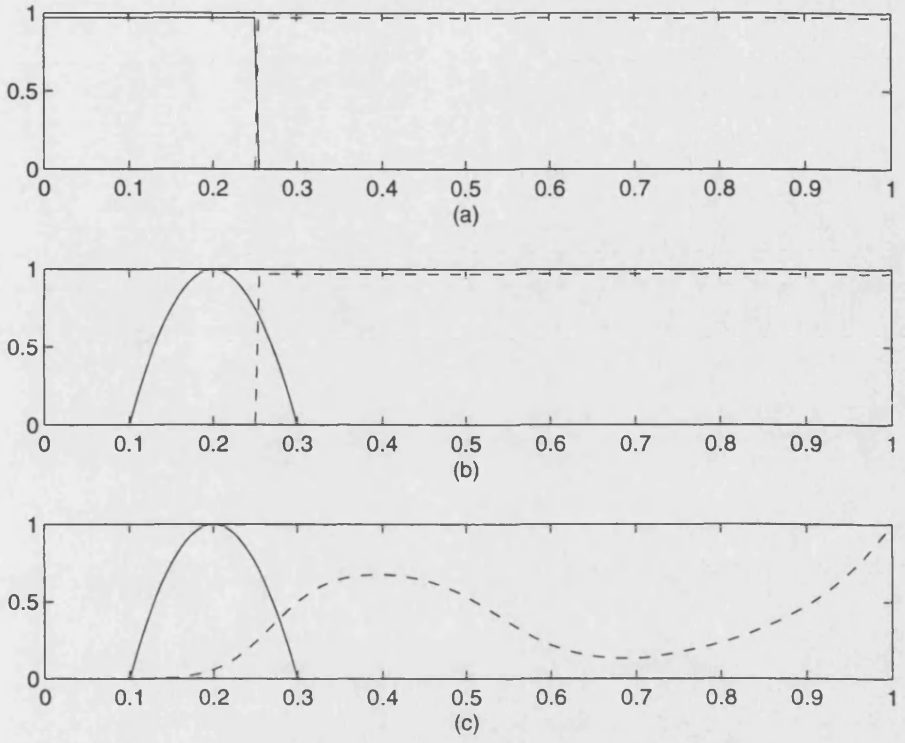

Figure 4-2: *The three different initial conditions used to test the model. The solid line represents the tumour cell distribution and the dashed line represents the vessel density. In figure (a) we have a block distribution of tumour cells and vessels. In figure (b) we have a Gaussian distribution of tumour cells centred at 0.2. In figure (c) we have the same Gaussian distribution for the tumour cells but for the vessels we have taken a profile from the model of angiogenesis by Chaplain & Stuart, (1993).*

order to allow more time for the overcrowding to take effect and also the tumour cell proliferation rate r was increased. Figure (4-5a) shows an advancing peak of tumour cells and a substantial increase in tumour cell density with time. Figure (4-5b) shows that the capillaries have penetrated the tumour mass but have collapsed at the centre and the vasculature within the tumour has regressed considerably.

We note that the qualitative form of the numerical solutions are wave-like. We can estimate the speed of the wave by examining the numerical solutions. For the first two simulations (figures (4-3) and (4-4)), we estimate that the dimensionless wavespeed varies between 11–15. With $L = 0.3$cm as a reference length and $\tau = 10$ days as a reference time, this gives a speed of invasion in the range of 3.3–4.5mm/day, which is quite high. In the last simulation (figure 4-5), which has the most realistic initial conditions

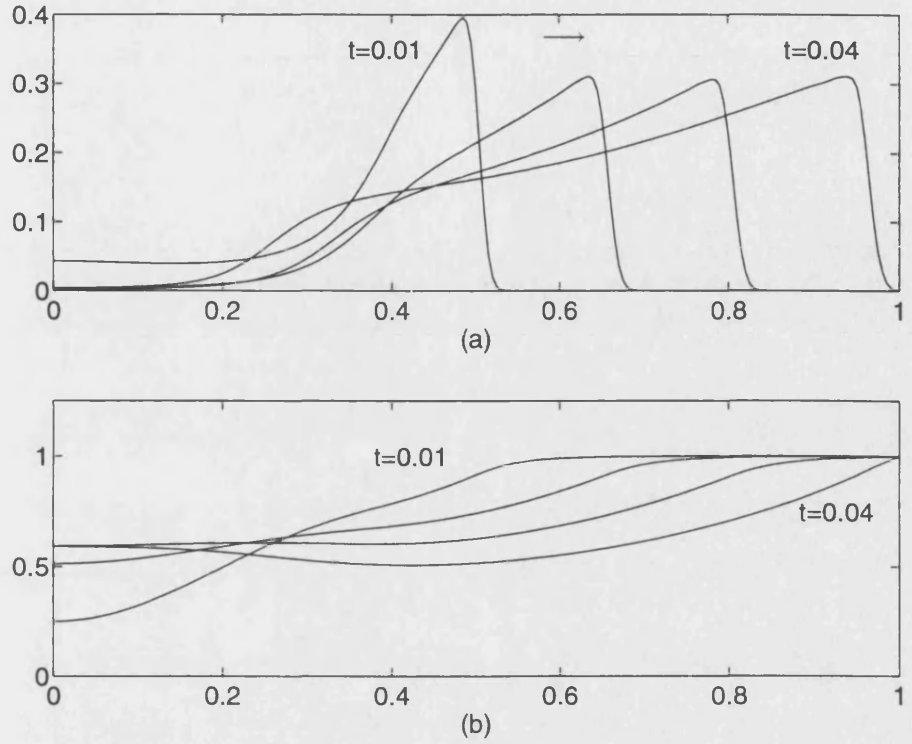

Figure 4-3: *With block initial conditions for the tumour cells and the vessels the system evolves as shown above. Figure (a) shows the tumour cells distribution and figure (b) the vessels. Plots were taken at times* $t = 0.01$, *0.02, 0.03 and 0.04. Parameters values were* $D = 0.01$, $\chi = 10$, $r = 100$, $\alpha = 10$, $S = 10$, $\beta = 1$, $A = 100$, $B = 0.01$.

and which best captures the key behaviour of the nascent tumour, the dimensionless wavespeed is approximately 4.5–5. This corresponds to an invasion speed of 1.4mm/day–1.5mm/day. This is not unreasonable given the simplicity of the model, though slightly overestimated in comparison to experimental observations of 0.2–0.5mm/day [Gimbrone *et al.*, (1974)] and 0.4–0.7mm/day [Shymko & Glass, (1976)]. We will suggest ways of reducing the wavespeed in the discussion section. In the next section we will investigate the possibility of travelling wave solutions with constant speed and profile.

4.2 Travelling wave analysis

In this section, we conduct a travelling wave analysis of the system of partial differential equations (4.1.8)–(4.1.9). We modify the original model by replacing the proliferation

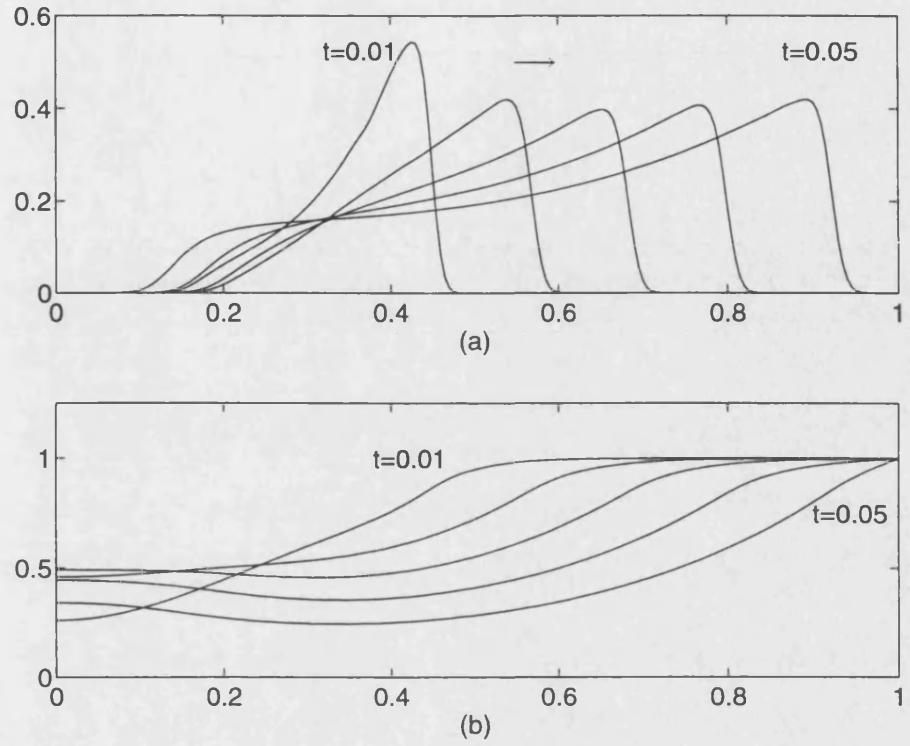

Figure 4-4: *With a Gaussian distribution of tumour cells and block initial conditions for the vessels the system evolves as shown. Figure (a) shows the tumour cell density while figure (b) shows the vessel distribution. Plots were taken at times* $t = 0.01$, *0.02, 0.03, 0.04 and 0.05. Parameters values were* $D = 0.01$, $\chi = 5$, $r = 100$, $\alpha = 10$, $S = 10$, $\beta = 1$, $A = 100$, $B = 0.01$.

term for the blood vessels by the logistic growth term $Sn_2(1 - n_2)$, where, once again the parameter S is dimensionless. The use of this term can be justified by assuming that the blood vessels have been saturated by TAF and hence the proliferation of vessels is independent of tumour cell density. Given that the rate of growth of the vascularized tumour is rapid, the tumour mass quickly increases in size [Gimbrone *et al.*, (1974)], [Muthukkaruppan *et al.*, (1982)]. We therefore conduct the travelling wave analysis using Cartesian coordinates as follows:

$$\frac{\partial n_1}{\partial t} = D\frac{\partial^2 n_1}{\partial x^2} - \chi\frac{\partial}{\partial x}\left(n_1\frac{\partial n_2}{\partial x}\right) + rn_1n_2 - \alpha n_1(1 - \tanh(n_2 - 1)), \quad (4.2.10)$$

$$\frac{\partial n_2}{\partial t} = \frac{\partial^2 n_2}{\partial x^2} + Sn_2(1 - n_2) - \frac{An_1n_2^2}{B + n_2^2}. \quad (4.2.11)$$

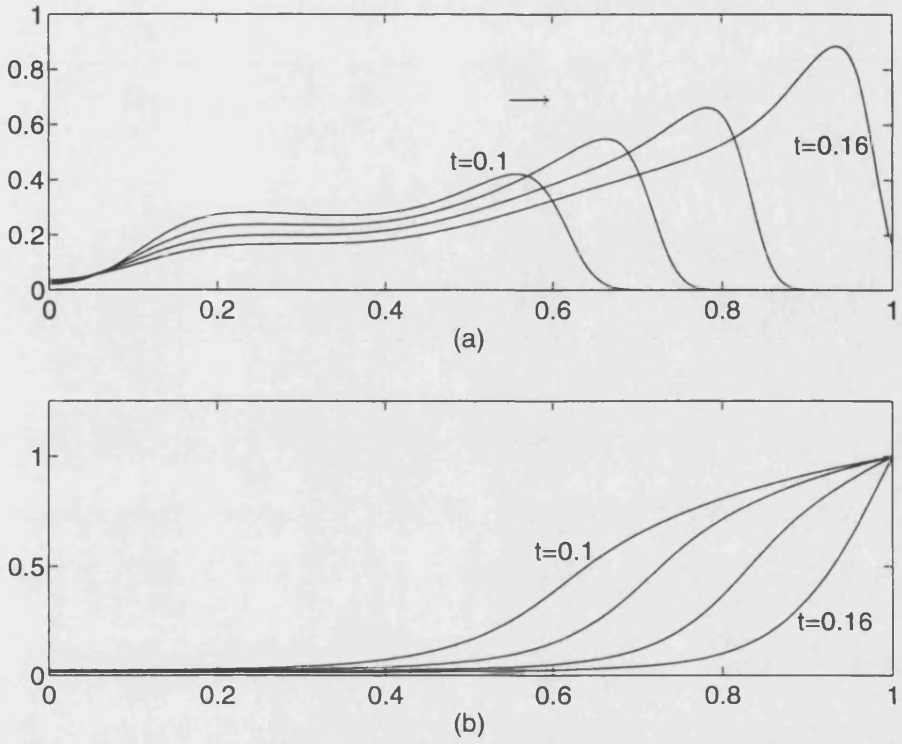

Figure 4-5: *With an initial profile for the vessels taken from Chaplain & Stuart, (1993) the system will evolve as shown. Figure (a) shows the tumour cell density while figure (b) shows the vessel distribution. Plots were taken at times* $t = 0.1$, *0.12, 0.14 and 0.16. Parameters values were* $D = 0.01$, $\chi = 1$, $r = 200$, $\alpha = 7$, $S = 10$, $\beta = 1$, $A = 100$, $B = 0.01$.

Numerical simulations of the above system do not vary significantly from the numerical simulations of the original system (see figure (4-6)).

The spatially homogeneous steady states are given by $(0,0)$, $(0,1)$ and $(n_1^\star, n_2^\star)$ where

$$n_1^\star = \frac{S(1-n_2^\star)(B+n_2^{\star 2})}{An_2^\star}, \tag{4.2.12}$$

and $n_2^\star$ uniquely satisfies

$$rn_2^\star - \alpha(1-\tanh(n_2^\star - 1)) = 0. \tag{4.2.13}$$

We look for solutions of the form $N_1(z) = n_1(x,t)$, $N_2(z) = n_2(x,t)$, where $z = x - ct$,

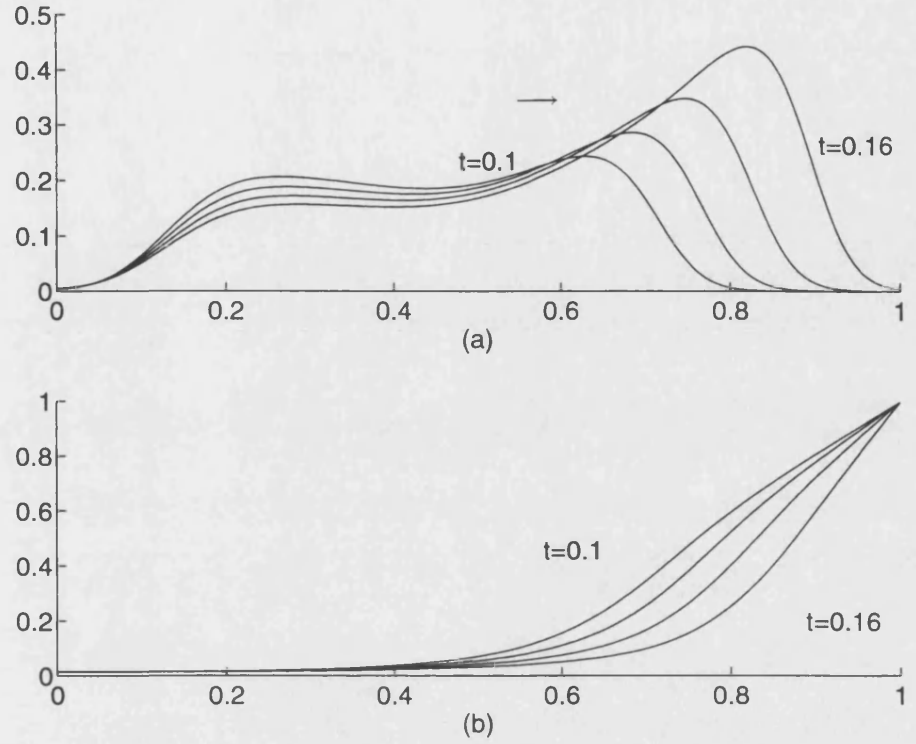

Figure 4-6: *A numerical simulation of the system (4.2.10)–(4.2.11) with initial profile for the vessels taken from Chaplain & Stuart, (1993). The solution compares well with figure (4-5). Figure (a) shows the tumour cell density while figure (b) shows the vessel distribution. Plots were taken at times* $t = 0.1$, *0.12, 0.14 and 0.16. Parameters values were* $D = 0.01$, $\chi = 1$, $r = 200$, $\alpha = 7$, $S = 10$, $\beta = 1$, $A = 100$, $B = 0.01$.

c being a constant positive wave speed, so that the waves travel from the left to the right along the x axis. Using the notation $'$ to denote differentiation with respect to z, we obtain a fourth order system of ordinary differential equations

$$-cN_1' = DN_1'' - \chi(N_1N_2')' + rN_1N_2 - \alpha N_1(1 - \tanh(N_2 - 1)), \quad (4.2.14)$$

$$-cN_2' = N_2'' + SN_2(1 - N_2) - \frac{AN_1N_2^2}{B + N_2^2}. \quad (4.2.15)$$

The appropriate boundary conditions are given below, i.e. non-negative solutions

satisfying

$$\begin{aligned} N_1(-\infty) &= n_1^* \quad , \quad N_1(+\infty) = 0, \\ N_2(-\infty) &= n_2^* \quad , \quad N_2(+\infty) = 1, \\ N_1'(\pm\infty) &= 0 \quad , \quad N_2'(\pm\infty) = 0. \end{aligned} \tag{4.2.16}$$

Waves satisfying (4.2.16) can be described as 'waves of invasion' [Dunbar, (1983)]. In this case, we have one population at its carrying capacity. Introducing a small amount of another species, the system evolves to a new steady state of co-existence where the original population has decreased and the new species has increased. From this description of invasion, we infer $n_2^* < 1$. In the biological situation that we are considering, tumour cells invade a population of endothelial cells.

We analyse the system (4.2.14) and (4.2.15) by considering two cases. First, we will simplify the system by setting $D = 0$, which is the limiting case of D small. In this case the vessels are diffusing much faster than the tumour cells. This implies that there is little random motion of tumour cells, therefore the emphasis is on the directed movement of tumour cells into the capillary vessels. Secondly, we consider D non zero.

Dunbar, (1983) gave a formal proof of the existence of travelling wave solutions for a predator-prey system with $D = 0$. Using a similar technique (a shooting argument), Dunbar went on to show a heteroclinic connection in $\mathbf{R}_4$, between the unstable steady state and the stable co-existence state for the case when $0 < D \leq 1$ [Dunbar, (1984)].

4.2.1 Case 1: $D = 0$.

Letting $W = N_2'$, we obtain the following system of 3 first-order ordinary differential equations:

$$\begin{aligned} N_1' &= \left(\frac{1}{\chi W - c}\right)[rN_1N_2 - \alpha N_1(1 - \tanh(N_2 - 1)) \\ &\qquad + \chi N_1(SN_2(1 - N_2) - \frac{AN_1N_2^2}{B + N_2^2} + cW)], \qquad (4.2.17) \\ N_2' &= W, \qquad (4.2.18) \\ W' &= \frac{AN_1N_2^2}{B + N_2^2} - SN_2(1 - N_2) - cW. \qquad (4.2.19) \end{aligned}$$

To remove the singularity at $W = \frac{c}{\chi}$, let $(\chi W - c)\frac{d}{dz} = \frac{d}{d\xi}$. Hence we obtain the following system:

$$\frac{dN_1}{d\xi} = rN_1N_2 - \alpha N_1(1 - \tanh(N_2 - 1)) + \chi N_1(SN_2(1 - N_2) - \frac{AN_1N_2^2}{B + N_2^2} + cW), \quad (4.2.20)$$

$$\frac{dN_2}{d\xi} = W(\chi W - c) \quad (4.2.21)$$

$$\frac{dW}{d\xi} = (\frac{AN_1N_2^2}{B + N_2^2} - SN_2(1 - N_2) - cW)(\chi W - c). \quad (4.2.22)$$

We carry out a phase plane analysis in the usual way by linearizing about each critical point to obtain a system of the form

$$\frac{d\mathbf{X}}{d\xi} = A\mathbf{X}, \text{ where } \mathbf{X} = (N_1, N_2, W)^T$$

and A is a 3×3 Jacobian matrix which has been evaluated at the critical point. The eigenvalues are then given by $\det(A - \lambda I)$=0. Using the notation A_{ij} to denote the element in the i^{th} row and j^{th} column of the matrix A, we obtain

$$\lambda^3 - \lambda^2(A_{11} + A_{33}) + \lambda(A_{11}A_{33} - A_{13}A_{31} - A_{23}A_{32}) + A_{11}A_{23}A_{32} - A_{12}A_{23}A_{31} = 0. \quad (4.2.23)$$

since A_{21} and A_{22} are always zero when evaluated at any of the critical points. The analysis of this phase space is given in appendix (A). A summary of the results are as follows.

- The critical point (0,0,0) is a stable node if $c^2 < \alpha(1 + \tanh 1) < S$. Otherwise, the critical point is a saddle point.
- For non-negative solutions passing through (0,0,0), the parameters must satisfy equations (A.1.4) and (A.1.5) as given in the appendix.
- Since $r > \alpha$ from equation (4.2.13), the critical point (0,1,0) is a saddle.
- For non-negative solutions passing through (0,1,0), the parameters must satisfy equations (A.1.7) and (A.1.8).

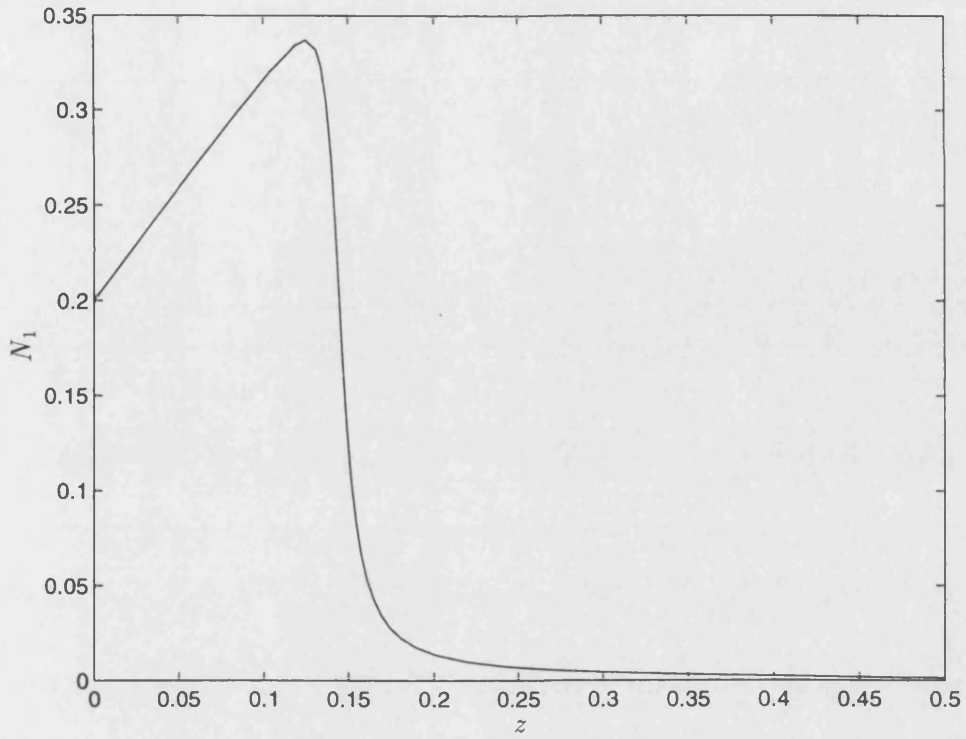

Figure 4-7: *Profile of tumour cells invading capillary network. Profile obtained from numerical solution to (4.2.20)-(4.2.22)* .

- The critical point $(n_1^\star, n_2^\star, 0)$ is a stable node if $c^2 < \chi S n_2^\star(1 - n_2^\star)$, otherwise it is a saddle.

We solved the system of equations (4.2.20)-(4.2.22) using an ODE solver implemented in MATLAB with the parameters $D = 0$, $\chi = 10$, $r = 100$, $\alpha = 10$, $S = 10$, $\beta = 1$, $A = 100$, $B = 0.01$ and the wavespeed $c = 16.9$ which was derived from conditions (A.1.7) and (A.1.8). Figures (4-7) and (4-8) show the profiles of the wave front for the tumour cell density and the vessel density respectively. Qualitatively, they illustrate the advance of the region of proliferating tumour cells with the collapse of the vasculature in its wake.

4.2.2 Case 2: $D > 0$

Letting $U = N_1'$ and $V = N_2'$, we obtain the following system of 4 ODE's:

$$N_1' = U, \tag{4.2.24}$$

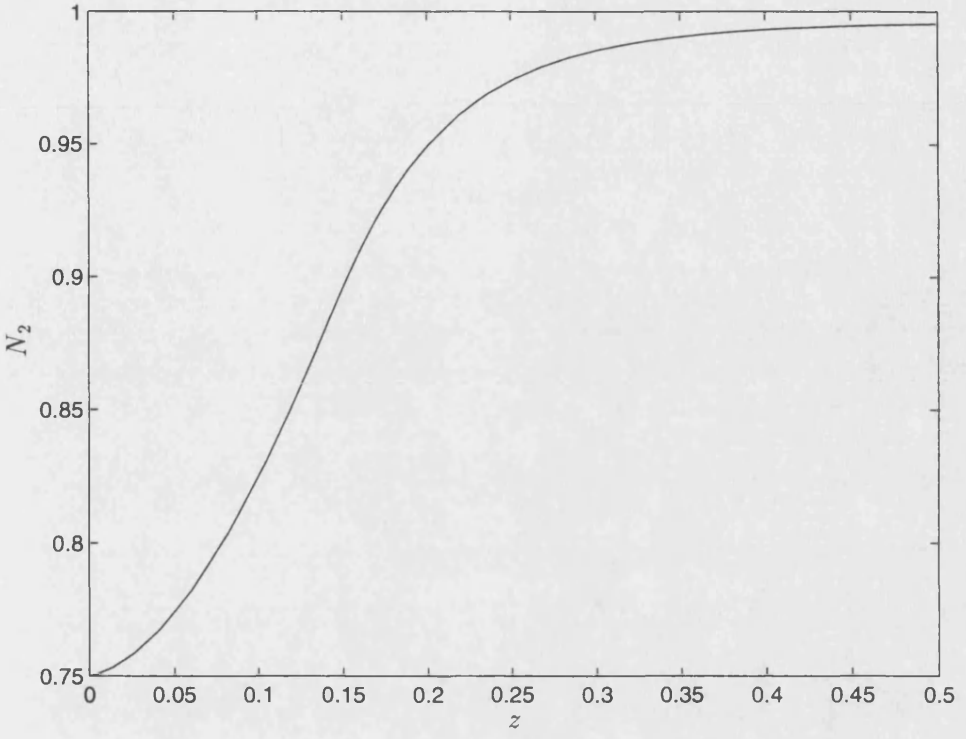

Figure 4-8: *Profile of vessel density being invaded by tumour cells. Profile obtained from numerical solution to (4.2.20)-(4.2.22) .*

$$N_2' = V, \tag{4.2.25}$$

$$U' = \frac{1}{D}[\chi(UV + N_1(\frac{AN_1N_2^2}{B+N_2^2} - SN_2(1-N_2) - cV)) + \alpha N_1(1 - \tanh(N_2 - 1)) - rN_1N_2 - cU], \tag{4.2.26}$$

$$V' = \frac{AN_1N_2^2}{B+N_2^2} - SN_2(1-N_2) - cV. \tag{4.2.27}$$

We carry out a phase plane analysis in the usual way by linearizing about each critical point to obtain a system of the form

$$\frac{d\mathbf{X}}{dz} = A\mathbf{X}, \text{ where } \mathbf{X} = (N_1, N_2, U, V)^T$$

and A is a 4×4 Jacobian matrix which has been evaluated at the critical point. The eigenvalues are then given by $\det(A - \lambda I)=0$. Using the notation A_{ij} to denote the

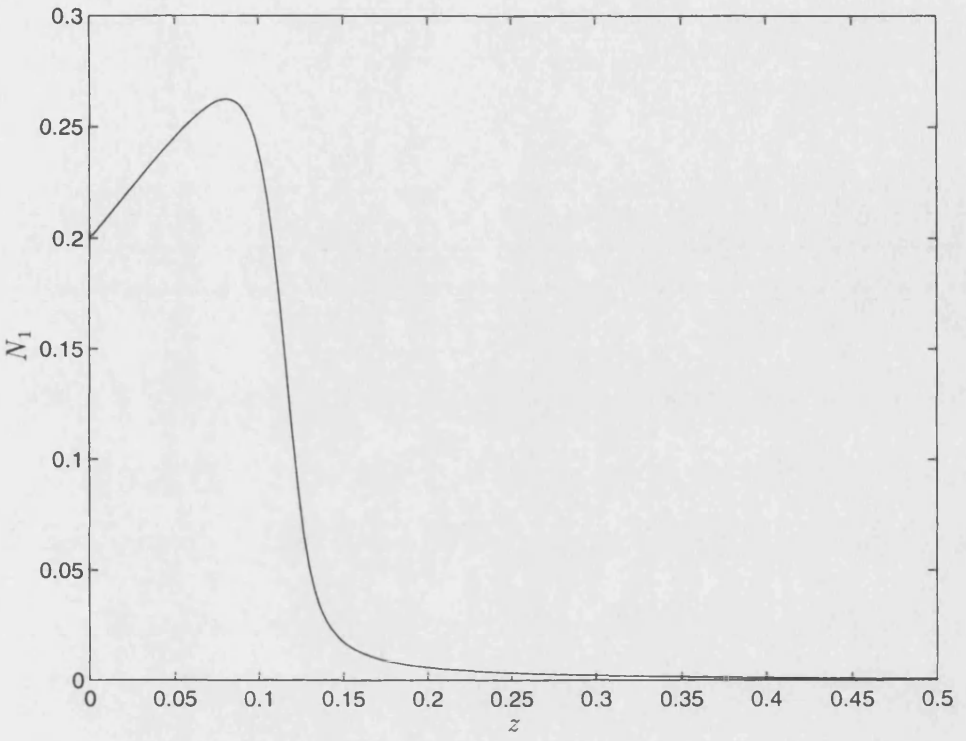

Figure 4-9: *Profile of tumour cells invading capillary network. Profile obtained from numerical solution to (4.2.24)-(4.2.27).*

element in the i^{th} row and j^{th} column of the matrix A, we obtain

$$\begin{aligned} \lambda^4 &+ \lambda^3(c - A_{33}) - \lambda^2(A_{42} + A_{31} + cA_{33}) \\ &+ \lambda(A_{33}A_{42} - cA_{31} - A_{34}A_{41}) + A_{31}A_{42} - A_{32}A_{41} = 0. \end{aligned} \tag{4.2.28}$$

The analysis of this phase space is given in appendix (A). A summary of the results are as follows.

- The condition $S < \alpha(1 + \tanh 1)$ is sufficient to ensure that the critical point (0,0,0,0) has an unstable manifold.
- The critical point (0,1,0,0) is a saddle since $r > \alpha$.
- The critical point $(n_1^\star, n_2^\star, 0, 0)$ is a stable node if $\frac{1}{27} > B > 0$ and $c^2 < \chi S n_2^\star(1-n_2^\star)$, otherwise it is a saddle.

Again, we solved the system of equations (4.2.24)-(4.2.27) using MATLAB with the

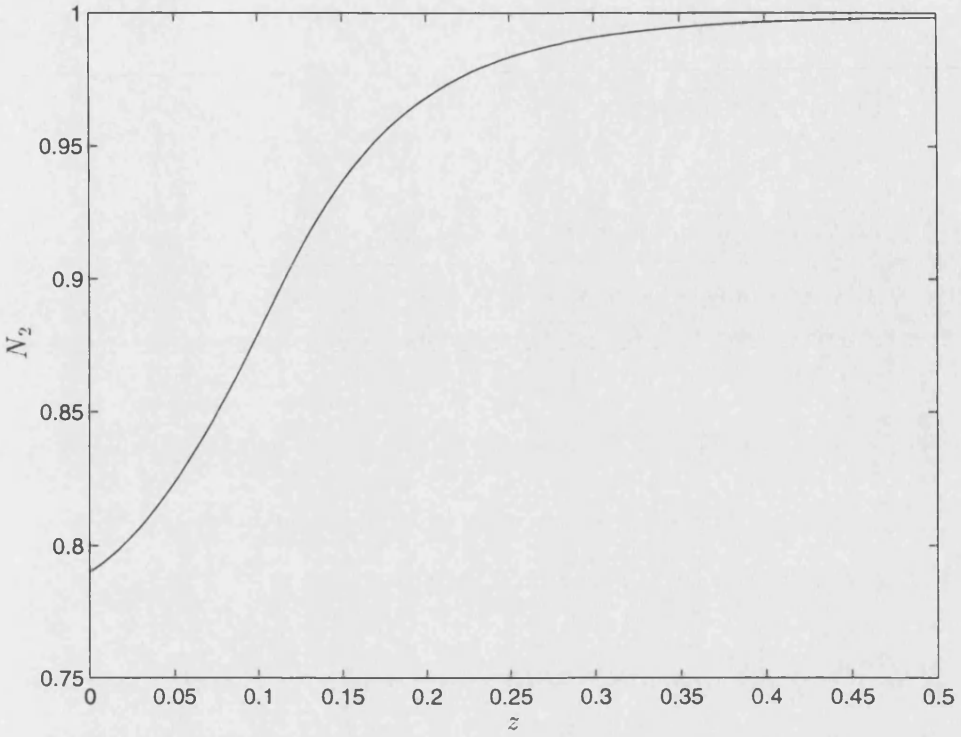

Figure 4-10: *Profile of capillary vessel density which is invaded by tumour cells. Profile obtained from numerical solution to (4.2.24)-(4.2.27).*

parameters $D = 0.01$, $\chi = 10$, $r = 100$, $\alpha = 10$, $S = 10$, $\beta = 1$, $A = 100$, $B = 0.01$ and the wavespeed $c = 15$ which was measured from the original numerical solutions of the PDE's. Figures (4-9) and (4-10) show the profiles of the wave front for the tumour cell density and the vessel density respectively. Once again the figures illustrate the advancing front of invading tumour cells leaving behind a compressed vasculature in its wake.

4.3 Discussion

We have developed a simple (minimal) mathematical model which has captured the key initial events of vascular invasive tumour growth such as the migrating front of tumour cells, central necrosis and the regression of blood vessels. The advance of tumour cells across the host tissue field is attributed to a combination of diffusion, active migration and proliferation of tumour cells. Liotta *et al.*, (1977) explains central necrosis as a failure of new blood vessels to reach the centre of the tumour fast enough. However,

shortly after vascularization, the whole of the tumour is criss-crossed by capillaries [Paweletz & Knierim, (1989)], with necrosis reappearing later. Hence, in this model the development of a necrotic core is due to overcrowding and the eventual collapse of the blood vessels at the centre of the tumour.

We note that the model is (necessarily) a simple one and neglects several features of tumour growth. For example, we do not consider the effect of extravascular pressure or the compression of host tissue which can obstruct the flow of blood to the tumour cells [Folkman, (1985)]. [Denekamp, (1984)] reports on the possibility of cyclic hypoxia, that is the temporary opening and closing of vessels for a few seconds or even for a few hours. We could include temporarily and permanently hypoxic cells by developing an age-structured model. This would involve two age classes for the tumour cells with 'young' proliferating cells in one class and 'old' reduced activity cells in the other, with cells switching from class to class whenever nutrient levels were above or below some threshold value.

Alternatively, we could develop a mechanical model which focuses on cell-matrix interactions [Murray, (1989)]. In the numerical simulations, the wavespeed was slightly larger than that observed experimentally [Gimbrone *et al.*, (1974)], [Shymko & Glass, (1976)]. No doubt this is due to the fact that the model is simple and does not consider other factors which may moderate the movement of the tumour cells. The extracellular matrix has an important role to play in tumour growth, especially invasive growth, since it can influence cell adhesion and motility [Blood & Zetter, (1990)], [Carter, (1965)], [Darling & Tarin, (1990)], [Schor & Schor, (1983)].

The model also assumes radial symmetry. It is unusual for tumours to grow outward to an equal extent in all directions except when grown in a homogeneous environment, e.g. in the liver. Studies on multicellular spheroids [Durand, (1990)], [Sutherland, (1988)] have shown that there is heterogeneity in both the spatial distribution of cells and the environment. A more realistic model should take this fact into account. We will look at a model of tumour growth in a heterogeneous environment in chapter (6).

Nevertheless, in spite of these simplifications, the model produces results which are in good qualitative agreement with *in vivo* observations, and gives a quantitative estimate of the invasive speed which is reasonable given the simplicity of the model. By improving the model as suggested above, no doubt, better results and predictions will be obtained.

Chapter 5

Travelling waves for a density-dependent diffusion-reaction system modelling tumour growth and invasion

Most cancers of epithelial origin are slow growing at first and can remain localised for many years before becoming invasive and metastatic [Ruddon, (1987)]. It can be supposed that the vascularization of a tumour promotes the propagation of the more aggressively growing tumour cells. In this chapter, we wish to develop a simple mathematical model which describes the growth of a solid tumour and its transition from a slowly growing *in situ* avascular carcinoma to a more aggressively growing phenotype which invades surrounding tissue and thus is assumed to metastasise. It provides an alternative to the model found in chapter (4) as a description of the interaction between the growing tumour mass and its vasculature. The main assumption of this model is that tumour cell proliferation, death and motility are all events which are dependent upon the density of the tumour cell population, and we show that changes in the model parameters relating to these events represent changes in the malignancy of the tumour. The model presented here is intended to be qualitative, so that it is amenable

to mathematical analysis. In section (5.2) we show some mathematical results for a density-dependent diffusion-reaction equation and in particular, we show the existence of travelling wave solutions with semi-infinite support. In section (5.3), we present some numerical simulations for a single density-dependent diffusion-reaction equation which describes the growth of the tumour, as well as some simulations of a PDE system representing the interaction of the nascent tumour with its vasculature.

5.1 The mathematical model

This model examines the pattern of tumour growth subsequent to vascularization, and how an increase in the malignancy of a tumour corresponds to a decrease in control over normal cellular functions. We make the assumption that angiogenesis has successfully occurred and model the growth of the tumour and its interplay with the newly formed vasculature.

Let $u(\mathbf{x},t)$ be the dimensionless tumour cell density and $v(\mathbf{x},t)$ be the dimensionless density of the capillary vessels which are composed of endothelial cells. The conservation equations are

$$\frac{\partial u}{\partial t} + \nabla.\mathbf{J_1} = f(u,v),$$

$$\frac{\partial v}{\partial t} + \nabla.\mathbf{J_2} = g(u,v),$$

where $\mathbf{J_{1,2}}$ is the flux and $f(u,v)$, $g(u,v)$ are functions containing the appropriate source/sink terms.

It is supposed that the transformation from an *in situ* avascular carcinoma to an invasive vascularized tumour may be caused in part by the process of angiogenesis [Blood & Zetter, (1990)], [Folkman, (1985)], [Gimbrone *et al.*, (1974)], [Paweletz & Knierim, (1989)], [Ruddon, (1987)]. The sudden increase in the supply of nutrients to the tumour leads to a rapid increase in growth and the development of less well differentiated malignant cells which bear little resemblance to the tissue of origin. In culture, normal epithelial cells are self-regulated by density-dependent mechanisms, such as contact inhibition [Clark *et al.*, (1982)b], [Ruddon, (1987)], [Stoker & Rubin, (1967)], that is, they cease movement at the point of contact with another cell and stop dividing once all available space is filled. However, malignant cells *in vitro* exhibit a decrease in density-dependent inhibition of growth [Stoker & Rubin, (1967)] and a loss of contact inhibition

of movement [Ruddon, (1987)]. Hence, as a cell becomes increasingly malignant, it loses the ability to regulate its growth and additionally, it displays an increase in motility

A common characteristic of solid tumours is the development of large regions of hypoxic cells within the tumour core [Brown & Giaccia, (1994)], [Denekamp, (1984)]. These are regions where the cells are unable to function because of an inadequate nutrient supply and so become inactive. Hypoxia can also occur in other pathological conditions, for example in a stroke, where the blood vessels in the brain may become damaged or blocked so that brain cells are starved of oxygen. The vasculature of a tumour is often inferior to normal vasculature [Harris *et al.*, (1996)], [Jain, (1994)], [Paweletz & Knierim, (1989)] and is insufficient in providing nutrients to the entire tumour, particularly if the growth is rapid. In normal tissue, the cells would prevent overcrowding by regulating growth and superfluous cells would be removed by programmed cell death (apoptosis) [Mirsky, (1995)], [Strano & Blandino, (1995)]. In a tumour there is no such control, so that the tumour outgrows its vasculature and hence a large number of tumour cells die or become hypoxic.

To summarise, cell motility, mitosis and programmed cell death are all cellular functions which are regulated to some extent by the density of the surrounding cell population. In other words, they are density-dependent events. The extent to which a cell population regulates these events varies inversely with the malignancy of the cells. In normal tissue, these functions are strictly controlled in order to prevent overcrowding and an excess of cells. Many models of population dynamics use density-dependent diffusion where it is assumed that individuals disperse in order to avoid crowding [Grindrod, (1991)], [Hosono, (1986)], [Hosono, (1987)], [Murray, (1989)]. Hence, we take the flux of the tumour cells to be governed by density-dependent diffusion, i.e.

$$\mathbf{J_1} = -D_1 u^m \nabla u, \tag{5.1.1}$$

where $D_1 > 0$, $m \geq 0$ are dimensionless parameters. For $m = 0$ we have the standard Fickian diffusion and for $m > 1$ we assume that the movement of the tumour cells is controlled to a certain extent by contact inhibition, i.e cells avoid compressing other cells by moving when intercellular spaces develop, but generally stay aggregated.

We assume that the proliferation of the tumour cells is also density dependent and that proliferation is increased in areas where the density of the vasculature is above a

threshold level. Furthermore, we assume that the death of the tumour cells can either be due to a lack of intercellular space and hence low oxygen levels, i.e. hypoxia, or due to programmed cell death, depending on how much control the tumour cell exerts over its behaviour. Hence we take our reaction term $f(u,v)$ to be given by

$$f(u,v) = au^p((1+v-v_0)^q - u^q), \tag{5.1.2}$$

where a, p, $q > 0$, $1 > v_0 \geq 0$ are dimensionless parameters. a represents the net rate at which the tumour cells proliferate, p measures the dependence of the proliferation on the density of tumour cells and q is a measure of control exercised by the tumour cells in order to prevent overcrowding. If q is decreased we assume that death is now uncontrolled and mainly due to hypoxia. v_0 is the threshold level of endothelial cell density above which the tumour cells have sufficient nutrients to proliferate above the normal level.

Though we do not model it directly, we suppose that the tumour has released TAF and this has an effect on the behaviour of the vasculature. We assume that the endothelial cells are stimulated to move and do so by random motion, i.e $\mathbf{J_1} = -D_2\nabla v$ where $D_2 > 0$. We also assume that there is a background level of proliferation in addition to proliferation due to the release of TAF by the tumour cells, and that the death of the vasculature is due to a combination of self population pressures and pressures due to the uncontrolled growth of the tumour. Hence we take our reaction term $g(u,v)$ to be given by

$$g(u,v) = bv(1-u(1-v_0)-v), \tag{5.1.3}$$

where $b > 0$ is the net rate of proliferation of the endothelial cells.

For simplicity, we assume a one-dimensional Cartesian geometry, and hence our system is

$$\frac{\partial u}{\partial t} = D_1\frac{\partial}{\partial x}\left(u^m\frac{\partial u}{\partial x}\right) + au^p((1+v-v_0)^q - u^q), \tag{5.1.4}$$

$$\frac{\partial v}{\partial t} = D_2\frac{\partial^2 v}{\partial x^2} + bv(1-u(1-v_0)-v). \tag{5.1.5}$$

This model is purely qualitative, since we do not attempt to estimate the values of our parameters because of a lack of experimental data concerning the decrease in self-

regulation in tumour cells. As the tumour becomes increasingly malignant, the parameters m, p and q will change. In order to focus attention upon these more important parameters, we set $D_2 = a = b = 1$, $D_1 \ll D_2$ and, for simplicity, we consider various integer values of m, p and q.

In the next section, we will look at a system of non-linear diffusion reaction equations and show that the system can be uncoupled to obtain the single equation describing the nascent tumour, i.e.

$$\frac{\partial u}{\partial t} = \frac{\partial}{\partial x}\left(u^m \frac{\partial u}{\partial x}\right) + u^p(1 - u^q), \tag{5.1.6}$$

which has weak solutions for $m \geq 1$. Murray, (1989) discusses the equation (5.1.6) in some detail and gives some exact solutions for particular values of m, p, and q. Recently, there has been a lot of interest in non-linear diffusion equations of the form

$$\frac{\partial u}{\partial t} = \frac{\partial}{\partial x}\left(D(u)\frac{\partial u}{\partial x}\right) + f(u), \tag{5.1.7}$$

and their applications in population dynamics. In particular, if $D(u) = mu^{m-1}$ and $f(u) = 0$, we have the porous media equation which describes the flow of a fluid through an absorbent media. Grindrod & Sleeman, (1987) showed the existence and the stability of weak travelling wave front solutions of the equation $u_t = (u^2/2)_{xx} + f(u)$ where $f(u)$ is a bistable function. Satsuma, (1987) derived some explicit solutions for the equation $u_t = (u^2)_{xx} + f(u)$ for a variety of $f(u)$. More generally, the equation $u_t = (u^m)_{xx} + \lambda u^n$ has been studied by de Pablo & Vazquez, (1991) for $\lambda > 0$ and by Grundy, (1988) for $\lambda = -1$. It is well known that if $D(u)$ is such that $D(u) = 0$ for some u, then the equation is degenerate at that point and discontinuities arise in the x and t derivatives. If the initial conditions for (5.1.7) have compact support, then the solution will have compact support for all time.

5.2 Travelling wave analysis of a density-dependent diffusion-reaction equation

Firstly, we shall show some results regarding the following system of equations:

$$u_t = \epsilon^2(u^m u_x)_x + f(u, v), \tag{5.2.8}$$

$$v_t = v_{xx} + g(u, v), \tag{5.2.9}$$

where $m \geq 1$ and $\epsilon > 0$. Note that when $u = 0$, the nonlinear diffusion term vanishes and the equation (5.2.8) becomes a first order ODE. Solutions do not exist in the classical sense. Later in this section, we will define a weak solution for u.

We make the following assumptions on f and g.

- $f(u,v)$ and $g(u,v)$ are continuously differentiable on

$$\bar{\mathbf{R}}^2_+ = \{(u,v) \mid u \geq 0,\ v \geq 0\},\ \mathbf{R} = (-\infty, \infty),$$

  where the bar denotes the closure of the set and $f(u,v) = uf_1(u,v)$, $g(u,v) = vg_1(u,v)$.

- $f(u,v) = 0$ has a positive solution $u = h(v)$ on some closed interval $\bar{J}_-$ where $J_- = (\beta_1, \beta_2)$, $0 \leq \beta_1 < \beta_2$.

- $f(u,v) = g(u,v) = 0$ has two solutions $P_\pm(u_\pm, v_\pm)$ such that $u_+ = 0$, $v_+ = 1$, $u_- = h(v_-)$, $v_- \in \bar{J}_-$ and $0 \leq v_- < v_+$.

We look for travelling wave solutions of the form $u(x,t) = U(z)$, $v(x,t) = V(z)$ where $z = x - c\epsilon t$. Then (5.2.8)–(5.2.9) becomes

$$\epsilon^2(U^m U')' + c\epsilon U' + Uf_1(U,V) = 0, \tag{5.2.10}$$

$$V'' + c\epsilon V' + Vg_1(U,V) = 0, \tag{5.2.11}$$

with boundary conditions

$$U(-\infty) = h(v_-), \qquad V(-\infty) = v_-, \tag{5.2.12}$$

$$U(+\infty) = 0, \qquad V(+\infty) = 1. \tag{5.2.13}$$

Definition 5.2.1 *The bounded piecewise smooth functions (U,V) with $z = x - c\epsilon t$ are said to be (weak) travelling wave solutions for (5.2.8)–(5.2.9) provided*

(a) $U^m U'$ exists and is continuous.

(b) U satisfies

$$\int_{-\infty}^{+\infty} (\epsilon^2 \xi'' \frac{U^{m+1}}{m+1} - c\epsilon\xi' U + \xi U f_1(U,V))dz = 0,$$

where $\xi(z)$ is any smooth function with compact support.

(c) V satisfies the equation (5.2.11)

(d) (U,V) satisfy the boundary conditions (5.2.12) and (5.2.13).

Following Hosono, (1986), Hosono, (1987) we will now construct an approximation to solutions of (5.2.10) and (5.2.11) with boundary conditions (5.2.12) and (5.2.13) using a standard singular perturbation technique.

5.2.1 First order approximation

First we will set $\epsilon = 0$ in (5.2.10) to obtain

$$Uf_1(U,V) = 0, \tag{5.2.14}$$

$$V'' + Vg_1(U,V) = 0, \quad z \in \mathbf{R}. \tag{5.2.15}$$

Equation (5.2.14) has two solutions $U \equiv 0$ and $U = h(V)$. Without loss of generality, we assume that we have a jump discontinuity some point at $z = z^\star$ and we impose $V(z^\star) = \beta$ in order to remove the invariance of solutions under translation. Hence we have

$$V'' + Vg_1(0,V) = 0, \quad z > z^\star, \tag{5.2.16}$$

$$V'' + Vg_1(h(V),V) = 0, \quad z < z^\star, \tag{5.2.17}$$

with $V(\pm\infty) = v_\pm$, $V(z^\star) = \beta$.

If we let $V' = W$ and

$$g_2(V) = \begin{cases} g_1(0,V), & z > z^\star, \\ g_1(h(V),V), & z < z^\star, \end{cases} \tag{5.2.18}$$

then we have the following system of two coupled nonlinear ODEs

$$W' + Vg_2(V) = 0, \tag{5.2.19}$$

$$V' = W, \quad z \in \mathbf{R}, \tag{5.2.20}$$

subject to the boundary conditions $W(\pm\infty) = 0$ and $V(\pm\infty) = v_\pm$. We will have a unique solution for $W(V)$ provided $g_2(V)$ is a bounded Lipschitz continuous function

on $\mathbf{R}$, i.e.

$$|g_2(a) - g_2(b)| \leq k\,|a-b|\,, \quad \forall a, b \in \mathbf{R}, \text{ for some constant } k > 0.$$

If we multiply (5.2.19) by W and integrate once, we have

$$\frac{1}{2}\left[\frac{d(V_+)}{dz}\right]^2 = -\int_{\beta}^{v_+} V g_1(0,V)dV,$$

$$\frac{1}{2}\left[\frac{d(V_-)}{dz}\right]^2 = -\int_{v_-}^{\beta} V g_1(h(V),V)dV,$$

where $V_\pm$ are defined as the solutions to (5.2.16) and (5.2.17) respectively, and

$$V_0(z;\beta) = \begin{cases} V_+(z;\beta), & z > z^\star, \\ V_-(z;\beta), & z < z^\star, \end{cases}$$

Then (5.2.17) and (5.2.16) has a unique solution $V_0(z;\beta) \in C^1(\mathbf{R})$. Therefore, by setting

$$U_0(z;\beta) = \begin{cases} h(V_0(z;\beta)), & z < z^\star, \\ 0 & z > z^\star, \end{cases}$$

(U_0, V_0) is a solution to (5.2.10)–(5.2.11) outside the neighbourhood of $z = z^\star$.

We will now construct an approximate solution in the neighbourhood of $z = z^\star$ using matched asymptotic expansions. Consider the stretched variable $\zeta = \frac{z}{\epsilon}$, $\zeta \in \mathbf{R}$. Then (5.2.10)–(5.2.11) becomes

$$(U^m U')' + cU' + U f_1(U,V) = 0, \tag{5.2.21}$$

$$V'' + c\epsilon^2 V' + \epsilon^2 V g_1(U,V) = 0, \tag{5.2.22}$$

where $'$ now denotes differentiation with respect to ζ. By setting $\epsilon = 0$, we get $V'' = 0$, i.e. $V = c_1\zeta + c_2$, where c_1 and c_2 are constants. By the matching principle we have

$$\lim_{\zeta \to \pm\infty} U(\zeta) = \lim_{z \to z_\pm^\star} U_0(z;\beta) = \lim_{V \to \beta_\pm} h_\beta(V), \tag{5.2.23}$$

where

$$h_\beta(V) = \begin{cases} 0, & \beta < V \leq v_+, \\ h(V), & v_- \leq V < \beta, \end{cases} \tag{5.2.24}$$

and

$$\lim_{\zeta \to \pm\infty} V(\zeta) = \lim_{z \to z_{\pm}^{*}} V_0(z;\beta) = \beta. \tag{5.2.25}$$

Hence $V = \beta$ and we must solve

$$(U^m U')' + cU' + U f_1(U,V) = 0, \tag{5.2.26}$$

subject to the boundary conditions

$$U(-\infty) = h(\beta), \quad U(+\infty) = 0. \tag{5.2.27}$$

Returning to our model, we have

$$U f_1(U,V) = U^p((1+V-v_0)^q - U^q), \tag{5.2.28}$$

$$V g_1(U,V) = V(1 - U(1-v_0) - V), \tag{5.2.29}$$

so that $f_1(U,V) = 0$ has a positive solution $U = h(V) = 1 + V - v_0$ and $u_- = h(v_-) = 1$ implies that $v_- = v_0$. Furthermore, $g_2(V)$, as defined by (5.2.18) is Lipschitz continuous for all a, b in the domain of g_2.

In the next section we will show the existence of travelling wave solutions to equations of the form (5.2.26) by following Sánchez-Garduño & Maini, (1994).

5.2.2 Existence of a travelling wave solution for a density dependent diffusion equation

Sánchez-Garduño & Maini, (1994) and Sánchez-Garduño & Maini, (1993) show the existence of travelling wave solutions, $u(x,t) = U(x - ct)$ for parabolic equations of the form

$$\frac{\partial u}{\partial t} = \frac{\partial}{\partial x}\left[D(u)\frac{\partial u}{\partial x}\right] + f(u), \tag{5.2.30}$$

where D and f are defined on [0,1] and satisfy

(1) $f(0) = f(1) = 0$, $f(u) > 0\ \forall u \in (0,1)$,

(2) $f \in C^2_{[0,1]}$ with $f'(0) > 0$, $f'(1) < 0$,

(3) $D(0) = 0$, $D(u) > 0\ \forall u \in (0,1]$,

(4) $D \in C^2_{[0,1]}$ with $D'(u) > 0$, $D''(u) \neq 0$, $\forall u \in [0,1]$,

with initial condition $u(x,0) = u_0(x)$, where u_0 is any piecewise differentiable function such that $0 \leq u_0(x) \leq 1$, and with boundary conditions $U(-\infty) = 1$ and $U(+\infty) = 0$. We will extend this further to show the existence of travelling wave solutions for equations of the above form for a particular $D(u)$ and $f(u)$ but with condition (4) replaced by

(4') $D \in C^2_{[0,1]}$ with $D'(u) \geq 0$, $\forall u \in [0,1]$,

In particular we let $D(u) = u^m$ and $f(u) = u^p(1-u^q)$. Then if we look for travelling wave solutions for (5.2.30) of the form $u(x,t) = U(z)$, where $z = x - ct$, we obtain

$$(U^m U')' + cU' + U^p(1-U^q) = 0, \tag{5.2.31}$$

with boundary conditions $U(-\infty) = 1$, $U(+\infty) = 0$. By a suitable change of variables, we can write (5.2.26) in the form (5.2.31). If we let

$$V = \left(-\frac{U^m}{m}\right)' = -U^{m-1}U', \tag{5.2.32}$$

and $r = m + p - 1$, then we have,

$$U' = -U^{1-m}V, \tag{5.2.33}$$

$$U^m V' = -V(c-V) + U^r(1-U^q), \tag{5.2.34}$$

To remove the singularity we set $U^m d\xi = dz$, hence the system becomes

$$\dot{U} = -UV = F(U,V), \tag{5.2.35}$$

$$\dot{V} = -V(c-V) + U^r(1-U^q) = G(U,V), \tag{5.2.36}$$

where we have used $\dot{}$ to denote differentiation with respect to ξ. It is easily seen that this system has three critical points,

$$P_0 = (0,0), \quad P_1 = (1,0), \quad P_c = (0,c). \tag{5.2.37}$$

A local stability analysis is given in Appendix B.1. Some of the results are included

here for the convenience of the reader. The eigenvectors at P_1 are

$$\mathbf{v_1} = \begin{bmatrix} 1 \\ -\lambda_1 \end{bmatrix}, \quad \mathbf{v_2} = \begin{bmatrix} 1 \\ -\lambda_2 \end{bmatrix},$$

where

$$\lambda_{1,2} = \frac{-c \pm \sqrt{c^2+q}}{2}, \quad \lambda_1 > 0, \ \lambda_2 < 0, \tag{5.2.38}$$

are the corresponding eigenvalues at P_1, whereas P_c has eigenvalues $\lambda_{1,2} = \pm c$ with associated eigenvectors

$$\mathbf{v_1} = \begin{bmatrix} 0 \\ 1 \end{bmatrix}, \quad \mathbf{v_2} = \begin{bmatrix} 1 \\ \dfrac{-K_1(0)}{2c} \end{bmatrix},$$

where

$$K_1(0) = U^{r-1}\big|_0 = \begin{cases} 0, & \text{if } r > 1, \\ 1, & \text{if } r = 1. \end{cases} \tag{5.2.39}$$

Hence, P_1 and P_c are saddle points. P_0 has a centre manifold (see Appendix (B.1)) and the behaviour of trajectories close to the origin is given in section (B.1.1). In general, if we have initial values (U_0, V_0) such that $\sqrt{U_0^2 + V_0^2}$ is sufficiently small and $U_0 > 0$, then solutions will tend to P_0 along the centre manifold.

5.2.3 Existence of travelling wave solutions for $c^2 \geq M > 0$

First, we introduce the following notation: Let $W_c^u(P_1)$ and $W_c^s(P_c)$ be the left–unstable manifold of P_1 and the right–stable manifold of P_c, respectively.

We have the following proposition:

Proposition 5.2.2 *No travelling wave solutions exist for $c \approx 0$.*

Proof. Consider $c = 0$. Then (5.2.35) and (5.2.36) becomes

$$\dot{U} = -UV = F_0(U,V), \tag{5.2.40}$$

$$\dot{V} = V^2 + U^r(1 - U^q) = G_0(U,V). \tag{5.2.41}$$

Now consider

$$\dot{U} = -U^2V = F_0^*(U,V), \tag{5.2.42}$$

$$\dot{V} = UV^2 + U^{r+1}(1-U^q) = G_0^*(U,V). \tag{5.2.43}$$

Since $U > 0$ and is well behaved, the trajectories of (5.2.40)–(5.2.41) and (5.2.42)–(5.2.43) coincide on the region

$$\mathcal{R} = \{(U,V) \mid 0 < U \leq 1,\ -\infty < V < +\infty\}.$$

Now, (5.2.42)–(5.2.43) can be written in Hamiltonian form, i.e.

$$\dot{U} = \frac{\partial H}{\partial V},\quad \dot{V} = \frac{-\partial H}{\partial U},$$

where

$$H(U,V) = -\frac{1}{2}[UV]^2 - \int_{U_0}^{U} \tilde{U}^{r+1}(1-\tilde{U}^q)d\tilde{U}, \tag{5.2.44}$$

$$= -\frac{1}{2}[UV]^2 + \hat{H}(U). \tag{5.2.45}$$

The trajectory of (5.2.42)–(5.2.43), (and also of (5.2.40)–(5.2.41)) passing through (1,0) is given by the level curve

$$-\frac{1}{2}[UV]^2 + \hat{H}(U) = H(1,0),$$

where

$$H(1,0) = U_0^{r+2}\left(\frac{1}{r+2} - \frac{U_0^q}{q+r+2}\right) - \left(\frac{q}{(q+r+2)(r+2)}\right).$$

Hence, for trajectories in the first quadrant we have

$$V(U) = \frac{1}{U}\sqrt{2(\hat{H}(U) - H(1,0))}.$$

Now for all $U \in (0,1]$, $\hat{H}(U)$ is strictly decreasing with its minimum at $U = 1$, where $\hat{H}(1) = H(1,0)$. So $\hat{H}(U) - H(1,0) \geq 0$ on (0,1] and hence $V(U)$ is a well defined function on (0,1] and $\lim_{U\to 0+} V(U) = \infty$. Hence for $c = 0$ there are no trajectories connecting P_1 to P_0.

Now consider $c \approx 0$. Since the vector field (5.2.35)-(5.2.36) depends continuously upon c, U and V, for c sufficiently small, the path of the unstable manifold of P_1, $W_c^u(P_1)$, is such that $V(U) \to \infty$ as $U \to 0^+$. Furthermore, the path of the stable manifold of P_c, $W_c^s(P_c)$, will leave the region

$$\mathcal{R}_2 = \{(U,V) \mid 0 < U \leq 1,\ 0 < V < \infty\}.$$

at some point U_0, $0 < U_0 \leq 1$, close to P_0, since it cannot cross $W_c^u(P_1)$. Hence, no travelling wave solutions exist for $c \approx 0$.

□

Proposition 5.2.3 *For each $c^2 \geq M$, where*

$$M = 4\left(\frac{r}{q+r}\right)^{\frac{r}{q}}\left(\frac{q}{q+r}\right),$$

there exists a travelling wave solution, $u(x,t) = U(x-ct)$ of (5.2.30), which satisfies $U(-\infty) = 1$ and $U(+\infty) = 0$.

Proof. Consider the vertical nullclines $\dot{V} = 0$, i.e.

$$V^2 - cV + U^r(1-U^q) = 0,$$

$$V_{1,2}(U) = \frac{c \pm \sqrt{c^2 - 4U^r(1-U^q)}}{2}. \tag{5.2.46}$$

So $V_1(0) = V_1(1) = c$, $V_2(0) = V_2(1) = 0$. Now consider $\mathcal{F}(U) = 4U^r(1-U^q)$ which has a maximum on [0,1] at $U_{max} = \left(\frac{r}{q+r}\right)^{\frac{1}{q}}$ given by

$$M = 4\left(\frac{r}{q+r}\right)^{\frac{r}{q}}\left(\frac{q}{q+r}\right).$$

Furthermore at U_{max}, V_1 attains its minimum and V_2 attains its maximum.

Suppose that $c^2 > M$. Then $V_1(U) > V_2(U)$ for all $U \in [0,1]$ and the nullclines are as shown below in figure (5-1 a). Now suppose $c^2 = M$. Then $V_1(U) \geq V_2(U)$ for all $U \in [0,1]$ with equality at $U = U_{max}$. The nullclines are as shown in figure (5-1 b). Finally, suppose that $c^2 < M$. Then there is a subinterval, $(U_1^\star, U_2^\star)$ say, of [0,1] for which V_1 and V_2 are imaginary, hence V_1 and V_2 are discontinuous at $U_1^\star$ and $U_2^\star$ where $\mathcal{F}(U_1^\star) = \mathcal{F}(U_2^\star) = c^2$. The nullclines are as shown below in figure (5-1 c).

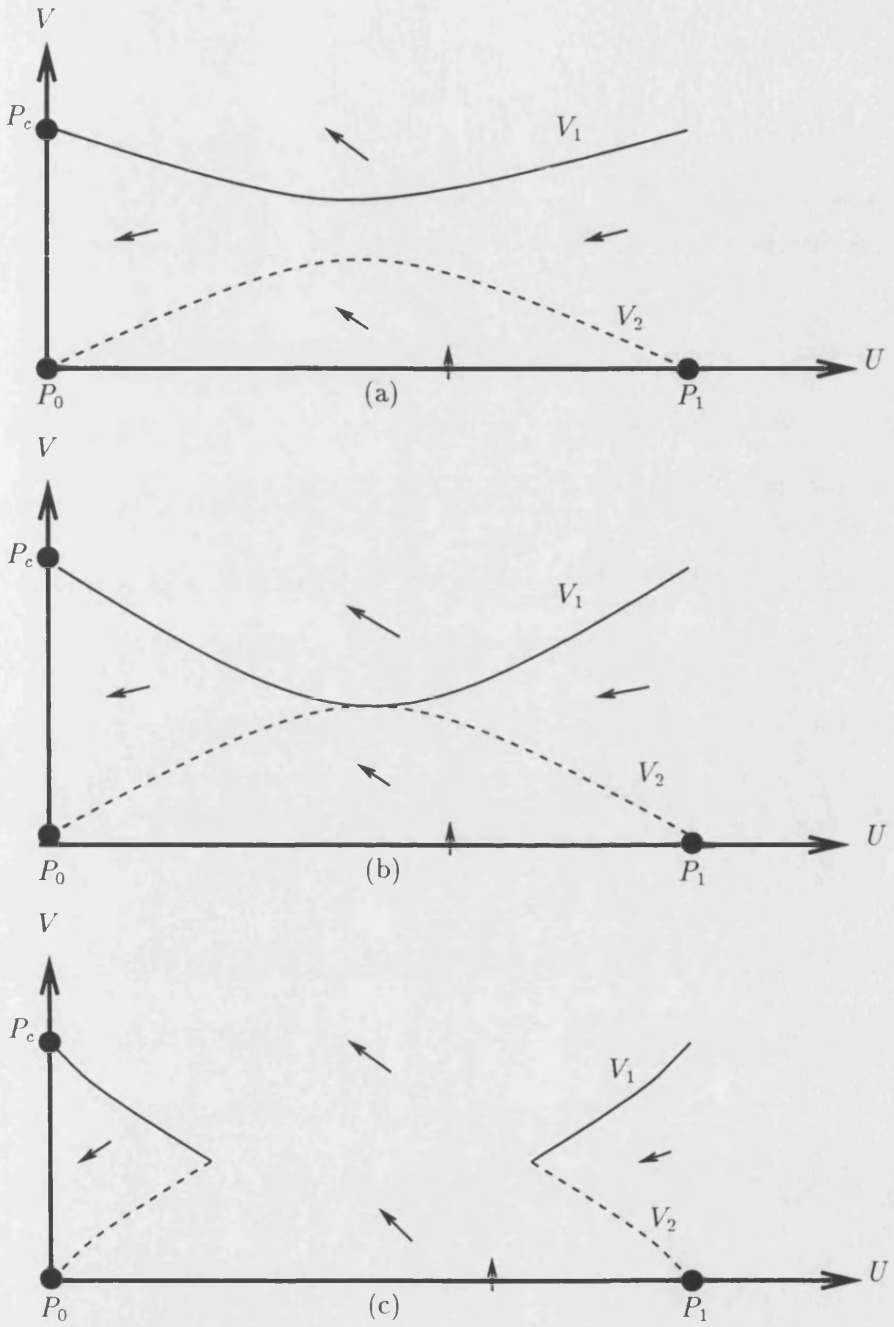

Figure 5-1: *The vertical nullclines of (5.2.35)-(5.2.36) for (a)* $c^2 > M$, *(b)* $c^2 = M$ *and (c)* $c^2 < M$.

Differentiating (5.2.46) with respect to U, we obtain

$$V_1'(0) = \frac{-K_1(0)}{c}, \quad V_1'(1) = \frac{q}{c}, \quad V_2'(0) = \frac{K_1(0)}{c}, \quad V_2'(1) = -\frac{q}{c},$$

with K_1 as in (5.2.39). From our linear analysis (see Appendix (B.1)), we know that the slope of $W_c^u(P_1)$ is

$$M_c^u(P_1) = \frac{c - \sqrt{c^2 + q}}{2},$$

and the slope of $W_c^s(P_c)$ is

$$M_c^s(P_c) = \frac{-K_1(0)}{2c}.$$

Comparing $V_2'(1)$ with $M_c^u(P_1)$ and $V_1'(0)$ with $M_c^s(P_c)$, we see that

$$M_c^u(P_1) > V_2'(1), \quad M_c^s(P_c) \geq V_1'(0),$$

for all positive c.

Now consider nullclines as in figure (5-1 a). Then, the region

$$\mathcal{R}_3 = \{(U,V) \mid 0 \leq U \leq 1,\ 0 \leq V \leq V(U_{max})\},$$

is a positive invariant set of (5.2.35)–(5.2.36) and hence by the Poincaré–Bendixson theorem, the unstable manifold of P_1 connects with the stable manifold of P_0. Furthermore, by examining the behaviour of $V_1(U)$ and $W_c^s(P_c)$ at P_c and the vector field, we see that the path of $W_c^s(P_c)$ will only intersect with $V_1(U)$ (in inverse time) at some point $(U_1, V(U_1))$ where $U_1 > U_{max}$. Therefore, $W_c^s(P_c)$ will leave (in inverse time) the region

$$\mathcal{R}_4 = \{(U,V) \mid 0 \leq U \leq 1,\ 0 < V < \infty\},$$

somewhere on $\{(U,V) \mid U = 1,\ V > 0\}$. Hence for each $c^2 > M$, there exists a travelling wave solution, $u(x,t) = U(x - ct)$, of (5.2.30) satisfying $U(-\infty) = 1$ and $U(+\infty) = 0$.

Now consider nullclines as in figure (5-1 b). The unstable manifold $W_c^u(P_1)$ will leave P_1 and will enter

$$\mathcal{R}_5 = \{(U,V) \mid 0 < U < 1,\ 0 < V \leq V_2(U)\},$$

and the vector field will push $W_c^u(P_1)$ towards V_2. Suppose that $W_c^u(P_1)$ leaves $\mathcal{R}_5$ at

some point $(U_2, V(U_2))$ such that $U_{max} < U_2$. Then the vector field will push $W_c^u(P_1)$ back into $\mathcal{R}_5$. If $U_{max} > U_2$ then the vector field pushes $W_c^u(P_1)$ towards P_0. Furthermore, we can show that the path of $W_c^s(P_c)$ leaves (in inverse time) the region $\mathcal{R}_4$ somewhere on $\{(U,V) \mid U = 1,\ V > 0\}$ by using the same argument as before. Hence for $c^2 = M$, there exists a travelling wave solution, $u(x,t) = U(x-ct)$, of (5.2.30) satisfying $U(-\infty) = 1$ and $U(+\infty) = 0$.

□

We have now shown the following theorem.

Theorem 5.2.4 *1. For each $c^2 \geq M$, there exists a travelling wave solution, $u(x,t) = U(x-ct)$, of (5.2.30) satisfying $U(-\infty) = 1$ and $U(+\infty) = 0$.*

2. There are no travelling wave solutions of (5.2.30) for sufficiently small c.

5.2.4 Existence of finite travelling waves

In this section we consider the possibility of the existence of travelling wave solutions for $c \in [c_0, \sqrt{M}]$, where c_0 is positive and sufficiently small.

Definition 5.2.5 *Suppose there exists a wave speed $c = c^\star > 0$ and a point $z = z^\star \in (-\infty, +\infty)$ such that $u(x,t) = U(z)$, $z = x - c^\star t$, satisfies*

(1) equation (5.2.31) $\forall z \in (-\infty, z^\star)$,

(2) $U(-\infty) = 1$, $U(z) \equiv 0\ \ \forall z \in (z^\star, +\infty)$, $U(z_\pm^\star) = 0$,

(3)

$$U'(z) = 0\ \ \forall z \in (z^\star, +\infty),\ \lim_{z \to z_-^\star} U'(z) = \begin{cases} -c & \text{if } m = 1, \\ -\infty & \text{if } m > 1. \end{cases}$$

Then $u(x,t) = U(z)$ is a finite travelling wave solution of (5.2.30).

Such a solution exists if there is a trajectory in the (U,V) phase plane (5.2.35)–(5.2.36) connecting (0,c) to (1,0).

Proposition 5.2.6 *Let c_1 and c_2 be two arbitrary speeds such that $c_0 < c_1 < c_2 < \sqrt{M}$ and define $V_{c_1}(U)$ and $V_{c_2}(U)$ as the paths of $W_{c_1}^s(P_{c_1})$ and $W_{c_2}^s(P_{c_2})$ respectively in the region*

$$\mathcal{R}_6 = \{(U,V) | 0 \leq U \leq 1,\ 0 \leq V < \infty\}.$$

Then,

$$V_{c_0}(U) < V_{c_1}(U) < V_{c_2}(U) < V_{\sqrt{M}}(U), \ \forall U \in [0,1].$$

Proof. First, note that the equilibrium P_c moves away from P_0 along the vertical axis as c increases. Consider the region

$$\mathcal{R}_0 = \{(U,V) \mid 0 \leq U \leq U_0,\ 0 \leq V(U) \leq V_{c_0}(U)\},$$

and a point $(\bar{U}, \bar{V}_{c_0}(\bar{U}))$ on the boundary of $\mathcal{R}_0$ and on the graph of $V_{c_0}(U)$. By considering the vector field (5.2.35)-(5.2.36) with $c = c_1$, we note that any trajectory that passes through the point $(\bar{U}, \bar{V}_{c_0}(\bar{U}))$ will enter $\mathcal{R}_0$ and will reach P_0 as $t \to \infty$. Furthermore, since $V_{c_1}(0) = c_1 > V_{c_0}(0) = c_0$, then (0,$c_1$) is outside of the region $\mathcal{R}_0$ and $W^s_{c_1}(P_{c_1})$ cannot enter $\mathcal{R}_0$ in inverse time. Hence $V_{c_0}(U) < V_{c_1}(U)$. By a similar argument we can show $V_{c_1}(U) < V_{c_2}(U) < V_{\sqrt{M}}(U)$.

□.

Proposition 5.2.7 *Let $\theta(U,V,c)$ be the angle between the positive U axis and the line connecting the origin to the point (U,V) where (U,V) is the solution to (5.2.35)-(5.2.36). Then $\theta(U,V,c)$ is an increasing function of c.*

Proof.

$$\theta(U,V,c) = \tan^{-1}\left(\frac{cV - V^2 - U^r(1-U^q)}{UV}\right),$$

so

$$\frac{\partial \theta}{\partial c} = \frac{UV^2}{(UV)^2 + (cV - V^2 - U^r(1-U^q))^2} > 0.$$

□.

Proposition 5.2.8 *There exists a critical wavespeed $c = c^\star$ such that the trajectory in the (U,V) phase plane defined by (5.2.35)-(5.2.36) leaving (1,0) and the trajectory approaching (0,c) coincide. Furthermore, $c^\star$ is unique.*

Proof. The existence of $c^\star$ follows from the continuity of solutions with respect to c and proposition (5.2.6).

Now suppose that $c_1^\star$ and $c_2^\star$ are two such wavespeeds such that a connection between P_1 and $P_{c_1^\star}$, and P_1 and $P_{c_2^\star}$ both exist and, without loss of generality, let $c_1^\star < c_2^\star$. Recall

that the slope of $W_c^u(P_1)$ at P_1 is given by

$$M_c^u(P_1) = \frac{c - \sqrt{c^2 + q}}{2} < 0,$$

and $M_c^u(P_1)$ is an increasing function of c. Hence, at P_1, $W_{c_1^*}^u(P_1) > W_{c_2^*}^u(P_1)$. However, since $c_1^* < c_2^*$, $P_{c_1^*}$ lies below $P_{c_2^*}$ on the positive V axis. So $W_{c_1^*}^u(P_1)$ and $W_{c_2^*}^u(P_1)$ must intersect at some point, (u^*, v^*). This contradicts proposition (5.2.7). Hence c^* is unique.

□.

Hence we have shown the following theorem:

Theorem 5.2.9 *There exists a unique $c = c^*$ such that $u(x,t) = U(x - c^*t)$ is a finite travelling wave solution of (5.2.30).*

We can obtain an upper bound on c^* by following de Pablo & Vazquez, (1991). Given that

$$\frac{dV}{dU} = \frac{c - V}{U} - \frac{U^{r-1}(1 - U^q)}{V}, \tag{5.2.47}$$

we have $V\dfrac{dV(U)}{dU} \geq -U^{r-1}(1 - U^q)$ for $0 \leq U \leq 1$. Integrating from $U = 0$ to $U = 1$ and $V = c^*$ to $V = 0$, we obtain

$$c^*(q,r) \leq \sqrt{\frac{2q}{r(r+q)}}.$$

Figure (5-2) shows the dependence of the bound of c^* on the parameters p, q and m.

We solved the ODE system (5.2.35)–(5.2.36) using MATLAB for $c > c^*$ and $m = p = q = 1$ (figure (5-3)). When $c \approx c^*$ (in this case we took $c = \sqrt{0.5} + 0.001$), the solution for $U(z)$ has a sharp front and the solution for $V(U)$ is approximately a straight line passing through $(1,0)$ and $(0,c^*)$. This can be exploited to find an exact solution for U (see Murray, (1989)). If we set

$$V = c^*(1 - U)$$

and substitute for V in (5.2.47), we obtain

$$c^* = \sqrt{\frac{U^{r-1}(1 - U^q)}{2(1 - U)}}, \tag{5.2.48}$$

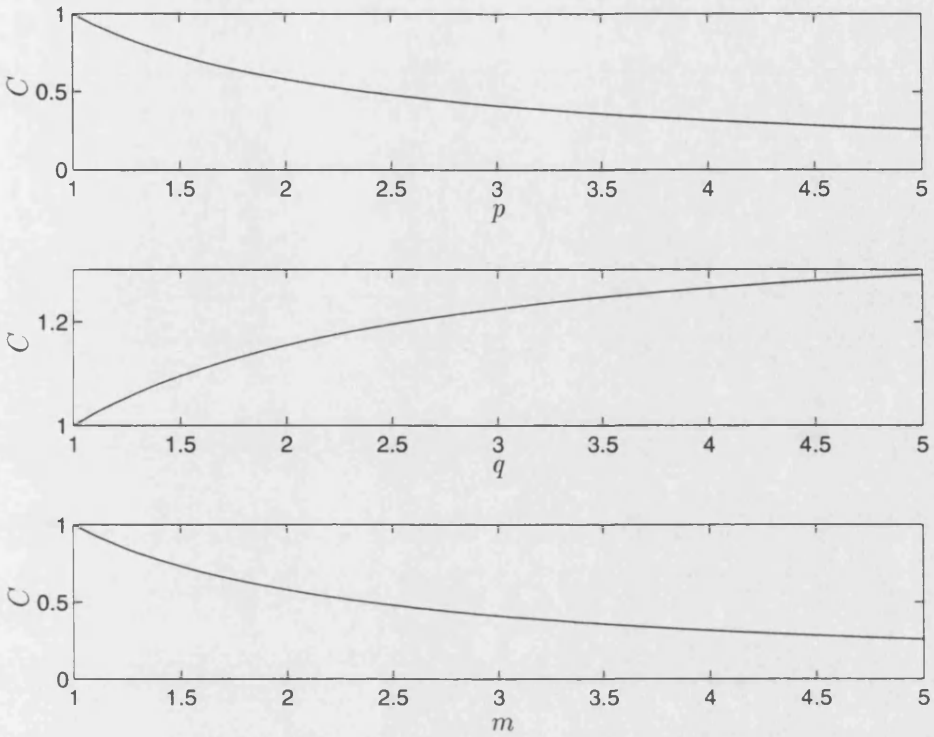

Figure 5-2: *The effect of varying p, q, and m on the bound C, where* $c^\star \leq C$, $C = (\frac{2q}{r(r+q)})^{1/2}$, *with the other parameters held fixed at 1.*

and when $m = p = q = 1$ we have $c^\star = \sqrt{0.5}$. When $m = 1$, we have from (5.2.33)

$$U' = -V = -\frac{(1-U)}{\sqrt{2}}, \tag{5.2.49}$$

which integrates to give

$$U = \begin{cases} 1 - \exp\left(\dfrac{z - z^\star}{\sqrt{2}}\right) & \text{for } z < z^\star \\ 0 \text{ for } z \geq z^\star \end{cases} \tag{5.2.50}$$

Figure (5-4) compares the exact solution for U (5.2.50) with the numerical solution of (5.2.35)–(5.2.36) with $m = p = q = 1$, $c \approx c^\star$.

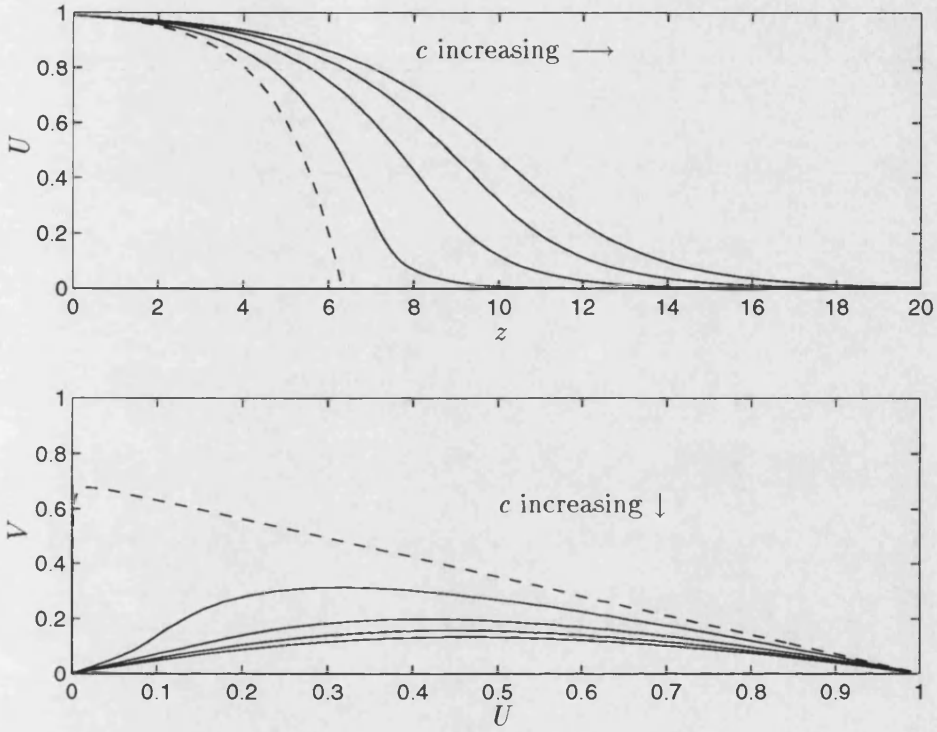

Figure 5-3: *A numerical solution of the ODE system (5.2.35)–(5.2.36) for* $m = p = q = 1$ *as* c *is increased above* $c^\star$. *The top figure shows the solution for* U *as a function of* $z = x - ct$. *The bottom figure shows the solution in the* $(U, -U^{m-1}U')$ *plane. The dotted line is the solution for* $c \approx c^\star$, *where* $c^\star \leq (0.5)^{1/2}$. *In this case, there is a heteroclinic connection between* P_1 *and* P_c *and the travelling wave solution has semi-infinite support.*

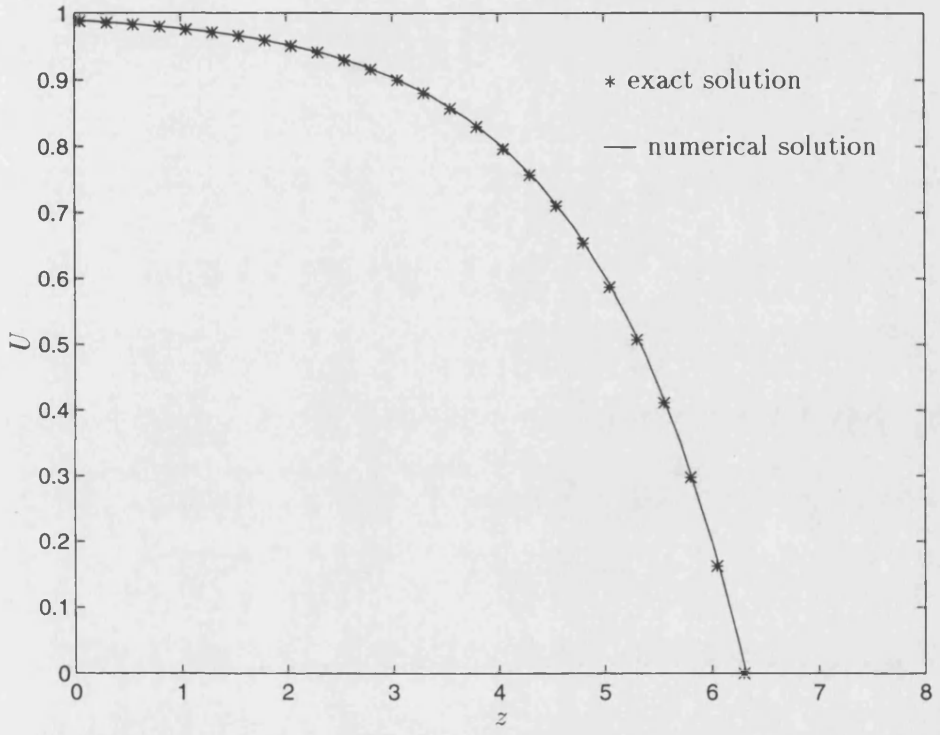

Figure 5-4: *The numerical solution for U of the ODE system (5.2.35)– (5.2.36) for $m = p = q = 1$, $c \approx c^*$ (solid line) as compared with the exact solution for U ($*$'s) with $z^* \approx 6.3$.*

5.3 Numerical simulations

We conducted our numerical simulations using a parabolic PDE solver available from the NAG library. We chose block initial conditions in all our simulations such that

$$\begin{aligned} &\text{if } 0 \leq x < 0.25, \quad u(x,0) = 1, \quad v(x,0) = 0, \\ &\text{if } x \geq 0.25, \quad\quad u(x,0) = 0, \quad v(x,0) = 1, \end{aligned} \tag{5.3.51}$$

In the simulations presented here, the boundary conditions were taken to be

$$u(0,t) = v(L,t) = 1, \quad \frac{\partial u(L,t)}{\partial x} = \frac{\partial v(0,t)}{\partial x} = 0, \tag{5.3.52}$$

where the right hand boundary (i.e. the limbus) was taken to be at $x = L$ and in general we took $L = 10$. Other boundary conditions for u were considered such as $u^{m-1}\dfrac{\partial u}{\partial x} = 0$ at both boundaries. This did affect the solution at the left hand boundary, which is where the diffusion term degenerates and hence there is a loss of accuracy in the numerical scheme (see NAG documentation). In simulations of the PDE system (5.2.8)–(5.2.9), $u(0,t) \approx 1$, but for the simulations of the single PDE equation (5.2.30), $u(0,t) < 1$. Fixing u at the left hand boundary allowed for direct comparisons between the PDE and ODE solutions.

First, we compared the solution of the PDE (5.2.30) with $m = p = q = 1$ with the exact solution of the ODE system given by (5.2.50). Figure (5-5) shows that the solution of the PDE system converges to a travelling wave front after finite time (see appendix (B.2)).

In the second set of simulations, we examined the effect of varying the parameters m, p and q on the single equation (5.2.30), which modelled solely the growth of the tumour. Figure (5-6) shows the effect of increasing m whilst fixing p and q. When $m = 2$ (bottom picture) the tumour has a distinct edge and expands slowly. For $m = 1$ (middle picture) the tumour is still encapsulated, but moves across the domain faster than before. The front of the tumour is less steep, indicating a more penetrative/invasive tumour. When $m = 0$ (top picture) we have Fisher's equation and the solution is no longer has compact support. The tumour cells quickly reach the right hand boundary. There is a small amount of tumour cells moving ahead of the bulk of the tumour mass, suggesting that the tumour is highly invasive. Hence an increase in m corresponds to a

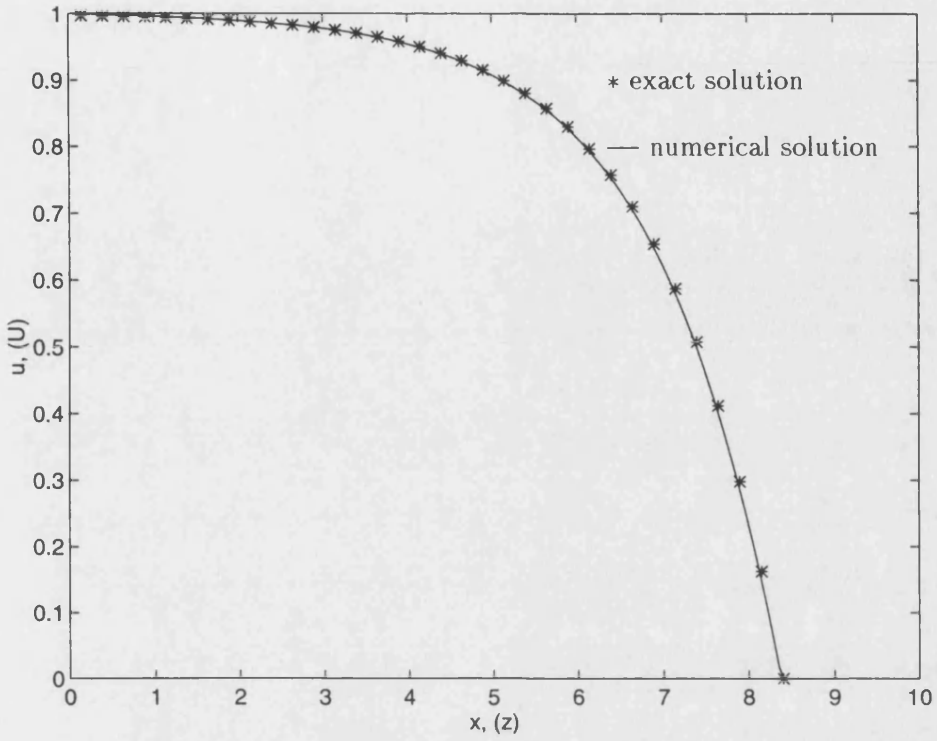

Figure 5-5: *A numerical solution of the PDE (5.2.30) for* $m = p = q = 1$, *(solid line) at* $t = 10$ *as compared with the exact solution (5.2.50) for* U *(* 's) with* $z^* \approx 8.4$.

decrease in the invasion speed and an increase in the steepness of the tumour front (cf. figure (5-2)).

Figure (5-7) shows the effect of increasing p whilst keeping m and q fixed. Examination of the three solutions shows that whilst the steepness of the tumour front stays the same, the tumour moves across the domain more slowly as p increases. The opposite effect can be obtained (figure (5-8)) whereby the tumour moves faster across the domain as parameter q is increased (cf. figure (5-2)). This scenario has interesting biological implications which we discuss later.

To summarise, these simulations (figures (5-6)–(5-8)) have the following biological interpretation:

- A decrease in m corresponds to a gradual loss in contact inhibition of motility and hence a more invasive tumour.
- A decrease in p corresponds to a decrease in density-dependent inhibition of growth and hence the loss of growth regulation.

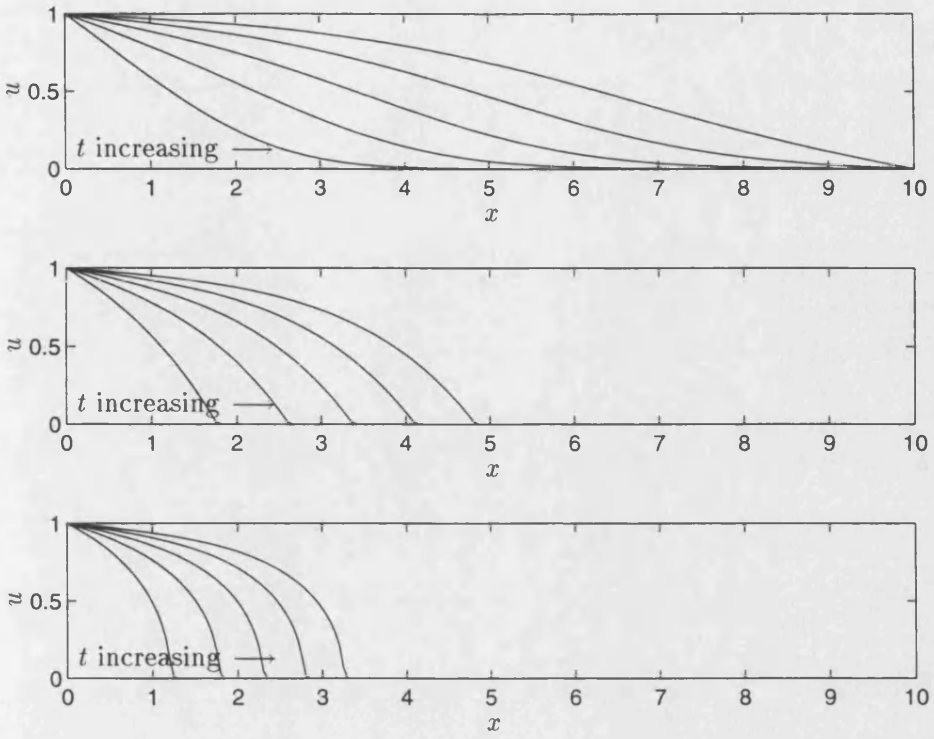

Figure 5-6: *A comparison of three numerical solutions of the PDE (5.2.30) for* $p = q = 1$, *with* $m = 0$ *(top picture),* $m = 1$ *(middle picture) and* $m = 2$ *(bottom picture). Plots drawn at* $t = 1, 2, 3, 4, 5$. *We conclude from this, that a decrease in* m *coincides with an increase in the invasive growth of the tumour.*

- A decrease in q corresponds to an decrease in density-dependent death (e.g. programmed cell death which prevents overcrowding) and hence a net increase in death due to population pressures which lead to a lack of oxygen (hypoxia).

In general, we conclude that a decrease in any of the parameters m, p, q is equivalent to an increase in the malignancy of a tumour. Many tumours grow slowly at first and become increasingly malignant over time. The suggestion is that as the tumour grows, it increasingly bears little resemblance to the tissue of origin and hence, gradually loses the ability to regulate its growth. We can model this by assuming that m is a decreasing function of time, for example, $m(t) = m_1(1-\tanh(t))$. Figure (5-10) shows the numerical simulation of (5.2.30) with $m = m(t)$ as in figure (5-9). However, because of difficulties with the numerical algorithm, we took integer values of m. Initially the tumour growth is compact, but gradually the tumour front becomes less steep, indicating that the tumour has developed into a more invasive phenotype as time progresses.

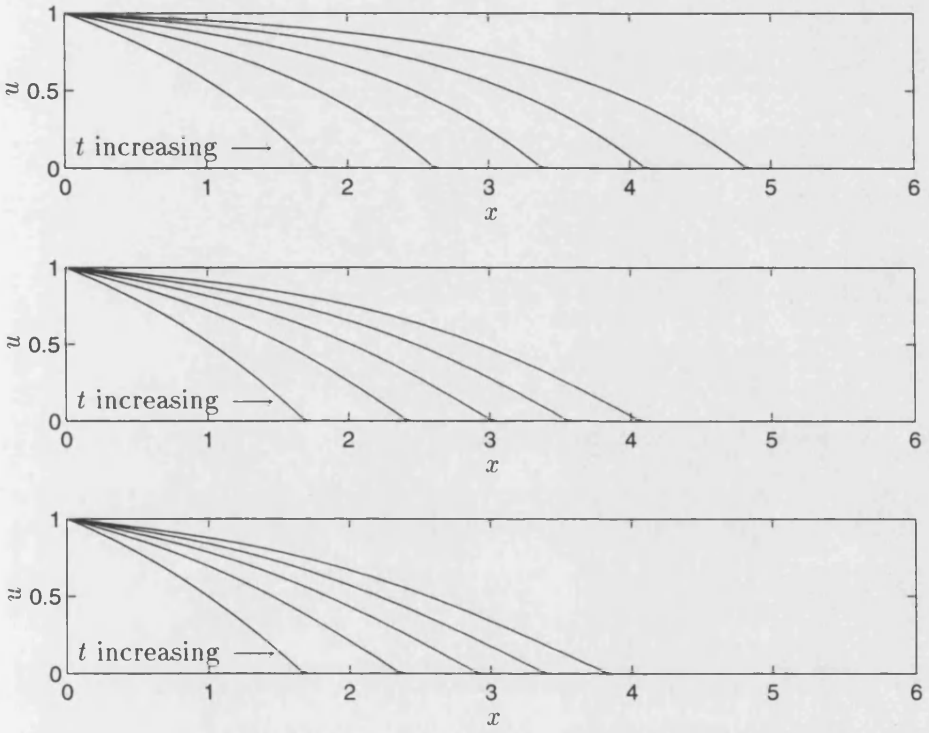

Figure 5-7: *A comparison of three numerical solutions of the PDE (5.2.30) for* $m = q = 1$, *with* $p = 1$ *(top picture),* $p = 2$ *(middle picture) and* $p = 3$ *(bottom picture). Plots drawn at* $t = 1, 2, 3, 4, 5$. *We infer from this simulation, that a decrease in* p *corresponds to an increase in expansive tumour growth.*

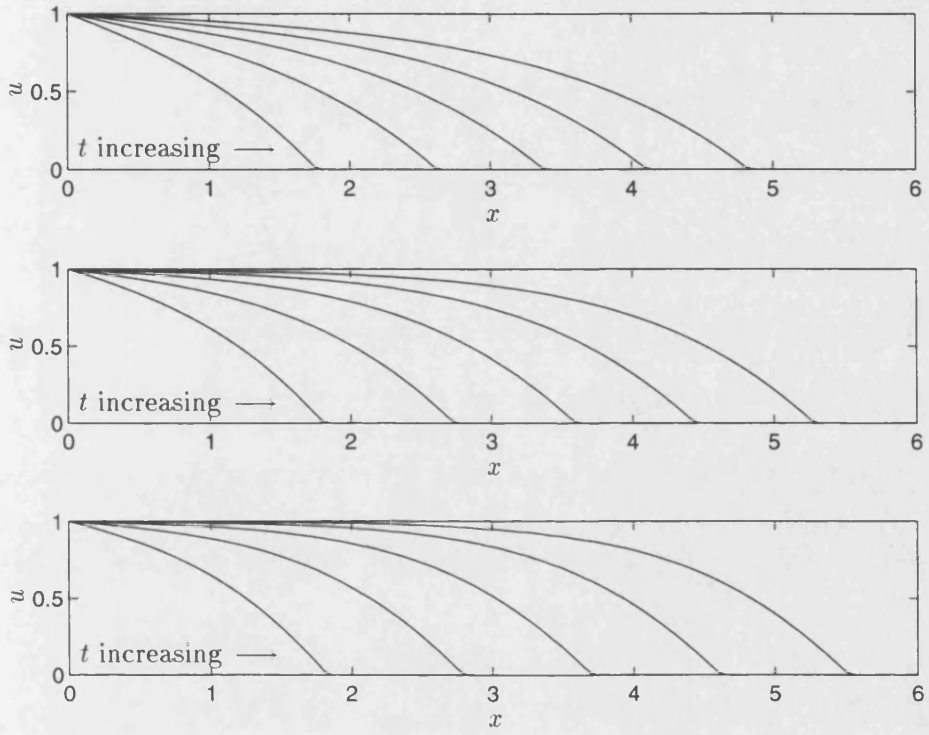

Figure 5-8: *A comparison of three numerical solutions of the PDE (5.2.30) for* $m = p = 1$, *with* $q = 1$ *(top picture),* $q = 2$ *(middle picture) and* $q = 3$ *(bottom picture). Plots drawn at* $t = 1, 2, 3, 4, 5$. *The simulations suggest that a decrease in* q, *results in an increase in overcrowding and hence an increase in tumour cell death.*

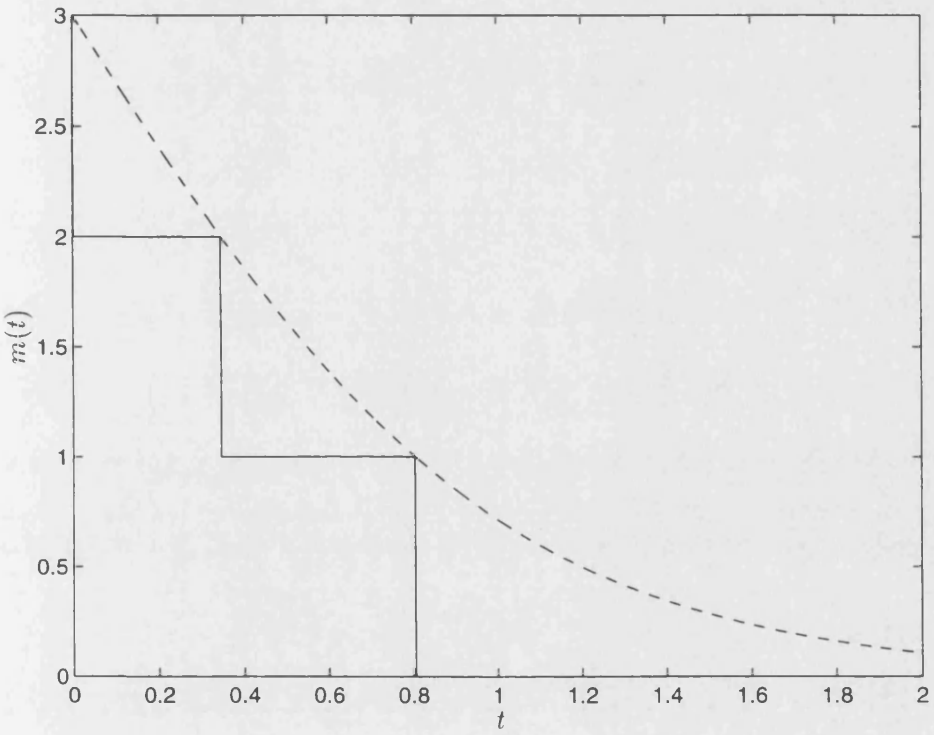

Figure 5-9: *An example of* $m = m(t)$ *as a decreasing function of* t. *This models the decrease in contact inhibition of movement over a period of time. We have* $m = m_1(1 - \tanh(t))$ *(dashed line) and* $m = INTEGER[m_1(1 - \tanh(t))]$ *(solid line). We took* $m_1 = 3$ *in the following numerical simulation.*

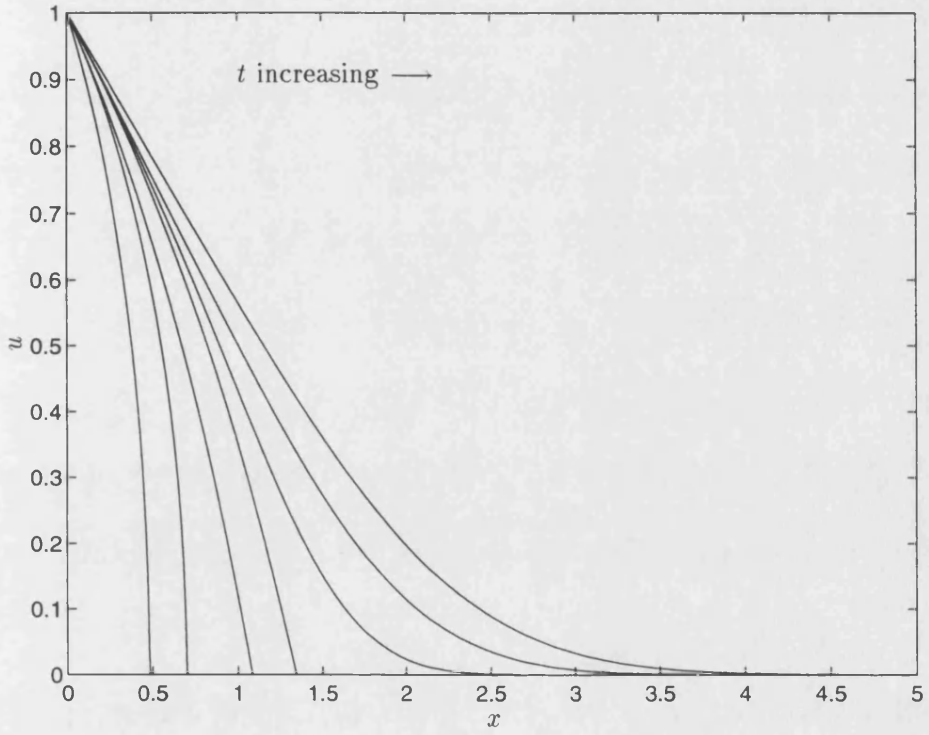

Figure 5-10: *A numerical solution of with $m = m(t)$, a decreasing function of t, which models a decrease in contact inhibition of movement over time. The tumour loses its compactness and becomes more invasive, which simulates the transformation of an in situ carcinoma into a more invasive, malignant phenotype. Plots drawn at* $t = 0.1, 0.3, 0.5, 0.7, 0.9, 1.1, 1.3$.

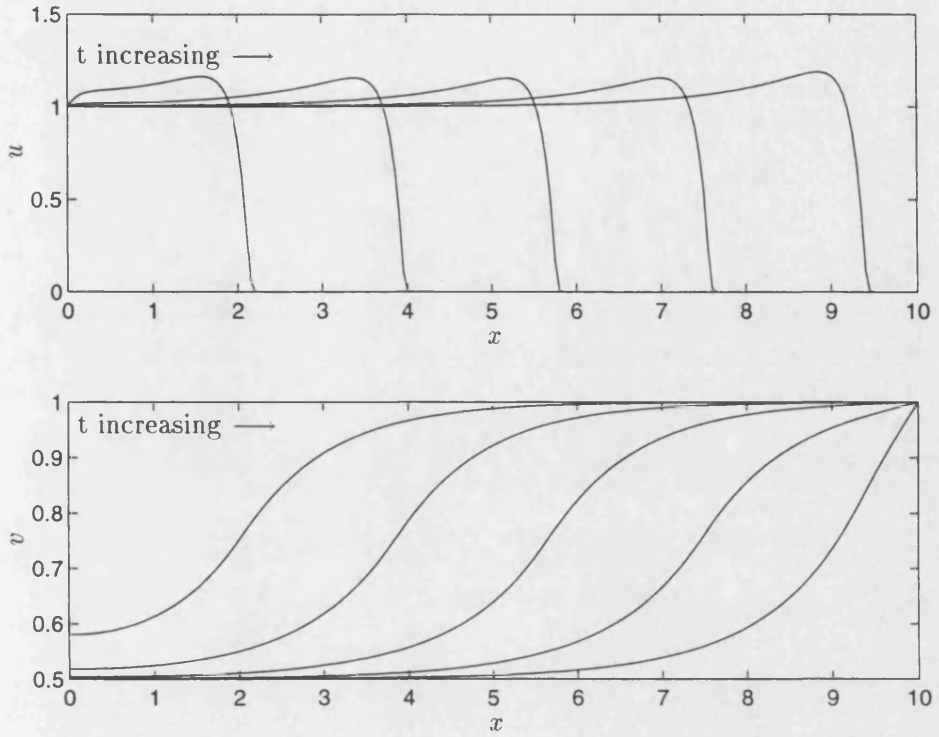

Figure 5-11: *A numerical solution of the PDE system (5.2.8) -(5.2.9) with* $m = p = q = 1$, $v_- = 0.5$ *and* $\epsilon = 0.1$. *The profile of the tumour is compact as it moves across the domain, with the vasculature regressing from the advancing front of tumour cells. Plots drawn at* $t = 2, 4, 6, 8, 10$.

Finally, we conducted numerical simulations of the PDE system (5.2.8)-(5.2.9) in order to show the interaction between the growing tumour and its vasculature. The previous simulations can be used to represent both benign or malignant tumours. In the following simulations the tumours are vascularized and it is more likely that such tumours will metastasise.

Figure (5-11) with $m = p = q = 1$ is a typical simulation. We see that the capillaries have quickly penetrated the entire tumour and the density at the centre subsequently decreases to v_- (in this case we arbitrarily took $v_- = 0.5$). The vessels regress as the tumour mass moves across the domain.

The simulations with $m = 3$, $p = q = 1$ (figure (5-12)) and with $p = 3$, $m = q = 1$ (figure (5-13)) were similar. However in each case the tumour grew quite slowly and the regression of the vasculature was not very severe. Interestingly, from a pathological point of view, the tumour invaded best when q was chosen to be greater than m and p (figure

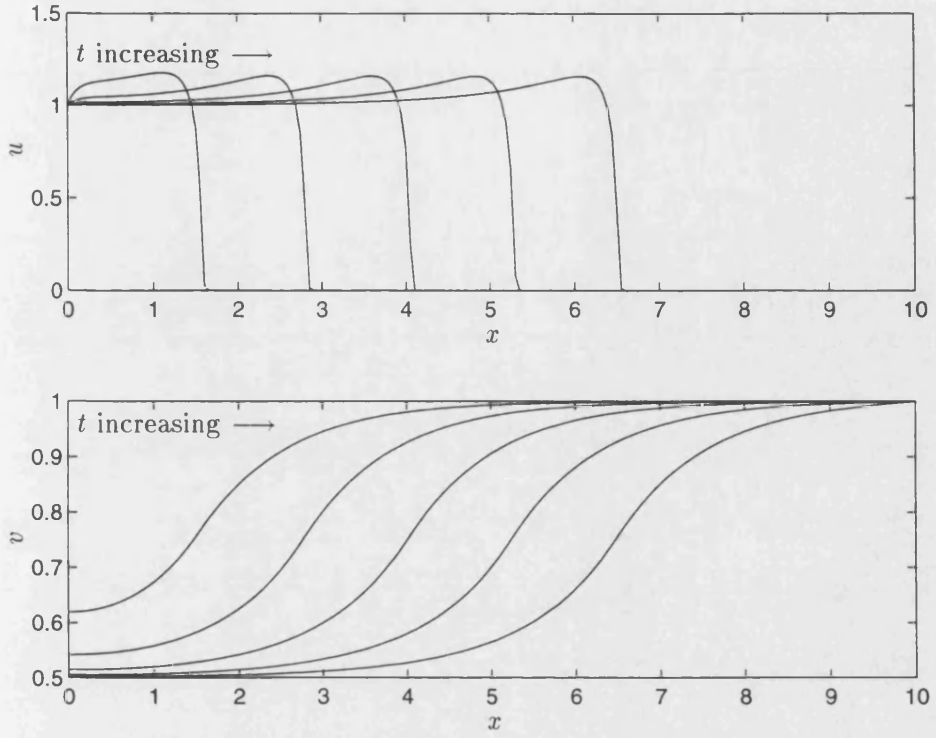

Figure 5-12: *A numerical solution of the PDE system (5.2.8) -(5.2.9) with* $m = 3$, $p = q = 1$, $v_- = 0.5$ *and* $\epsilon = 0.1$. *In this simulation, the tumour moves more slowly across the domain, and the regression of the capillary vessels is less marked. Plots drawn at* $t = 2, 4, 6, 8, 10$.

(5-14)). The tumour mass quickly invades the vasculature, the regression of which is quite acute. At first this case seemed to be counter-intuitive in that a large density-dependent death rate appears to benefit the tumour. It can be supposed however, that by selectively killing some cells, overcrowding can be prevented thus avoiding hypoxia. The increase in oxygen levels can help promote the proliferation of the remaining cells and hypoxia can be prevented further by the cells invading the vasculature where oxygen levels are high.

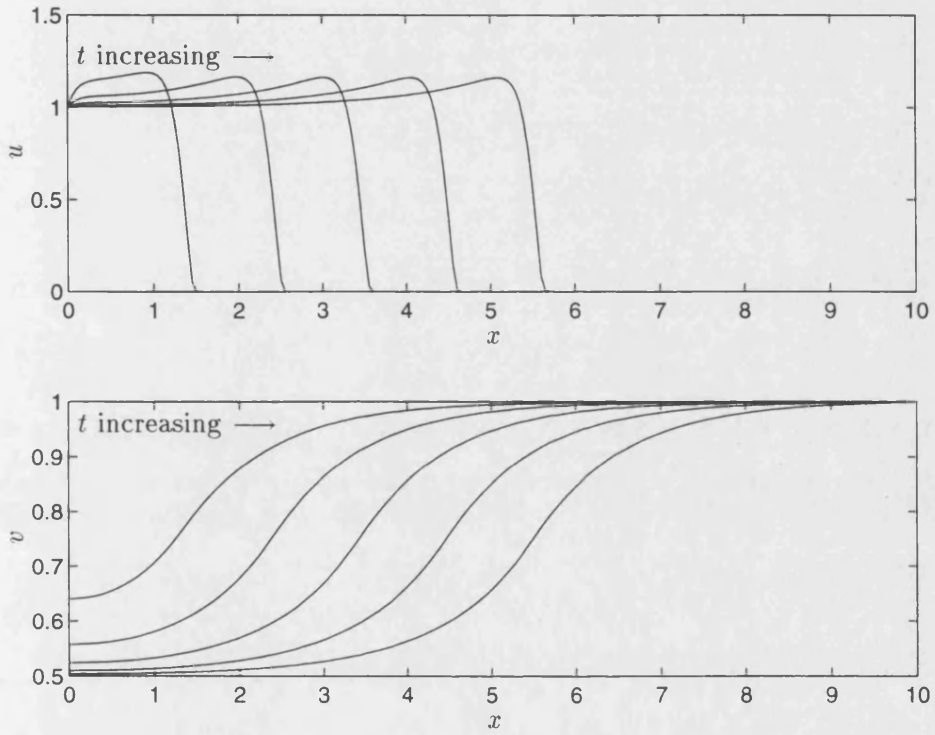

Figure 5-13: *A numerical solution of the PDE system (5.2.8) –(5.2.9) with* $p = 3$, $m = q = 1$, $v_- = 0.5$ *and* $\epsilon = 0.1$. *This solution is similar to the simulation shown in figure (5-12). Plots drawn at* $t = 2, 4, 6, 8, 10$.

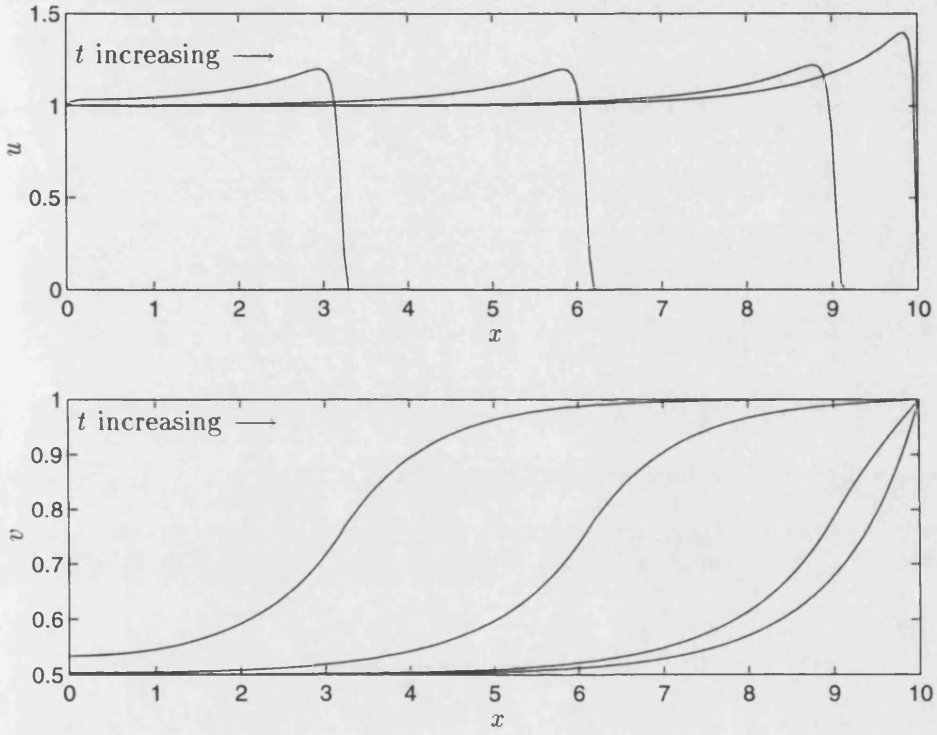

Figure 5-14: *A numerical solution of the PDE system (5.2.8) –(5.2.9) with* $q = 3$, $m = p = 1$, $v_- = 0.5$ *and* $\epsilon = 0.1$. *Here the speed of the advancing tumour front has noticeably increased and the regression of the vasculature is more pronounced. Plots drawn at* $t = 2, 4, 6, 8$.

Chapter 6

Two-dimensional models of tumour invasion in heterogeneous host tissue

One of the characteristics of a malignant tumour is the invasion of the neighbouring host tissue. Local dissemination of the tumour can have a number of serious consequences. Firstly, it can compromise the function of normal adjacent tissue. Secondly, it can result in an indistinct tumour boundary, which makes the carcinoma difficult to remove surgically. Furthermore, the invasive tumour cells can infiltrate local blood vessels and consequently metastasise.

In this chapter, we examine how the structure of the host tissue contributes to the metastatic potential of the tumour by assisting or hindering the invasion process. Furthermore, we show that the irregular shape, which is typical of an invading carcinoma, can be caused in part by the heterogeneities in the surrounding host tissue. We develop a two dimensional model of tumour invasion in heterogeneous host tissue, whereby a spatially dependent diffusion coefficient is used to model the variations in the tissue structure. In section (6.2), we present some two-dimensional numerical simulations of a tumour grown in four different domains, which capture the irregular and indistinct shape of the tumour. By estimating the speed at which the tumour cells reach the boundary, we show that some host tissue structures can impede or contribute to the invasion process. Furthermore, we show that, whilst the infiltration of some host tissue structures is limited when the proliferation of tumour cells is low, an increase in the

proliferation rate can facilitate the invasion of the entire host tissue. In section (6.3), we present an informal travelling wave analysis of the model in one space dimension and show that the spatially dependent diffusion term is equivalent to a combination of diffusion and nonlinear convection.

6.1 A mathematical model of tumour invasion

The majority of models of solid tumour growth are based on the idealisation that growth is isotropic. Whilst benign tumours grow by expansion [Ruddon, (1987)] and many are quasi-spherical in shape, for example, leiomyoma of the uterus (fibroid) [MacSween & Whaley, (1992)], this is rarely true of malignant neoplasms which tend to be irregular in shape [Darling & Tarin, (1990)], [Eaves, (1973)], [Ruddon, (1987)]. [Gimbrone *et al.*, (1974)] observed that a prevascular tumour implanted into a rabbit cornea, grew as thin circular plates. On closer examination, the tumour appeared to have penetrated the corneal lamellae, resulting in a feathered edge. A common feature of liver cell carcinomas is the permeation of the surrounding vein branches resulting in an irregular shape [MacSween & Whaley, (1992)]. Suh & Weiss, (1984) used cancer cell density maps to study the distribution of tumour cells at the advancing edge of an invasive melanoma and found that the outline of the tumour was irregular with a gradual centrifugal diminution in cancer cell density towards the advancing edge. It can be supposed that the composition of the host tissue surrounding a tumour can determine the shape of the neoplasm.

Primary tumours originating in different anatomical sites exhibit wide variations in metastatic potential. For example, benign tumours of the liver are extremely rare [MacSween & Whaley, (1992)]. Tumours of smooth (involuntary) muscle can be benign or, more infrequently, malignant, whereas striated (striped or voluntary) muscle tumours are nearly always highly malignant [MacSween & Whaley, (1992)]. (Note that smooth muscle lacks the highly organised structure found in striated muscle). It is also known that certain anatomical structures are relatively resistant to invasion by tumour cells [MacSween & Whaley, (1992)], [Nicolson, (1988)], [Ruddon, (1987)], for example, cartilage, aorta, cornea lens. It can therefore be hypothesised that the type of tissue surrounding a neoplasm can influence a tumour's latent ability to metastasise.

The main assumption in this model is that the heterogeneity of the host tissue

affects the ability of the tumour to invade and also contributes to the tumour's irregular shape. We incorporate heterogeneity into the model by assuming that the diffusion of the tumour cells is spatially dependent, reflecting the fact that some areas of host tissue are easier to invade than others.

If $u(\mathbf{x},t)$ is the density of the cancer cells at position $\mathbf{x}$ and time t then, assuming that the tumour cells simply diffuse and proliferate, the equation modelling invasion of the local tissue by the cancer cells is given by

$$\frac{\partial u}{\partial t} = \nabla.(D(\mathbf{x})\nabla u) + au(1 - \frac{u}{U}), \tag{6.1.1}$$

where $D(\mathbf{x})$ is the spatially-dependent diffusion coefficient and a is the net rate of production of the tumour cells and U is the carrying capacity of the environment.

We assume that $\mathbf{x} = (x,y)$ and $x,\ y \in [0,L]$, so that our model represents a two-dimensional cross-section of a tumour. We introduce dimensionless parameters into the system by making the following substitutions;

$$x^\star = \frac{x}{L}, \qquad y^\star = \frac{y}{L}, \qquad t^\star = \frac{dt}{L^2},$$

$$u^\star = \frac{u}{U}, \quad D^\star(x^\star,y^\star) = \frac{D(x,y)}{d}, \quad a^\star = \frac{aL^2}{d},$$

where U is the maximum tumour cell density and d is the average diffusion rate over an area L^2. Hence, dropping the $\star$'s for notational convenience, equation (6.1.1) becomes

$$\frac{\partial u}{\partial t} = \frac{\partial}{\partial x}\left(D(x,y)\frac{\partial u}{\partial x}\right) + \frac{\partial}{\partial y}\left(D(x,y)\frac{\partial u}{\partial y}\right) + au(1-u). \tag{6.1.2}$$

In order to close the system, we choose zero flux boundary conditions. By this we assume that the host tissue is surrounded by some (semi)impermeable barrier (i.e. mature vasculature) or is somehow contained *in vitro*, (e.g. within a square Petri dish). In the majority of the numerical simulations shown here, we choose initial conditions as follows;

$$u(x,y,0) = \begin{cases} 1, & \text{if } (x-0.5)^2 + (y-0.5)^2 \leq 0.1, \\ 0, & \text{otherwise.} \end{cases} \tag{6.1.3}$$

This corresponds to a circular cross-section of a spherical tumour in the centre of the host tissue. In some of the numerical simulations shown here, we assume the initial

distribution of tumour cells to be a rectangular strip of width 0.1 placed along the x-axis. This represents a cross-section of a squamous cell carcinoma (of the skin, for example) at the edge of the host tissue.

6.2 Numerical simulations

In the numerical simulations that follow, we used the method described in chapter (2), section (2.2) which was extended to two space dimensions by approximating the spatial derivatives using five point differencing. Note that, (using the notation of chapter (2), section (2.2)), we now obtain $(J+1)^2 \times (NPDE)$ coupled ODEs, which significantly increases the time taken to solve the system. The numerical simulations are conducted for different $D(x,y)$ in order to model a variety of host micro-environments (i.e. randomly mixed tissue, cartilage, immature vasculature) and for different values of a. In this way a comparison between the importance of diffusion and proliferation for invasion can be made.

The four different functions of $D(x,y)$ that we used in this model, which represent four different host tissue domains, are shown in figure (6-1). Each domain was divided into 100 equal regions and the diffusion coefficient in each region was chosen at random from a set of diffusion coefficients which represents the type of tissue to be modelled in each simulation. The overall structure of the host tissue varies from a domain consisting of randomly mixed, dissimilar tissue, to domains containing structures resistant or susceptible to invasion by the tumour cells.

In the first set of simulations, $D(x,y)$ is randomly generated such that the diffusion coefficients are uniformly distributed between 0 and 1. This corresponds to a domain consisting of a variety of dissimilar tissue. Initially the tumour is circular with radius 0.1. Figure (6-2) shows how the growth of the tumour progresses in such a randomly mixed domain. The growth is evenly spread in all directions but the surface of the tumour is irregular and appears to be covered in small protrusions which is typical of an invading carcinoma. Figure (6-3) is a contour plot of the solution shown in figure (6-2). This represents the portion of the tumour visible to the eye, assuming that tumour cell densities below 0.i cannot be detected. Comparison of figure (6-2) with figure (6-3) shows that surgical excision of the tumour is required beyond the observed tumour boundary in order to prevent regrowth. From the simulations, we estimate the

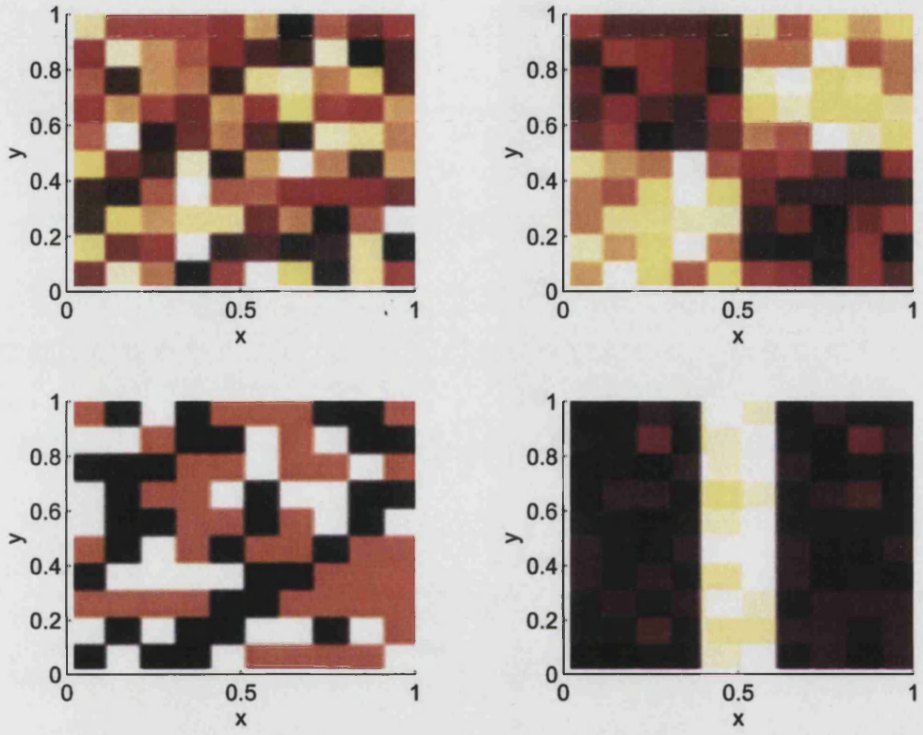

Figure 6-1: *Four different domains corresponding to the four different values of D(x,y) used in the numerical simulations. The light colour indicates a region of high permeability. The first domain represents randomly mixed, dissimilar tissue. The second domain consists of large areas of high and low permeability, which represents large structures that are relatively resistant to invasion. In the third, the host environment is more polarised and contains small areas of very low permeability, for example small fragments of cartilage. Finally, the fourth contains a path of high permeability such as an immature blood vessel.*

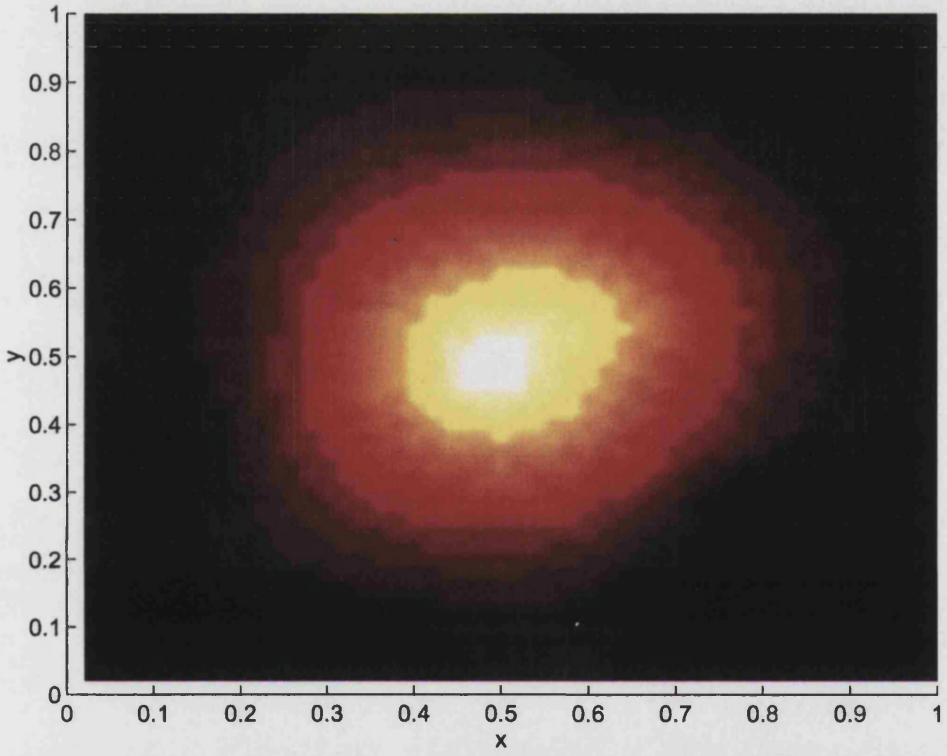

Figure 6-2: *A colour surface plot showing the growth of a circular tumour in a randomly mixed tissue after time* $t = 0.06$ *with* $a = 0.5$. *The light colour indicates a region of high tumour cell density. The periphery of the tumour is covered in small protrusions, indicating local invasion of the host tissue, a characteristic typical of malignant carcinomas.*

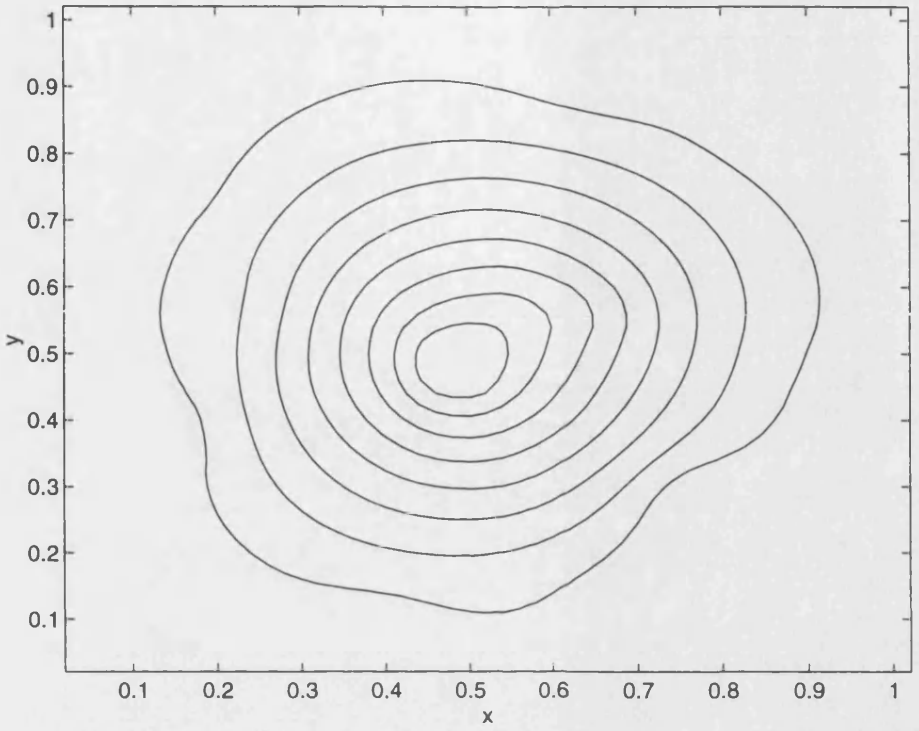

Figure 6-3: *A contour plot showing the growth of a circular tumour in a randomly mixed domain after time* $t = 0.06$ *with* $a = 0.5$. *By comparing this simulation with the simulation shown in figure (6-2), we see that the perceived tumour boundary is within that actual tumour boundary. The (dimensionless) invasion speed is estimated to be 6.7.*

dimensionless invasion speed to be 6.7.

Next, we took $D(x, y)$ as in figure (6-1b), which corresponds to a domain containing large areas of high and low permeability. In the low areas the diffusion coefficients are uniformly distributed between 0 and 0.5 and in the high areas the distribution is between 0.5 and 1. Again, we took the tumour to be circular initially and figure (6-4) shows that the growth of the tumour in such a domain is biased in the direction of least resistance. It is interesting to note that the presence of large and relatively impenetrable areas seem to have assisted the invasion process since the edge of the tumour appears to have reached the boundary quicker than in the previous example. This time the dimensionless invasion speed is estimated to be 10.

From our third set of simulations, it became clear that the heterogeneity of the domain could also hamper the invasion process. This time $D(x, y)$ was more polarised

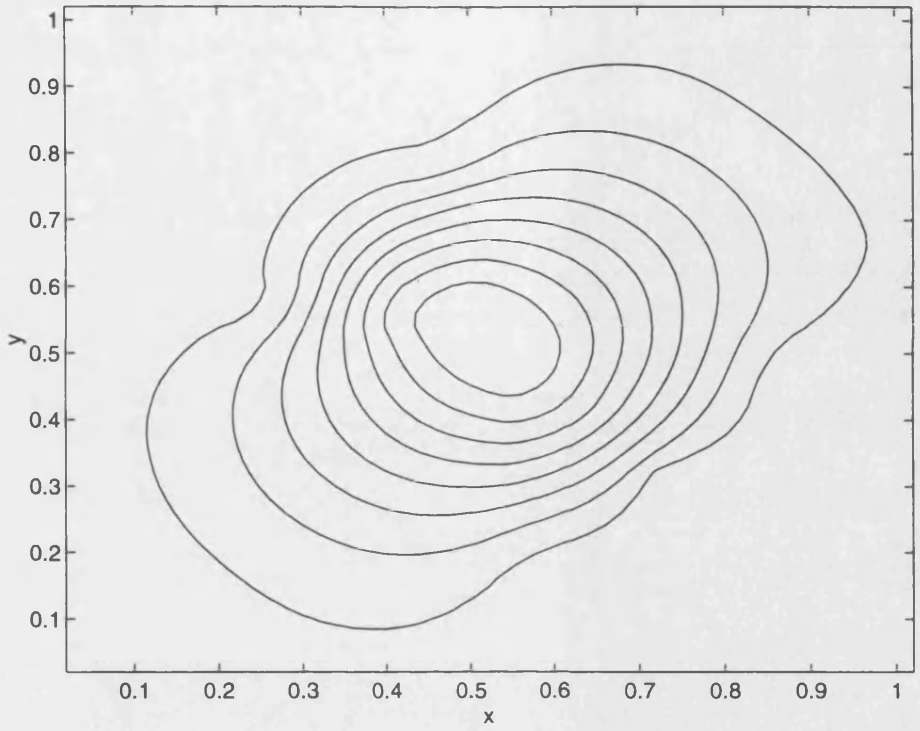

Figure 6-4: *The growth of a circular tumour in a domain consisting of large areas of high and low permeability. In this example, the structure of the host tissue enables the tumour to reach the boundary quicker with an estimated invasion speed of 10. Plot taken at time* $t = 0.04$ *with* $a = 0.5$.

in the sense that the diffusion coefficients were randomly chosen to be 0.001, 0.3 or 0.6. This corresponds to a domain containing small regions of high, medium or very low permeability. In figure (6-5), we see that the tumour has taken a much longer time to reach the boundary. Here the dimensionless invasion speed is about 0.1. However, the invasion process can be assisted by increasing the proliferation rate. By doubling the proliferation rate, we obtained the solution as shown in figure (6-6). Here, the tumour has been more successful in invading the entire domain. The role of proliferation in the invasion process becomes more apparent if we take different initial conditions. For example, if initially we have a band of tumour cells of width 0.1, then the growth progresses as shown in figure (6-7). Even after time $t = 10$, the tumour has grown very little and invasion into the local tissue appears to have stopped completely. However, by increasing the proliferation rate, the tumour successfully invades the entire domain (figure (6-8)).

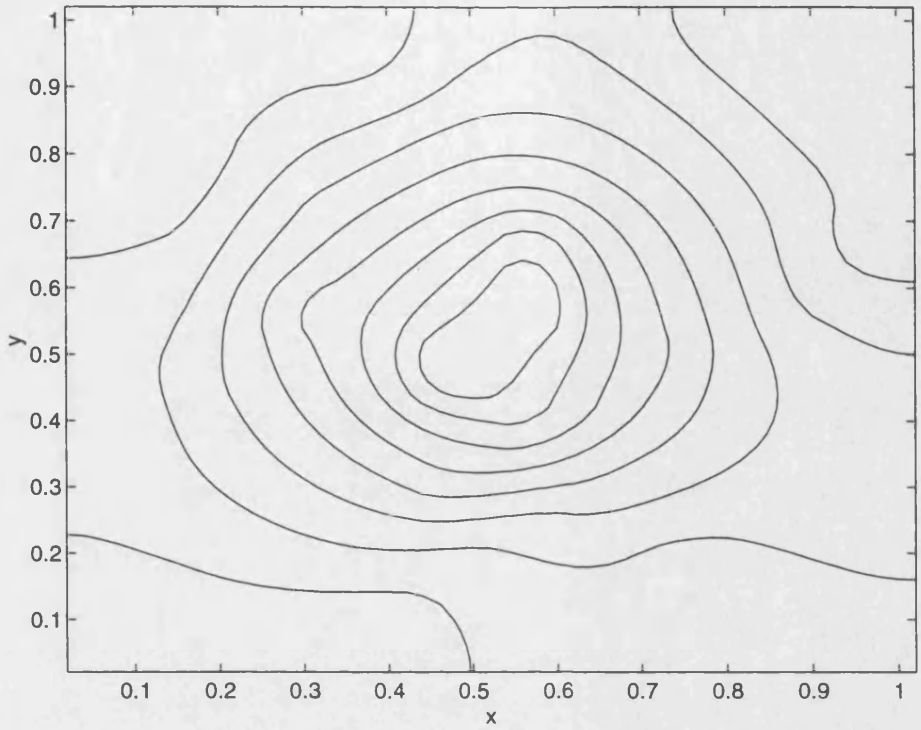

Figure 6-5: *The growth of a circular tumour in a domain consisting of small regions of very low permeability (i.e. cartilage). In this case, the tumour takes much longer to reach the boundary. Plot taken at time* $t = 5$ *with* $a = 0.5$.

In the final set of simulations, we took $D(x, y)$ as in figure (6-1d), in which an area of high permeability represents a structure such as immature vessels in the host environment. The rest of the domain consists of tissue which is unfavourable to invasion. Figure (6-9) shows that the tumour growth, in general, is biased in the direction of the vasculature, parallel to the y-axis. However, one interesting occurrence was that there was a moderate amount of movement out of, and perpendicular to, the vasculature. The tumour cells have reached the boundary quite quickly with an estimated (dimensionless) invasion speed of about 5. The overall pattern of tumour growth was not affected by varying the proliferation rate.

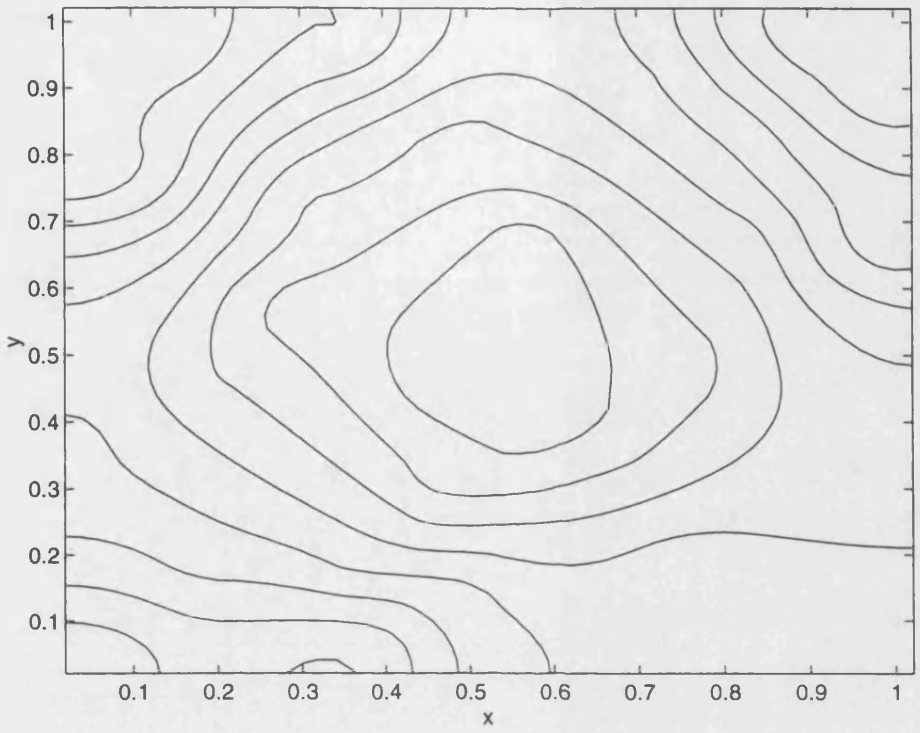

Figure 6-6: *The growth of a circular tumour in a domain consisting of small regions of very low permeability but with increased proliferation rate. In this case, the invasion of the host tissue is noticeably more widespread. Plot taken at time* $t = 5$ *with* $a = 1$.

6.3 Travelling wave analysis of invasion in a heterogeneous domain

We will now consider a one-dimensional analogue of the two-dimensional model given in (6.1). Firstly, consider the equation

$$\frac{\partial u}{\partial t} = \frac{\partial}{\partial x}\left(D(x)\frac{\partial u}{\partial x}\right) + au(1-u), \tag{6.3.4}$$

which can be expanded to

$$\frac{\partial u}{\partial t} = D(x)\frac{\partial^2 u}{\partial x^2} + D'(x)\frac{\partial u}{\partial x} + au(1-u). \tag{6.3.5}$$

When viewed in this form, we can see that the nonlinear diffusion term consists of two terms—diffusion, which attempts to smooth out the solution, and a nonlinear convective

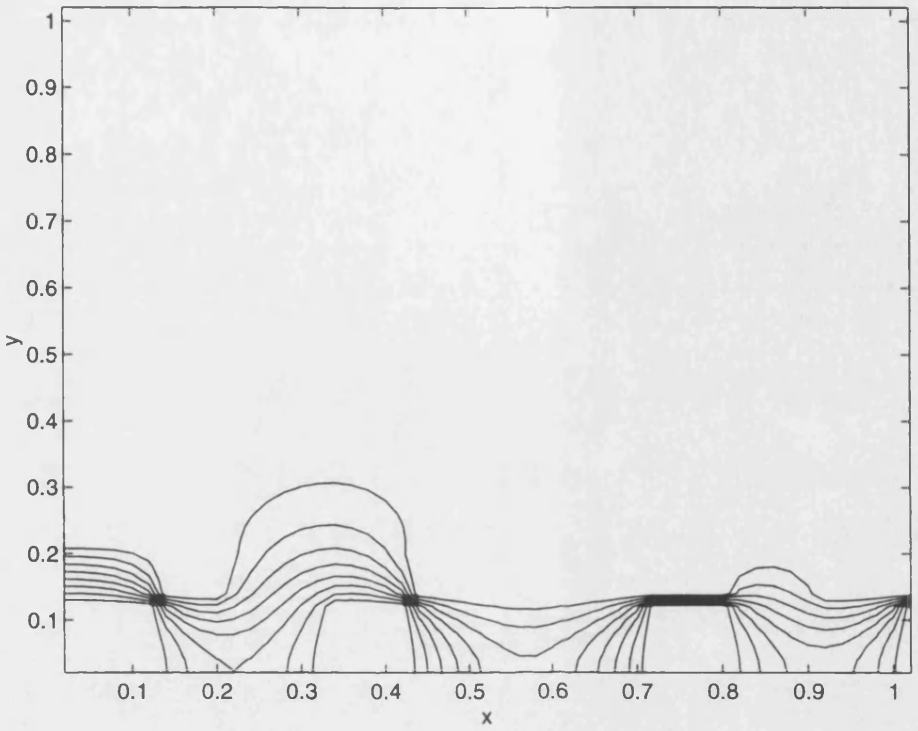

Figure 6-7: *The growth of a band of tumour cells (for example, squamous cell carcinoma) in a domain consisting of small regions of very low permeability (i.e. cartilage). The tumour fails to fully invade the local tissue and stops growing. Plot taken at time* $t = 10$ *with* $a = 0.5$.

term, which can lead to shocks in the absence of diffusion [Logan, (1994)], [Murray, (1989)]. Whether or not the convection process enhances the diffusion effect, or hinders it, depends on the sign and size of $D'(x)$.

We assume block initial conditions as follows;

$$u(x,0) = \begin{cases} 1, & \text{for } 0 \leq x \leq 0.1, \\ 0, & \text{otherwise.} \end{cases}$$

This could represent approximately a vertical cross-section of a circular tumour with centre at $x = 0$.

As previously, we assume that the tumour is growing in a mixture of tissue with different permeabilities. Within one tissue type, $D(x) \simeq$ constant, $D'(x) \simeq 0$. Hence, we assume that, in the interior of tissue i, the permeability corresponds to the constant

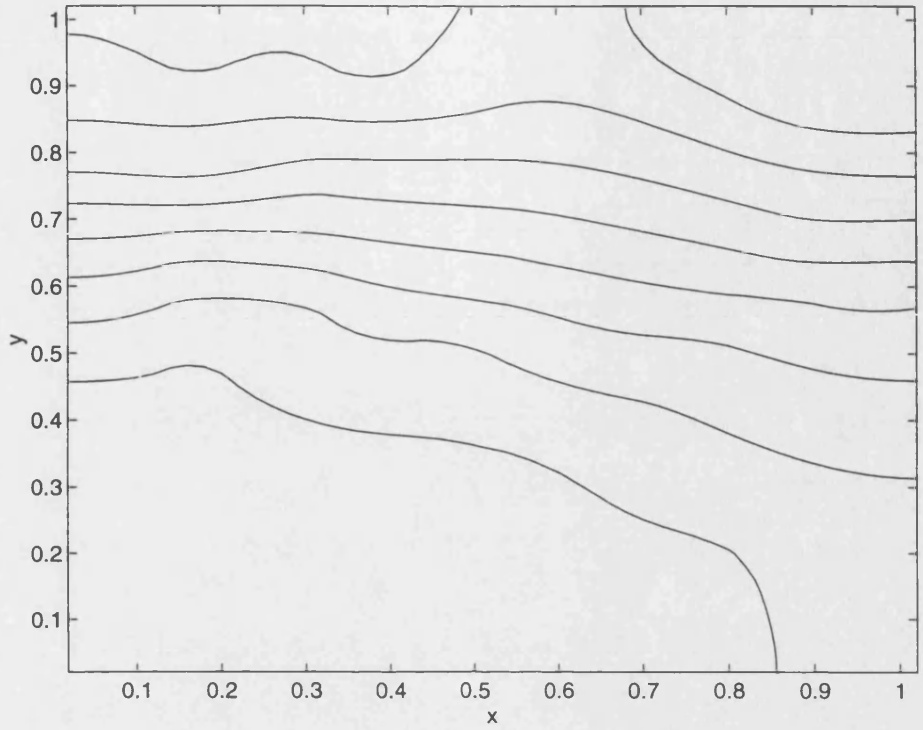

Figure 6-8: *The growth of a band of tumour cells (for example, squamous cell carcinoma) in a domain consisting of small regions of very low permeability. By increasing the proliferation rate, the tumour has now successfully penetrated the entire host tissue. Plot taken at time* $t = 7$ *with* $a = 1$.

diffusion coefficient D_i, and thus, equation (6.3.5) can be approximated by

$$\frac{\partial u}{\partial t} = D_i \frac{\partial^2 u}{\partial x^2} + au(1-u). \tag{6.3.6}$$

Therefore, in the interior of tissue i, the equation (6.3.5) can be approximated by a travelling wave solution of the form $u(x,t) = U(z)$, $z = x - ct$, where $c = 2\sqrt{D_i a}$ (by standard analysis of Fisher's equation [Murray, (1989)]).

During the transition from one tissue type to another, the non-linear convection term will come into play. Hence in this transition region, i.e. the transition from tissue i to tissue $i+1$, we approximate equation (6.3.5) by

$$\frac{\partial u}{\partial t} = D_i \frac{\partial^2 u}{\partial x^2} + k_i \frac{\partial u}{\partial x} + au(1-u), \tag{6.3.7}$$

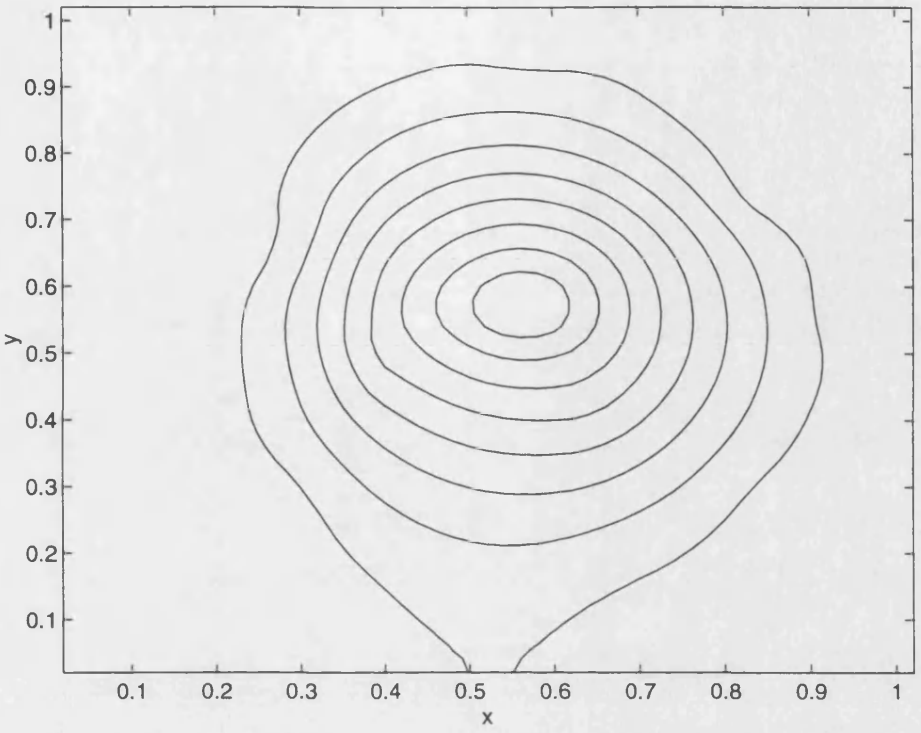

Figure 6-9: *The growth of a circular tumour in a domain consisting of high areas of permeability which simulates the path of a blood vessel. Growth of the tumour is biased in the direction parallel to the vessel, though there is some lateral movement. Plot taken at time* $t = 0.09$ *with* $a = 0.5$

where $\text{sgn}(k_i) = \text{sgn}(D_{i+1} - D_i)$. We seek a travelling wave solution to this equation, of the above form with $c > 0$ and hence, we have

$$-cU' = D_iU'' + k_iU' + aU(1-U). \tag{6.3.8}$$

Let $V = U'$. It is easily seen that

$$\frac{dU}{dV} = \frac{D_iV}{-(c+k_i)V - aU(1-U)}, \tag{6.3.9}$$

has two critical solutions $(0,0)$ and $(1,0)$. At (0,0) the eigenvalues are given by

$$\lambda_{1,2} = \frac{1}{2}\left[-(c + D'(x)) \pm \sqrt{(c+k_i)^2 - 4D_ia}\right]. \tag{6.3.10}$$

Since D_i and a are positive, (0,0) is stable if $k_i > -c$ and unstable otherwise. Further-

more, the eigenvalues are real if $(c+k_i)^2 > 4D_ia$, i.e. if $p(c) > 0$ where

$$p(c) = c^2 + 2ck_i + k_i^2 - 4D_ia.$$

We have three possibilities.

1. $k_i > 2\sqrt{D_ia} > 0$. Then $p(c) = 0$ has two negative solutions and $p(0) > 0$. Hence, $c > 0 > -k_i + 2\sqrt{D_ia}$ satisfies $p(c) > 0$ and $k_i > -c$.

2. $k_i < -2\sqrt{D_ia} < 0$. Then $p(c) = 0$ has two positive solutions and $p(0) > 0$. Hence, $c > -k_i + 2\sqrt{D_ia} > 0$ satisfies $p(c) > 0$ and $k_i > -c$.

3. $-2\sqrt{D_ia} < k_i < 2\sqrt{D_ia} < 0$. Then $p(c) = 0$ has one positive and one negative solution and $p(0) < 0$. Hence, $c > -k_i + 2\sqrt{D_ia} > 0$ satisfies $p(c) > 0$ and $k_i > -c$.

Therefore, the minimum wave speed $c = c_{min}$ is given by

$$c_{min} = \begin{cases} -k_i + 2\sqrt{D_ia}, & \text{for } k_i < 2\sqrt{D_ia}, \\ 0, & \text{for } k_i \geq 2\sqrt{D_ia}. \end{cases} \tag{6.3.11}$$

Hence, we conclude that, if $k_i < 0$, then the tumour invasion of the host tissue is assisted by the convective effect, but if $k_i > 0$ then invasion is hindered. Furthermore, if k_i is positive and sufficiently large, i.e. $k_i > 2\sqrt{D_ia}$, then the growth can stop altogether (see figure (6-7)).

To illustrate how changes in the tissue type can effect the invasion process, we solved equation (6.3.4) numerically. We took $D(x) = D_1(x)$, where $D_1(x)$ represents a tissue domain divided into ten subdomains, with the diffusion coefficient in each subdomain chosen at random from a uniform distribution (see figure (6-10)). Figure (6-11) shows that whilst the majority of the tumour is confined to the region below $x = 0.3$, where there is an abrupt increase in the diffusion coefficient, a very small density of tumour cells quickly invade the rest of the host tissue. From a surgical point of view, this tumour is deceptive, since it appears to have a distinct edge. By analysing the properties and composition of the host tissue at the perceived tumour boundary, a surgeon may anticipate that the tumour has invaded the host tissue beyond, and prevent tumour regrowth by adjusting the treatment strategy accordingly.

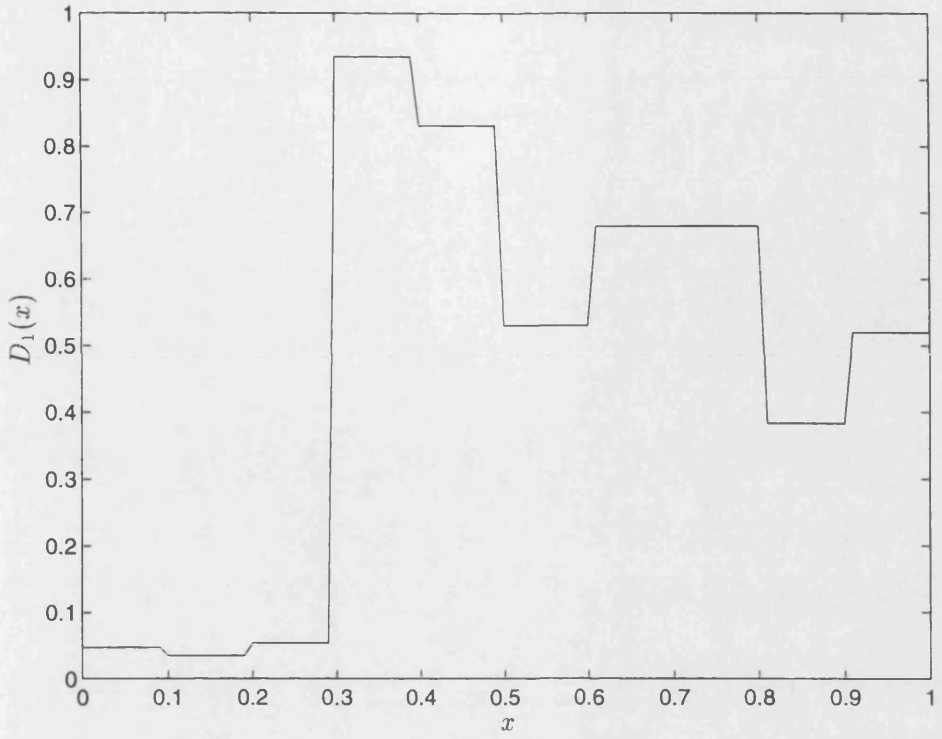

Figure 6-10: *A plot of the spatially dependent diffusion coefficient* $D_1(x)$. *Note that, at* $x = 0.3$ *there is an abrupt increase in the diffusion coefficient.*

6.4 Discussion

This model is a first attempt at introducing heterogeneity into a mathematical model of tumour growth. The model is very simple, with no sophisticated mechanism required to produce the fingering effect which is typical of an invading carcinoma. The model highlights the problem faced by a surgeon during the excision of a locally invading carcinoma. The surgeon must be satisfied that the tumour is completely removed and at the same time must minimise the damage to normal healthy tissue.

In theory, the model is experimentally testable. For example, it should be possible to grow cancer cells in a petri-dish containing dissimilar tissue. This would be an extension of multicellular spheroid models [Adam & Maggelakis, (1990)], [Durand, (1990)], [Sutherland, (1988)], which are normally grown in homogeneous cultures. The numerical simulations allow us to estimate the speed at which the cancer cells invade different tissue types and these suggest that there is a link between the metastatic potential of the tumour and the composition of the host tissue. Certain tissue combinations can provide

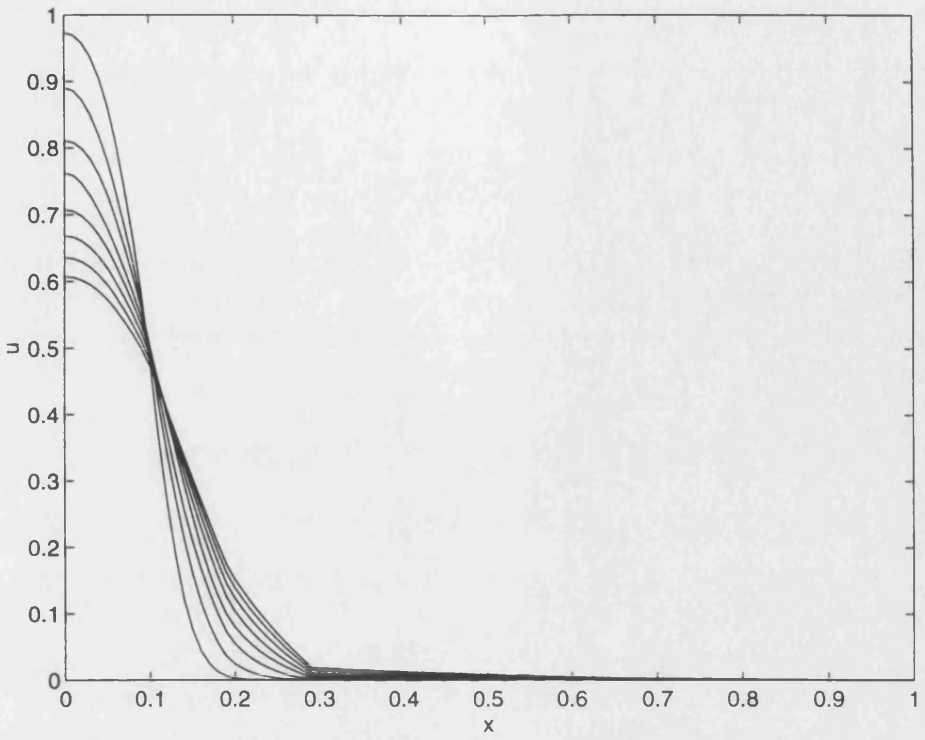

Figure 6-11: *A numerical simulation of equation (6.3.4) with* $D(x) = D_1(x)$ *as shown in figure (6-10).*

paths of least resistance which are quickly and easily penetrated by the tumour. This can assist the invasion process and may eventually lead to metastases. On the other hand, some tissue structures can restrict the tumour growth or even stop it altogether.

One way the model can be improved is to introduce heterogeneous cell populations instead of (or as well as) a heterogeneous environment. It is known that a tumour consists of sub-populations of tumour cells of varying malignancies, and may even incorporate normal cells [Fidler, (1978)], [MacSween & Whaley, (1992)]. This could be reflected in a simple model where each sub-population had a different (and perhaps density dependent) diffusion coefficient and proliferation rate.

A vascularized tumour may not have an evenly distributed blood supply and may contain *hot spots* of dense vasculature [Ellis & Fidler, (1995)] and hence there is an uneven distribution of metabolites throughout the tumour. This could lead to an irregularly shaped tumour and may affect the tumour's latent ability to metastasise. We could include active invasion mechanisms in the model, whereby the tumour cells react to blood vessels in a similar manner to that of 'taxis' [Orme & Chaplain, (1996)b] in

order to maintain their supply of nutrients.

Finally, an alternative approach would be to use a mechanochemical model [Oster & Murray, (1989)], with different constitutive equations representing different host tissue-tumour cell interactions. Byrne & Chaplain, (1996) showed that different constitutive equations led to different dispersion relations. Hence, the constitutive equation could be used as a way of classifying a tumour.

Chapter 7

Two-dimensional models of tumour angiogenesis and anti-angiogenesis strategies

There is a very strong link between the vascularization of a tumour and the spread of the disease, both locally and to distant sites. The direct supply of nutrients into the tumour results in a rapid increase in growth [Ellis & Fidler, (1995)], [Gimbrone *et al.*, (1974)], [Muthukkaruppan *et al.*, (1982)]. Solid tumour growth is dependent on angiogenesis and any significant increase in tumour size must be preceded by an increase in the vasculature [Norton, (1995)], [Paweletz & Knierim, (1989)]. Furthermore, vascularization increases the possibility of tumour cells entering the blood stream [Blood & Zetter, (1990)], [Ellis & Fidler, (1995)], [McCulloch *et al.*, (1995)], which may consequently lead to metastases. It has been suggested that some measure of the intensity of the tumour vasculature could be used as a prognostic factor [Ellis & Fidler, (1995)], [Folkman, (1995)], [McCulloch *et al.*, (1995)], [Norton, (1995)]. For example, Frank *et al.*, (1995) have developed a technique for grading angiogenesis in order to determine whether increased angiogenesis correlates to higher recurrence and reduced survival in patients suffering from cancer of the colon.

It seems clear that anti-angiogenesis strategies could be used to augment existing treatment modalities [Folkman, (1985)], [Harris *et al.*, (1996)]. Mathematical models such as the one given here can help us to understand the mechanisms behind angiogenesis and to identify the different ways by which the angiogenic process can be interrupted.

In this chapter we will develop a two-dimensional model of capillary vessel formation. As before in chapter (3), we examine the role that haptotaxis may play during the growth of the neovasculature. By suitable manipulation of the model parameters, we simulate a variety of anti-angiogenic strategies and examine the effect on the pattern of capillary growth. Finally, we suggest an alternative mechanism to capillary vessel formation which does not involve haptotaxis.

7.1 The mathematical model

This mathematical model is based on the assumption that diffusible chemicals, generically referred to as tumour angiogenesis factors (TAFs), are released by the tumour cells and that these chemicals stimulate the endothelial cells (EC) in nearby blood vessels to grow and migrate towards the tumour. It is known that different TAFs provoke different responses in the EC [Folkman & Klagsbrun, (1987)]. For example,

- Some TAFs act as a chemoattractant, whereby the EC move up the chemical gradient towards the tumour (chemotaxis).
- Some TAFs induce the EC into secreting adhesive substances (e.g. fibronectin, collagens) and this creates an adhesive gradient which the EC move up (haptotaxis [Carter, (1965)]).

If $n(\mathbf{x},t)$ denotes the density of the EC, $c(\mathbf{x},t)$ the concentration of TAF, $p(\mathbf{x},t)$ the density of an adhesive chemical, such as fibronectin, at position $\mathbf{x}$ and time t, then the general conservation equations are

$$\frac{\partial n}{\partial t} = -\nabla.\mathbf{J} + P_1(n,p,c), \tag{7.1.1}$$

$$\frac{\partial p}{\partial t} = D_2\nabla^2 p + S_1(n,p,c) + P_2(n,p,c), \tag{7.1.2}$$

$$\frac{\partial c}{\partial t} = D_3\nabla^2 c + S_2(n,p,c) + P_3(n,p,c), \tag{7.1.3}$$

where $\mathbf{J}$ is the flux of the EC, D_i, $(i = 2,3)$ are the (constant) diffusion coefficients, P_i, $(i = 1,2,3)$ are net production/loss terms and S_i, $i = 1,2$ are sink terms modelling the uptake of the chemotactic/haptotactic chemical by the EC. These terms will be made explicit below.

First, we assume that the flux of the EC is governed by diffusion, haptotactic and chemotactic movement, such that we have

$$\mathbf{J} = -D_1 \nabla n + \chi n \nabla p + \kappa n \nabla c,$$

where D_1 is the diffusion coefficient, χ is the haptotaxis coefficient and κ is the chemotaxis coefficient. For simplicity, we assume that D_1, χ, κ are all constant. We further assume that the proliferation of the EC is governed by logistic type growth and that any cell loss is linear. Hence we assume that P_1 takes the form

$$P_1(n,p,c) = \mu n(1 - \frac{n}{n_0}) - \beta n,$$

where μ is the proliferation rate of the cells, n_0 is the maximum sustainable cell density and β is the rate of cell loss. In their one dimensional model of tumour angiogenesis, Chaplain *et al.*, (1995) considered the first order loss term $-\beta n$ to be a loss due to the formation of secondary capillary buds. In two or more dimensions however, such a term represents a loss due to cell death. Since EC have a long half life [Paweletz & Knierim, (1989)], we assume that any death occurs due to external intervention, i.e. the introduction of a cytotoxic drug. In this model, we suppose that the initial release of TAF induces the EC into secreting an adhesive (haptotactic) chemical p, which saturates as p increases. If B is the threshold level of the haptotactic chemical above which the production of p by the EC is switched on and if α is the maximum production rate per cell, then

$$P_2 = \frac{\alpha n p}{B + p} - \text{decay}.$$

Here, the chemical production term shows the response of the endothelial cells to changes in the adhesive chemical density and the term saturates as p increases, as required. We assume that any uptake of the haptotactic and chemotactic chemical by the EC to be of the form

$$S_1 = -s_1 np, \quad S_2 = -s_2 nc,$$

where s_1 and s_2 are the rate of uptake of the haptotactic and chemotactic chemical, per cell. The decay of the two chemicals is assumed to be linear.

Hence, the full model is

$$\frac{\partial n}{\partial t} = D_1\nabla^2 n - \chi\nabla.(n\nabla p) - \kappa\nabla.(n\nabla c) + \mu n(1 - \frac{n}{n_0}) - \beta n, \qquad (7.1.4)$$

$$\frac{\partial p}{\partial t} = D_2\nabla^2 p + \frac{\alpha np}{B+p} - s_1 np - \lambda_1 p, \qquad (7.1.5)$$

$$\frac{\partial c}{\partial t} = D_3\nabla^2 c - s_2 nc - \lambda_2 c, \qquad (7.1.6)$$

We assume a two-dimensional geometry such that the model equations hold on the square domain $\mathcal{D} = [0, L] \times [0, L]$. We assume that the tumour is located along the x-axis and that the parent capillary vessel lies along the line $y = L$ so that L is the perpendicular distance from the tumour to the parent vessel. By using the above two dimensional geometry, the model is, in theory, *experimentally reproducible*. For example, this model could represent an *in vitro* experiment, whereby tumour cells are placed in a line along one edge of a square petri-dish with EC placed along the opposite edge. Alternatively, we could focus upon the role of haptotaxis by suspending TAF in gel, so that the gradient of TAF is constant.

In order to normalize the equations, we define the following reference variables. Let n_0 be a reference endothelial cell density, such as the carrying capacity of the system, p_0 be a typical density of the adhesive chemical during angiogenesis and c_0 be the initial density of TAF concentration at the tumour boundary. Hence, we non-dimensionalize by making the following substitutions;

$$\tilde{n} = \frac{n}{n_0}, \quad \tilde{p} = \frac{p}{p_0}, \quad \tilde{c} = \frac{c}{c_0}, \quad \tilde{t} = \frac{t}{\tau}, \quad \tilde{x} = \frac{x}{L}, \quad \tilde{y} = \frac{y}{L},$$

$$\tilde{\chi} = \frac{p_0\tau\chi}{L^2}, \quad \tilde{\kappa} = \frac{c_0\tau\kappa}{L^2}, \quad \tilde{\mu} = \mu\tau, \quad \tilde{\beta} = \beta\tau, \quad \tilde{D}_i = \frac{D_i\tau}{L^2}, \quad i = 1,2,3, \qquad (7.1.7)$$

$$\tilde{\alpha} = \frac{\alpha n_0\tau}{p_0}, \quad \tau = \frac{1}{s_1 n_0}, \quad \tilde{s_2} = \frac{s_2}{s_1}, \quad \tilde{B} = \frac{B}{p_0}, \quad \tilde{\lambda_i} = \lambda_i\tau, \quad i = 1,2.$$

Dropping the tildes for notational convenience, the full model equations are

$$\frac{\partial n}{\partial t} = D_1\left(\frac{\partial^2 n}{\partial x^2} + \frac{\partial^2 n}{\partial y^2}\right) - \chi\left(\frac{\partial n}{\partial x}\frac{\partial p}{\partial x} + \frac{\partial n}{\partial y}\frac{\partial p}{\partial y} + n\left(\frac{\partial^2 p}{\partial x^2} + \frac{\partial^2 p}{\partial y^2}\right)\right)$$

$$-\kappa\left(\frac{\partial n}{\partial x}\frac{\partial c}{\partial x} + \frac{\partial n}{\partial y}\frac{\partial c}{\partial y} + n\left(\frac{\partial^2 c}{\partial x^2} + \frac{\partial^2 c}{\partial y^2}\right)\right) + \mu n(1-n) - \beta n, \quad (7.1.8)$$

$$\frac{\partial p}{\partial t} = D_2\left(\frac{\partial^2 p}{\partial x^2} + \frac{\partial^2 p}{\partial y^2}\right) + \frac{\alpha n p}{B+p} - np - \lambda_1 p, \quad (7.1.9)$$

$$\frac{\partial c}{\partial t} = D_3\left(\frac{\partial^2 c}{\partial x^2} + \frac{\partial^2 c}{\partial y^2}\right) - s_2 nc - \lambda_2 c, \quad (7.1.10)$$

Initial and boundary conditions

The initial conditions are as follows;

- If $y \geq 0.9$ and $0.11 \leq x \leq 0.17$, or $0.35 \leq x \leq 0.41$, or $0.59 \leq x \leq 0.65$, or $0.83 \leq x \leq 0.89$, then $n(x, y, 0) = 1$. Otherwise, $n(x, y, 0) = 0$.
- $p(x, y, 0) = \dfrac{n(x, y, 0)}{2}$.
- $c(x, y, 0) = 1 - y$.

Thus, we assume that there are initially four capillary sprouts and equivalently, four foci of fibronectin. For all the numerical simulations, we took zero flux boundary conditions, except for the endothelial cells at the boundary $y = 1$, for which we assumed that the capillary sprouts were fixed to the parent vessel, i.e. if $0.11 \leq x \leq 0.17$, or $0.35 \leq x \leq 0.41$, or $0.59 \leq x \leq 0.65$, or $0.83 \leq x \leq 0.89$, then $n(x, y = 1, t) = 1$. Otherwise, $n(x, y = 1, t) = 0$.

7.1.1 Estimation of parameter values

Whenever possible, experimental data was used to estimate the parameter values. If this was not possible, then the parameters were chosen in order to give the best qualitative results, provided those parameters did not correspond to unrealistic dimensional quantities.

Estimation of fibronectin uptake time τ

Terranova *et al.*, (1985) found that doses of fibronectin between 10^{-8}M and 10^{-10}M stimulated cell migration and Yamada & Olden, (1978) gave the generation time of fibronectin to be 18 hours. Assuming that 10^{-8}M of fibronectin is produced by n_0 cells in 18 hours, we estimate the rate of the secretion of the fibronectin as $\frac{10^{-8}}{18} n_0^{-1} \mathrm{h}^{-1}\mathrm{M}$ [Orme & Chaplain, (1996)a]. We would expect the secretion rate to be higher than the uptake rate, say five times higher, i.e. $\alpha = 5$. Hence taking p_0 in the range $10^{-8} - 10^{-10}$M [Terranova *et al.*, (1985)], we have $\tau = \frac{1}{s_1 n_0}$ in the range 90–9000 h.

Estimation of diffusion coefficients D_1, D_2, D_3

In their model of epidermal wound healing, Sherratt & Murray, (1990) used values of $3 \times 10^{-9}\mathrm{cm}^2\mathrm{s}^{-1}$, $3.5 \times 10^{-10}\mathrm{cm}^2\mathrm{s}^{-1}$ and $6.9 \times 10^{-11}\mathrm{cm}^2\mathrm{s}^{-1}$ for the diffusion of the cells. In their study of individual endothelial cells, Stokes *et al.*, (1991) calculated a random motility coefficient of $(7.1 \pm 2.7) \times 10^{-9}\mathrm{cm}^2\mathrm{s}^{-1}$ for endothelial cells migrating in a culture containing an angiogenic factor αFGF [Folkman & Klagsbrun, (1987)], heparin and fetal calf serum. Assuming that the diffusion of the EC is in the range $10^{-9} - 10^{-11}\mathrm{cm}^2\mathrm{s}^{-1}$, then D_1 is in the range $3.6 \times 10^{-5} - 5.06$. Since we want to focus upon the roles of haptotaxis and chemotaxis in this model, we want the diffusion coefficient to be as small as possible without running into difficulties with the numerical simulations. Hence, we chose $D_1 = 0.0025$.

For the diffusion coefficient of the chemotactic chemical, Sherratt & Murray, (1990) took values of $3.1 \times 10^{-7}\mathrm{cm}^2\mathrm{s}^{-1}$ and $5.9 \times 10^{-6}\mathrm{cm}^2\mathrm{s}^{-1}$ and Chaplain *et al.*, (1995) took $3.3 \times 10^{-8}\mathrm{cm}^2\mathrm{s}^{-1}$. Assuming that the diffusion coefficient of the haptotactic and chemotactic chemical is in the range $10^{-6} - 10^{-8}\mathrm{cm}^2\mathrm{s}^{-1}$, we obtain D_2 and D_3 in the range $3.6 \times 10^{-2} - 5.06$. We chose $D_2 = D_3 = 0.5$, which is in the middle of the range and is 200 times larger than the diffusion coefficient of the tumour cells.

Haptotaxis coefficient χ and chemotaxis coefficient κ

In the absence of reliable empirical data, we chose $\chi = 0.5$, which leads to a dimensional value of the haptotaxis coefficient in the range $10^{-2} - 1389\mathrm{cm}^2\mathrm{s}^{-1}\mathrm{M}^{-1}$. Stokes *et al.*, (1991) estimated the chemotaxis coefficient of EC migrating in a culture containing αFGF, to be $2600\mathrm{cm}^2\mathrm{s}^{-1}\mathrm{M}^{-1}$. Choosing $\kappa = 0.65$ the non-dimensionalization gives a

value of c_0 in the range $6.7 \times 10^{-11} - 4.9 \times 10^{-14}$M. From this, we infer that the TAF mobilizes EC at a smaller concentration than that of the fibronectin.

Proliferation rate μ and death rate β

The proliferation rate of the EC is estimated to be in the range 0.04h^{-1} [Sherratt & Murray, (1990)] to 0.056h^{-1} [Stokes & Lauffenburger, (1991)], assuming that all cells undergo mitosis. However, fibronectin can inhibit EC proliferation by up to 23% [Bowersox & Sorgente, (1982)]. Furthermore, during angiogenesis, proliferation is generally confined to a region near the tips of the capillary sprouts. Hence, assuming that the proliferation rate is 0.02h^{-1} [Chaplain *et al.*, (1995)], [Stokes & Lauffenburger, (1991)], we obtain μ in the range 1.8 to 180.

Brooks *et al.*, (1994) found that EC underwent apoptosis 48 hours after injecting integrin $\alpha_v\beta_3$ antagonists into the site. Taking $\frac{1}{48}\text{h}^{-1}$ as the death rate, we have β in the range 1.875-187.5.

Fibronectin density ratio B

We would expect that the secretion of fibronectin to have been switched on by the initial release of TAF by the tumour, so that the typical threshold fibronectin density p_0, is greater than the threshold level, i.e. $B < 1$. We take $B = 0.001$.

Decay of haptotactic and chemotactic chemicals λ_1, λ_2

If we take $\lambda_i = 0.5$, $i = 1, 2$, then the dimensional estimate for the decay of the chemicals is $5.6 \times 10^{-3} - 5.6 \times 10^{-5}\text{h}^{-1}$.

7.1.2 Model simplification which focuses upon the role of haptotaxis

In order to focus attention upon the role of haptotaxis in angiogenesis, we simplify the profile of the chemotactic chemical. In Chaplain *et al.*, (1995), the TAF concentration profile does not vary drastically over time. They concluded that it is reasonable to assume that the TAF profile is in some kind of steady state, since the TAF diffuses much faster than the endothelial cells. Henceforth, we assume that the TAF has reached its steady state and we approximate the TAF profile by $c(x, y) = 1 - y$ (cf. Chaplain *et al.*, (1995)). Thus, in the next section, we solve numerically the simplified model,

$$\frac{\partial n}{\partial t} = D_1\left(\frac{\partial^2 n}{\partial x^2} + \frac{\partial^2 n}{\partial y^2}\right) - \chi\left(\frac{\partial n}{\partial x}\frac{\partial p}{\partial x} + \frac{\partial n}{\partial y}\frac{\partial p}{\partial y} + n\left(\frac{\partial^2 p}{\partial x^2} + \frac{\partial^2 p}{\partial y^2}\right)\right)$$

$$+\kappa\frac{\partial n}{\partial y} + \mu n(1-n) - \beta n, \tag{7.1.11}$$

$$\frac{\partial p}{\partial t} = D_2\left(\frac{\partial^2 p}{\partial x^2} + \frac{\partial^2 p}{\partial y^2}\right) + \frac{\alpha n p}{B+p} - np - \lambda_1 p. \tag{7.1.12}$$

7.2 Numerical simulations of simplified model

The system of equations (7.1.11)-(7.1.12) was solved using a routine available from the NAG library, which integrates using the method of lines and Gear's method. In our first numerical simulation, we solved the system (7.1.11)-(7.1.12) with parameters $\kappa = 0.65$, $\mu = 5$, $\beta = 0$, $\chi = 0.5$, $\lambda_1 = 0.5$, $\alpha = 5$, $B = 0.001$, $D_1 = 0.0025$, $D_2 = 0.5$. Figure (7-1) and figure (7-2) show the resultant growth of the capillary vessels through the host tissue. In figure (7-1), we can see the beginning of secondary branch formation at the tip of each capillary sprout, and these branches subsequently merge to form anastomoses (figure(7-2)) via branch-tip to branch-tip fusion [Konerding *et al.*, (1992)]. Furthermore, the capillaries have a well defined structure (cf. figure (7-7)) which is necessary for blood to flow through the vessels. Note that there is a higher density of endothelial cells at the front of the capillary vessel which is where the brush border effect is observed by Muthukkaruppan *et al.*, (1982).

7.2.1 Anti-angiogenesis strategies

In the numerical simulations, we consider four different ways by which the angiogenic process can be disrupted. These four approaches represent viable anti-angiogenesis strategies, which can be used in conjunction with more established treatment modalities [Folkman, (1995)], [Norton, (1995)]. Furthermore, we explicitly target the endothelium in the neovasculature so that, in theory, the damage to normal tissue is minimised [Brooks *et al.*, (1994)], [Folkman, (1995)].

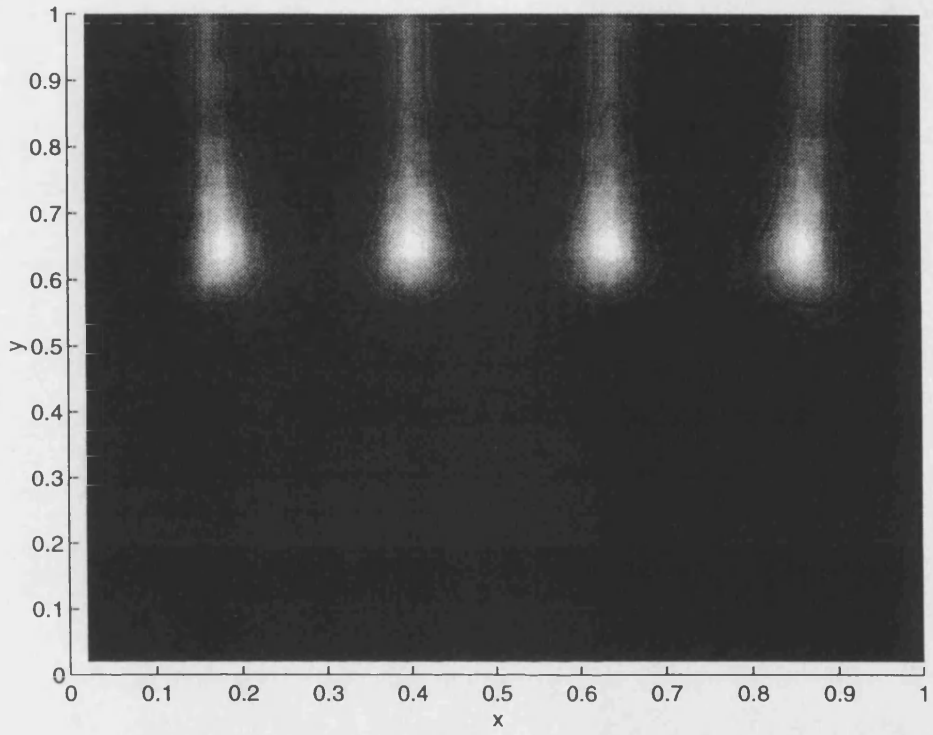

Figure 7-1: *Numerical solution of the system (7.1.11)-(7.1.12) with fixed TAF profile* $c = 1 - y$ *and parameters* $\kappa = 0.65$, $\mu = 5$, $\beta = 0$, $\chi = 0.5$, $\lambda_1 = 0.5$, $\alpha = 5$, $B = 0.001$, $D_1 = 0.0025$, $D_2 = 0.5$. *This simulation shows the distribution of the EC at time* $t = 0.8$. *We can see the beginning of T shaped branch formation at the tip of each capillary sprout.*

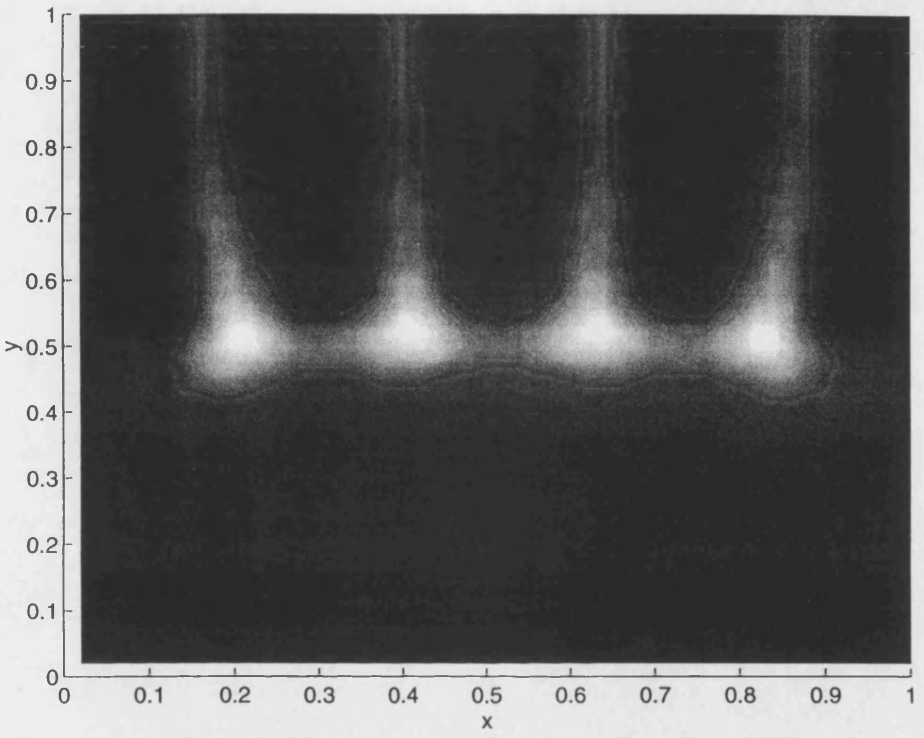

Figure 7-2: *Numerical solution of the system (7.1.11)-(7.1.12) with fixed TAF profile* $c = 1 - y$ *and parameters* $\kappa = 0.65$, $\mu = 5$, $\beta = 0$, $\chi = 0.5$, $\lambda_1 = 0.5$, $\alpha = 5$, $B = 0.001$, $D_1 = 0.0025$, $D_2 = 0.5$. *At time* $t = 1.2$, *we can see the formation of anastomoses via branch-tip to branch-tip fusion. Furthermore, the capillaries have a well-defined structure which correlates to a good flow of blood.*

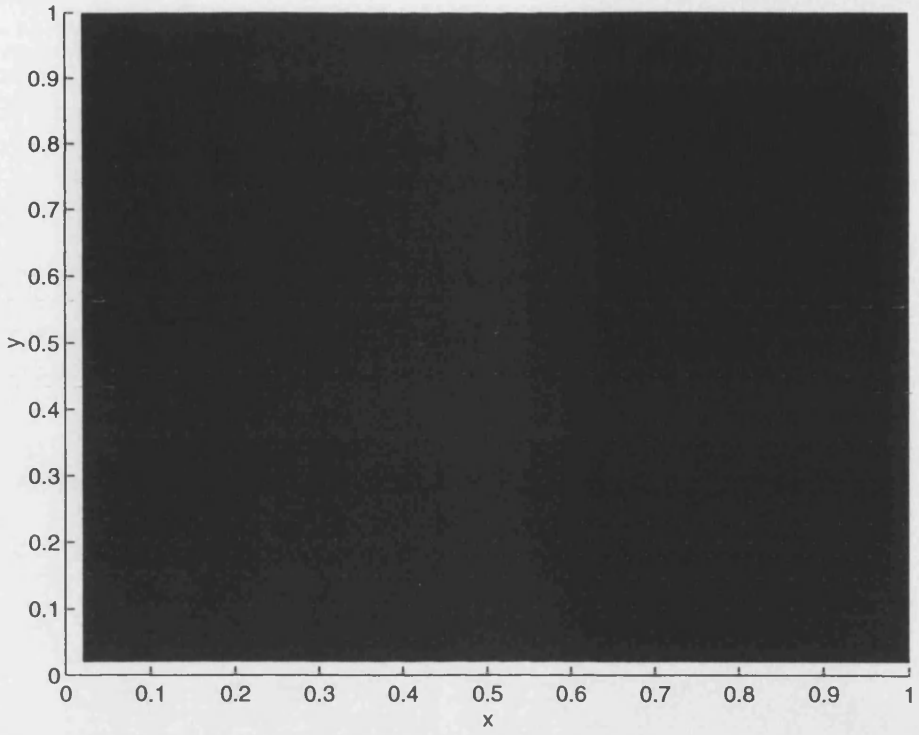

Figure 7-3: *Numerical solution of the system (7.1.11)-(7.1.12) with fixed TAF profile* $c = 1 - y$ *and parameters* $\kappa = 0.65$, $\mu = 5$, $\beta = 50$, $\chi = 0.5$, $\lambda_1 = 0.5$, $\alpha = 5$, $B = 0.001$, $D_1 = 0.0025$, $D_2 = 0.5$. *This models an anti-angiogenesis strategy whereby the angiogenic process is impeded by the use of endothelial cell-specific drugs, i.e. cytotoxic agents which preferentially kill EC. At time* $t = 0.1$, *the capillary sprouts have died away.*

Cytotoxic targeting of endothelial cells

First, we consider the use of cytotoxic therapy which preferentially kills EC. Such a strategy is most beneficial if preexisting blood vessels can be left unaffected. For example, Brooks *et al.*, (1994) demonstrated that antagonists of integrin $\alpha_\nu\beta_3$ disrupted tumour angiogenesis by selectively inducing apoptosis in EC during the proliferative phase of the cell cycle. Since only the EC in the neovasculature undergo mitosis on the time scale under consideration, the adjacent vessels are left intact. We model this by setting $\beta = 50$. As expected such a strategy results in the complete regression of the capillary sprouts (see figure (7-3)).

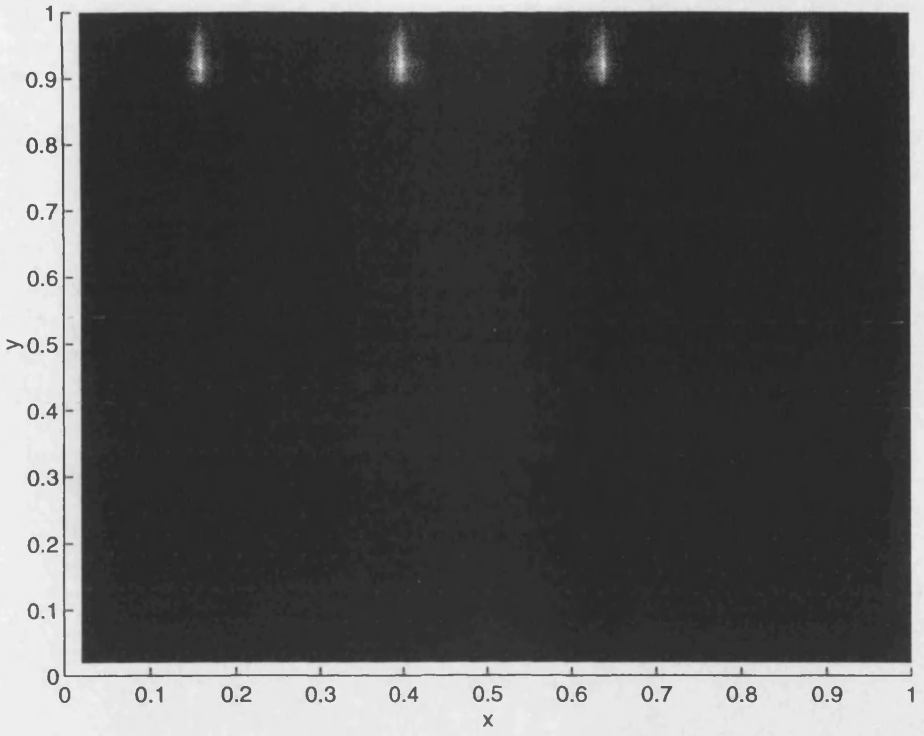

Figure 7-4: *Numerical solution of the system (7.1.11)-(7.1.12) with fixed TAF profile* $c = 1 - y$ *and parameters* $\kappa = 0.65$, $\mu = 0$, $\beta = 0$, $\chi = 0.5$, $\lambda_1 = 0.5$, $\alpha = 5$, $B = 0.001$, $D_1 = 0.0025$, $D_2 = 0.5$. *Another potential anti-angiogenesis strategy is the prevention of EC mitosis, i.e. by irradiation or by use of an inhibitor. At time* $t = 0.1$, *the growth of the capillary sprouts has been arrested.*

Inhibition of cell mitosis

It has been demonstrated that proliferation of EC is vital for the successful completion of angiogenesis [Ausprunk & Folkman, (1977)], [Paweletz & Knierim, (1989)]. Recently, chemical agents, such as angiostatin [Folkman, (1995)], [O'Reilly *et al.*, (1994)] have been isolated, which specifically inhibit EC proliferation and thus inhibit angiogenesis. Since the cell doubling time of EC in the absence of TAF is long (months [Paweletz & Knierim, (1989)]) in comparison with the half life of angiostatin (2.5 days [Folkman, (1995)], only the newly formed vasculature would be affected. We model this by setting the cell proliferation rate μ to zero. In the numerical simulation, the capillary sprouts stopped growing after a time $t = 0.1$ (figure (7-4)). O'Reilly *et al.*, (1994) found that angiostatin inhibited angiogenesis 48 hours after implantation, which gives us a value of $\tau = 480$, which is within our estimated range.

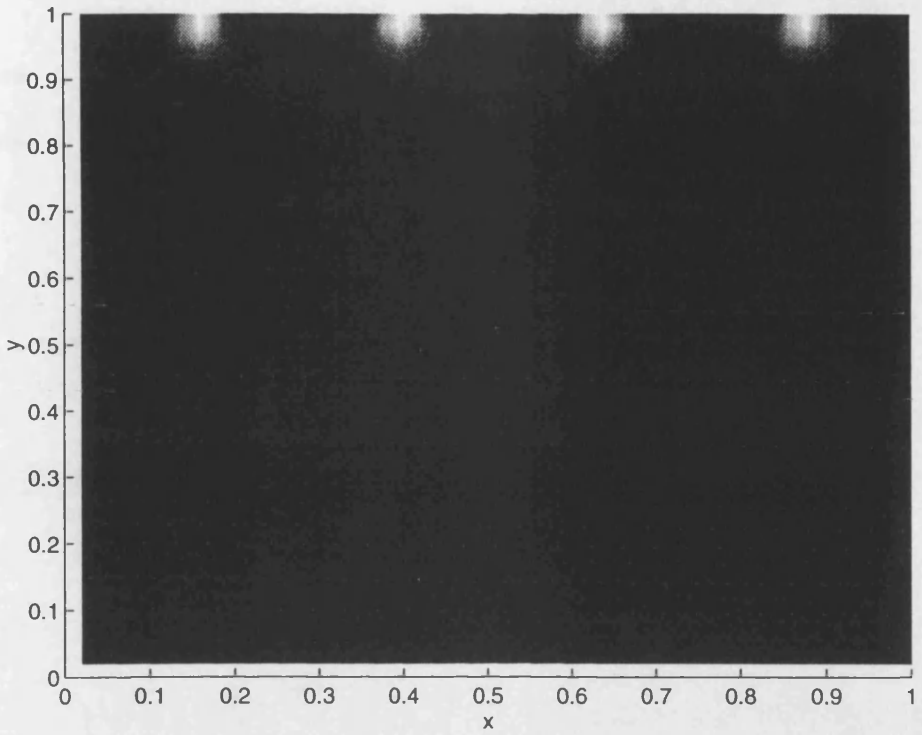

Figure 7-5: *Numerical solution of the system (7.1.11)-(7.1.12) with fixed TAF profile* $c = 1 - y$ *and parameters* $\kappa = 0$, $\mu = 5$, $\beta = 0$, $\chi = 0.5$, $\lambda_1 = 0.5$, $\alpha = 5$, $B = 0.001$, $D_1 = 0.0025$, $D_2 = 0.5$. *Plot taken at time* $t = 0.2$. *This simulates an anti-angiogenesis strategy whereby the EC are unable to react to the chemotactic stimulus, i.e by disrupting the appropriate receptors on the surface of the cell. The capillary vessels regress and angiogenesis fails.*

Prevention of cell migration: (1) Anti-chemotaxis

Cell migration has been identified as a key event in tumour angiogenesis. Cell migration can be disrupted by interfering with the cells' ability to detect local chemical gradients. For example, endothelial cells are known to react chemotactically to hepatocyte growth factor (HGF) [Bussolino *et al.*, (1992)]. It is possible to cultivate antibodies against the HGF receptor [Bussolino *et al.*, (1992)] and hence prevent chemotaxis. We model this by setting our chemotaxis coefficient κ to zero to obtain the numerical solution as shown in figure (7-5). This shows that in the absence of a detectable TAF gradient, angiogenesis fails.

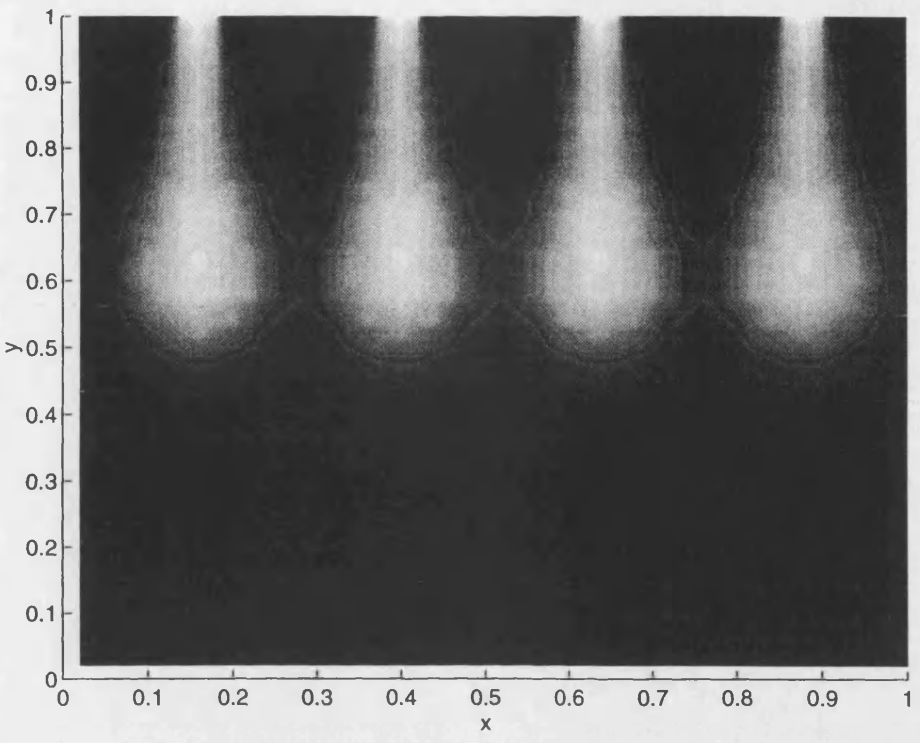

Figure 7-6: *Numerical solution of the system (7.1.11)-(7.1.12) with fixed TAF profile* $c = 1 - y$ *and parameters* $\kappa = 0.65$, $\mu = 5$, $\beta = 0$, $\chi = 0$, $\lambda_1 = 0.5$, $\alpha = 5$, $B = 0.001$, $D_1 = 0.0025$, $D_2 = 0.5$. *Plot taken at time* $t = 0.6$. *The anti-angiogenesis strategy adopted here prevents the EC from reacting to the haptotactic chemical, i.e. by affecting the receptors on the cell surface. Though the capillary sprouts continue to grow under the influence of chemotaxis, the sprouts are not as distinct as those in figures (7-1) and (7-2) .*

Prevention of cell migration: (2) Anti-haptotaxis

It is known that fibronectin increases cell-cell and cell-matrix adhesiveness. Yamada & Olden, (1978) showed that EC have a specific receptor for fibronectin. By blocking the fibronectin receptors, we prevent the EC from reacting haptotactically to fibronectin. We model this by setting the haptotaxis coefficient χ to zero. At first, this method does not seem to have impeded the growth of the capillary sprouts. At time $t = 0.6$ there is some evidence of anastomoses (figure (7-6)), though the loops do not appear to have been formed by the fusion of branch tips. Furthermore, the capillary vessels are not as distinct in comparison with the vessels in figures (7-1) and (7-2). This becomes more evident in figure (7-7) where we can see that the endothelial cells have not formed

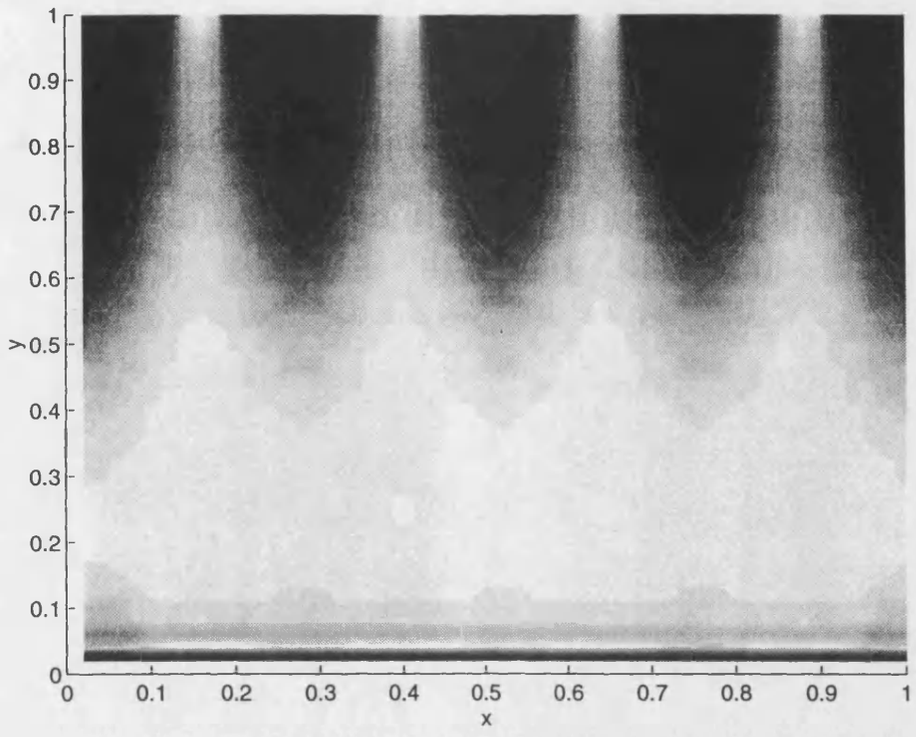

Figure 7-7: *Numerical solution of the system (7.1.11)-(7.1.12) with fixed TAF profile* $c = 1 - y$ *and parameters* $\kappa = 0.65$, $\mu = 5$, $\beta = 0$, $\chi = 0$, $\lambda_1 = 0.5$, $\alpha = 5$, $B = 0.001$, $D_1 = 0.0025$, $D_2 = 0.5$. *Plot taken at time* $t = 1.2$. *The anti-angiogenesis strategy adopted here prevents the EC from reacting to the haptotactic chemical, i.e. by affecting the receptors on the cell surface. Though the strategy has not prevented the outgrowth of endothelial cells, the EC have not formed well-defined structures, and hence there will be a poor circulation of blood.*

well-defined structures. We would expect the circulation of blood through such inferior vessels to be poor and hence, the angiogenic process has failed to produce a viable network of capillaries. Hence, we conclude that the compactness of the vessels shown in in figures (7-1) and (7-2) as compared to figures (7-6) and (7-7) is due to haptotaxis.

Finally, we conducted a parameter sensitivity analysis on this model and found that the following parameter changes had an equivalent effect on the resultant solutions. Increasing the EC proliferation rate, increasing the diffusion coefficient of the haptotactic chemical or decreasing the haptotaxis coefficient all resulted in a loss of definition (compactness) of the capillary sprouts (a similar result is shown in figure (7-7)). Furthermore, the same effect could be achieved by increasing *or* decreasing the secretion rate of the

haptotactic chemical. This implies that there is some optimal level of (fibronectin) production, such that the EC cannot respond to too little chemical or become saturated when there is too much. A summary of the different numerical simulations conducted and the parameter sensitivity analysis is given in table (7.1).

7.3 Alternative chemotaxis model

We will now briefly consider an alternative mechanism for the formation of capillary sprouts during angiogenesis, which does not involve haptotaxis. We assume that the TAF produced by the tumour does not induce the secretion of fibronectin (or other such adhesive material) by the EC. Hence, by setting $p(x,y,t) = 0$ in the system (7.1.8)-(7.1.10), we obtain the sub-model

$$\frac{\partial n}{\partial t} = D_1\left(\frac{\partial^2 n}{\partial x^2} + \frac{\partial^2 n}{\partial y^2}\right) - \kappa\left(\frac{\partial n}{\partial x}\frac{\partial c}{\partial x} + \frac{\partial n}{\partial y}\frac{\partial c}{\partial y} + n\left(\frac{\partial^2 c}{\partial x^2} + \frac{\partial^2 c}{\partial y^2}\right)\right)$$

$$+\mu n(1-n) - \beta n, \tag{7.3.13}$$

$$\frac{\partial c}{\partial t} = D_3\left(\frac{\partial^2 c}{\partial x^2} + \frac{\partial^2 c}{\partial y^2}\right) - s_2 nc - \lambda_2 c, \tag{7.3.14}$$

Here, the capillary vessels act as sinks, which absorb the TAF and hence, create local chemical gradients. This may provide an alternative mechanism for the formation of capillary branches and anastomoses. This is investigated in a preliminary numerical simulation of the system (7.3.13)-(7.3.14) with parameter values $\kappa = 0.65$, $\mu = 5$, $\beta = 0$, $\lambda_2 = 0.5$, $s_2 = 1$, $D_1 = 0.0025$, $D_3 = 0.5$. The resultant pattern of capillary growth is shown in figure (7-8). We see the beginnings of capillary outgrowth towards the tumour located at $y = 0$. However, in the absence of haptotaxis, the vessels are not as well-defined when compared with figure (7-1) and figure (7-2). After a time $t = 0.8$, the vessels are almost indistinguishable, and such poor definition would result in poor circulation of blood. In this case, the angiogenic process has failed to produce a viable capillary network.

Anti-angiogenesis strategies

Action	*Change in parameter*	*Effect on solution*
Cytotoxic targeting of EC [Brooks *et al.*, (1994)]	$\beta = 50$	Complete regression of capillary sprouts
Inhibit EC mitosis [O'Reilly *et al.*, (1994)]	$\mu = 0$	Capillary sprouts stop growing
Anti-chemotaxis	$\kappa = 0$	Capillary sprouts stop growing
Anti-haptotaxis	$\chi = 0$	Loss of compactness

Parameter sensitivity analysis

Action	*Change in parameter*	*Effect on solution*
Increase proliferation	Increase μ	Loss of compactness
Increase diffusion of haptotactic chemical	Increase D_2	" "
Increase secretion of haptotactic chemical	Increase α	" "
Decrease secretion of haptotactic chemical	Decrease α	" "

Table 7.1: *A summary of the different anti-angiogenesis strategies and a parameter sensitivity analysis and the effect on the solution as compared to figures (7-1) and (7-2).*

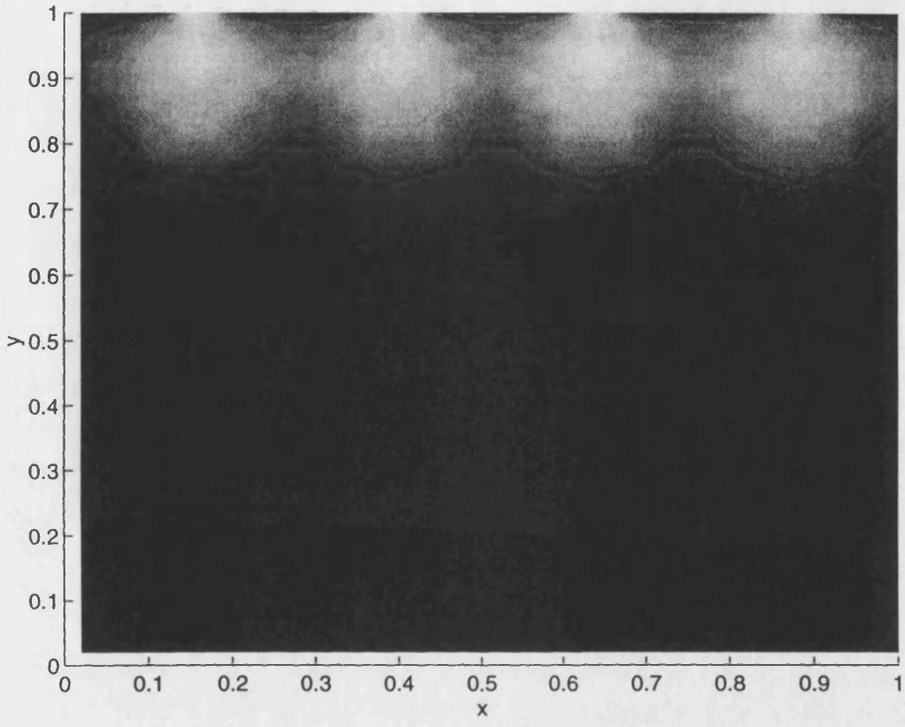

Figure 7-8: *Numerical solution of the chemotaxis sub-model (7.3.13)-(7.3.14) with model parameters* $\kappa = 0.65$, $\mu = 5$, $\beta = 0$, $\lambda_2 = 0.5$, $s_2 = 1$, $D_1 = 0.0025$, $D_3 = 0.5$. *Plot taken at time* $t = 0.8$. *Though the capillary sprouts grow towards the tumour, the vessels are not well-defined and as a result the flow of blood through the vasculature would be poor. In this case, we consider angiogenesis to have failed*

7.4 Discussion

This model has captured key features of angiogenesis, namely, the outgrowth of capillary sprouts, branching and loop formation (anastomoses). In this model, anastomoses is brought about as a result of the haptotactic movement of the EC in response to an adhesive chemical which the EC themselves secrete. This is considered to be an improvement on the model of Chaplain, (1995), where the steady-state profile of the TAF was assumed to be radially symmetric and hence, anastomosis occurs simply as a consequence of the geometry.

We have used two dimensional geometry in this model, so that, in theory, the results are experimentally testable. The initial and boundary conditions used in the model suggest an *in vitro* experiment, where a square petri-dish contains TAF suspended in gel and four clusters of EC located at the edge of the dish. Such an experiment has yet to be carried out.

The numerical simulations presented in the previous sections imply that both chemotaxis and haptotaxis are required for successful vascularization of the tumour, though they have different roles in the angiogenic process. Chemotaxis is the underlying mechanism which drives the outgrowth of the complete capillary network, whereas haptotaxis controls the finer structure and continuity of the vasculature. Though it has been shown that the proliferation of the EC is not required for the initial stages of capillary sprout formation [Sholley *et al.*, (1984)], it is essential for the successful completion of angiogenesis [Ausprunk & Folkman, (1977)].

We have identified a number of ways by which the angiogenic process can be disrupted. Anti-angiogenesis has a lot of potential as an adjunctive therapy, whereby it is used alongside conventional treatments, or on its own in circumstances where other methods result in unacceptable damage of normal host tissue [Folkman, (1995)], [Harris *et al.*, (1996)]. One problem for pathologists is the variety of metastatic patterns in patients with the same type of cancer [Frank *et al.*, (1995)], [Nicolson, (1988)]. By establishing a range of different therapies, treatment can be tailored to meet the individual requirements of each patient. Furthermore, anti-angiogenesis can be used to control the growth of the metastases as well as the primary tumour.

Chapter 8

Conclusions and future work

In this final chapter, we will look at the models presented in this thesis in a more general context and highlight areas of research which are currently underway or which may be realised in the future. The focus in this thesis has been upon events prior to metastasis, as there is more potential for the development of viable treatment modalities in this area. In particular, we have looked at models of tumour angiogenesis and tumour invasion as these events have many serious consequences. It would be extremely difficult to model metastases formation using a continuum approach. The potential of each tumour to metastasise depends upon numerous factors, such as the tumour type, the site of the primary tumour relative to the circulatory system, and the probability of the tumour cells surviving in the blood stream. Once a secondary tumour has been initiated, it will develop in a similar manner to the primary tumour. Hence, the models in this thesis can also describe the progress of established tumour metastases.

In chapter (2), we presented a mathematical model which showed that the growth of an avascular tumour can be modulated by the immune response of the host as well as other host factors. In the future, we can expect the development of cancer 'vaccines', whereby tumour antibodies are administered intravenously, which mark the tumour cells for destruction by the host's immune cells [Lineham *et al.*, (1996)]. However, progress in this area may be hampered by a lack of suitable *in vivo* models which represent a spontaneously growing human tumours. Mathematical models of post vaccine host-tumour interactions may prove a useful tool to screen out invalid treatment modalities.

In chapter (3), we looked at the formation of capillary buds and secondary branching during the early stages of angiogenesis. We considered haptotaxis to be an important

mechanism for the formation of capillary buds and sprouts. The model was very simple, which is an advantage from a mathematical perspective, but may not be entirely appropriate from a biological point of view, since the early stages of angiogenesis involve many complex interactions between different cells and a number of chemicals with competing effects. However, a highly detailed model may obscure the important features and would be difficult to analyse. One way to overcome this may be to use a stochastic model (for example [Dickinson & Tranquillo, (1993)], [Stokes & Lauffenburger, (1991)]), which can go some way towards modelling sources of variation which are too difficult to incorporate directly. In a stochastic model the same initial conditions can produce different end results. Hence, stochastic variation in a model of a capillary network formation may result in more realistic branching structures.

In chapter (4), we examined the vascularization and subsequent invasive growth of a solid tumour. We used this model to estimate the invasion speed of the tumour. One of the features captured by this model is the development of a necrotic/hypoxic core. The current thinking regarding hypoxia has changed recently [Brown & Giaccia, (1994)]. Previously regarded as a problem, researchers now view hypoxia as a feature of the tumour which can be exploited. Hypoxia activated pro-drugs are currently in development and have a lot of potential, particularly when combined with conventional treatments [Harris *et al.*, (1996)]. Mathematical models can be used to examine the growth kinetics of subpopulations of active and hypoxic tumour cells after hypoxic targeting, in much the same way that models can be used to optimise drug delivery during chemotherapy [Usher & Henderson, (1996)].

Chapter (5) was largely a mathematical exercise to show the existence of travelling wave solutions with semi-infinite support for a density-dependent diffusion equation,although the model also acts as a qualitative description of solid tumour growth. The dilemma that faces the mathematical biologist is how to produce a model which is biologically realistic, yet mathematically tractable. The mathematical biologist must balance a number of disciplines in order to produce a useful model. This includes obtaining a thorough knowledge of the biological and experimental background, using techniques to analyse systems of ODEs and PDEs, and producing computer simulations of the modelled phenomena.

The numerical analysis of equations arising from complex biological systems that is also in need of further development, since the PDEs which arise are often non-standard

(cf. Oster & Murray, (1989)). For example, a preliminary investigation into the numerical solution of the mechanochemical model [Oster & Murray, (1989)], [Perelson *et al.*, (1986)], revealed a number of problems, such as stability, accuracy of the solution and problems associated with the use of periodic boundary conditions. The proper numerical treatment of the mechanochemical model is certainly non-trivial and could be considered as a research project in its own right.

Detailed mathematical models of solid tumour growth can prove difficult and time-consuming to solve numerically, particularly if large numbers of parameters are involved. The models found in chapters (6) and (7) were simulated in two space dimensions. This considerably increased the number of computations required to produce a solution. A cellular automaton approach can offer an alternative, with a set of simple rules replacing the physical interactions and reactions of the cells (see Ermentrout & Edelstein-Keshet, (1993) for a review). They have the advantage of being quick and easy to compute for large data sets, and involve discrete numbers of cells. The disadvantage is they are not accessible to mathematical analysis.

In chapter (6), we introduced heterogeneity into a mathematical model in a very simple way. This model demonstrated that heterogeneity in the tumour environment can directly affect the invasion process, in addition to highlighting the problems arising during surgical excision of a tumour. One improvement that could be made is to include heterogeneity in the model in a more sophisticated way. e.g. by having heterogeneous cell populations or a heterogeneous nutrient field. Cellular automata could be ideal for modelling heterogeneous populations of cells [Stott, (1996)].

Finally, in chapter (7), we produced a two-dimensional model of tumour angiogenesis, which we used to test a number of hypothetical anti-angiogenesis strategies. A very positive feature of this model is that it directly feeds back to the biology by suggesting a viable and potentially informative set of experiments. We have already seen a number of recent developments in anti-angiogenesis and anti-vascular treatments [Harris *et al.*, (1996)]. Angiogenesis has been the focus of much attention for the past few decades, and no doubt will continue to be of importance in the future.

Bibliography

Adam, J. A. (1993). The dynamics of growth-factor-modified immune response to cancer growth: One dimensional model. *Mathl. Comput. Modelling.*, **17**(3), 83–106.

Adam, J. A., & Maggelakis, S. A. (1990). Diffusion regulated growth characteristics of a spherical prevascular carcinoma. *Bull. Math. Biol.*, **52**(4), 549–582.

Ausprunk, D. H., & Folkman, J. (1977). Migration and proliferation of endothelial cells in preformed and newly formed blood vessels during tumor angiogenesis. *Microvasc. Res.*, **14**, 53–65.

Balding, D., & McElwain, D. L. S. (1985). A mathematical model of tumour induced capillary growth. *J. Theor. Biol.*, **114**, 53–73.

Ben-Yu, G., Mitchell, A. R., & Sleeman, B. D. (1986). Spatial effects in a two-dimensional model of the budworm-balsam fir ecosystem. *Comp. & Maths. with Appls.*, **12B**(5/6), 1117–1132.

Ben-Yu, G., Mitchell, A. R., & Sleeman, B. D. (1991). Spatial patterning of spruce budworm in circular region. *Science in China, Series A*, **34**(6), 676–688.

Blood, C. H., & Zetter, B. R. (1990). Tumor interactions with the vasculature: angiogenesis and tumor metastasis. *Biochim. Biophys. Acta*, **1032**, 89–118.

Bowersox, J. C., & Sorgente, N. (1982). Chemotaxis of aortic endothelial cells in response to fibronectin. *Cancer Res.*, **42**, 2547–2551.

Brooks, P. C., Montgomery, A. M. P., Rosenfeld, M., Reisfled, R. A., Hu, T., Klier, G., & Cheresh, D. A. (1994). Integrin $\alpha_v\beta_3$ antagonists promote tumor regression by inducing apoptosis of angiogenic blood vessels. *Cell*, **79**, 1157–1164.

Brown, J. M., & Giaccia, A. J. (1994). Tumour hypoxia: The picture has changed in the 1990s. *Int. J. Radiat. Biol.*, **65**, 95–102.

Bussolino, F., Renzo, M. F. Di, Ziche, M., Bocchietto, E., Olivero, M., Naldini, L., Gaudino, G., Tamagnone, L., Coffer, A., & Comoglio, P. M. (1992). Hepatocyte growth factor is a potent angiogenic factor which stimulates endothelial cell motility and growth. *J. Cell. Biol.*, **119**(9), 629–641.

Byrne, H. M, & Chaplain, M. A. J. (1996). *On the importance of constitutive equations in mechanochemical models of pattern formation. Appl. Math. Lett..*, to appear.

Carr, J. (1981). *Applications of centre manifold theory.* New York: Springer-Verlag.

Carter, S. B. (1965). Principles of cell motility: The direction of cell movement and cancer invasion. *Nature*, **208**, 1183–1187.

Chaplain, M. A. J. (1995). The mathematical modelling of tumour angiogenesis and invasion. *Acta Biotheoretica*, **43**, 387–402.

Chaplain, M. A. J., & Stuart, A. M. (1993). A model mechanism for the chemotactic response of endothelial cells to tumour angiogenesis factor. *IMA J. Math. Appl. Med. Biol.*, **10**, 149–168.

Chaplain, M. A. J., Giles, S. M., Sleeman, B. D., & Jarvis, R. J. (1995). A mathematical analysis of a model for tumour angiogenesis. *J. Math. Biol.*, **33**, 744–770.

Clark, R. A. F., DellaPelle, P., Manseau, E., Lanigan, J. M, Dvorak, H. F., & Colvin, R. B. (1982)a. Blood vessel fibronectin increases in conjunction with endothelial cell proliferation and capillary ingrowth during wound healing. *J. Invest. Dermatol.*, **79**, 269–276.

Clark, R. A. F., Lanigan, J. M., DellaPelle, P., Manseau, E., Dvorak, H. F., & Colvin, R. B. (1982)b. Fibronectin and fibrin provide a provisional matrix for epidermal cell migration during wound re-epithelialization. *J. Invest. Dermatol.*, **79**, 264–269.

Darling, D., & Tarin, D. (1990). The spread of cancer in the human body. *New Scientist*, July, 50–53.

de Pablo, A., & Vazquez, J. L. (1991). Travelling waves and finite propagation in a reaction-diffusion equation. *J. Diff. Eqn.*, **93**, 19–61.

Denekamp, J. (1984). Vascular endothelium as the vulnerable element in tumours. *Acta Radiol. Oncol.*, **23**, 217–225.

Dickinson, R. B., & Tranquillo, R. T. (1993). A stochastic model for adhesion mediated cell random motility and haptotaxis. *J. Math. Biol.*, **31**, 563–600.

Dunbar, S. R. (1983). Travelling Wave Solutions of diffusive Lotka–Volterra equations. *J. Math. Biol.*, **17**, 11–32.

Dunbar, S. R. (1984). Travelling Wave Solutions of diffusive Lotka–Volterra equations: A heteroclinic connection in R^4. *Trans. Amer. Math. Soc.*, **286**(2), 557–594.

Durand, R. E. (1990). Multicell spheroids as a model for cell kinetic studies. *Cell Tissue Kinet.*, **23**, 141–159.

Eaves, G. (1973). The invasive growth of malignant tumours as a purely mechanical process. *J. Path.*, **109**, 233–237.

Edelstein, L. (1982). The propagation of fungal colonies: A model for tissue growth. *J. Theor. Biol.*, **98**, 679–701.

Edelstein-Keshet, L. (1988). *Mathematical models in biology.* Random House.

Ellis, L. E, & Fidler, I. J. (1995). Angiogenesis and breast cancer metastasis. *Lancet*, **346**(August 12), 388–389.

Ermentrout, G. Bard, & Edelstein-Keshet, L. (1993). Cellular automata approaches to biological modelling. *J. Theor. Biol.*, **160**, 97–133.

Fenselau, A., & Mello, R. J. (1976). Growth stimulation of cultured endothelial cells by tumor cell homogenates. *Cancer Res.*, **36**, 3269–3273.

Fidler, I. J. (1978). Tumor heterogeneity and the biology of cancer invasion and metastasis. *Cancer Res.*, **38**, 2651–2660.

Fife, P. C. (1979). *Mathematical aspects of reacting and diffusing systems.* Berlin: Springer-Verlag.

Folkman, J. (1985). Tumor angiogenesis. *Adv. Cancer Res.*, **43**, 175–203.

Folkman, J. (1995). Angiogenesis in cancer, vascular, rheumatoid and other disease. *Nature Medicine*, **1**(1), 21–31.

Folkman, J., & Haudenschild, C. (1980). Angiogenesis in vitro. *Nature*, **288**, 551–556.

Folkman, J., & Klagsbrun, M. (1987). Angiogenic Factors. *Science*, **235**, 442–447.

Frank, R. E., Saclarides, T. J., Leurgans, S., Speziale, N. J., Drab, E. A., & Rubin, D. B. (1995). Tumor angiogenesis as a predictor of recurrence and survival in patients with node-negative colon cancer. *Ann. Surg.*, **222**(6), 695–699.

Gimbrone, M. A., Cotran, R. S., Leapman, S. B., & Folkman, J. (1974). Tumor growth and neovascularization: An experimental model using the rabbit cornea. *J. Natl. Cancer Inst.*, **52**(2), 413–427.

Goldwasser, L., Maini, P. K., & Murray, J. D. (1989). Splitting of cell clusters and bifurcation of bryozoan branches. *J. Theor. Biol.*, **137**, 271–279.

Goodall, C. M., Sanders, A. G., & Shubik, P. (1965). Studies of vascular patterns in living tumors with a transparent chamber inserted in hamster cheek pouch. *J. Natl. Cancer Inst.*, **35**, 497–505.

Greenspan, H.P. (1972). Models for the growth of a solid tumor by diffusion. *Stud. Appl. Math.*, **51**, 317–340.

Greenspan, H.P. (1976). On the growth and stability of cell cultures and solid tumours. *J. Theor. Biol.*, **56**, 229–242.

Grindrod, P. (1991). *Pattern and waves. The theory and applications of reaction-diffusion equations.* Oxford: Clarendon Press.

Grindrod, P., & Sleeman, B. D. (1987). Weak travelling fronts for population models with density dependent dispersion. *Math. Meth. in the Appl. Sci.*, **9**, 576–586.

Grundy, R. E. (1988). Asymptotic solutions of a model diffusion-reaction equation. *IMA J. Appl. Maths.*, **40**(1), 53–72.

Harris, A. L., Zhang, H. T., Moghaddam, A., Fox, S., Scott, P., Pattison, A., Gatter, K., Stratford, I., & Bicknell, R. (1996). Breast cancer angiogenesis- New approaches

to therapy via anti-angiogenesis, hypoxic activated drugs, and vascular targeting. *Breast Cancer Research and Treatment*, **38**(1), 97–108.

Hosono, Y. (1986). Travelling waves for some density dependent diffusion equations. *Japan J. Appl. Math.*, **3**, 163–196.

Hosono, Y. (1987). Travelling waves for some biological systems with density dependent diffusion. *Japan J. Appl. Math.*, **4**, 297–359.

Jain, R. K. (1994). Barriers to drug delivery in solid tumors. *Sci. Am.*, **271**(1), 58–65.

Jones, D. S., & Sleeman, B. D. (1983). *Differential equations and mathematical biology.* London: George Allen and Unwin.

Kalebic, T., Garbisa, S., Glaser, B., & Liotta, L. A. (1983). Basement membrane collagen: Degradation by migrating endothelial cells. *Science*, **221**, 281–283.

Kennedy, K. A., Teicher, B. A., Rockwell, S., & Sartorelli, A. C. (1980). The hypoxic tumor cell: A target for selective cancer chemotherapy. *Biochem. Pharmocol.*, **29**, 1–8.

Klein, G. (1980). Immune and non-immune control of neoplastic development. *Cancer*, **45**(10), 2486–2499.

Konerding, M. A., van Ackern, C., Steinberg, F., & Streffer, C. (1992). The development of the tumour vascular system: 2-D and 3-D approaches to network formation in human xenografted tumours. *In:* Maragoudakis, M. E., Gullino, P., & Lelkes, P. I. (eds), *Angiogenesis in Health and Disease.* New York: Plenum Press.

LaBarbera, M., & Vogel, S. (1982). The design of fluid transport systems in organisms. *American Scientist*, **70**, 54–60.

Langer, R., Brem, H., Falterman, K., Klein, M., & Folkman, J. (1976). Isolation of a cartilage factor that inhibits tumor neovascularization. *Science*, **193**, 70–72.

Lefever, R., & Horsthemke, W. (1979). Bistability in fluctuating environments. Implications in tumour immunology. *Bull. Math. Biol.*, **41**, 469–490.

Lineham, D. C., Goedegebuure, P. S., & Eberlein, T. J. (1996). Vaccine therapy for cancer. *Annals Surg. Oncol.*, **3**(2), 219–228.

Liotta, L.A., Saidel, G. M., & Kleinerman, J. (1977). Diffusion model of tumor vascularization and growth. *Bull. Math. Biol.*, **39**, 117–128.

Logan, J. David. (1994). *An introduction to nonlinear partial differential equations.* New York: John Wiley and Sons, Inc.

Ludwig, D., Jones, D. D., & Holling, C. S. (1978). Qualitative analysis of insect outbreak systems: The spruce budworm and forest. *J. Animal Ecol.*, **47**, 315–332.

MacSween, R.N.M., & Whaley, K. (eds). (1992). *Muir's textbook of pathology.* 13th edn. London: Edward Arnold.

Maini, P K. (1989). Spatial and spatio-temporal patterns in a cell-haptotaxis model. *J. Math. Biol.*, **27**, 507–522.

Marrack, P., & Kappler, J. (1986). The T-cell and its receptor. *Sci. Am.*, **254**(2), 28–37.

McCulloch, P., Choy, A., & Martin, L. (1995). Association between tumour angiogenesis and tumour cell shedding into effluent venous blood during breast cancer surgery. *Lancet*, **346**(November 18), 1334–1335.

McElwain, D. L. S., & Pettet, G. J. (1993). Cell migration in multicell spheroids: Swimming against the tide. *Bull. Math. Biol.*, **55**(3), 655–674.

Mirsky, R. (1995). Death and suicide in the world of the cell. *MRC News*, **65**, 13–16.

Murray, J. D. (1989). *Mathematical biology.* Berlin: Springer-Verlag.

Muthukkaruppan, V. R., Kubai, L., & Auerbach, R. (1982). Tumor-induced neovascularization in the mouse eye. *J. Natl. Cancer Inst.*, **69**, 699–704.

Myerscough, M. R., & Murray, J. D. (1992). Analysis of propagating pattern in a chemotaxis system. *Bull. Math. Biol.*, **54**(1), 77–94.

Nicolson, G. L. (1988). Cancer metastasis: tumor cell and host organ properties important in metastasis to specific secondary sites. *Biochim. Biophys. Acta*, **948**, 175–224.

Norton, J. A. (1995). Tumor angiogenesis: The future is now. *Ann. Surg.*, **222**(6), 693–694.

OPCS. (1989). *Cancer Statistics, Registrations.* Series MB1, No. 22.

OPCS. (1993). *Mortality Statistics, Cause.* Series DH2, No. 20.

O'Reilly, M. S., Holmgren, L., Shing, Y., Chen, C., Rosenthal, R. A., Moses, M., Lane, W. S., Cao, Y., Sage, E. Helene, & Folkman, J. (1994). Angiostatin: A novel angiogenesis inhibitor that mediates the suppression of metastases by a Lewis lung carcinoma. *Cell*, **79**, 315–328.

Orme, M. E., & Chaplain, M. A. J. (1996)a. A mathematical model of the first steps of tumour-related angiogenesis: capillary sprout formation and secondary branching. *IMA J. Math. Appl. Med. Biol.*, **13**, 73–98.

Orme, M. E., & Chaplain, M. A. J. (1996)b. A mathematical model of vascular tumour growth and invasion. *Mathl. Comput. Modelling*, **23**(10), 43–60.

Oster, G.K., & Murray, J.D. (1989). Pattern formation models and developmental constraints. *J. Exp. Zool.*, **251**, 186–202.

Paweletz, N., & Knierim, M. (1989). Tumor related angiogenesis. *Crit. Rev. Oncol. Hematol.*, **9**, 197–242.

Perelson, A.S., Maini, P. K., Murray, J. D., Hyman, J. M., & Oster, G. F. (1986). Nonlinear pattern selection in a mechanical model for morphogenesis. *J. Math. Biol.*, **24**, 525–541.

Prehn, R. T. (1994). Stimulatory effects of immune reactions upon growth of untransplanted tumors. *Cancer Res.*, **54**(February 15), 908–914.

Prigogine, I., & Lefever, R. (1980). Stability problems in cancer growth and nucleation. *Comp. Biochem. Physiol.*, **67B**, 389–393.

Ruddon, R. W. (1987). *Cancer biology.* 2nd edn. New York: Oxford University Press.

Sánchez-Garduño, F., & Maini, P. K. (1993). Wave Patterns in one-dimensional nonlinear degenerate diffusion equations. *Chap. 10 of:* Othmer, H. G., *et al.* (eds), *Experimental and theoretical advances in biological pattern formation.* New York: Plenum Press.

Sánchez-Garduño, F., & Maini, P. K. (1994). Existence and uniqueness of a sharp travelling wave in degenerate non-linear diffusion Fisher-KPP equations. *J. Math. Biol.*, **33**, 163–192.

Satsuma, J. (1987). Explicit solutions of nonlinear equations with density dependent diffusion. *J. Phys. Soc. Japan*, **56**(6), 1947–1950.

Saunders, P. T., & Ho, M. W. (1995). Reliable segmentation by successive bifurcation. *Bull. Math. Biol.*, **57**(4), 539–556.

Schirrmacher, V. (1985). Cancer metastasis: Experimental approaches, theoretical concepts, and impacts for treatment strategies. *Adv. Cancer Res.*, **43**, 1–73.

Schor, A.M., & Schor, S.L. (1983). Tumour angiogenesis. *J. Pathol.*, **141**, 385–413.

Sherratt, J. A., & Murray, J. D. (1990). Models of epidermal wound healing. *Proc. R. Soc. Lond. B*, **241**, 29–36.

Sholley, M.M., Ferguson, G. P., Seibel, H. R., Montour, J. L., & Wilson, J. D. (1984). Mechanisms of neovascularization. Vascular sprouting can occur without proliferation of endothelial cells. *Lab. Invest.*, **51**, 624–634.

Shymko, R. M., & Glass, L. (1976). Cellular and geometric control of tissue growth and mitotic instability. *J. Theor. Biol.*, **63**, 355–374.

Stoker, M. G. P., & Rubin, H. (1967). Density dependent inhibition of cell growth in culture. *Nature*, **215**, 171–172.

Stokes, C. L., & Lauffenburger, D. A. (1991). Analysis of the roles of microvessel endothelial cell random motility and chemotaxis in angiogenesis. *J. Theor. Biol.*, **152**, 377–403.

Stokes, C. L., Lauffenburger, D. A., & Williams, S. K. (1991). Migration of individual microvessel endothelial cells: stochastic model and parameter measurement. *J. Cell. Sci.*, **99**, 419–430.

Stott, E. L. (1996) (September). *Initial growth of cancer and simulation of cell movements within a tumour.* First year report.

Strano, S., & Blandino, G. (1995). Apoptosis: cell death or suicide. This is the problem! *J. Exp. Clin. Cancer Res.*, **14**(3), 275–281.

Suh, O., & Weiss, L. (1984). The development of a technique for the morphometric analysis of invasion in cancer. *J. Theor. Biol.*, **107**, 547–561.

Sutherland, R. M. (1988). Cell and environment interaction in tumor microregions: the multicell spheroid model. *Science*, **240**, 177–184.

Terranova, V. P., DiFlorio, R., Lyall, R. M., Hic, S., Friesel, R., & Maciag, T. (1985). Human endothelial cells are chemotactic to endothelial cell growth factor and heparin. *J. Cell. Biol.*, **101**, 2330–2334.

Ungari, S., Katari, R. S., Alessandri, G., & Gullino, P. M. (1985). Cooperation between fibronectin and heparin in the mobilisation of capillary endothelium. *Invas. Metast.*, **5**, 193–205.

Usher, J. R., & Henderson, D. (1996). Some drug-resistant models for cancer-chemotherapy. 1). cycle-nonspecific drugs. *IMA J. Math. Appl. Med. Biol.*, **13**(2), 99–126.

Weiss, J. B. (1992). Assays for angiogenic factors. *In:* Maragoudakis, M. E., Gullino, P., & Lelkes, P. I. (eds), *Angiogenesis in health and disease.* New York: Plenun Press.

Yamada, K. M., & Olden, K. (1978). Fibronectin-adhesive glycoproteins of cell surface and blood. *Nature*, **275**, 179–184.

Zetter, B. R. (1980). Migration of capillary endothelial cells is stimulated by tumor-derived factors. *Nature*, **285**, 41–43.

Appendix A

Appendix to chapter 4

A.1 Analysis of the three-dimensional phase space

At the critical point (0,0,0)

$$A_{11} = -\alpha(1+\tanh 1), \quad A_{12} = 0, \quad A_{13} = 0, \quad A_{23} = -c,$$
$$A_{31} = 0, \quad A_{32} = Sc, \quad A_{33} = c^2.$$

Hence the eigenvalues are given by the roots of

$$p(\lambda) = \lambda^3 + \lambda^2 a_1 + \lambda a_2 + a_3, \tag{A.1.1}$$

where

$$a_1 = \alpha(1+\tanh 1) - c^2,$$

$$a_2 = c^2(S - \alpha(1+\tanh 1)),$$

$$a_3 = Sc^2\alpha(1+\tanh 1).$$

If $c^2 < \alpha(1+\tanh 1) < S$ then the origin is a stable node. Otherwise, the critical point is a saddle point.

For non-negative solutions, we require these roots to be real. We must impose the conditions $\alpha_1 > 0$ and $\beta_1 = 0$ [Murray, (1989)] where

$$\alpha_1 = \left(\frac{a_1}{3}\right)^2 - \left(\frac{a_2}{3}\right), \tag{A.1.2}$$

$$\beta_1 = 2\left(\frac{a_1}{3}\right)^3 - \frac{a_1 a_2}{3} + a_3. \tag{A.1.3}$$

From the first condition we have

$$\alpha^2(1+\tanh 1)^2 + c^4 - 3c^2 S + c^2\alpha(1+\tanh 1) > 0. \tag{A.1.4}$$

A sufficient condition to satisfy $\alpha_1 > 0$ is $c^2 > 3S$ or $\alpha(1+\tanh 1) > 3S$.

From the second condition $\beta_1 = 0$, we have

$$\begin{aligned} &2(\alpha(1+\tanh 1))^3 + 3(\alpha(1 + \tanh 1))^2(3-2c^2) \\ &\quad +3\alpha(1+\tanh 1)(2c^4 + 3(3S-1)c^2 - 3S) + c^2(9S - 2c^4) = 0. \end{aligned} \tag{A.1.5}$$

Since α is real and positive, as a minimum requirement, we need the above polynomial to have one positive root. By Descartes Rule of Signs we require

$$3 > 2c^2,\ \ 2c^4 + 3(3S-1)c^2 - 3S > 0,\ \ 2c^4 > 9S.$$

c^2 is real and positive for $S > 0$. Hence combining these conditions $\frac{3}{2} > c^2 > 3\sqrt{\frac{S}{2}}$ is sufficient for α real and positive.

At the critical point (0,1,0)

$$\begin{aligned} &A_{11} = r - \alpha, \quad A_{12} = 0, \quad A_{13} = 0, \quad A_{23} = -c, \\ &A_{31} = \frac{-A}{B+1}, \quad A_{32} = -Sc, \quad A_{33} = c^2. \end{aligned}$$

Hence the eigenvalues are given by solutions of

$$\lambda^3 + \lambda^2(\alpha - r - c^2) + \lambda c^2(r - \alpha - S) + Sc^2(r - \alpha) = 0. \tag{A.1.6}$$

i.e. the roots of $p(\lambda) = \lambda^3 + \lambda^2 a_1 + \lambda a_2 + a_3$, where

$$a_1 = \alpha - r - c^2,$$

$$a_2 = c^2(r - \alpha - S),$$

$$a_3 = Sc^2(r-\alpha).$$

(0,1,0) is a saddle point. If $r > \alpha$, the polynomial $p(\lambda)$ will have two positive roots and one negative root. If $\alpha > r$ we will have one positive root and two negative roots. However by examination of equation (4.2.13) combined with the condition for invasion $n_2^\star < 1$, we conclude that $r > \alpha$.

Again we must impose conditions on our parameters so that the solutions are non-negative, i.e. the eigenvalues must be real. From the condition $\alpha_1 > 0$ where α_1 is given by (A.1.2) we obtain

$$\alpha^2 + r^2 + c^4 + 3Sc^2 - 2r\alpha > 0. \tag{A.1.7}$$

$r > 2\alpha$ is a sufficient but not necessary condition which satisfies (A.1.7). From $\beta_1 = 0$ where β_1 is given by (A.1.3) we obtain

$$\frac{2}{27}[-(r-\alpha)-c^2]^3 - \frac{c^2}{3}[-(r-\alpha)-c^2][(r-\alpha)-S] + Sc^2(r-\alpha) = 0.$$

$$\frac{2}{27}[-(r-\alpha)-c^2]^3 - \frac{c^2}{3}[-(r-\alpha)-c^2][(r-\alpha)-S] + Sc^2(r-\alpha) = 0.$$

After some algebra this becomes

$$2(r-\alpha)^3 - 3c^2(r-\alpha)^2 - c^2(r-\alpha)(18S+6c^2) + c^4(2c^2+9S) = 0. \tag{A.1.8}$$

At the third critical point $(n_1^\star, n_2^\star, 0)$

Using equations (4.2.12) and (4.2.13), the eigenvalues are given by solving the cubic equation

$$\lambda^3 + \lambda^2[\chi n_2^\star S(1-n_2^\star) - c^2] + \lambda Sc^2\left[\frac{2n_2^\star(1-n_2^\star)}{(B+n_2^{\star 2})^2}[n_2^\star - \chi(B+n_2^{\star 2})] - 1\right]$$

$$+ c^2 n_2^\star S(1-n_2^\star)[r + \alpha\,\mathrm{sech}^2(n_2^\star - 1)] = 0 \tag{A.1.9}$$

i.e. the roots of $p(\lambda) = \lambda^3 + \lambda^2 a_1 + \lambda a_2 + a_3$ where

$$a_1 = \chi n_2^\star S(1-n_2^\star) - c^2,$$

$$a_2 = Sc^2\left[\frac{2n_2^\star(1-n_2^\star)}{(B+n_2^{\star 2})^2}[n_2^\star - \chi(B+n_2^{\star 2})] - 1\right].$$

$$a_3 = c^2 n_2^\star S(1 - n_2^\star)[r + \alpha \mathrm{sech}^2(n_2^\star - 1)].$$

There are four possible cases, all roots negative, one root positive and two negative, one negative and two positive and all roots positive.

Suppose all the roots are negative. By the Routh-Hurwitz conditions

$$a_1,\ a_2,\ a_3 > 0.$$

The condition $n_2^\star < 1$ is satisfied and we obtain a bound on the wavespeed,

$$\text{i.e. } c^2 < \chi n_2^\star S(1 - n_2^\star).$$

Consider the limiting case $a_3 = 0$. Then the roots of $p(\lambda)$ are

$$\lambda = 0,\ \lambda_{1,2} = -a_1 \pm \sqrt{a_1^2 - 4a_2},$$

The maximum λ_M and minimum λ_m are given by

$$\frac{dp}{d\lambda} = 3\lambda^2 + 2\lambda a_1 + a_2 = 0,$$

$$\Rightarrow \lambda_{m,M} = \frac{1}{3}(-a_1 \pm \sqrt{a_1^2 - 3a_2}).$$

These are independent of a_3. As a_3 increases from zero, $p(\lambda)$ has three real negative roots. There is a critical value of a_3, $a_3^\star$ say, for which two of the roots are equal where

$$a_3^\star = \frac{1}{27}\left(a_1 + 2\sqrt{a_1^2 - 3a_2}\right)\left(a_1 - \sqrt{a_1^2 - 3a_2}\right)^2. \qquad \text{(A.1.10)}$$

So for $a_3 > a_3^\star$, we have only one real root and two complex roots. Hence the solutions approach the critical point in an oscillatory manner for $a_3 > a_3^\star$ and for $0 < a_3 < a_3^\star$ they are monotonic (figure (A-1)).

Suppose that one of the roots of $p(\lambda)$ is positive and two roots are negative. This implies that $a_3 < 0$ and so $n_2^\star > 1$ which contradicts our previous assumption. We dismiss this case on the grounds that this situation does not arise in the biological context that we are considering.

Now suppose that two of the roots are positive and one root is negative. Then $a_3 > 0$.

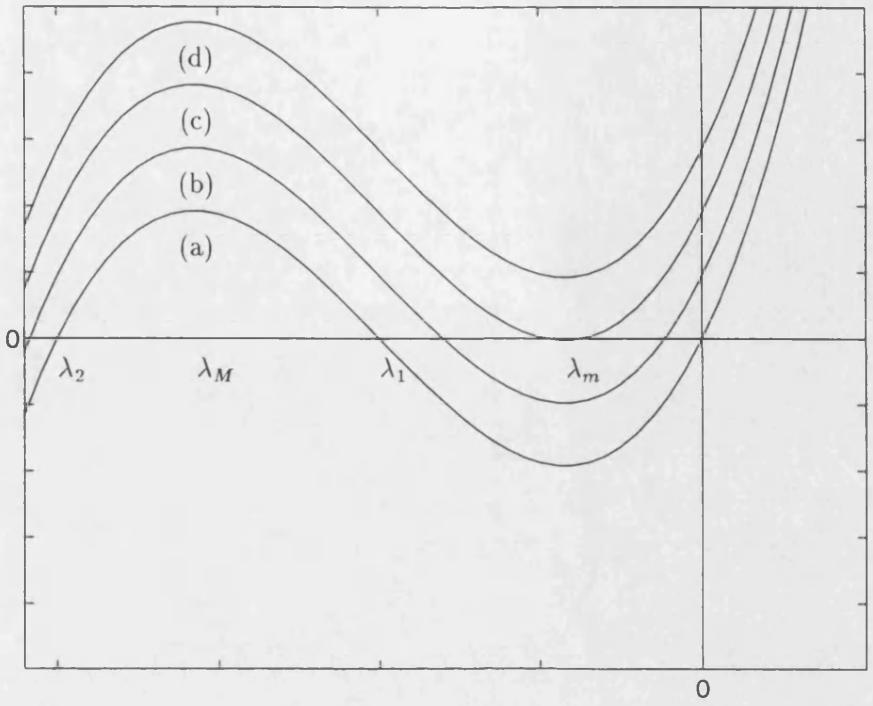

Figure A-1: *The general form of* $p(\lambda)$ *as* a_3 *increases from zero.* *(a)* $a_3 = 0$, *(b)* $0 < a_3 < a_3^\star$, *(c)* $a_3 = a_3^\star$ *and (d)* $a_3 > a_3^\star$.

Either of or both of a_1 and a_2 must be negative. If $a_1 < 0$, then $c^2 > \chi n_2^\star S(1 - n_2^\star)$. If $a_2 < 0$, then we obtain the inequality

$$(2\chi - 1)n_2^{\star 4} - 2(\chi + 1)n_2^{\star 3} + 2(1 + B(\chi - 1))n_2^{\star 2} - 2\chi B n_2^\star - B^2 < 0.$$

As before in the case where all the roots were negative, there is a critical value of a_3. As a_3 increases to this critical value, the two positive real roots become equal. So for $a_3 > a_3^\star$ we have a trajectory which oscillates away from $(n_1^\star, n_2^\star)$.

Finally, if all the roots are positive we have $a_3 < 0$. Again, we dismiss this case as it is not of biological relevance.

A.2 Analysis of the four-dimensional phase space

At the critical point (0,0,0,0)

$$A_{31} = \frac{\alpha}{D}(1+\tanh 1), \quad A_{32} = 0, \quad A_{33} = -\frac{c}{D},$$
$$A_{41} = 0, \quad A_{42} = -S.$$

Hence the eigenvalues are given by the roots of

$$p(\lambda) = \lambda^4 + \lambda^3 a_1 + \lambda^2 a_2 + \lambda a_3 + a_4,$$

where

$$a_1 = c + \frac{c}{D},$$

$$a_2 = \frac{c^2}{D} + S + \frac{\alpha}{D}(1+\tanh 1),$$

$$a_3 = \frac{cS}{D} - \frac{\alpha c}{D}(1+\tanh 1),$$

$$a_4 = -\frac{\alpha S}{D}(1+\tanh 1).$$

By examination of a_3 we see that the origin is a saddle. In particular it has an unstable manifold if $S < \alpha(1+\tanh 1)$ which agrees with the result found in appendix A.

At the critical point (0,1,0,0)

$$A_{31} = \frac{\alpha - r}{D}, \quad A_{32} = 0, \quad A_{33} = -\frac{c}{D},$$
$$A_{34} = 0, \quad A_{41} = \frac{A}{B+1}, \quad A_{42} = S.$$

Hence the eigenvalues are given by the roots of

$$p(\lambda) = \lambda^4 + \lambda^3 a_1 + \lambda^2 a_2 + \lambda a_3 + a_4,$$

where

$$a_1 = c + \frac{c}{D},$$

$$a_2 = \frac{1}{D}(c^2 + r - \alpha - DS),$$

$$a_3 = \frac{c}{D}(r - \alpha - S),$$

$$a_4 = \frac{S}{D}(\alpha - r).$$

Since $r > \alpha$, we can see that (0,1,0,0) is always a saddle.

At the critical point $(n_1^\star, n_2^\star, 0, 0)$

$$A_{31} = \frac{\chi}{D}\left(\frac{2An_1^\star n_2^\star}{B + n_2^{\star 2}} - Sn_2^\star(1 - n_2^\star)\right),$$

$$A_{32} = \frac{1}{D}(\chi A_{42} - rn_1^\star + \alpha n_1^\star \mathrm{sech}^2(n_2^\star - 1),$$

$$A_{33} = -\frac{c}{D},$$

$$A_{34} = -\frac{\chi c n_1^\star}{D},$$

$$A_{41} = \frac{An_2^\star}{B + n_2^\star},$$

$$A_{42} = \frac{2An_1^\star n_2^\star}{B + n_2^{\star 2}}\left(1 - \frac{n_2^{\star 2}}{B + n_2^{\star 2}}\right) - S(1 - 2n_2^\star).$$

Using equations (4.2.12) and (4.2.13), the eigenvalues are given by the roots of

$$p(\lambda) = \lambda^4 + \lambda^3 a_1 + \lambda^2 a_2 + \lambda a_3 + a_4,$$

where

$$a_1 = c + \frac{c}{D},$$

$$a_2 = \frac{c^2}{D} + S\left(\left(\frac{2}{B + n_2^{\star 2}} - \frac{\chi}{D}\right) n_2^{\star 2}(1 - n_2^\star) - 1\right),$$

$$a_3 = \frac{cS}{D}\left(\frac{2n_2^{\star 2}(1 - n_2^\star)}{B + n_2^{\star 2}} - 1\right),$$

$$a_4 = \frac{\chi}{D} Sn_2^\star(1 - n_2^\star)(r + \alpha \mathrm{sech}^2(n_2^\star - 1).$$

Since $n_2^\star < 1$, $a_4 > 0$. If either $a_2 < 0$ and/or $a_3 < 0$ then the critical point $(n_1^\star, n_2^\star, 0, 0)$ is a saddle. If both $a_2 > 0$ and $a_3 > 0$ then the critical point is a stable node, i.e. if

$$\frac{c^2}{D} + S\left(\left(\frac{2}{B + n_2^{\star 2}} - \frac{\chi}{D}\right) n_2^{\star 2}(1 - n_2^\star) - 1\right) > 0, \qquad \text{(A.2.11)}$$

and

$$2n_2^{\star 2}(1 - n_2^{\star}) > B + n_2^{\star 2}. \tag{A.2.12}$$

From (A.2.12), we have $n_2^{\star 2} - 2n_2^{\star 3} > B > 0$. Consider the function $f(n_2^{\star}) = n_2^{\star 2} - 2n_2^{\star 3}$ for $0 < n_2^{\star 2} < 1$. Then clearly $\frac{1}{27} > B > 0$. Hence if (A.2.12) is satisfied then $c^2 > \chi S n_2^{\star 2}(1 - n_2^{\star})$ is sufficient to satisfy (A.2.11).

Appendix B

Appendix to chapter 5

B.1 Local stability analysis of a density-dependent diffusion equation

The Jacobian for all points (U,V) is

$$J[F,G]_{(U,V)} = \begin{bmatrix} -V & -U \\ rU^{r-1} - (r+q)U^{r+q-1} & -c+2V \end{bmatrix}. \tag{B.1.1}$$

B.1.1 At the critical point (0,0)

At $P_0 = (0,0)$ the Jacobian is,

$$J[F,G]_{(0,0)} = \begin{bmatrix} 0 & 0 \\ K_1(0) & -c \end{bmatrix}, \tag{B.1.2}$$

where

$$K_1(0) = U^{r-1}|_0 = \begin{cases} 0, & \text{if } r > 1, \\ 1, & \text{if } r = 1. \end{cases}$$

The eigenvalues are $\lambda_1 = 0$, $\lambda_2 = -c$, with corresponding eigenvectors

$$\mathbf{v_1} = \begin{bmatrix} 1 \\ \frac{K_1(0)}{c} \end{bmatrix}, \quad \mathbf{v_2} = \begin{bmatrix} 0 \\ 1 \end{bmatrix}.$$

We will use centre manifold theory in order to determine the behaviour of the trajectories around (0,0). We will consider two separate cases $r \leq 2$, $r > 2$.

First consider $r \leq 2$. If we expand (5.2.35)–(5.2.36) about (0,0) up to second order, we have

$$\dot{U} = -UV = F_2(U,V), \tag{B.1.3}$$

$$\dot{V} = K_1(0)U - cV + K_2(0)U^2 + V^2 + h.o.t. = G_2(U,V), \tag{B.1.4}$$

where

$$K_2(0) = \begin{cases} -1, & \text{if } r = 1 \text{ and } q = 1, \\ 1, & \text{if } r = 2, \\ 0, & \text{otherwise.} \end{cases} \tag{B.1.5}$$

In our analysis, we will use the following theorems.

Theorem B.1.1 *Consider the system*

$$\begin{aligned} \dot{x}(t) &= Ax(t) + f(x(t), y(t)), \\ \dot{y}(t) &= By(t) + g(x(t), y(t)), \end{aligned} \tag{B.1.6}$$

$x \in \mathbf{R}^n$, $y \in \mathbf{R}^m$, A and B constant matrices such that all of the eigenvalues of A have zero real parts and all of the eigenvalues of B have negative real parts, with f and g, C^2 and $f(0,0) = g(0,0) = f'(0,0) = g'(0,0) = 0$, where $'$ denotes the Jacobian matrix of the function.

Then, there exists a centre manifold

$$y = h(x),\ h(0) = 0,\ h'(0) = 0,\ |x| < \delta,$$

for (B.1.6), where $h(x) \in C^2$. Furthermore, the flow on the centre manifold is given by

$$\dot{w} = Aw + f(w, h(w)). \tag{B.1.7}$$

We see that (B.1.7) contains all the information needed to determine the asymptotic behaviour of small solutions as seen by the next theorem.

Theorem B.1.2 *(a) Suppose the zero solution of (B.1.7) is stable,asymptotically stable or unstable. Then the zero solution of (B.1.6) is also stable, asymptotically stable*

or unstable respectively.

(b) Suppose the zero solution of (B.1.7) is stable, then, if $(x(t), y(t))$ *is a solution of (B.1.6) with* $(x(0), y(0))$ *sufficiently small, then there exist a solution* $u(t)$ *of (B.1.7) such that as* $t \to \infty$

$$x(t) = u(t) + O(e^{-\gamma}),$$

$$y(t) = h(u(t)) + O(e^{-\gamma}),\ \gamma > 0 \text{ some constant.}$$

The next theorem tells us how to approximate the centre manifold.

Theorem B.1.3 *For functions* $\phi : \mathbf{R}^n \to \mathbf{R}^m$, *which are* C^1 *in the neighbourhood of the origin, define*

$$(M\phi)(x) = \phi'(x)[Ax + f(x, \phi(x))] - B\phi(x) - g(x, \phi(x)).$$

Suppose that as $x \to 0$, $(M\phi)(x) = O(|x|^q)$, $q > 1$. *Then as* $x \to 0$, $|h(x) - \phi(x)| = O(|x|^q)$.

Proof For the proofs of theorems (B.1.1) to (B.1.3) see Carr, (1981).

In order to apply the centre manifold theory, we need to re–write (B.1.3)–(B.1.4) in normal form. First we write (B.1.3)–(B.1.4) in the form

$$\dot{\underline{X}} = J[F, G]_{(0,0)}\underline{X} + \underline{f}(\underline{X}), \tag{B.1.8}$$

where $\underline{X} = \begin{bmatrix} U \\ V \end{bmatrix}$, $\underline{f}(\underline{X}) = \begin{bmatrix} -UV \\ K_2(0)U^2 + V^2 \end{bmatrix}$.

Let

$$P = \begin{bmatrix} 1 & 0 \\ \frac{K_1(0)}{c} & 1 \end{bmatrix}, \quad D = \begin{bmatrix} 0 & 0 \\ 0 & -c \end{bmatrix}, \quad \underline{Y} = \begin{bmatrix} \tilde{U} \\ \tilde{V} \end{bmatrix},$$

then $\underline{X} = P\underline{Y}$ is an orthogonal transformation such that $P^{-1}J[F, G]_{(0,0)}P = D$, i.e. (B.1.8) becomes

$$\dot{\underline{Y}} = D\underline{Y} + P^{-1}\underline{f}(P\underline{Y}).$$

Hence

$$\frac{d\tilde{U}}{d\xi} = -\frac{1}{c}K_1(0)\tilde{U}^2 - \tilde{U}\tilde{V}, \tag{B.1.9}$$

$$\frac{d\tilde{V}}{d\xi} = -c\tilde{V} + \left[\frac{2K_1^2(0)}{c^2} + K_2(0)\right]\tilde{U}^2 + \frac{3K_1(0)}{c}\tilde{U}\tilde{V} + \tilde{V}^2. \qquad \text{(B.1.10)}$$

By theorem (B.1.1), (B.1.9)–(B.1.10) has a centre manifold $\tilde{V} = \tilde{h}(\tilde{U})$. To approximate $\tilde{h}$ (up to second order), we set

$$\begin{aligned}(M\phi)(\tilde{U}) &= \phi'(\tilde{U})\left[\frac{1}{c}K_1(0)\tilde{U}^2 - \tilde{U}\phi(\tilde{U})\right] + c\phi(\tilde{U}) \\ &\quad - \left[\frac{2}{c^2}K_1^2(0) + K_2(0)\right]\tilde{U}^2 - \frac{3}{c}K_1(0)\tilde{U}\phi(\tilde{U}) + \phi^2(\tilde{U}). \qquad \text{(B.1.11)}\end{aligned}$$

If $\phi(\tilde{U}) = \frac{1}{c}\left[\frac{2}{c^2}K_1^2(0) + K_2(0)\right]\tilde{U}^2$ then $(M\phi)(\tilde{U}) = O(\tilde{U}^3)$, and $\phi(0) = \phi'(0) = 0$. Hence by theorem (B.1.3)

$$\tilde{h}(\tilde{U}) = \frac{1}{c}\left[\frac{2}{c^2}K_1^2(0) + K_2(0)\right]\tilde{U}^2 + O(\tilde{U}^3).$$

In terms of (U, V), the centre manifold is given by

$$h(U) = \frac{1}{c}\left[\frac{2}{c^2}K_1^2(0) + K_2(0)\right]U^2 + \frac{1}{c}K_1(0)U + O(U^3). \qquad \text{(B.1.12)}$$

By theorem (B.1.1), the flow on the centre manifold of (B.1.3)–(5.2.36) is given by

$$\dot{w} = -\frac{w^2}{c}\left[\left(\frac{2}{c^2}K_1^2(0) + K_2(0)\right)w + K_1(0)\right] + O(w^4).$$

Recall that

$$K_1(0) = \begin{cases} 0 & \text{if } r > 1, \\ 1 & \text{if } r = 1, \end{cases} \qquad K_2(0) = \begin{cases} -1, & \text{if } r = 1 \text{ and } q = 1, \\ 1, & \text{if } r = 2, \\ 0 & \text{otherwise,} \end{cases} \qquad \text{and } r = m + p - 1,$$

We have three possibilities;

1. $r = 2$. Then the flow on the centre manifold is

$$\dot{w} = -\frac{1}{c}w^3 + O(w^4),$$

so $w \equiv 0$ is stable.

2. $r = 1$ and $q = 1$. The flow on the centre manifold is

$$\dot{w} = -\frac{w^2}{c}\left[\left(\frac{2}{c^2} - 1\right) w + \mathbb{1}\right] + O(w^4).$$

Hence the flow on the centre manifold varies with c. When $c = \sqrt{2}$, we have one equilibrium $w \equiv 0$. When $c \neq \sqrt{2}$, we have two equilibria $w \equiv 0$ and $w = c^2/(c^2 - 2)$. In any case $w \equiv 0$ is unstable. (*cf* [Sánchez-Garduño & Maini, (1994)].)

3. $r = 1$ and $q \neq 1$. In this case the flow is given by

$$\dot{w} = -\frac{1}{c} w^2 \left[\frac{2w}{c^2} + 1\right] + O(w^4),$$

so $w \equiv 0$ is unstable.

Now consider $r > 2$. We need to obtain a better approximation to the centre manifold. Recall (5.2.35)–(5.2.36)

$$\begin{aligned} \dot{U} &= -UV = F(U,V), \\ \dot{V} &= -V(c - V) + U^r(1 - U^q) = G(U,V). \end{aligned}$$

For $r > 2$, we have eigenvalues $\lambda_1 = 0$ and $\lambda_2 = -c$ corresponding to eigenvectors $\mathbf{v}_1 = [1,0]^T$ and $\mathbf{v}_2 = [0,1]^T$. We can approximate the centre manifold up to order r by setting

$$(M\phi)(U) = -U\phi(U)\phi'(U) + c\phi(U) - \phi^2(U) - U^r(1 - U^q).$$

Let $\phi(U) = \frac{1}{c}U^r$, then $(M\phi)(U) = O(U^{r+1})$ and $\phi(0) = \phi'(0) = 0$. Hence by theorem (B.1.3)

$$h(U) = \frac{1}{c}U^r + O(U^{r+1}),$$

and by theorem (B.1.1), the flow on the centre manifold is

$$\dot{w} = -\frac{1}{c} w^{r+1}.$$

Hence, if r is odd $w \equiv 0$ is unstable and if r is even $w \equiv 0$ is stable.

In general, if we have initial values (U_0, V_0) such that $\sqrt{U_0^2 + V_0^2}$ is sufficiently small

and $U_0 > 0$, then solutions will tend to P_0 along the centre manifold.

B.1.2 At the critical point P_1

At $P_1 = (1,0)$,

$$J[F,G]_{(1,0)} = \begin{bmatrix} 0 & -1 \\ -q & -c \end{bmatrix}. \tag{B.1.13}$$

The eigenvalues are given by

$$\lambda_{1,2} = \frac{-c \pm \sqrt{c^2+q}}{2}, \quad \lambda_1 > 0, \ \lambda_2 < 0. \tag{B.1.14}$$

Eigenvectors are

$$\mathbf{v_1} = \begin{bmatrix} 1 \\ -\lambda_1 \end{bmatrix}, \quad \mathbf{v_2} = \begin{bmatrix} 1 \\ -\lambda_2 \end{bmatrix}.$$

Hence P_1 is a saddle.

B.1.3 At the critical point P_c

At $P_c = (0,c)$

$$J[F,G]_{(0,c)} = \begin{bmatrix} -c & 0 \\ K_1(0) & c \end{bmatrix}. \tag{B.1.15}$$

This has eigenvalues $\lambda_{1,2} = \pm c$ with associated eigenvectors

$$\mathbf{v_1} = \begin{bmatrix} 0 \\ 1 \end{bmatrix}, \quad \mathbf{v_2} = \begin{bmatrix} 1 \\ \frac{-K_1(0)}{2c} \end{bmatrix}.$$

Hence, P_c is also a saddle.